

Department of Civil Engineering

**Shear and Bond Behaviour of Reinforced Fly Ash-Based
Geopolymer Concrete Beams**

Ee Hui Chang

**This thesis is presented for the Degree of
Doctor of Philosophy
of
Curtin University of Technology**

January 2009

Declaration

To the best of my knowledge and belief this thesis contains no material previously published by any other person except where due acknowledgment has been made.

This thesis contains no material which has been accepted for the award of any other degree or diploma in any university.

Signature:

Date:

ABSTRACT

Concrete is by far the most widely used construction material worldwide in terms of volume, and so has a huge impact on the environment, with consequences for sustainable development. Portland cement is one of the most energy-intensive materials of construction, and is responsible for some emissions of carbon dioxide — the main greenhouse gas causing global warming. Efforts are being made in the construction industry to address these by utilising supplementary materials and developing alternative binders in concrete; the application of geopolymer technology is one such alternative. Indeed, geopolymers have emerged as novel engineering materials with considerable promise as binders in the manufacture of concrete. Apart from their known technical attributes, such as superior chemical and mechanical properties, geopolymers also have a smaller greenhouse footprint than Portland cement binders.

Research on the development, manufacture, behaviour and applications of low calcium fly ash-based geopolymer concrete has been carried out at Curtin University of Technology since 2001. Past studies of the structural behaviour of reinforced fly ash-based geopolymer concrete members have covered the flexural behaviour of members. Further studies are needed to investigate other aspects of the structural behaviour of geopolymer concrete. Design for both shear and bond are important in reinforced concrete structures. Adequate shear resistance in reinforced concrete members is essential to prevent shear failures which are brittle in nature. The performance of reinforced concrete structures depends on sufficient bond between concrete and reinforcing steel. The present research therefore focuses on the shear and bond behaviour of reinforced low calcium fly ash-based geopolymer concrete beams.

For the study of shear behaviour of geopolymer concrete beams, a total of nine beam specimens were cast. The beams were 200 mm x 300 mm in cross section with an effective length of 1680 mm. The longitudinal tensile reinforcement ratios were 1.74%, 2.32% and 3.14%. The behaviour of reinforced geopolymer concrete beams

failing in shear, including the failure modes and crack patterns, were found to be similar to those observed in reinforced Portland cement concrete beams. Good correlation of test-to-prediction value was obtained using *VecTor2* Program incorporating the Disturbed Stress Field Model proposed by Vecchio (2000). An average test-to-prediction ratio of 1.08 and a coefficient of variation of 8.3% were obtained using this model. It was also found that the methods of calculations, including code provisions, used in the case of reinforced Portland cement concrete beams are applicable for predicting the shear strength of reinforced geopolymer concrete beams.

For the study of bond behaviour of geopolymer concrete beams, the experimental program included manufacturing and testing twelve tensile lap-spliced beam specimens. No transverse reinforcement was provided in the splice region. The beams were 200 mm wide, 300 mm deep and 2500 mm long. The effect of concrete cover, bar diameter, splice length and concrete compressive strength on bond strength were studied. The failure mode and crack patterns observed for reinforced geopolymer concrete beams were similar to those reported in the literature for reinforced Portland cement beams. The bond strength of geopolymer concrete was observed to be closely related to the tensile strength of geopolymer concrete. Good correlation of test bond strength with predictions from the analytical model proposed by Canbay and Frosch (2005) were obtained when using the actual tensile strength of geopolymer concrete. The average ratio of test bond strength to predicted bond strength was 1.0 with a coefficient of variation of 15.21%. It was found that the design provision and analytical models used for predicting bond strength of lap-splices in reinforced Portland cement concrete are applicable to reinforced geopolymer concrete beams.

ACKNOWLEDGEMENTS

The author expresses her sincere thanks to Dr Prabir Sarker, Dr Natalie Lloyd and Prof B. Vijaya Rangan for their guidance, constructive advice and valuable assistance throughout the study.

The technical assistance provided by the laboratory staff for the experimental works is appreciated. Special thanks to Mr John Murray, Mr Rob Cutter, Mr Mike Elliss, Mr Mike Appleton and other staff for their support.

Special thanks are extended to Dr Paul Y. L. Kong and Mr Gerard Chin, for valuable inputs into the *ShearCalculator* Program. Other contributions made by Dr Djwantoro Hardjito, Dr Steenie Wallah, Dr Dody Sumajouw, Dr John Fielder, Professor Hamid Nikraz and Professor Frank J Vecchio are also acknowledged.

The author thanks Curtin University of Technology for providing the Curtin University Postgraduate Scholarship (CUPS) for the tenure of 2006-2008. The fly ash was obtained from Fly Ash Australia.

Last, but not least, thanks to my family for their continuing support and encouragement throughout the entire study. Special thanks to my husband, Mr Kian Huat Tan, for providing encouragement and assistance in the experimental works; also to my parents, Mr and Mrs Tien Sung Chang, and sisters, Kathleen and Ee Ling Chang, for the love and moral support that helped me to carry out this research.

TABLE OF CONTENTS

ABSTRACT	i
ACKNOWLEDGEMENTS	iii
TABLE OF CONTENTS	iv
LIST OF FIGURES	x
LIST OF TABLES	xvi
NOTATION	xviii
CHAPTER 1	1
INTRODUCTION	1
1.1 Background.....	1
1.2 Research Objectives	3
1.3 Scope of Work.....	3
1.4 Organisation of Thesis.....	4
CHAPTER 2	6
LITERATURE REVIEW	6
2.1 Geopolymers.....	6
2.1.1 General	6
2.1.2 Fly Ash-Based Geopolymers.....	9
2.1.3 Low Calcium Fly Ash-Based Geopolymer Concrete	12
2.1.3.1 Constituents of Geopolymer Concrete	12
2.1.3.2 Manufacturing of Geopolymer Concrete – Mixing, Casting and Curing	14
2.1.3.3 The Effect of Salient Parameters on the Properties of Geopolymer Concrete	15
2.1.3.4 Engineering Properties of Geopolymer Concrete.....	16
2.1.3.5 Structural Applications of Geopolymer Concrete	17
2.1.3.6 Geopolymer Precast Concrete Products	18
2.1.3.7 Economic Benefits of Geopolymer Concrete.....	19
2.2 Shear Strength of Reinforced Concrete Beams with Shear Reinforcement	20
2.2.1 General	20
2.2.2 Predictions by using Analytical Models.....	23
2.2.2.1 von Ramin (2004).....	23

2.2.2.2	Kong and Rangan (1998).....	31
2.2.2.3	Disturbed Stress Field Model by Vecchio (2000).....	39
2.2.3	Code Provisions.....	50
2.2.3.1	Australian Standard AS 3600-01 (2001) and Draft Australian Standard AS3600 (2005).....	50
2.2.3.2	American Concrete Institute Building Code ACI318-08	52
2.3	Bond Strength of Lap-Spliced Bars in Beams.....	53
2.3.1	General	53
2.3.2	Modelling Approaches for Bond Strength of Lap-Spliced Bars in Beams	55
2.3.2.1	Canbay and Frosch (2005).....	55
2.3.2.2	Esfahani and Rangan (1998)	60
2.3.2.3	Orangun et al (1977).....	62
2.3.2.4	Zuo and Darwin (2000)	63
2.3.2.5	ACI Committee 408	63
2.3.3	Code Provisions.....	64
2.3.3.1	Australian Standard AS3600-01 (2001)	64
2.3.3.2	Draft Australian Standard AS3600 (2005).....	65
2.3.3.3	American Concrete Institute Building Code ACI318-08 (2008)	67
2.3.4	Summary.....	68
SECTION ONE.....		69
SHEAR BEHAVIOUR OF REINFORCED FLY ASH-BASED GEOPOLYMER CONCRETE BEAMS		69
CHAPTER 3		70
MANUFACTURE AND TESTING OF BEAMS FOR SHEAR STUDY		70
3.1	Experimental Aims	70
3.2	Design of Test Specimens	70
3.3	Materials	76
3.3.1	Aggregates.....	76
3.3.2	Fly Ash	78
3.3.3	Alkaline Liquid.....	79
3.3.4	Superplasticiser.....	80
3.4	Mixture Proportions for Geopolymer Concrete	80
3.5	Properties of Reinforcement.....	82
3.6	Manufacture of Test Specimens	83

3.6.1	Mould Preparation	83
3.6.2	Reinforcement Cage	84
3.6.3	Mixing	84
3.6.4	Steam Curing	88
3.7	Test Set-up and Instrumentation.....	91
3.8	Testing Procedure.....	93
CHAPTER 4	94
PRESENTATION AND DISCUSSION OF TEST RESULTS FOR SHEAR		
STUDY	94
4.1	Behaviour of Test Beams Failing in Shear.....	94
4.2	Load-Deflection Curves	114
4.3	Shear Cracking Load	120
4.4	Shear Strength of Test Beams	121
4.4.1	General	121
4.4.2	Influence of the Longitudinal Tensile Reinforcement Ratio on Shear Strength of Test Beams	122
CHAPTER 5	124
ANALYTICAL MODELLING OF BEAMS IN SHEAR STUDY		
5.1	Introduction	124
5.2	<i>ShearCalculator</i>	124
5.2.1	Calculation Steps	124
5.2.2	Input Data for Beam	126
5.2.3	Numerical Example	127
5.3	<i>VecTor2</i>	131
5.3.1	Calculation Procedure	131
5.3.1.1	Input using <i>Formworks</i> Program.....	132
5.3.1.2	<i>VecTor2</i>	139
5.3.1.3	<i>Augustus</i> Program.....	140
CHAPTER 6	141
DISCUSSION AND CORRELATION OF TEST AND CALCULATED RESULTS		
FOR SHEAR STUDY	141
6.1	Shear at Diagonal Cracking.....	141
6.2	Shear Strength of Test Beams	144
6.2.1	Comparison with Prediction using Analytical Models.....	144

6.2.2	Comparison with Prediction using Code Provisions	146
6.3	Cracking/Crushing Patterns and Failure Modes	149
6.4	Comparison of Shear Strength Between Geopolymer Concrete and Portland Cement Concrete Beams	159
SECTION TWO		162
BOND BEHAVIOUR OF REINFORCED FLY ASH-BASED GEOPOLYMER CONCRETE BEAMS		162
CHAPTER 7.....		163
MANUFACTURE AND TESTING OF BEAMS FOR BOND STUDY		163
7.1	Experimental Aims	163
7.2	Design of Test Specimens	163
7.3	Materials	172
7.4	Mixture Proportions for Geopolymer Concrete	173
7.5	Properties of Reinforcement.....	174
7.6	Manufacture of Test Specimens	175
7.7	Steam Curing	179
7.8	Test Set-up and Instrumentation.....	180
7.9	Testing Procedure.....	181
CHAPTER 8.....		183
PRESENTATION AND DISCUSSION OF TEST RESULTS FOR BOND STUDY		183
8.1	General Behaviour of Test Specimens	183
8.2	Failure Modes and Crack Patterns.....	185
8.3	Observation on Steel-Geopolymer Concrete Interface at Splice Region After Failure.....	191
8.4	Test Results	193
8.4.1	Failure Loads and Moments	194
8.4.2	Test Bond Strength.....	195
8.4.3	Effect of Parameters on Bond Stress.....	197
8.4.3.1	Effect of C/d_b	197
8.4.3.2	Effect of L_s/d_b	198
8.4.3.3	Effect of Concrete Compressive Strength	199
8.5	Load-Deflection Curves	201
CHAPTER 9.....		206

DISCUSSION AND CORRELATION OF TEST RESULTS AND CALCULATED RESULTS FOR BOND STUDY	206
9.1 Bond strength of Lap Splices in Geopolymer Concrete Beams	206
9.1.1 Comparison with Prediction using Analytical Models.....	206
9.1.2 Comparison of Bond Strength using Code Provisions	211
9.2 Comparison of Bond Strength between Geopolymer Concrete and Portland Cement Concrete Beams	213
9.2.1 Relationship between Splitting Tensile Strength and Bond Strength of Geopolymer Concrete.....	215
CHAPTER 10.....	217
CONCLUSIONS AND RECOMMENDATIONS.....	217
10.1 Conclusions	217
10.1.1 Shear Behaviour of Reinforced Fly Ash-Based Geopolymer Concrete Beams	217
10.1.2 Bond Behaviour of Reinforced Fly Ash-Based Geopolymer Concrete Beams	219
10.2 Recommendations for Future Research.....	221
10.2.1 Shear behaviour of Reinforced Fly Ash-Based Geopolymer Concrete	221
10.2.2 Bond Behaviour of Lap Splices in Geopolymer Concrete	222
REFERENCES	223
APPENDICES.....	237
APPENDIX A1	238
WATER ADJUSTED FOR THE MIX ACCORDING TO MOISTURE CONDITIONS OF AGGREGATES (SHEAR STUDY).....	238
APPENDIX A2	244
WATER ADJUSTED FOR THE MIX ACCORDING TO MOISTURE CONDITIONS OF AGGREGATES (BOND STUDY).....	244
APPENDIX B1.....	251
TRIAL MIX DATA FOR MIXTURE GP1	251
APPENDIX B2.....	253
TRIAL MIX DATA FOR MIXTURE GP2	253
APPENDIX C.....	255
TEST DATA FOR BEAMS (SHEAR STUDY).....	255
APPENDIX D	266

SAMPLE OF BEAM ANALYSIS REPORT USING <i>ShearCalculator</i>	266
APPENDIX E	304
INPUT DATA FOR ANALYSIS USING VECTOR2	304
APPENDIX F	350
CRACK PATTERN OF EACH PAIR OF GEOPOLYMER CONCRETE BEAMS FOR D-SERIES AND L-SERIES (SIDE VIEW AND BOTTOM VIEW)	350
APPENDIX G	363
STEEL- GEOPOLYMER CONCRETE INTERFACE AT SPLICE REGION.....	363
AFTER FAILURE.....	363
APPENDIX H	370
TEST DATA FOR BEAMS (BOND STUDY).....	370

LIST OF FIGURES

Figure 2.1: Reinforced Concrete Panel with Inclined Strut	24
(von Ramin, 2004).....	24
Figure 2.2: Definition of Strut Width in Deep Beam (von Ramin, 2004).....	25
Figure 2.3: Constant Distribution of Friction Stresses along Crack (Reineck, 1991)	29
Figure 2.4: Stress Analysis of a Reinforced Concrete Element	31
(Kong and Rangan, 1998).....	31
Figure 2.5: Reinforced Concrete Element – Reinforcement and Loading Conditions (Vecchio, 2000)	40
Figure 2.6: Mohr’s Circle for Average Stresses in Concrete (Vecchio, 2000)	41
Figure 2.7: Bearing Forces and Tensile Forces in Concrete (Warner et al., 1998) ...	53
Figure 2.8: Potential Splitting Surfaces (Warner et al., 1998)	54
Figure 2.9: Beam Tests to Measure Bond Strength.....	54
Figure 2.10: Side Splitting Failure (Canbay and Frosch, 2005).....	56
Figure 2.11: Face Splitting Failure (Canbay and Frosch, 2005)	56
Figure 2.12: Relationship between longitudinal and splitting forces	58
Figure 3.1: Cross-section and Elevation View of Beams for Series 1	73
Figure 3.2: Cross-section and Elevation View of Beams for Series 2	74
Figure 3.3: Cross-section and Elevation View of Beams for Series 3	75
Figure 3.4: Particle Size Distributions of Fly Ash	79
Figure 3.5: Mould for Beam Specimens.....	83
Figure 3.6: Reinforcement Cage.....	84
Figure 3.7: Materials for making Fly Ash- Based Geopolymer Concrete	85
Figure 3.8: Pan Mixer.....	86
Figure 3.9: Fresh Geopolymer Concrete	86
Figure 3.10: Casting and Compacting Geopolymer Concrete.....	87
Figure 3.11: Typical Set-up of Steam Curing Chamber.....	89
Figure 3.12: Steam boiler system	89
Figure 3.13: Complete Set-Up of Steam Curing Chamber.....	90
Figure 3.14: De-moulded Beams in Laboratory.....	90
Figure 3.15: Loading Arrangement for Beam Tests.....	91

Figure 3.16: Typical Test Set-Up for Beam Tests.....	92
Figure 3.17: LVDTs for Vertical Displacement Measurement.....	92
Figure 4.1: Concrete Crushing in Compression Zone for Beam S1-1	96
Figure 4.2: Overall Crack Pattern for Beam S1-1 (Front Face).....	97
Figure 4.3: Overall Crack Pattern for Beam S1-1 (Back Face).....	97
Figure 4.4: Concrete Crushing in Compression Zone for Beam S1-2	98
Figure 4.5: Overall Crack Pattern for Beam S1-2 (Front Face).....	99
Figure 4.6: Overall Crack Pattern for Beam S1-2 (Back Face).....	99
Figure 4.7: Principal Diagonal Crack Near Loading Point for Beam S1-3.....	100
Figure 4.8: Overall Crack Pattern for Beam S1-3 (Front Face).....	101
Figure 4.9: Overall Crack Pattern for Beam S1-3 (Back Face).....	101
Figure 4.10: Principal Diagonal Crack for Beam S2-1	102
Figure 4.11: Overall Crack Pattern for Beam S2-1 (Front Face).....	103
Figure 4.12: Overall Crack Pattern for Beam S2-1 (Back Face).....	103
Figure 4.13: Concrete Crushing in Compression Zone for Beam S2-2	104
Figure 4.14: Overall Crack Pattern for Beam S2-2 (Front Face).....	105
Figure 4.15: Overall Crack Pattern for Beam S2-2 (Back Face).....	105
Figure 4.16: Concrete Crushing in Compression Zone for Beam S2-3	106
Figure 4.17: Overall Crack Pattern for Beam S2-3 (Front Face).....	107
Figure 4.18: Overall Crack Pattern for Beam S2-3 (Back Face).....	107
Figure 4.19: Principal Diagonal Crack for Beam S3-1	108
Figure 4.20: Overall Crack Pattern for Beam 3-1 (Front Face).....	109
Figure 4.21: Overall Crack Pattern for Beam 3-1 (Back Face).....	109
Figure 4.22: Principal Diagonal Crack for Beam S3-2	110
Figure 4.23: Overall Crack Pattern for Beam 3-2 (Front Face).....	111
Figure 4.24: Overall Crack Pattern for Beam 3-2 (Back Face).....	111
Figure 4.25: Principal Diagonal Crack for Beam S3-3	112
Figure 4.26: Overall Crack Pattern for Beam 3-3 (Front Face).....	113
Figure 4.27: Overall Crack Pattern for Beam 3-3 (Back Face).....	113
Figure 4.28: Load versus Mid-span Deflection for Beam S1-1	115
Figure 4.29: Load versus Mid-span Deflection for Beam S1-2	115
Figure 4.30: Load versus Mid-span Deflection for Beam S1-3	116
Figure 4.31: Load versus Mid-span Deflection for Beam S2-1	116
Figure 4.32: Load versus Mid-span Deflection for Beam S2-2	117

Figure 4.33: Load versus Mid-span Deflection for Beam S2-3	117
Figure 4.34: Load versus Mid-span Deflection for Beam S3-1	118
Figure 4.35: Load versus Mid-span Deflection for Beam S3-2	118
Figure 4.36: Load versus Mid-span Deflection for Beam S3-3	119
Figure 4.37: Effect of Longitudinal Tensile Reinforcement Ratio on the Shear Capacity of Beams for Shear Reinforcement Ratio of 0.10%.....	122
Figure 4.38: Effect of Longitudinal Tensile Reinforcement Ratio on the Shear Capacity of Beams for Shear Reinforcement Ratio of 0.13%.....	123
Figure 4.39: Effect of Longitudinal Tensile Reinforcement Ratio on the Shear Capacity of Beams for Shear Reinforcement Ratio of 0.17%.....	123
Figure 5.1: Input Dialog of ShearCalculator Program for Beam S1-1	126
Figure 5.2: $V-\gamma_t$ curve for Beam S1-1	131
Figure 5.3: A Typical <i>FormWorks</i> Application Window.....	132
Figure 5.4: Job Control Property Page Display.....	133
Figure 5.5: Models Property Page Display.....	134
Figure 5.6: The Structure Information Dialog.....	135
Figure 5.7: Reinforced Concrete Materials Property Dialog Box.....	136
Figure 5.8: Reinforcement Material Properties Dialog Box	136
Figure 5.9: Load Information Dialog Box.....	137
Figure 5.10: Typical Finite Element Meshes For Beam S3-1	138
Figure 5.11: <i>VecTor2</i> Analysis Dialog.....	139
Figure 5.12: Crack Pattern of Beam S3-1 at Failure	140
Figure 6.1: Comparison of Crack Patterns for Beam S1-1.....	150
Figure 6.2: Comparison of Crack Patterns for Beam S1-2.....	151
Figure 6.3: Comparison of Crack Patterns for Beam S1-3.....	152
Figure 6.4: Comparison of Crack Patterns for Beam S2-1.....	153
Figure 6.5: Comparison of Crack Patterns for Beam S2-2.....	154
Figure 6.6: Comparison of Crack Patterns for Beam S2-3.....	155
Figure 6.7: Comparison of Crack Patterns for Beam S3-1.....	156
Figure 6.8: Comparison of Crack Patterns for Beam S3-2.....	157
Figure 6.9: Comparison of Crack Patterns for Beam S3-3.....	158
Figure 7.1: Geometry and Reinforcement Arrangement.....	166
for Beams N-D-1.0 and H-D-1.0.....	166

Figure 7.2: Geometry and Reinforcement Arrangement	167
for Beams N-D-1.5 and H-D-1.5	167
Figure 7.3: Geometry and Reinforcement Arrangement for	168
Beams N-D-2.2 and H-D-2.2	168
Figure 7.4: Geometry and Reinforcement Arrangement for	169
Beams N-L-12.5 and H-L-12.5	169
Figure 7.5: Geometry and Reinforcement Arrangement for	170
Beams N-L-18.8 and H-L-18.8	170
Figure 7.6: Geometry and Reinforcement Arrangement for	171
Beams N-L-30.0 and H-L-30.0	171
Figure 7.7: Particle Size Distributions of Fly Ash	173
Figure 7.8: Typical Test Set-Up for Modulus of Elasticity of Concrete	178
and Poisson Ratio	178
Figure 7.9: Loading Arrangement for Beam Tests	180
Figure 7.10: Typical Test Set-Up for Beam Tests	181
Figure 8.1: Crack Pattern of Beam N-D-1.0 over the Splice Region After Failure (Side Face)	184
Figure 8.2: Crack Pattern of Beam N-D-1.0 over the Splice Region After Failure (Bottom Face)	184
Figure 8.3 : Crack Pattern of Normal Strength Geopolymer Concrete Beams over the Splice Region After Failure (D-Series)	186
Figure 8.4 : Crack Pattern of High Strength Geopolymer Concrete Beams over the Splice Region After Failure (D-Series)	187
Figure 8.5 : Crack Pattern of Normal Strength Geopolymer Concrete Beams over the Splice Region After Failure (L-Series)	188
Figure 8.6 : Crack Pattern of High Strength Geopolymer Concrete Beams over the Splice Region After Failure (L-Series)	189
Figure 8.7 : Comparison of Crack Width In Splice Region for	190
Beam N-D-1.0 and Beam H-D-1.0	190
Figure 8.8: Surface Condition of Reinforcing Bars After Failure	191
(Normal Strength Concrete – Beam N-L-30)	191
Figure 8.9: Rib Patterns of Bar on Geopolymer Concrete	192
(Normal Strength Concrete – Beam N-L-30)	192
Figure 8.10: Effect of C/d_b on Bond Stress	198

Figure 8.11: Effect of L_s/d_b on Bond Stress	199
Figure 8.12: Effect of Concrete Compressive Strength on Bond Stress (D-Series)	200
Figure 8.13: Effect of Concrete Compressive Strength on Bond Stress (L-Series)	201
Figure 8.14: Load versus Mid-span Deflection for Beams N-D-1.0 and H-D-1.0	202
Figure 8.15: Load versus Mid-span Deflection for Beams N-D-1.5 and H-D-1.5	203
Figure 8.16: Load versus Mid-span Deflection for Beams N-D-2.2 and H-D-2.2	203
Figure 8.17: Load versus Mid-span Deflection for Beams N-L-12.5 and H-L-12.5	204
Figure 8.18: Load versus Mid-span Deflection for Beams N-L-18.8 and H-L-18.8	204
Figure 8.19: Load versus Mid-span Deflection for Beams N-L-30.0 and H-L-30.0	205
Figure B1.1: Concrete Compressive Strength Development for Trial Mix 1 (GP1)	252
Figure B2.1: Concrete Compressive Strength Development for Trial Mix 1 (GP2)	254
Figure F.1: Crack Pattern for Beam N-D-1.0 and H-D-1.0 (Side View)	351
Figure F.2: Crack Pattern for Beam N-D-1.5 and H-D-1.5 (Side View)	352
Figure F.3: Crack Pattern for Beam N-D-2.2 and H-D-2.2 (Side View)	353
Figure F.4: Crack Pattern for Beam N-L-12.5 and H-L-12.5 (Side View)	354
Figure F.5: Crack Pattern for Beam N-L-18.8 and H-L-18.8 (Side View)	355
Figure F.6: Crack Pattern for Beam N-L-30.0 and H-L-30.0 (Side View)	356
Figure F.7: Crack Pattern for Beam N-D-1.0 and H-D-1.0 (Bottom View)	357
Figure F.8: Crack Pattern for Beam N-D-1.5 and H-D-1.5 (Bottom View)	358
Figure F.9: Crack Pattern for Beam N-D-2.2 and H-D-2.2 (Bottom View)	359
Figure F.10: Crack Pattern for Beam N-L-12.5 and H-L-12.5 (Bottom View)	360
Figure F.11: Crack Pattern for Beam N-L-18.8 and H-L-18.8 (Bottom View)	361
Figure F.12: Crack Pattern for Beam N-L-30.0 and H-L-30.0 (Bottom View)	362
Figure G.1: Steel-Geopolymer Concrete Interface for Beam N-D-1.0 and H-D-1.0	364
Figure G.2: Steel-Geopolymer Concrete Interface for Beam N-D-1.5 and H-D-1.5	365
Figure G.3: Steel-Geopolymer Concrete Interface for Beam N-D-2.2 and H-D-2.2	366

Figure G.4: Steel-Geopolymer Concrete Interface for Beam N-L-12.5 and H-L-12.5	
.....	367
Figure G.5: Steel-Geopolymer Concrete Interface for Beam N-L-18.8 and H-L-18.8	
.....	368
Figure G.6: Steel-Geopolymer Concrete Interface for Beam N-L-30.0 and H-L-30.0	
.....	369

LIST OF TABLES

Table 2.1: Applications of Geopolymers based on Si:Al ratio (Davidovits, 1999)	8
Table 3.1: Details of the Test Beams for Shear Study	71
Table 3.2: SSD Moisture Conditions for Aggregates.....	77
Table 3.3: Grading Combination of Aggregates	78
Table 3.4: Chemical Composition of Fly Ash (mass %).....	79
Table 3.5: Mixture Proportions of Geopolymer Concrete (GP1).....	81
Table 3.6: Longitudinal Reinforcement Properties	82
Table 3.7: Transverse Reinforcement Properties	82
Table 3.8: Concrete Properties of Geopolymer Concrete	88
Table 4.1: Effect of Beam Slenderness on Mode of Failure (Nawy, 2005)	94
Table 4.2: Test Results for Shear Cracking Load.....	120
Table 4.3: Test Results for Shear Strength, V_{uTEST}	121
Table 6.1: Correlation of Test and Predicted Shear Cracking Load.....	143
Table 6.2: Summary of Predicted Shear Strength using Analytical Models.....	144
Table 6.3: Summary of Test-to-Predicted Ratio using Analytical Models	145
Table 6.4: Summary of Predicted Shear Strength using Code Provisions	147
Table 6.5: Summary of Test-to-Predicted Ratio using Code Provisions.....	148
Table 6.6: Comparison of Shear Strength of Geopolymer Concrete and Portland Cement Concrete Beams using Analytical Models	160
Table 7.1: Details of the Test Beams for Bond Study	165
Table 7.2: Chemical composition of fly ash (mass %).....	172
Table 7.3: Mixture Proportions of Geopolymer Concrete.....	174
Table 7.4: Longitudinal Reinforcement Properties	175
Table 7.5: Transverse Reinforcement Properties	175
Table 7.6: Concrete Properties	177
Table 7.7: Modulus of Elasticity and Poisson's Ratio	179
Table 8.1: Actual Details of Test Beams.....	193
Table 8.2: Failure Loads and Moments	194
Table 8.3: Summary of Test Results for Steel Stress and Average Bond Stress.....	196
Table 9.1: Summary of Predicted Bond Strength using Analytical Models	207
Table 9.2: Summary of Test-to-Predicted Ratio using Analytical Models	208

Table 9.3: Predicted Bond Strength from Canbay and Frosch Model using Actual Tensile Strength Results	210
Table 9.4: Bond Strength: Summary of Results by Code Provisions.....	212
Table 9.5: Summary of Test-to-Predicted Ratio for Bond Strength of Portland Cement Concrete Beams	214
Table 9.6: Comparison of Test/Prediction Ratio between Geopolymer Concrete and Portland Cement Concrete Beams using Same Prediction Methods.....	215
Table B1.1: Cylinder Compressive Strength Data for Trial Mix 1 (GP1)	252
Table B2.1: Cylinder Compressive Strength Data for Trial Mix 1 (GP2)	254
Table C.1: Test Data for Beam S1-1	256
Table C.2: Test Data for Beam S1-2	257
Table C.3: Test Data for Beam S1-3	259
Table C.4: Test Data for Beam S2-1	260
Table C.5: Test Data for Beam S2-2	261
Table C.6: Test Data for Beam S2-3	262
Table C.7: Test Data for Beam S3-1	263
Table C.8: Test Data for Beam S3-2	264
Table C.9: Test Data for Beam S3-3	265
Table H.1: Test Data for Beam N-D-1.0	371
Table H.2: Test Data for Beam N-D-1.5	372
Table H.3: Test Data for Beam N-D-2.2	373
Table H.4: Test Data for Beam H-D-1.0	374
Table H.5: Test Data for Beam H-D-1.5	375
Table H.6: Test Data for Beam H-D-2.2	376
Table H.7: Test Data for Beam N-L-12.5.....	377
Table H.8: Test Data for Beam N-L-18.8.....	378
Table H.9: Test Data for Beam N-L-30.0.....	379
Table H.10: Test Data for Beam H-L-12.5.....	380
Table H.11: Test Data for Beam H-L-18.8.....	381
Table H.12: Test Data for Beam H-L-30.0.....	382

NOTATION

a	= shear span
A_b	= cross-sectional area of a bar being developed
A_g	= gross concrete area of the beam cross section
A_{sl}	= total cross-sectional area of longitudinal tensile steel
A_{sIM}	= cross-sectional area of longitudinal tensile steel attributed to flexure
A_{sIV}	= cross-sectional area of longitudinal tensile steel attributed to shear
A_{sv}	= cross-sectional area of shear reinforcement
$A_{sv.max}$	= cross-sectional area of maximum shear reinforcement
$A_{sv.min}$	= cross-sectional area of minimum shear reinforcement
b	= member width
b_v	= effective web width
C	= minimum cover
c	= smaller of the distance from the centre of the bar to the nearest concrete surface and one half of the centre-to-centre spacing of bars being developed (ACI318)
c_b	= bottom cover
c_d	= the smaller of the concrete cover to the deformed bar or half the clear distance to the next parallel bar provided at least 3 transverse bars are located within the development length (AS3600)
c_{max}	= maximum (c_b , c_s)
c_{med}	= median (c_b , c_{so} , $c_{si} + d_b/2$)
c_{min}	= minimum (c_b , c_s)
c_{min}	= minimum (c_b , c_{so} , $c_{si} + d_b/2$) (Esfahani and Rangan)
c_s	= $\min(c_{si}+0.25, c_{so})$ (in)

C_s	= the concrete strut
c_{si}	= half of the clear spacing between bars
c_{so}	= side cover
d	= effective depth
d_b	= bar diameter
d_o	= distance from the extreme compression fibre to the centroid of the outermost layer of longitudinal tensile reinforcement
$[D_c]$	= concrete stiffness matrices
$[D_s]_i$	= reinforcement stiffness matrices
E_c	= modulus of elasticity of concrete
E_s	= modulus of elasticity of steel
E_{sh}	= strain hardening modulus
f'_c	= concrete compressive strength
f'_{ct}	= tensile strength of concrete
F_b	= bearing force developed at a rib
f_b	= steel stress (Canbay and Frosch)
f_{c1}	= principal tensile stress
f_{c1}^a	= concrete post-cracking stress associated with tensile softening
f_{c1}^b	= concrete tension stiffening stresses
f_{c2}	= principal concrete compressive stress
f_{cc}	= concrete cube strength
f_{cr}	= concrete cracking stress
f_{cx}	= concrete stress in x-direction
f_{cy}	= concrete stress in y-direction
F_l	= concrete tensile force in the longitudinal direction

F_{long}	= longitudinal bar force
f_p	= peak stress for cracked concrete in compression
f_s	= stress in steel reinforcement (Vecchio, 2000)
f_{scri}	= local reinforcement stress
f_{si}	= average stress for the i-th reinforcement component
f_{sl}	= stresses in longitudinal reinforcement (Kong and Rangan, 1998)
f_{sty}	= yield stresses of the longitudinal steel reinforcement
$F_{splitting}$	= force to cause splitting
f_{st}	= stresses in transverse reinforcement (Kong and Rangan, 1998)
f_{svy}	= yield stress of shear reinforcement
f_{sy}	= yield stress of steel being develop or spliced
F_t	= concrete tensile force in the transverse direction
$f_{t,v}$	= stress in the compression field induced by vertical truss mechanism
f_y	= yield strength of steel reinforcement (Vecchio, 2000)
f_{yi}	= yield stress for the i-th reinforcement component
G_f	= fracture energy parameter
h_a	= twice the cover depth of the longitudinal reinforcement
jd	= lever arm
k_a	= transition factor for arch action
K_{tr}	= transverse reinforcement index
l_b	= dimension of the loading plate in the axial direction of the member
L_d	= development length
L_r	= characteristic length
L_s	= splice length
$L_{st,t}$	= development length in tension (AS3600)
$L_{st,tb}$	= basic development length (AS3600)

M	= bending moment
M_{max}	= maximum bending moment
n	= ratio of modulus of elasticity of steel to that of concrete
n_b	= numbers of bars being spliced
N	= axial force in a beam (Kong and Rangan, 1998)
P_{max}	= failure load
R_a	= reduction factor for arch action
R_v	= reduction factor for truss mechanism
s	= spacing of stirrups
s_a	= average crack spacing (Vecchio, 2000)
s_{ax}	= average cracking spacing in the x-direction
s_{ay}	= average cracking spacing in the y-direction
S_{cr}	= average cracking spacing (von Ramin, 2004)
T_s	= tie formed by the longitudinal reinforcement
u	= average bond stress
u_c	= average bond stress (Esfahani and Rangan, 1998)
u_m	= bond stress of splices in beam (Esfahani and Rangan, 1998)
V	= shear force
V_a	= shear capacity of arch mechanism
V_c	= concrete contribution to shear
V_{cr}	= shear cracking load
V_{cz}	= shear capacity from un-cracked compression zone
V_f	= shear capacity from friction
V_n	= nominal shear strength
V_s	= steel contribution to shear
V_t	= shear capacity of truss mechanism

- V_u = shear strength of beam
- w = average crack width
- w_a = width of strut
- Δw_u = limiting crack width
- α_i = angle of orientation of the reinforcement
- β_d = reduction factor for cracked concrete
- β_s = reduction factor for effective concrete compressive strength
- β_1 = factor to account for effect of depth (AS3600)
- β_2 = factor to account for effect of axial force (AS3600)
- β_3 = factor to account for the effect of a concentrated load near a support
(AS3600)
- δ_s = slip along the crack surface
- $[\varepsilon^s]$ = slip strain
- $[\varepsilon_c]$ = net strains in concrete
- $[\varepsilon_c^\circ]$ = elastic strain offset
- $[\varepsilon_c^p]$ = plastic offset
- ε_{cr} = concrete cracking strain
- ε_{cx} = average concrete strain in the x-direction
- ε_{c1} = principal tensile strain
- ε_{c2} = principal compressive strain
- ε_d = average principal strains in the element in d - directions and is positive for
tension
- ε_l = average strains in the element in l - directions and is positive for tension

- ε_o = strain corresponding to the peak concrete compressive stress
- ε_p = strain corresponding to peak stress for cracked concrete in compression
- ε_r = average principal strains in the element in r - directions and is positive for tension
- ε_s = strain in steel reinforcement
- $[\varepsilon_s]_i$ = net strains in reinforcement
- $[\varepsilon_{s_i}^o]$ = initial prestrain in the reinforcement
- ε_{scr_i} = local reinforcement strains
- ε_{sh} = strain at start of strain hardening
- ε_t = average strains in the element in t - directions and is positive for tension
- ε_{ts} = terminal strain
- ε_u = ultimate strain
- ε_x^s = slip strain in the x-direction
- ε_{xy} = average concrete strain in the y-direction
- ε_y = yield strain of steel reinforcement
- ε_y^s = slip strain in the y-direction
- $\Delta\varepsilon_{lcr}$ = local incremental strain
- ϕ = angle of inclination of the compression field with respect to the longitudinal reinforcement (von Ramin, 2004)
- γ_{cxy} = concrete shear strain
- γ_{lt} = average shear strain in the element in the l - and t -coordinate system
- γ_s = average slip strain

- γ_{xy}^s = shear slip strain
- v_{ci} = shear stresses along the crack surfaces
- v_{cxy} = concrete normal shear stress
- v_{lt} = average shear stress in the l and t -coordinate system and is taken as
- $$= \frac{V}{b_v(0.9d_o)}$$
- θ = angle of inclination of the concrete compression strut
- θ_a = angle of inclination of the strut, approximately calculated from shear span to depth ratio (von Ramin, 2004)
- θ_{n_i} = the difference between the angle of orientation of the reinforcement α_i and the normal to the crack surface, θ_N
- θ_N = normal to the crack surface
- θ_ε = apparent principal strain
- θ_σ = inclination of the principal stress
- ρ_i = reinforcement ratio
- ρ_l = smeared longitudinal tensile reinforcement ratio attributed to shear
- ρ_{sl} = longitudinal tensile reinforcement ratio
- ρ_{sv} = shear reinforcement ratio
- ρ_t = smeared transverse reinforcement ratio
- σ_d = principal stresses in the d - directions respectively and is positive for tension
- σ_l = normal stress in l - directions respectively and is positive for tension
- σ_r = principal stresses in the r - directions respectively and are positive for tension

σ_t = normal stress in t -directions respectively and is positive for tension

τ_{fu} = limiting friction stress at the crack surface

ζ = stress and strain softening factor (Kong and Rangan, 1998)

CHAPTER 1

INTRODUCTION

1.1 Background

Concrete is second only to water as the most consumed material on earth. Portland cement has been used as a binder to combine the coarse and fine aggregates to make concrete since the 19th century. The demand for concrete is increasing with the growing demands of infrastructure, energy and resources. However, there are some issues associated with cement production, for not only it is one of the most energy-intensive materials used in construction, but it is also responsible for some carbon dioxide (CO₂) emissions, the gas most implicated in global warming. Several efforts are in progress to address the global warming issue. These include the utilisation of supplementary materials such as fly ash, granulated blast furnace slag, silica fume and rice-husk ash, and also the development of alternative binders to Portland cement.

In view of sustainable development in the construction industry, geopolymer technology shows considerable promise as an alternative binder to Portland cement. Geopolymers are emerging materials which, since being proposed by Davidovits in 1979, have been used in applications ranging from waste management to the building industry. Their difference in chemical process and matrix formation means geopolymers have technical performance advantages over conventional cement binders, such as early compressive strength gain, higher acid and fire resistance, low alkali-aggregate expansion and sulphate and corrosion resistance (Lee and van Deventer, 2002; Davidovits, 1991; García-Lodeiro et al., 2008; Bakharev 2005a and 2005c). In addition, with correct mix design and formation development, fly ash-based geopolymer concrete can exhibit superior chemical and mechanical properties to those of Portland cement concrete (Duxson et al., 2007b). All of these benefits make geopolymers promising construction materials.

Apart from these technical attributes, there are numerous environmental benefits associated with waste utilisation in geopolymer technology applications. Over the past two decades, it has been found that widely available industry by-products such as fly ash can be used as feedstock for geopolymer materials. In terms of global warming, using geopolymers as binder in concrete has the potential to reduce CO₂ emission (Gartner, 2004).

Although numerous studies of geopolymers have been carried out worldwide, the majority have focused on material characterisation, the enhancement of physical and chemical properties of the material, the effects of source material and engineering properties (Duxson et al., 2007b). Past studies on the structural behaviour of reinforced fly ash-based geopolymer concrete members are scarce. Studies on structural applications of fly ash-based geopolymer concrete are important, not only because of the difference in terms of chemical reaction and matrix formation compared to Portland cement concrete, but also because of the need to examine the suitability of current code provisions and theories for Portland cement concrete to be used for geopolymer concrete.

Design for both shear and bond are important in the design of reinforced concrete structures. The behaviour of reinforced concrete beams at failure in shear is distinctly different from their behaviour in flexure. As shear failures are brittle in nature, it is vital to provide adequate design for shear resistance in concrete members. Apart from this, the lap splice of reinforcing bars is one of the practical aspects of bond between concrete and reinforcing bars. Given their inevitable use in most reinforced concrete structures, accurate prediction of splice length is important as the performance of reinforced concrete structures depends on adequate bond between concrete and reinforcing steel.

Currently, the steel reinforcing bars available in the market have been designed and developed for use with Portland cement concrete. Furthermore, all the analytical models and code provisions for both shear and bond are based on test results using Portland cement concrete. The present research is therefore dedicated to the study of

shear behaviour of geopolymer concrete beams and the bond performance of lap splices in geopolymer concrete beams.

1.2 Research Objectives

The aims of this research program are:

1. to investigate the shear behaviour of reinforced geopolymer concrete beams.
2. to investigate the bond behaviour of tensile lap splices in geopolymer concrete beams.
3. to compare the experimental results with prediction methods currently used for reinforced Portland cement concrete structural members, and to evaluate the suitability of these methods for geopolymer concrete.

1.3 Scope of Work

The scope of work of this research is as below:

1. Produce geopolymer concrete mixtures with target compressive strength for the manufacture of all the beams.
2. Manufacture and test nine reinforced fly ash-based geopolymer concrete beams under monotonically increasing load with longitudinal tensile reinforcement ratio as test variable.
3. Manufacture and test twelve tensile lap-spliced geopolymer concrete beams under monotonically increasing load with concrete cover, bar diameter, splice length and concrete compressive strength as test variables.
4. Perform calculation on shear strength of geopolymer concrete beams using current code provisions and analytical models available for Portland cement concrete members.

5. Perform calculation of bond strength of lap splices in geopolymer concrete beams using current methods available for Portland cement concrete members, including code provisions and analytical models.
6. Study the correlation of the test and calculated results.

1.4 Organisation of Thesis

This thesis comprises ten chapters.

Chapter 2 presents a brief overview of geopolymer technology, particularly of fly ash-based geopolymers and geopolymer concrete. A review of current approaches used to predict the shear strength of reinforced concrete beams and the bond strength of lap splices in beams is also included.

Section 1 consists of Chapters 3, 4, 5 and 6, and describes the works conducted on the study of shear behaviour of geopolymer concrete beams. Chapter 3 describes the experimental work including the specimen details, materials, manufacturing and testing procedures of the test specimens. Chapter 4 presents the test results for beams failing in shear, including their behaviour and strength. Chapter 5 describes the analytical modelling of the beams and Chapter 6 consists of the correlation of test results with predictions from the code provisions and theoretical models outlined in Chapter 2.

Section 2 consists of Chapters 7, 8 and 9, and describes the work conducted on the study of the bond behaviour of geopolymer concrete beams. Chapter 7 describes the test program for the twelve lap-spliced geopolymer concrete beams, including the specimen details, materials, manufacturing and testing procedures. Chapter 8 presents the results of the experimental investigation for the beams, including their behaviour and strength. Chapter 9 consists of the correlation of test results with predictions from the code provisions and theoretical models outlined in Chapter 2.

Chapter 10 outlines the conclusions of this study and presents recommendations for future research.

The thesis ends with a list of references and a number of appendices detailing the experimental data and other supporting results.

CHAPTER 2

LITERATURE REVIEW

This chapter presents a review of recent research on geopolymers and geopolymer concrete, with an emphasis on low calcium fly ash-based geopolymer paste and concrete. A review of current approaches and models available to predict shear strength and bond strength of Portland cement concrete members is also included. These approaches will be used to predict the shear and bond strength of geopolymer concrete beams in this study.

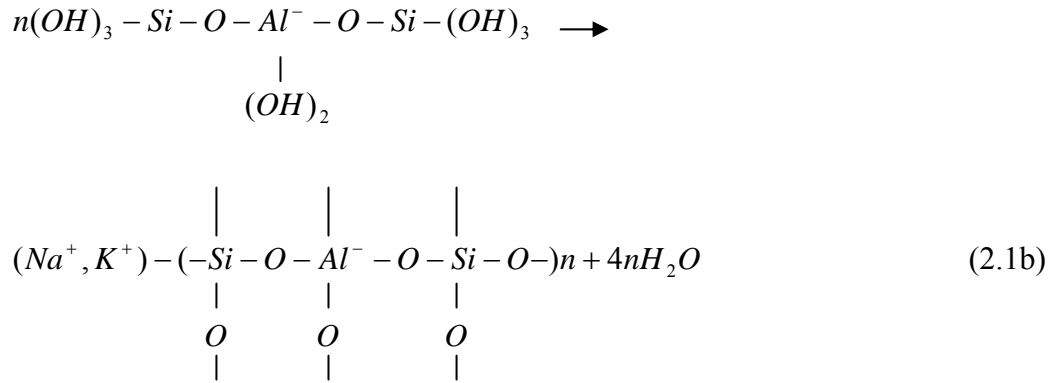
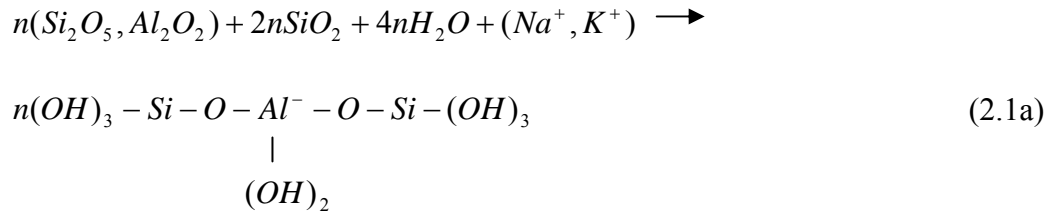
2.1 Geopolymers

2.1.1 General

The term geopolymer was first introduced by Davidovits in 1979 to name the tri-dimensional alumino-silicates material, which is a binder produced from the reaction of a source material or feedstock rich in silicon (Si) and aluminium (Al) with a concentrated alkaline solution.

The source materials may be natural minerals, such as kaolinite, calcined kaolinite (metakaolin) and clays (Davidovits, 1991; Barbosa et al., 2000; Xu and Van Deventer, 2002). Alternatively, industry waste products such as fly ash, slag, red mud, rice-husk ash and silica fume may be used as feedstock for the synthesis of geopolymers. The alkaline liquids are concentrated aqueous alkali hydroxide or silicate solution, with soluble alkali metals, usually Sodium- (Na) or Potassium- (K) based (Davidovits, 1991). High alkaline liquids are used to induce the silicon and aluminium atoms in the source materials to dissolve and form the geopolymeric binder.

The geopolymerisation process involves a substantially fast chemical reaction between various alumino-silicate oxides and silicates under alkaline conditions, yielding polymeric Si-O-Al-O bonds (Davidovits 1991). The schematic formation of geopolymer material may be described by Equations 2.1a and 2.1b (Davidovits, 1999).



It can be seen from the last term in Equation 2.1b that water is released from the geopolymer matrix during the chemical reaction. It is important to note the role of water in the formation of geopolymers. This water, expelled from the geopolymer matrix during the curing and further drying periods, leaves discontinuous nano-pores in the matrix which are beneficial to the performance of geopolymers. It provides the workability of the mixture during handling and plays no role in the chemical reaction that takes place, which is in contrast to the chemical reaction of water in a Portland cement mixture during the hydration process (Hardjito and Rangan, 2005; Rangan, 2008b).

Geopolymers are members of the inorganic polymers. Geopolymers comprise mixtures of amorphous to semi-crystalline structure and crystalline Al-Si particles (Davidovits, 1991). Amorphous geopolymers are obtained at condensation temperatures ranging from 20°C to 90°C, whereas crystalline ones are formed in autoclave at 150°C to 200°C, and resemble those of zeolite (Andini et al., 2008).

According to Davidovits (1999), the atomic ratio of Si:Al in the poly(sialate) structure determines the properties and applications of geopolymers. A low ratio of Si:Al (1:1; 2:1;

3:1) initiates a three-dimensional network that is very rigid. A high ratio, Si:Al higher than 15, gives a polymeric character to the geopolymeric material. It is also found that different Si-Al ratios result in different properties and applications, as listed in Table 2.1.

Table 2.1: Applications of Geopolymers based on Si:Al ratio (Davidovits, 1999)

Si-Al Ratio	Characteristics/ Applications
1 : 1	Rigid, poor adhesion: bricks and ceramics
2 : 1	Cements and concretes, waste encapsulation
3 : 1	Foundry moulds, heat resistant fibre reinforced composites
> 3 : 1	Sealants and adhesives (resin-like)
> 20 : 1 and < 35:1	Fire and heat resistant carbon fibre mat composites

Numerous studies have been conducted to investigate the properties, performance and applications of geopolymers over the past two decades. It has been proven that calcined materials, such as slag, fly ash and metakaolin, which are mostly amorphous, usually display a higher reactivity during geopolymerisation than non-calcined materials (Palomo et al., 1999; Xu and Deventer, 2000). For fly ash-based geopolymers, mechanical strength increases, due to the formation of an Al-rich alumino-silicate gel during the first stage of alkaline activation of fly ash particles, and may further increase as a result of the Si enrichment of the material (Fernández-Jiménez et al., 2006). It has also been found that geopolymers derived from metakaolin may require too much water due to porosity increase and therefore become too soft for construction application, although metakaolin remains important in the production of geopolymers for applications as adhesives, coatings and hydroceramics. Also, the microstructure and properties of geopolymers depend strongly on the nature of the initial source materials (Duxson et al., 2007a). As a result, it is important to understand the reactivity and chemistry of raw materials in order to optimise both cost and technical performance for certain applications.

2.1.2 Fly Ash-Based Geopolymers

Fly ash is a by-product from the combustion of coal at coal-fired power stations. It is the most available supplementary cementing material worldwide, and is commonly used as a supplementary material in concrete. Most of the fly ash available globally is low calcium (ASTM Class F) fly ash from the burning of bituminous and anthracite coal, whereas high calcium (ASTM Class C) fly ash is formed by burning lignite and subbituminous coal (Manz, 1998). Fly ash-based geopolymerisation was intensively studied in the past decade, especially on the development of different characterisation techniques, the effects of different chemical additives and/or contaminants and the influence of curing conditions such as humidity, time and temperature on compressive strength (Duxson et al., 2007b).

The influence of curing temperature and curing time on the compressive strength of fly ash based-geopolymer paste has been studied by Palomo et al. (1999), Swanepoel and Strydom (2002) and van Jaarsveld et al. (2002). It has been found that both curing temperature and curing time influence compressive strength. Compressive strength up to 60MPa is obtained when cured at 85°C for five hours. In addition, the utilisation of sodium hydroxide (NaOH) combined with sodium silicate solutions ($\text{Na}_2\text{O} \cdot \text{SiO}_2$) results in the highest strength for the paste (Palomo et al., 1999). Swanepoel and Strydom (2002) report that curing time and curing temperature are found to affect compressive strength, with the optimum condition being curing at 60°C for a period of 48 hours. Van Jaarsveld et al. (2002) confirm the importance of curing at an elevated temperature for fly ash-based geopolymer materials and observe that curing for a longer period of time at an elevated temperature weakens the microstructure and thus reduces the compressive strength of fly ash-based geopolymer materials.

Bakharev (2005a) investigated the influence of elevated temperature curing on phase composition, microstructure and strength development in ASTM Class F fly ash-based geopolymer materials with sodium silicate and sodium hydroxide solutions as alkaline activators. He finds that long pre-curing at room temperature is beneficial for strength development as it allows for shortening the time of heat treatment to achieve high

strength. Samples with sodium silicate solution as activator are found to have more strength development in 6 hours of heat curing than 24 hours of heat treatment. An increase in curing temperature causes a decrease of Si/Al ratios in aluminosilicate gel, while long curing at room temperature narrows the range in Si/Al ratios distribution.

Van Jaarsveld et al. (2003) studied the various parameters that affect the final structure and physical properties of fly ash-based geopolymers. They find that the zeta-potential of fly ash particles and calcium content has a vital effect on the setting time and final hardening of the geopolymer. It is also suggested that calcium-containing compounds, such as calcium silicates, calcium aluminates hydrates and calcium-silico-aluminates, which form during the geopolymerisation of fly ash, affect both the setting and workability of the mix and the strength development. The degree of crystallinity (the amorphous nature) of the resultant geopolymer, the CaO content of fly ash and the water/fly ash ratio are found to affect the compressive strength of geopolymers.

The interface between mineral aggregates such as sand and natural rocks, and fly ash-based geopolymers has been studied by Lee and Van Deventer (2004). They find that the presence of soluble silicates in the initial activating solution is effective in improving the interfacial bond strength. A denser binder, as well as stronger aggregate/binder interfaces, is formed by increasing the soluble silicate dosage.

Fernandez-Jimenez, Palomo and Criado (2004) conducted a study on the microstructure development of alkali-activated fly ash cement using microscopic tools to establish a model. They find that electron microscopy is a useful tool in monitoring the microstructural development of the cementitious matrix generated over time. The activation reaction rate, as well as the chemical composition of the reaction products, is found to depend on several factors such as particle size distribution, the mineral composition of fly ash and the type and concentration of fly ash.

Bakharev's (2005b, 2005c) studies on the durability of fly ash-based geopolymers when exposed to a sulfate environment and to 5% solutions of acetic and sulfuric acid find that

high performance geopolymer materials deteriorate with the formation of fissures in an amorphous polymer matrix, while low performance geopolymers deteriorate through the crystallisation of zeolites and the formation of fragile grainy structures. In addition, the type of activator used in specimen preparation and the concentration and type of cation in the sulfate media are found to affect the stability of geopolymer materials when exposed to a sulfate environment. Specimens prepared with sodium hydroxide and cured at an elevated temperature show the best performance in different sulfate solutions. A strength increase of 4% to 12% is found when specimens are immersed in a sulfate solution.

The effect of mechanical activation of fly ash on the structure and properties of geopolymer mortar was studied by Kumar et al. (2005). They conclude that the mechanical activation of fly ash through high energy milling devices, namely attrition and vibratory mills, favours the geopolymerisation process by increasing the reactivity of fly ash. Through the mechanical activation of fly ash, lower temperatures and less time were needed for geopolymerisation, and an improvement in the compressive strength resulted from the formation of a compact microstructure. In addition, Kumar et al. (2007) report that the compressive strength of fly ash-based geopolymer mortar can be tailored over a wide range through the selection of the mechanical activation device and alkali addition.

Studies conducted by Sindhunata et al. (2006) observe that the fly ash-based geopolymer is an amorphous material with nanosize pore characteristics. A well-reacted fly ash-based geopolymer shows a mesoporous structure (3.6 – 50nm) that develops with increasing curing temperature and silicate ratio. However, the kinetics appear to be temperature-controlled only before the material is hardened.

García-Lodeiro et al. (2007) evaluated the performance of low-calcium fly ash-based geopolymer mortars in the context of an alkali-aggregate reaction. It was found that fly ash-based geopolymer binders are less likely to generate expansion by alkali-silica reaction than Portland cement binders. García-Lodeiro et al. suggest that the calcium in the materials plays an essential role in the expansive nature of gels.

Andini et al. (2008) used fly ash as feedstock for the synthesis of geopolymers of the polysialatesiloxo (Si/Al ratio of 2:1) and polysialatedisiloxo (Si/Al ratio of 3:1) classes in different experimental conditions in terms of temperature and time of polycondensation. The physico-structural and mechanical characterisation of the geopolymeric products was calculated through the measurement of several properties, including compressive strength, elasticity modulus, porosity and specific surface area and microscopic observations. It was found that lightweight fly ash-based geopolymer building materials (pre-formed blocks) can be manufactured at room temperature, with the properties of the products depending on the composition of the starting mixture, the nature of alkali metal silicate and the polycondensation conditions (temperature and time).

2.1.3 Low Calcium Fly Ash-Based Geopolymer Concrete

Low calcium fly ash is preferred as a source material in fly ash-based geopolymer concrete, as the presence of calcium in high amounts may interfere with the polymerisation process and result in an alteration of the microstructure (Gourley, 2003; Gourley and Johnson, 2005). Low calcium fly ash has been successfully used as the source material to manufacture geopolymer concrete (Gourley, 2003; Gourley and Johnson, 2005; Hardjito and Rangan, 2005; Song et al., 2005; Wallah and Rangan, 2006; Sumajouw and Rangan, 2006; Fernández-Jiménez et al., 2006; Sofi et al., 2007a; Sofi et al., 2007b; Chang et al., 2007; Sarker et al., 2007).

2.1.3.1 Constituents of Geopolymer Concrete

Hardjito and Rangan (2005) conducted studies on the development of mixture proportions and the manufacturing of geopolymer concrete using low calcium fly ash. The details of the mixture proportions developed are reported elsewhere (Hardjito and Rangan, 2005; Wallah and Rangan, 2006; Sumajouw and Rangan, 2006). The design of geopolymer concrete mixtures is also reported by Rangan (2008b). The constituents of geopolymer concrete from the studies are summarised as follows:

- Coarse and fine aggregates

The coarse and fine aggregates currently used by the concrete industry are found to be suitable for producing geopolymer concrete. As in the case of Portland cement concrete, coarse and fine aggregates occupy about 75% to 80% of the mass of geopolymer concrete. The aggregates are prepared in saturated-surface dry (SSD) condition, which means that the aggregates, both coarse and fine, are neither too dry to absorb water from the mixture nor too wet to preclude adding water to the mixture. This is important as the water in the mixture plays an important role, affecting the compressive strength and workability of the mixture.

- Low calcium fly ash

The silicon and aluminium oxides in low-calcium fly ash constitute about 80% by mass, with the atomic ratio of Si-to-Al of about 2. The chemical composition and particle size distribution of the fly ash must be established prior to use. For low calcium fly ash, the calcium oxide content is less than 5% by mass. Iron oxide content ranges from 10 – 20 % by mass. The carbon content of the fly ash is less than 2% by mass as indicated by the loss on ignition (LOI) value.

- Alkaline liquid

The alkaline liquid, which is a combination of sodium silicate solution and sodium hydroxide solution, reacts with the silicon and aluminium in the fly ash to form the paste which binds the loose coarse and fine aggregates, to produce the geopolymer concrete. The sodium silicate solution is commercially available in different grades, with different weight ratios of silica to alkali (SiO_2 to Na_2O) ranging from 1.60 to 3.25 for different application needs. The sodium silicate solution (grade A-53 in Western Australia, commonly known as D-grade in the eastern states of Australia) with a weight ratio of SiO_2 to Na_2O of 2, is recommended. The sodium hydroxide (NaOH) solution can be made by dissolving NaOH solids (pellet or flake form) in water. The amount of NaOH solids in a solution can vary depending on the concentration of solution needed, which is expressed in terms of Molarity, M. The concentration of the solution is in the range of 8 Molar to 16 Molar.

- High range water reducer and extra water

High range water reducer superplasticiser available commercially for Portland cement concrete and any extra water may be added to the mixture to improve the workability of the mix. The high range water reducer superplasticiser used is a naphthalene sulphonate superplasticiser.

2.1.3.2 Manufacturing of Geopolymer Concrete – Mixing, Casting and Curing

The manufacture of geopolymer concrete can be carried out using conventional techniques for manufacturing Portland cement concrete. For this study, the fly ash, coarse and fine aggregates, are first mixed in a dry state in the laboratory pan mixer for about three minutes. At the end of this mixing, the alkaline liquid together with the superplasticiser and the extra water are combined and added into the dry mixture. The mixing continues for another four minutes. The fresh concrete is cohesive; the workability is measured by using the conventional slump test. The fresh geopolymer concrete is easily handled for up to 120 minutes without any sign of setting and without any degradation in the compressive strength. The fresh concrete is cast and compacted using methods adopted for Portland cement concrete as reported by Hardjito and Rangan (2005), Wallah and Rangan (2006) and Sumajouw and Rangan (2006).

Heat-curing of fly ash-based geopolymer concrete is recommended and can be achieved by either steam-curing or dry-curing. Heat curing assists the chemical reaction that occurs in the geopolymer binder (Rangan, 2008a). It is found that both curing time and curing temperature influence the compressive strength of geopolymer concrete. Curing at 60°C for 24 hours is found to be sufficient to achieve the required compressive strength. Higher curing temperature and longer curing time improve the polymerisation process and result in higher compressive strength (Hardjito and Rangan, 2005). Tests by Hardjito and Rangan (2005) show that a delay in the start of heat curing of up to five days increases the compressive strength of geopolymer concrete.

2.1.3.3 The Effect of Salient Parameters on the Properties of Geopolymer Concrete

The effect of various salient parameters that influence the compressive strength and workability of geopolymer concrete has been investigated by Hardjito and Rangan (2005). Some significant results of their findings are summarised below:

1. Higher compressive strength can be achieved by
 - higher concentration (in terms of Molar) of sodium hydroxide solution
 - higher ratio of sodium silicate to sodium hydroxide by mass
 - longer curing time in the range of 4 to 96 hours (however, the increase in strength after 48 hours is not significant)
 - increasing the curing temperature in the range of 30°C to 90°C
 - having a Rest Period, which is defined by the delay at the start of heat curing as mentioned earlier
2. As the H₂O-to-Na₂O molar ratio increases, the compressive strength of geopolymer concrete decreases.
3. The workability of fresh geopolymer concrete can be improved by the addition of naphthalene-based super plasticiser for up to approximately 4% of the fly ash by mass; however, a slight degradation of compressive strength is observed when the super plasticiser dosage is greater than 2%.
4. The slump value of fresh geopolymer concrete increases as the water content of the mixture increases.

From tests performed to study the effect of water-to-geopolymer solids ratio by mass on compressive strength and workability, it was observed that compressive strength of geopolymer concrete decreases as the water-to-geopolymer solids ratio by mass increases. This trend is analogous to the well-known effect of the water-to-cement ratio on the compressive strength of Portland cement concrete. On the other hand, as the water-to-geopolymer solids ratio by mass increases, workability increases (Hardjito and Rangan, 2005).

2.1.3.4 Engineering Properties of Geopolymer Concrete

The engineering properties of geopolymer concrete, including compressive strength, indirect tensile strength, modulus of elasticity and Poisson's ratio have been reported by Hardjito and Rangan (2005) and Sofi et al. (2007a). Test data from Hardjito and Rangan (2005) show that the modulus of elasticity increases with increasing compressive strength and the Poisson's ratio of fly ash-based geopolymer concrete is in the range of 0.12 to 0.16. The indirect tensile strength of geopolymer concrete is found to be only a fraction of the compressive strength, as in the case of Portland cement concrete. These properties compare favourably to those predicted by the relevant Australian Standards for Portland cement concrete.

Hardjito and Rangan (2005) observe that the behaviour and failure mode of fly ash-based geopolymer concrete in compression is similar to that of Portland cement concrete. The stress-strain curve of geopolymer concrete shows that the strain at peak stress is in the range of 0.0024 to 0.0026.

The studies of long-term properties by Wallah and Rangan (2006) show that fly ash-based geopolymer concrete undergoes very little shrinkage: in the order of about 100 micro strains after one year, which is significantly smaller than the range of values experienced in Portland cement concrete, which are 500 to 800 micro strains. Test data also show that geopolymer concrete has excellent resistance to sulfate attack, with no damage to the surface of test specimens after exposure to a sodium sulfate solution for up to one year.

Song et al. (2005) carried out a study on the sulphuric acid attack on fly ash-based geopolymer concrete. They find that the sulphuric acid ingress in geopolymer concrete is controlled by a diffusion process. Excellent gel-aggregate interface was observed from SEM micrographs, where the geopolymer matrix at the corroded region remains identical to the unaffected one and still serves the binding function to the surrounding aggregates.

2.1.3.5 Structural Applications of Geopolymer Concrete

The behaviour and the strength of reinforced geopolymer concrete slender columns and the flexural behaviour of reinforced geopolymer concrete beams have been studied by Sumajouw and Rangan (2006). The experimental work involved testing twenty-four fly ash-based geopolymer concrete columns and beams. The tests results gathered included deflection and load capacity of members at failure. Test results show that the behaviour, failure mode and load carrying capacity of column members are similar to those of Portland cement concrete, and good correlations of results can be obtained by using current calculation methods for Portland cement concrete members. The behaviour and failure mode of beams tested in flexure were also observed to be similar to those of Portland cement concrete. The results of flexure capacity and deflection of beams agree well with the current design provisions used for Portland cement concrete members.

Fernández-Jiménez et al. (2006) conducted experimental research on engineering properties of fly ash-based geopolymer concrete. Pull-out tests were conducted on 20 x 20 x 20cm concrete cubes to determine the bond strength between geopolymer concrete and reinforcing bars. From their investigation, it is found that geopolymer concrete shows rapid development of initial mechanical strength, very low drying shrinkage and excellent bond strength. The researchers suggest that the rapid development of high mechanical strength can be attributed to the microstructure characteristics of the high compactness of the binder with the three-dimensional skeleton, which provides exceptional physical solidity, and also to the smaller mean size of the pores in the alkaline systems compared to the pores in Portland cement systems. In addition, Fernández-Jiménez et al. observe that no special microstructures developed in the interfacial areas that constitute a weak point in the material, that might make them prone to cracking or other types of failure. The interfaces between the alkaline cement and the reinforcement and aggregates are characterised by the same dense and compact microstructure as found in the bulk of the material.

The bond performance of reinforcing bars in geopolymer mortars and concrete has been studied by Sofi et al. (2007b). A total of 27 beam-end specimens and 58 cubic direct pullout-type specimens were manufactured and tested. A splitting type of failure was

observed for all beam-end specimens, and the failures were irrespective of the size of reinforcing bar. They find that all beam specimens failed by splitting of concrete surrounding the bar, and that the normalised bond strength increased with a reduction in rebar size. Conservative results were obtained when the test results were compared with predictions from code provisions such as AS3600, ACI 318-02 and Eurocode 2.

The bond strength of geopolymer concrete was also investigated by Sarker et al. (2007). A total of 24 geopolymer concrete and 6 Portland cement beam-end specimens were tested according to ASTM standard A944 to study the bond behaviour of geopolymer concrete. From the analysis of results, it was found that both geopolymer concrete and Portland cement concrete specimens show similar patterns of bond stress-slip graphs. The design expressions proposed by Orangun et al. (1977), Esfahani and Rangan (1998) and ACI-408R (2003) resulted in conservative predictions of bond strength for both geopolymer concrete and Portland cement concrete.

2.1.3.6 Geopolymer Precast Concrete Products

Gourley and Johnson (2005) report the properties of precast geopolymer concrete products, such as sewer pipes, railway sleepers and wall panels produced on a commercial scale. For sewer pipes, conventional pipe-making processes were used to make geopolymer concrete pipes with diameters in the range of 375 mm to 1800 mm. From the test results, it was found that these pipes pass the structural load capacity strength required by the Australian Standard.

Geopolymer concrete railway sleepers were also manufactured using conventional prestressing processes. These products were in the concrete compressive strength range of 60 to 80 MPa. It was found that the products passed all Australian Standard static and cyclic load tests. In addition, it was observed that the bond strength of geopolymer concrete–steel was great, with no steel slippage at ultimate load. These railway sleeper products were interspersed in mainline tracks from 2002 and showed good performance.

A modular wall panel system using foamed fibre reinforced geopolymer mortar was developed together with an installation system. The panels were found to have excellent resistance to fire. This demonstrated the applicability of geopolymer concrete manufactured by conventional methods to the precast concrete industry, satisfying Australian concrete product standards at commercially viable costs.

2.1.3.7 Economic Benefits of Geopolymer Concrete

The economic benefits of low calcium fly ash-based geopolymer concrete have been reported by Hardjito and Rangan (2005) and Rangan (2008a, 2008b). When compared to Portland cement concrete, several economic benefits are found. The price of fly ash-based geopolymer concrete is estimated to be 10 to 30 percent cheaper than Portland cement concrete due to the lower cost of fly ash compared to the same weight of Portland cement. This includes an allowance for the price of the alkaline liquids needed to make geopolymer concrete.

There are also monetary benefits through carbon-credit trade. The appropriate usage of one ton of fly ash, creates approximately one carbon-credit, with a redemption value of 10 to 20 Euros. It is estimated that one ton of fly ash can be utilised to make approximately 2.5 cubic meters of good quality fly ash-based geopolymer concrete.

Additional economic benefits can be found in using fly ash-based geopolymer concrete with its superior chemical and mechanical properties, such as little drying shrinkage, low creep, excellent resistance to sulfate attack, and good acid resistance. These technical attributes yield economic benefits in the construction industry, such as infrastructure applications.

2.2 Shear Strength of Reinforced Concrete Beams with Shear Reinforcement

2.2.1 General

In reinforced concrete members, flexure and shear combine to create a biaxial state of stress. Cracks form when the principal tensile stresses exceed the tensile strength of concrete (Park and Paulay, 1975). In a beam subjected to transverse loading, the stress resultants at a typical cross section consist of shear force V and a bending moment M . The relative magnitudes of M and V have an effect on the manner in which inclined cracks form, and also on post-cracking behaviour. Therefore, the moment-to-shear ratio, M/Vd finds frequent use in the study of shear failure in structural concrete beams (Warner et al., 1998).

In reinforced concrete beams with stirrups, the resistance to shear is distributed between the concrete and the stirrups. At the initial loading stage, the shear reinforcements carry only a small portion of shear force. As a result, neither the load at inclined cracking nor the position and inclination of the inclined cracks are significantly affected by the presence of the shear reinforcement. After the formation of the first inclined crack, redistribution of shear stresses occur, with part of the shear force being carried by the concrete, V_c , and the rest being carried by the stirrups, V_s (Pendyala and Mendis, 2000).

The concrete component V_c is the sum of the resistances to shear due to various shear mechanisms. In the ASCE-ACI Committee 445 report (1998), four mechanisms of shear transfer in reinforced concrete members are identified:

1. Un-cracked compressive concrete above the inclined crack
2. Interface shear transfer, often known as “aggregate interlock” or “crack friction”
3. Dowel action of the longitudinal reinforcing bars
4. Residual tensile stresses transmitted directly across the cracks

These mechanisms of shear transfer in reinforced concrete beams are well documented in many research publications and textbooks (ASCE-ACI Committee 445, 1998; Warner et al., 1998; Park and Paulay, 1975).

The tensile stresses in the stirrups at inclined cracking, and in the overload stage just before failure, depend on the relative efficiency of these various mechanisms of shear transfer. It is difficult to know which mechanism of shear transfer will contribute most to the resistance of a beam as a cracked concrete beam member is a highly indeterminate system affected by many parameters. Some of the important parameters influencing shear capacity identified in past research include size effect or depth of member, shear span-to-depth ratio (a/d) and support conditions, longitudinal reinforcement and axial force (ASCE-ACI Committee 445, 1998).

Because the shear failure mechanism of reinforced concrete beams is affected by various parameters, it is not easy to evaluate the shear strength of reinforced concrete beams accurately, and many experimental and theoretical studies have been performed to investigate the behavioural characteristics and shear failure of reinforced concrete beams (Choi and Park, 2007).

Since the early twentieth century, truss models have been used to follow the flow of internal forces in structural concrete members and to provide structural systems made out of concrete and reinforcement that ensure equilibrium. The original 45° truss model advocated by Ritter in 1899 and Morsch in 1920 has been adopted, either explicitly or implicitly, by most major codes for shear design specifications. This conceptual model has been adopted in sectional truss models and compression field approaches to strut-and-tie models, and is applicable for members with and without web reinforcements (ASCE-ACI 445, 1998).

In more modern design specifications, a variable angle truss model supplemented by a concrete contribution term has been used. In 1964, Kupfer provided a solution to diagonal cracking from an analysis of a truss model consisting of linearly elastic members and

neglecting the tensile strength of the concrete. Bazant and Kim (1984) developed a theoretical strength model based on fracture mechanics. Hoang and Nielsen (1998) developed a strength model based on a theory of plasticity. Various refined truss models, such as the variable angle truss model supplemented by a concrete contribution term, were used.

Vecchio and Collins (1986) introduced the Modified Compression Field Theory (MCFT) based on the assumption that tensile stresses in the concrete between the cracks contribute significantly to shear resistance. It is a full rotating-crack model built around constitutive relations derived from experimental investigations. An extension of the MCFT-Disturbed Stress Field Model (DSFM) has been developed by Vecchio (2000), which incorporates rigid slipping along crack surfaces into the compatibility relations for the element, and provides a better phenomenological representation of the behaviour of concrete.

In parallel with the developments of these truss models, other refinements based on the shear friction theory have undergone development in the last decade. This approach considers the discrete formation of cracks, crack spacing, determination of crack width and equilibrium check along the crack in the evaluation of the crack-slip mechanism of failure (ASCE-ACI 445, 1998).

The research on shear behaviour of reinforced concrete beams has been carried out for about a century (Regan, 1993). As such, it is beyond the scope of this study to include extensive reviews here. A comprehensive review of recent approaches to shear design of reinforced concrete can be found in ASCE-ACI Committee 445 report (1998).

The following section presents a detailed descriptions of recent analytical models based on different approaches and code provisions used to calculate the shear strength of Portland cement concrete members. These theoretical models include models proposed by von Ramin (2004), Kong and Rangan (1998) and Vecchio (2000), and will be used to predict the shear strength of geopolymer concrete beams in this study. A brief review of the shear provisions in the Draft Australian Standard for Concrete Structures AS 3600 (2005) and the American Concrete Institute Building Code ACI 318-08 are also discussed.

2.2.2 Predictions by using Analytical Models

2.2.2.1 von Ramin (2004)

The model proposed by von Ramin (2004) is a physical model which includes the contribution of various significant shear transfer mechanisms identified in the research literature for reinforced concrete members: arch action (V_a), truss action (V_t), friction between crack surfaces or aggregate interlock (V_f) and the contribution of the un-cracked compression zone (V_{cz}). This model is directly applicable and does not rely on iterations that are computer based.

The nominal shear strength of a reinforced concrete member is given by

$$V_n = V_a + V_t + (V_{cz} + V_f) \quad (2.2)$$

Where V_a , V_b , V_{cz} and V_f are the contributions resulting from arch action, truss, compression zone and friction, respectively. These mechanisms are described in detail in the following:

Arch Component

Arch action is assumed to be related to a single strut directed from the loading point towards the support, as shown in Figure 2.1.

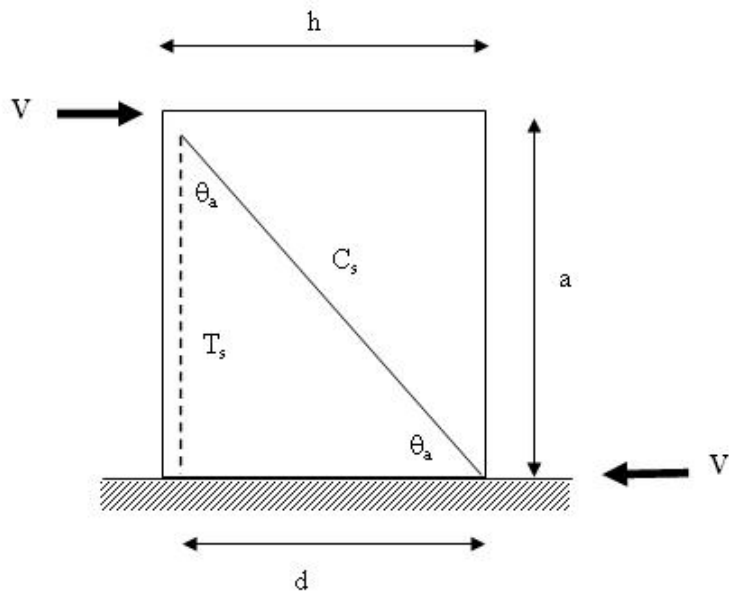


**Figure 2.1: Reinforced Concrete Panel with Inclined Strut
(von Ramin, 2004)**

Where

C_s = concrete strut

T_s = tie formed by the longitudinal reinforcement

θ_a = angle of inclination of the strut, approximately calculated from shear span to depth ratio, where

$$\cot \theta_a = \frac{a}{d} \quad (2.3)$$

The width of the strut, w_a , depends on the loading conditions of the member and is given by

$$w_a = h_a \cos \theta_a + l_b \sin \theta_a \quad (2.4)$$

with

h_a = twice the cover depth of the longitudinal reinforcement

l_b = dimension of the loading plate in the axial direction of the member as shown in

Figure 2.2.

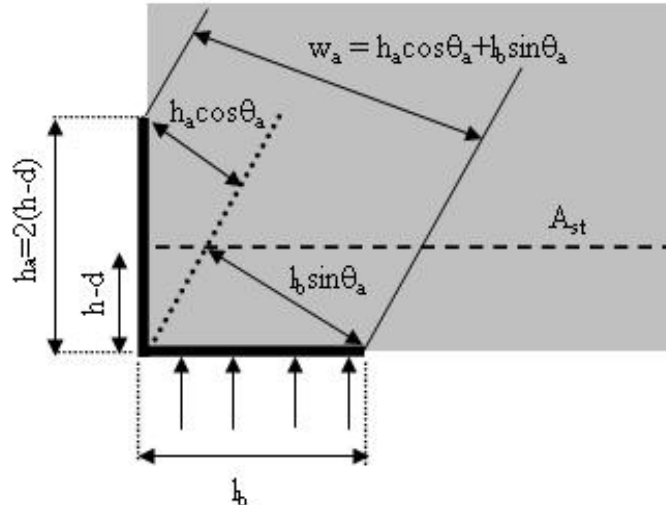


Figure 2.2: Definition of Strut Width in Deep Beam (von Ramin, 2004)

The strength of arch mechanism is defined based on the geometric configuration of the strut as described above, the effective strength of concrete, the reduction factor related to truss action and the transition function as given in Equation 2.5:

$$V_a = k_a R_a \beta_s f'_c w_a b \sin \theta_a \quad (2.5)$$

As arch action is a major shear-carrying mechanism in squat members, this mechanism becomes negligible in slender members. To allow for a smooth transition between deep and slender members, a transition factor k_a is introduced to describe the decreasing influence of arch action with an increasing aspect ratio. For members with web reinforcement, the transition factor is given by the following equation:

$$k_a = \frac{4.6}{6.5 + 0.13(a/d)^5} \quad (2.6)$$

The reduction factor for the effective strength of concrete is defined as a function of the compressive strength of concrete f'_c , which is given by

$$\beta_s = 0.85 - 0.004 f'_c \geq 0.5 \quad (2.7)$$

The contribution of arch action to shear strength is reduced by a factor R_a to account for additional stress demand due to truss action. This will be explained further in the interaction between the truss and arch mechanisms in the truss component presented next.

Truss Component

The strength of the truss component is calculated using a variable angle truss model, based on the yield strength of the transverse reinforcement, the internal arm jd and the angle of the inclination of the compression field. This is expressed by

$$V_{t,v} = \rho_{sv} f_{svy} bjd \cot \phi \quad (2.8)$$

With

ρ_{sv} = transverse reinforcement ratio

f_{svy} = yield strength of the vertical transverse reinforcement

b = member width

jd = lever arm (distance between the centroid of the flexural reinforcement and the compression force in the concrete)

ϕ = inclination of the compression field with respect to the longitudinal reinforcement

= 30 degrees due to simplicity of calibration of the model

As mentioned before, the arch action component is reduced based on the stress demand induced by the truss. It is assumed that the truss develops its full capacity as it is the more reliable shear carrying mechanism.

The stress in the compression field which is induced by the vertical truss mechanism, represented by $f_{t,v}$, is given by

$$f_{t,v} = \frac{P_{sv} f_{svy}}{\sin^2 \phi} \quad (2.9)$$

The compressive strength of the concrete in the arch is given by the effective compressive strength $\beta_s f'_c$. A factor R_v can be defined as a fraction of the effective compressive strength taken by the truss mechanism, as given in Equation 2.10:

$$R_v = \frac{f_{t,v}}{\beta_s f'_c} \quad (2.10)$$

However, there are two limitations for R_v . When the stress in the inclined compression field exceeds the allowable compressive stress, that is $f_{t,v} \geq \beta_s f'_c$, the strength of the truss must be lowered by the ratio of stress demand to effective compressive strength. As a result, V_t , must be reduced by the inverse of R_v , which is given by

$$\frac{1}{R_v} = \frac{\beta_s f'_c}{f_{t,v}} \leq 1.0 \quad (2.11)$$

R_a , as mentioned in the arch component earlier, is the factor accounting for the fraction of the effective compressive strength taken by the arch mechanism. Thus, the sum of these two terms must be equal to unity: that is,

$$R_v + R_a = 1 \quad (2.12)$$

The allowable demand on the strut without exceeding the effective compressive strength of concrete is obtained by solving for R_a , given by Equation 2.13:

$$R_a = 1 - \frac{f_{t,v}}{\beta_s f'_c} \quad (2.13)$$

Un-cracked Compression Zone

The shear strength of the un-cracked compression zone V_{cz} is calculated as a function of the tensile strength of concrete f'_{ct} , and the area of the un-cracked compression zone as

$$V_{cz} = \lambda f'_{ct} bkd \quad (2.14)$$

With the tensile strength of concrete given by

$$f'_{ct} = \sqrt[3]{f'_c} \quad (2.15)$$

and

$$k = \sqrt{(p_{sl}n)^2 + 2p_{sl}n} - \rho_{sl}n \quad (2.16)$$

where

p_{sl} = longitudinal reinforcement ratio

n = ratio of modulus of elasticity of steel to that of concrete

λ = 0.4 from the calibration of the model.

Friction

The friction component, V_f is calculated using a formulation similar to Reineck (1991). Figure 2.3 shows the distribution of friction stresses adopted in the model by Reineck.

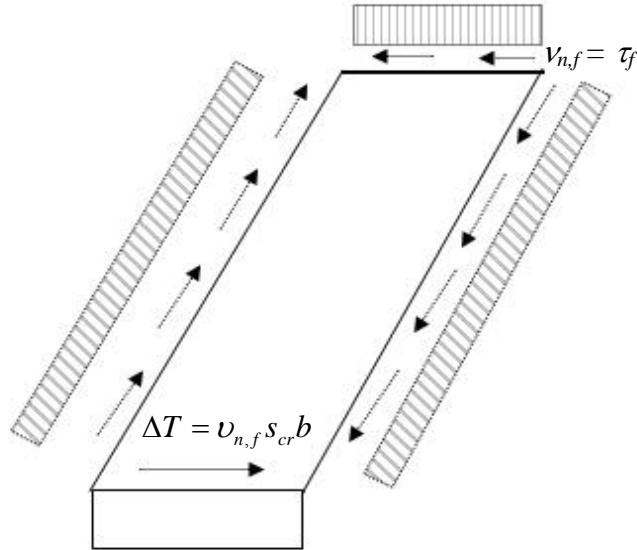


Figure 2.3: Constant Distribution of Friction Stresses along Crack (Reineck, 1991)

According to Reineck, the friction strength is obtained by the integration of a constant friction stress over the area of the surface of the crack, which yields

$$V_f = \tau_{fu} b(d - kd) \quad (2.17)$$

where

τ_{fu} = the limiting friction stress at the crack surface and is given by

$$\tau_{fu} = \lambda f'_{ct} \left(1 - \frac{w}{\Delta w_u}\right) \quad (2.18)$$

It is found that, through calibration based on experimental results from shear tests, the value of limiting crack width, $\Delta w_u = 1.0$ mm gives the best reflection on the reduction in strength observed with increasing crack width. The average crack width, w , is calculated

based on the strain in the longitudinal reinforcement, ε_s , and the orientation of the crack. By assuming an angle of inclination of the crack equal to the inclination of the compression field induced truss action ($\phi = 30$ degrees), the average crack width is given by

$$w = \frac{0.5\varepsilon_s S_{cr}}{\sin 30^\circ(1 - 0.336 \cot 30^\circ)} + \frac{0.01 \cot 30^\circ}{1 - 0.336 \cot 30^\circ} \cong 2.4\varepsilon_s S_{cr} + 0.04 \quad (2.19)$$

where the strain in the longitudinal reinforcement is calculated based on the properties of the cracked transformed section and at a critical distance d from the support as below:

$$\varepsilon_s = \frac{Vd}{p_{sl} b d j d E_s} \quad (2.20)$$

and the average cracking spacing is calculated from

$$S_{cr} = (d - kd) \quad (2.21)$$

The sum of the compression zone V_{cz} and friction V_f components constitutes the term V_c . For members with web reinforcement, V_c can be expressed as

$$V_c = \lambda f'_{ct} b k d + \lambda f'_{ct} b (d - kd) \left(1 - \frac{w}{\Delta w_u}\right) \quad (2.22)$$

Rearranging Equation 2.22 gives

$$V_c = \lambda f'_{ct} b d \left[k + (1 - k) \left(1 - \frac{w}{\Delta w_u}\right) \right] \quad (2.23)$$

From the model calibration, it is found that $\lambda = 0.4$.

2.2.2.2 Kong and Rangan (1998)

The theory developed by Kong and Rangan (1998) to calculate the shear strength of reinforced concrete beam is based on the stress analysis of the web portion of a beam and is adopted from work by Hsu (1988, 1993) and Vecchio and Collins (1982, 1993).

In this model, the shear response and shear strength of a region of a beam can be evaluated by performing a stress analysis of a cracked concrete element, as shown in Figure 2.4. This element is presented in the form of a strut-and-tie model comprising a concrete strut inclined at an angle θ , tied in place by reinforcing bars in the longitudinal and transverse direction. This concrete strut develops a compressive stress σ_d along its axis (d -direction) and a tensile stress σ_r in the orthogonal direction (r -direction), which are taken as principal stresses. These stresses can be transformed into longitudinal l - and transverse t -directions using Mohr's stress circle, and then superimposed on the stresses in the reinforcement.

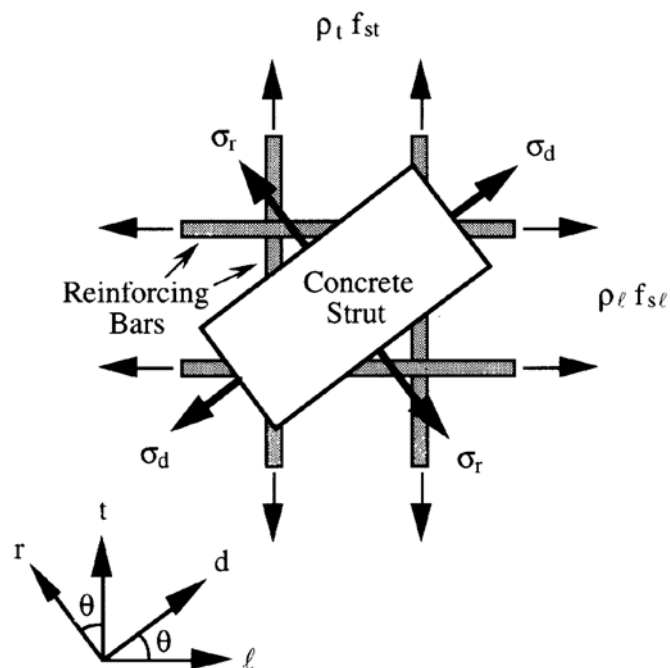


**Figure 2.4: Stress Analysis of a Reinforced Concrete Element
(Kong and Rangan, 1998)**

The stress analysis of the element can be solved by using equilibrium, strain compatibility and constitutive laws for stress and strain relationships of concrete and steel. The method of analysis is described below.

Equilibrium

The equilibrium equations are:

$$\sigma_\ell = \sigma_d \cos^2 \theta + \sigma_r \sin^2 \theta + \rho_\ell f_{sl} \quad (2.24)$$

$$\sigma_t = \sigma_d \sin^2 \theta + \sigma_r \cos^2 \theta + \rho_t f_{st} \quad (2.25)$$

$$v_{lt} = -(\sigma_d - \sigma_r) \sin \theta \cos \theta \quad (2.26)$$

where

σ_ℓ, σ_t = normal stress in l - and t -directions respectively and are positive for tension

σ_d, σ_r = principal stresses in the d -and r -directions respectively and are positive for tension

v_{lt} = average shear stress in the l and t -coordinate system and is taken as $\frac{V}{b_v(0.9d_o)}$

p_l = smeared longitudinal tensile reinforcement ratio attributed to shear

$$= \frac{A_{slV}}{b_v(0.9d_o)}$$

p_t = smeared transverse reinforcement ratio

$$= \frac{A_{sv}}{b_v s}$$

A_{sv} = total area of all legs of vertical stirrups across the width of the beam

s = spacing of stirrups along the longitudinal axis of a beam

f_{sl}, f_{st} = stresses in longitudinal and transverse reinforcement respectively

Strain Compatibility

The principal strain directions are assumed to coincide with the corresponding principal stress directions. The average strains in the l - and t -directions may be related to principal strains by using Mohr's strain circle, as below:

$$\varepsilon_l = \varepsilon_d \cos^2 \theta + \varepsilon_r \sin^2 \theta \quad (2.27)$$

$$\varepsilon_t = \varepsilon_d \sin^2 \theta + \varepsilon_r \cos^2 \theta \quad (2.28)$$

$$\gamma_{lt} = -2(\varepsilon_d - \varepsilon_r) \sin \theta \cos \theta \quad (2.29)$$

where

$\varepsilon_l, \varepsilon_t$ = average strains in the element in l - and t -directions respectively and are positive
for tension

$\varepsilon_d, \varepsilon_r$ = average principal strains in the element in d - and r - directions respectively and
are positive for tension

γ_{lt} = average shear strain in the element in the l - and t -coordinate system

Stress and Strain Relationships of Concrete

- Softened concrete in compression

The stress and strain curve of softened concrete in compression is adopted from Vecchio and Collins (1993), where the effective compressive strength of a strut in a reinforced concrete element is less than the uniaxial concrete compression strength due to the presence of tensile strains in the perpendicular directions. This softening effect is taken into account by means of a softening factor.

The stress and strain curve of a softened concrete in compression may be described as follows:

For $\zeta\varepsilon_o \leq \varepsilon_d \leq 0$ (the initial part of the curve where both stress and strain softening are applied):

$$\sigma_d = -\xi f'_c \left(\frac{\varepsilon_d}{\zeta \varepsilon_o} \right) \left(\frac{n'}{n'-1 + \left(\frac{\varepsilon_d}{\zeta \varepsilon_o} \right)^{n'k'}} \right) \quad (2.30)$$

For $\varepsilon_o \leq \varepsilon_d \leq \zeta\varepsilon_o$ (the middle part of the curve where Vecchio and Collins (1993) propose a flat region throughout this range of ε_d):

$$\sigma_d = -\xi f'_c \quad (2.31)$$

For $\varepsilon_d \leq \varepsilon_o$ (the post-peak branch where only stress softening is applied):

$$\sigma_d = -\xi f'_c \left(\frac{\varepsilon_d}{\varepsilon_o} \right) \left(\frac{n'}{n'-1 + \left(\frac{\varepsilon_d}{\varepsilon_o} \right)^{n'k'}} \right) \quad (2.32)$$

where

f'_c = concrete cylinder compressive strength in MPa

$$n' = 0.8 + \frac{f'_c}{17}$$

$$k' = 1.0 \text{ when } \frac{\varepsilon_d}{\varepsilon_o} \leq 1.0$$

$$= 0.67 + \frac{f'_c}{62} \text{ when } \frac{\varepsilon_d}{\varepsilon_o} > 1.0$$

ε_o = strain corresponding to the peak concrete compressive stress

$$= -\frac{f'_c}{E_c} \left(\frac{n'}{n'-1} \right)$$

E_c = modulus of elasticity of concrete (from Carrasquillo et al., 1981)

$$= 3320\sqrt{f'_c} + 6900$$

ζ = softening factor applicable for all grades of concrete, proposed by Vecchio and Collins (1993)

$$= \frac{1}{1.0 + K_f K_c}$$

where

$$K_f = 0.1825\sqrt{f'_c} \geq 1.0 \quad \text{and}$$

$$K_c = 0.35 \left(-\frac{\varepsilon_r}{\varepsilon_d} - 0.28 \right)^{0.8} \geq 1.0$$

- Concrete in tension

The stress and strain relationship of concrete in tension is given by Collins et al. (1996) as follows:

For $\varepsilon_r \leq \varepsilon_{cr}$

$$\sigma_r = E_c \varepsilon_r \tag{2.33}$$

For $\varepsilon_r \geq \varepsilon_{cr}$

$$\sigma_r = \frac{f_{cr}}{1 + \sqrt{500\varepsilon_r}} \tag{2.34}$$

where

ε_{cr} = concrete cracking strain

$$= \frac{f_{cr}}{E_c}$$

f_{cr} = concrete cracking stress

$$= 0.33\sqrt{f'_c}$$

Stress and strain relationship for steel

The stress and strain relationship of longitudinal and transverse steel reinforcement is represented by elasto-plastic curves as follows:

$$f_{s\ell} = E_s \varepsilon_\ell \text{ when } \varepsilon_\ell \leq f_{s\ell y} / E_s \quad (2.35a)$$

$$= f_{s\ell y} \text{ when } \varepsilon_\ell > f_{s\ell y} / E_s \quad (2.35b)$$

$$f_{st} = E_s \varepsilon_t \text{ when } \varepsilon_t \leq f_{svy} / E_s \quad (2.36a)$$

$$= f_{svy} \text{ when } \varepsilon_t > f_{svy} / E_s \quad (2.36b)$$

where

$f_{s\ell y}, f_{svy}$ = yield stresses of the longitudinal and transverse steel reinforcement

respectively

E_s = modulus of elasticity of steel

$$= 200 \times 10^3 \text{ MPa}$$

Solution

The stress analysis involves thirteen unknowns, which are $\sigma_l, \sigma_t, \sigma_d, \sigma_r, V_{lt}, \varepsilon_l, \varepsilon_t, \varepsilon_d, \varepsilon_r, \gamma_{lt}, f_{sl}, f_{st}$. From the equilibrium, strain compatibility and stress and strain

relationships for concrete and steel, ten equations are obtained. Three more equations are needed to obtain a solution.

The axial force N at a certain region of the beam is assumed to produce a uniform stress on the beam cross section. The intensity of this stress in the web of the beam in the l -direction is equal to N/A_g , where A_g is the gross concrete area of the beam cross section. This assumption is not entirely true as the stress distribution is non-uniform because of flexural cracks. In the case of a reinforced concrete beam, N/A_g is zero and the accuracy of this assumption does not affect the stress analysis of the beam. Therefore,

$$\sigma_\ell = \frac{N}{A_g} \quad (2.37)$$

As the beam is not subjected to any axial force in the transverse direction, it is assumed that the resultant tensile stress in that direction is zero:

$$\sigma_t = 0 \quad (2.38)$$

In order to trace the load-deformation response of the beam region in terms of average shear stress, ν_{lt} , and average shear strain, γ_{lt} , the strain ε_d can be specified for each load stage. This requires the area of the longitudinal tensile steel, A_{sIV} , which resists the shear force, to be defined as below:

$$A_{sIV} = A_{s\ell} - A_{s\ell M} \quad (2.39)$$

where

$A_{s\ell}$ = total longitudinal steel in the tension zone

$A_{s\ell M}$ = part of the $A_{s\ell}$ required to resist the bending moment

$$\approx \frac{M}{(0.9d_o)f_{sly}} \quad (2.40)$$

and M is the bending moment co-existing with the shear force V . Also, A_{sIV} is always positive and taken as greater than zero.

For the simplification of the solution process, some of the equations are rearranged as follows:

The longitudinal strain ε_ℓ can be expressed as

$$\varepsilon_\ell = \frac{\varepsilon_r(\sigma_d - \sigma_r) + (\sigma_\ell - \sigma_r)(\varepsilon_d - \varepsilon_r)}{\sigma_d - \sigma_r + \rho_\ell E_s(\varepsilon_d - \varepsilon_r)} \quad \text{when } \varepsilon_\ell \leq f_{s\ell y} / E_s \quad (2.41)$$

$$\varepsilon_\ell = \left(\frac{\sigma_\ell - \sigma_r - \rho_\ell f_{s\ell y}}{\sigma_d - \sigma_r} \right) (\varepsilon_d - \varepsilon_r) + \varepsilon_r \quad \text{when } \varepsilon_\ell > f_{s\ell y} / E_s \quad (2.42)$$

The transverse strain ε_t can be expressed as

$$\varepsilon_t = \frac{\varepsilon_r(\sigma_d - \sigma_r) - \sigma_r(\varepsilon_d - \varepsilon_r)}{\sigma_d - \sigma_r + \rho_t E_s(\varepsilon_d - \varepsilon_r)} \quad \text{when } \varepsilon_t \leq f_{svy} / E_s \quad (2.43)$$

$$\varepsilon_t = \left(\frac{-\sigma_r - \rho_t f_{svy}}{\sigma_d - \sigma_r} \right) (\varepsilon_d - \varepsilon_r) + \varepsilon_r \quad \text{when } \varepsilon_t > f_{svy} / E_s \quad (2.44)$$

The principal concrete tensile strain ε_r is obtained from combining Equations 2.27 and 2.28, which yield

$$\varepsilon_r = \varepsilon_\ell + \varepsilon_t - \varepsilon_d \quad (2.45)$$

The angle of inclination of the concrete compressive strut θ is given by

$$\theta = \tan^{-1}\left(\sqrt{\frac{\varepsilon_\ell - \varepsilon_d}{\varepsilon_t - \varepsilon_d}}\right) \quad (2.46)$$

For simplicity, the value of $A_{s\ell M}$ is calculated at the load stage corresponding to the peak of the $\nu_{lt} - \gamma_{lt}$ curve, which represents the shear strength V_u of the region. Since V_u is unknown in the beginning, some iteration is required. Initially, a trial value of V_u from the initial stress analysis is selected and A_{sIV} is calculated using Equations 2.39 and 2.40 for a known value of moment to shear ratio, M/V . The stress analysis of the model is then performed to establish the peak of the $\nu_{lt} - \gamma_{lt}$ curve, and hence V_u . Using this new value of V_u , A_{sIV} is calculated and the stress analysis is repeated. The entire process is continued until convergence is reached.

2.2.2.3 Disturbed Stress Field Model by Vecchio (2000)

The Disturbed Stress Field Model (DSFM) was introduced by Vecchio (2000) as an extension of the Modified Compression Field Theory (MCFT) developed by Vecchio and Collins (1986) to describe the behaviour of cracked reinforced concrete elements. Equilibrium, compatibility and constitutive response are formulated in terms of average stresses and average strains. The new formulation provides advancements made with relation to the inclusion of crack shear slip in the element compatibility relations, the removing of the restriction of coincidence between inclination of principal stress and principal strain directions and a revised look at compression softening and tension stiffening mechanisms (Vecchio, 2001).

With the incorporation of the slip formulation, the analytical procedure of DSFM occupies a middle ground between fixed crack models and rotating crack models, giving an improved representation of crack mechanisms and resulting in increased accuracy. Unlike conventional fixed crack models, the DSFM allows for a gradual progressive orientation of the concrete principal stresses direction (and crack direction), although

delayed to a certain extent. Unlike common rotating crack models, the DSFM allows for the divergence of principal stress and principal strain directions.

Equilibrium Conditions

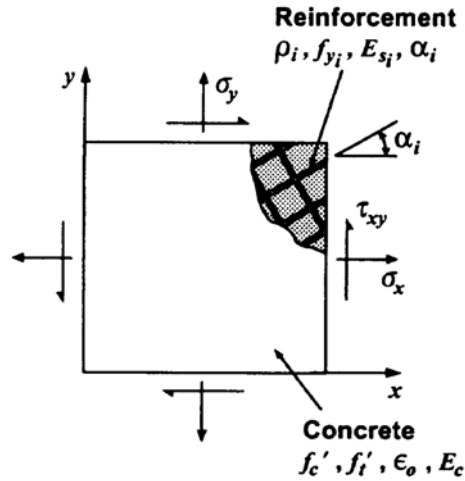


Figure 2.5: Reinforced Concrete Element – Reinforcement and Loading Conditions (Vecchio, 2000)

Figure 2.5 shows a reinforced concrete element subjected to uniform stresses along the element boundaries. The reinforcement of the element is assumed to be smeared and evenly distributed within the element. The force applied to the element is resisted by internal stresses in the concrete and in the reinforcement. The element equilibrium is considered in terms of both average stresses smeared over the area of the element and local conditions along the crack surfaces. The equilibrium conditions are given by

$$[\sigma] = [D_c][\varepsilon_c] + \sum_{i=1}^n [D_s]_i [\varepsilon_s]_i \quad (2.47)$$

Where n is the number of reinforcement components, $[D_c]$ and $[D_s]_i$ are the concrete and reinforcement stiffness matrices and $[\varepsilon_c]$ and $[\varepsilon_s]_i$ are net strains in the concrete and

reinforcement components respectively. For the special case where the panel is orthogonally reinforced and the reinforcement is aligned with the reference axes, the equilibrium conditions become:

$$\sigma_x = f_{cx} + \rho_x f_{sx} \quad (2.48)$$

$$\sigma_y = f_{cy} + \rho_x f_{sy} \quad (2.49)$$

$$\tau_{xy} = v_{cxy} \quad (2.50)$$

The concrete stresses f_{cx} , f_{cy} and v_{cxy} can be determined from the principal stresses using Mohr's circle of stress as shown in Figure 2.6.

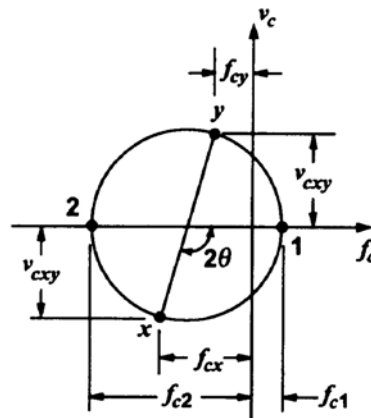


Figure 2.6: Mohr's Circle for Average Stresses in Concrete (Vecchio, 2000)

The magnitude of the average tensile stress in the concrete, f_{c1} , that can be transmitted across cracks is limited by the following condition:

$$f_{c1} \leq \sum_{i=1}^n \rho_i (f_{y_i} - f_{s_i}) \cdot \cos^2 \theta_{n_i} \quad (2.51)$$

where ρ_i is the reinforcement ratio, f_{s_i} is the average stress, f_{y_i} is the yield stress for the i -th reinforcement component, and θ_{n_i} is the difference between the angle of orientation of the reinforcement, α_i and the normal to the crack surface, θ_N :

$$\theta_{n_i} = \theta_N - \alpha_i \quad (2.52)$$

The local reinforcement stresses, f_{scr_i} are determined from local reinforcement strains, ε_{scr_i} . These local reinforcement stresses must meet the equilibrium condition that the average concrete tensile stresses be transmitted across the cracks: that is,

$$\sum_{i=1}^n \rho_i (f_{scr_i} - f_{s_i}) \cdot \cos^2 \theta_{n_i} = f_{c1} \quad (2.53)$$

The local increases in reinforcement stresses at crack locations lead to the development of shear stresses along the crack surfaces, v_{ci} . From the equilibrium requirement, the relationship is

$$v_{ci} = \sum_{i=1}^n \rho_i (f_{scr_i} - f_{s_i}) \cdot \cos \theta_{n_i} \cdot \sin \theta_{n_i} \quad (2.54)$$

Compatibility Relations

Consider the compatibility conditions in a reinforced concrete element that is experiencing deformation composed of both continuum straining and discontinuous slip

along the crack surfaces. The continuum straining is the result of mechanical compliance to stress and to the smearing of crack widths over a finite area. The slip component is the result of the rigid body movement along a crack interface. Using extensometers of a gauge length sufficient to span several cracks, one could make a measure of the average strains within the element.

Relative to a reference x, y system, the measured strains would intrinsically contain both components of deformation. These measured or “apparent” strains will be denoted as $[\varepsilon] = \{\varepsilon_x \varepsilon_y \gamma_{xy}\}$. The apparent inclination of the principal strain, θ_ε is given by

$$\theta_\varepsilon = \frac{1}{2} \tan^{-1} \left[\frac{\gamma_{xy}}{\varepsilon_x - \varepsilon_y} \right] \quad (2.55)$$

Decoupling the two strain effects, the actual (net) strains within the continuum will be denoted as $[\varepsilon_c] = \{\varepsilon_{cx} \varepsilon_{cy} \gamma_{cxy}\}$. These are employed in appropriate constitutive relations to determine the average stresses from the average strains for the concrete. For this purpose, the principal strains are determined from the net strains using the standard transformations:

$$\varepsilon_{c1}, \varepsilon_{c2} = \frac{(\varepsilon_{cx} + \varepsilon_{cy})}{2} \pm \frac{1}{2} [(\varepsilon_{cx} - \varepsilon_{cy})^2 + \gamma_{cxy}^2]^{1/2} \quad (2.56)$$

The actual inclination of the principal strains in the continuum θ and the assumed inclination of the principal stresses θ_σ will be:

$$\theta_\sigma = \theta = \frac{1}{2} \tan^{-1} \left[\frac{\gamma_{cxy}}{\varepsilon_{cx} - \varepsilon_{cy}} \right] \quad (2.57)$$

where ε_{c1} is the principal tensile strain, ε_{c2} is the principal compressive strain, ε_{cx} is the average strain in the x-direction, ε_{cy} is the average strain in the y-direction and γ_{cxy} is the shear strain.

An average shear slip strain can be defined as in Equation 2.58 by assuming that the cracks are inclined in the direction of the net principal tensile strain and with an average width and spacing of w and s_a , respectively; and that the slip along the crack surface is of magnitude δ_s .

$$\gamma_s = \frac{\delta_s}{s_a} \quad (2.58)$$

Using a Mohr's circle construction, the slip strain can be resolved into orthogonal components relative to the reference system, thus $[\varepsilon^s] = \{\varepsilon_x^s \ \varepsilon_y^s \ \gamma_{xy}^s\}$ where

$$\varepsilon_x^s = -\gamma_s / 2 \cdot \sin(2\theta) \quad (2.59)$$

$$\varepsilon_y^s = \gamma_s / 2 \cdot \sin(2\theta) \quad (2.60)$$

$$\gamma_{xy}^s = \gamma_s \cdot \cos(2\theta) \quad (2.61)$$

The element may have experienced strains due to elastic or plastic offsets. The elastic strain offsets, $[\varepsilon_c^e]$ will include effects due to thermal expansion, mechanical expansion (e.g. Poisson's effect, aggregate alkali activity), and shrinkage. Plastic offsets, $[\varepsilon_c^p]$, will arise from cyclic loading conditions or loading into post-peak levels. The apparent (total) strains will be the summation of the continuum stress-induced strains, the shear slip

strains, and the elastic and plastic offset strains. Thus, the following compatibility condition is obtained:

$$[\varepsilon] = [\varepsilon_c] + [\varepsilon^s] + [\varepsilon_c^o] + [\varepsilon_c^p] \quad (2.62)$$

The “lag” in the rotation of the principal stresses in the continuum, relative to the rotation of the apparent principal strains, will be defined as:

$$\Delta\theta = \theta_\varepsilon - \theta_\sigma \quad (2.63)$$

In relating the apparent strain condition to the actual orientation of the stress and strain field within the continuum, the following relation is used:

$$\gamma_s = \gamma_{sy} \cdot \cos 2\theta_\sigma + (\varepsilon_y - \varepsilon_x) \cdot \sin 2\theta_\sigma \quad (2.64)$$

The reinforcement is assumed perfectly bonded to the concrete. Hence, the average strain in a reinforcement component is calculated from the total strains as follows:

$$\varepsilon_{s_i} = \frac{\varepsilon_x + \varepsilon_y}{2} + \frac{\varepsilon_x - \varepsilon_y}{2} \cdot \cos 2\alpha_i + \frac{\gamma_{xy}}{2} \sin 2\alpha_i + \varepsilon_{s_i}^o \quad (2.65)$$

where α_i is the angle of orientation of the reinforcement and $[\varepsilon_{s_i}^o]$ is the initial prestrain in the reinforcement. At crack locations, the local stresses and strains in the reinforcement must increase in order to compensate for the local reduction in the concrete average tensile stress. The local strain in the reinforcement is expressed by Equation 2.66:

$$\varepsilon_{scr_i} = \varepsilon_{s_i} + \Delta\varepsilon_{1cr} \cdot \cos^2 \theta_{n_i} \quad (2.66)$$

where $\Delta\varepsilon_{1cr}$ is the local incremental strain.

Given nominal crack spacing in the reference x- and y- directions, s_{ax} and s_{ay} , the average cracking spacing in the cracked continuum can be estimated as follows:

$$s = \frac{1}{\frac{\sin \theta}{s_x} + \frac{\cos \theta}{s_y}} \quad (2.67)$$

The values s_x and s_y can be estimated from standard crack spacing formulations. From the average crack spacing, the average crack width w can then be calculated from the average tensile strain, given by Equation 2.68:

$$w = \varepsilon_{c1} \cdot s \quad (2.68)$$

Constitutive Relations

The compression response of cracked reinforced concrete is characterised by significant degrees of softening arising from the effects of transverse cracking. The principal compressive stress in the concrete, f_{c2} , is found to be a function of not only the principal compressive strain but also of the co-existing principal tensile strain. This influence is captured by the reduction factor β_d , as below:

$$\beta_d = \frac{1}{1 + C_s \cdot C_d} \leq 1.0 \quad (2.69)$$

where

$$C_d = 0.35(-\varepsilon_{c1} / \varepsilon_{c2} - 0.28)^{0.8} \quad (2.70)$$

The factor β_d is used to define both the peak stress, f_p , and the strain at peak stress, ε_p , in the compression response of the concrete, where

$$f_p = -\beta_d \cdot f_c' \quad (2.71)$$

$$\varepsilon_p = -\beta_d \cdot \varepsilon_o \quad (2.72)$$

The compression response curve is given by using Equation 2.73:

$$f_{c2} = f_p \cdot \frac{n \cdot (\varepsilon_{c2} / \varepsilon_p)}{(n-1) + (\varepsilon_{c2} / \varepsilon_p)^{nk}} \quad (2.73)$$

where

$$n = 0.8 - f_p / 17 \quad (2.73a)$$

$$k = 1.0, \varepsilon_p < \varepsilon_{c2} < 0; k = (0.67 - f_p / 62), \varepsilon_{c2} < \varepsilon_p \quad (2.73b)$$

A linear relation is used for concrete in tension prior to cracking as follows:

$$f_{c1} = E_c \varepsilon_{c1}, \quad 0 < \varepsilon_{c1} < \varepsilon_{cr} \quad (2.74)$$

where E_c is the modulus elasticity of concrete and ε_{cr} is the cracking strain, given by

$$E_c = 2 \frac{f'_c}{\varepsilon_o} \quad (2.74a)$$

$$\varepsilon_{cr} = \frac{f'_c}{E_c} \quad (2.74b)$$

The concrete tensile strength, f'_{ct} is taken as

$$f'_{ct} = 0.65(f'_c)^{0.33} \quad (2.74c)$$

Tension softening is particularly significant in concrete structures containing little or no reinforcement, such as beams containing no web steel. Here, the concrete post-cracking tensile stress associated with tension softening f'_{c1}^a is calculated as

$$f'_{c1}^a = f'_{ct} \left[1 - \frac{(\varepsilon_{c1} - \varepsilon_{cr})}{(\varepsilon_{ts} - \varepsilon_{cr})} \right] \quad (2.75)$$

where the terminal strain ε_{ts} is calculated from the fracture energy parameter, G_f and characteristic length, L_r as follows:

$$\varepsilon_{ts} = 2.0 \frac{G_f}{f'_{ct} \cdot L_r} \quad (2.76)$$

where G_f is taken as having a constant value of 75 N/m.

Post-cracking tensile stresses in the concrete also arise from interactions between the reinforcement and the concrete. In areas between cracks, load is transferred from the reinforcement to the concrete via bond stresses, producing significant levels of average

tensile stress in the concrete. These concrete tension stiffening stresses are modelled as follows:

$$f_{c1}^b = \frac{f'_{ct}}{1 + \sqrt{c_t \varepsilon_{c1}}} \quad (2.77)$$

where

$$c_t = 2.2m \quad (2.77a)$$

$$\frac{1}{m} = \sum_{i=1}^n \frac{4\rho_i}{d_{b_i}} \cdot |\cos\theta_{n_i}| \quad (2.77b)$$

$$f_{c1} = \max(f_{c1}^a, f_{c1}^b) \quad (2.77c)$$

A tri-linear stress-strain relation is used to model the response of reinforcement in tension and compression as expressed in Equations 2.78 and 2.79:

$$f_s = E_s \varepsilon_s, \quad 0 < \varepsilon_s < \varepsilon_y; \quad f_s = f_y, \quad \varepsilon_y < \varepsilon_s < \varepsilon_{sh} \quad (2.78)$$

$$f_s = f_y + E_{sh}(\varepsilon_s - \varepsilon_{sh}), \quad \varepsilon_{sh} < \varepsilon_s < \varepsilon_u; \quad f_s = 0, \quad \varepsilon_s > \varepsilon_u \quad (2.79)$$

where f_y is the yield strength, E_s is the modulus of elasticity, E_{sh} is the strain hardening modulus, ε_y is the yield strain, ε_{sh} is the strain at start of strain hardening and ε_u is the ultimate strain.

Slip Model

The relationship used for calculate the amount of slip adopted in the DSFM was adopted from Walraven (1981), as given below:

$$\delta_s^a = \frac{\nu_{ci}}{1.8w^{-0.8} + (0.234w^{-0.707} - 0.20) \cdot f_{cc}} \quad (2.80)$$

where ν_{ci} is the shear stress along the crack surface, w is the average crack width and f_{cc} is the concrete cube strength.

2.2.3 Code Provisions

2.2.3.1 Australian Standard AS 3600-01 (2001) and Draft Australian Standard AS3600 (2005)

The Australian Standard AS3600 adopts a variable angle truss model for shear design. The shear resistance consists of concrete and steel contributions:

$$V_u = V_c + V_s \quad (2.81)$$

where

The concrete contribution, V_c , is given by

$$V_c = \beta_1 \beta_2 \beta_3 b_v d_o \left[\frac{A_{st}}{b_v d_o \times f'_c} \right]^{1/3} \quad (2.82)$$

With factors $\beta_1, \beta_2, \beta_3$ accounting for size factor of a section, axial force effects and presence of large concentrated load near support respectively.

$$\beta_1 = 1.1 \left(1.6 - \frac{d_o}{1000} \right)$$

$$\beta_2 = 1.0$$

$$\beta_3 = 1.0$$

A_{st} = cross-sectional area of longitudinal tensile steel reinforcement

b_v = effective web width

d_o = distance from the extreme compression fibre to the centroid of the outermost layer of longitudinal tensile reinforcement.

The stirrup contribution, V_s , is taken as

$$V_s = \frac{A_{sv} f_{svy} d_o}{s \cot \theta} \quad (2.83)$$

The angle of inclination of the concrete compression strut, θ , is given by

$$\theta = 30^\circ + 15^\circ \left[\frac{A_{sv} - A_{sv.min}}{A_{sv.max} - A_{sv}} \right] \quad (2.84)$$

A_{sv} = cross-sectional area of shear reinforcement

f_{svy} = yield stress of shear reinforcement

s = spacing of stirrups

With minimum and maximum shear reinforcements given by

$$A_{sv.min} = \frac{0.06 \sqrt{f'_c} b_v s}{f_{svy}} \geq \frac{0.35 b_v s}{f_{svy}} \quad (2.85)$$

$$A_{sv,max} = \frac{b_v s}{f_{svy}} \left[0.2 f'_c - \frac{V_c}{b_v d_o} \right] \quad (2.86)$$

2.2.3.2 American Concrete Institute Building Code ACI318-08

The shear resistance in the American Code consists of contributions from the concrete and steel, where

$$V_u = V_c + V_s \quad (2.87)$$

The American Code ACI318 adopts the 45° truss model with an additional term for concrete contribution, V_c , given by

$$V_c = 2\lambda\sqrt{f'_c} b_w d \quad (\text{for members subject to shear and flexure only}) \quad (2.88)$$

where

$\lambda = 1.0$ for normal weight concrete

b_v = effective web width

d = effective depth

For stirrup contribution to shear, V_s is given by:

$$V_s = \frac{A_{sv} f_{svy} d}{s} \quad (2.89)$$

where

A_{sv} = cross-sectional area of shear reinforcement

f_{svy} = yield stress of shear reinforcement

s = spacing of stirrups

2.3 Bond Strength of Lap-Spliced Bars in Beams

2.3.1 General

The bond between concrete and the reinforcing bar is an important mechanism for ensuring that the structural concrete functions effectively as a composite material. Without any bond or other mechanical connection, the steel is completely ineffective. Basically, the interaction between a reinforcing bar and the surrounding concrete generates bond resistance by three different mechanisms: chemical adhesion, mechanical friction and the bearing of the concrete against deformations or ribs on bars. The most effective way of achieving a good bond is by the use of deformed reinforcing bars instead of plain bars (Warner et al., 1998).

The stresses produced in the concrete by bearing at the deformations on the bar surface can be represented by a simplified two-dimensional force diagram as shown in Figure 2.7.

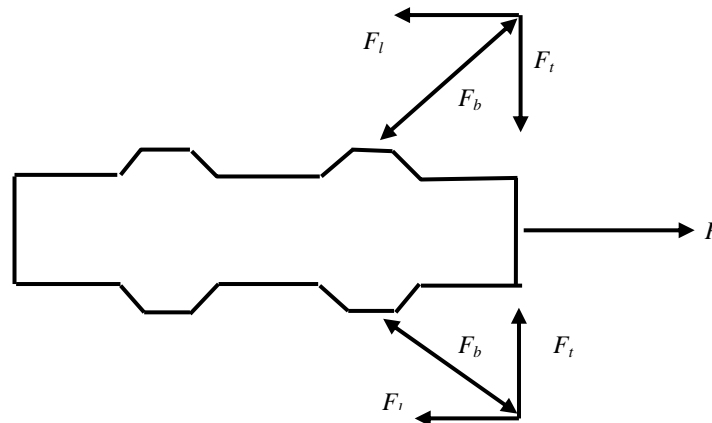


Figure 2.7: Bearing Forces and Tensile Forces in Concrete (Warner et al., 1998)

From Figure 2.7, the inclined bearing force F_b developed at a rib is equilibrated by concrete tensile forces, namely F_l in the longitudinal direction and F_t in the transverse direction. The transverse tensile forces F_t play an important role in any bond failure as they are responsible for longitudinal splitting in the concrete around the bar. Failures take

place when there is insufficient concrete to carry the transverse tensile forces. Potential splitting surfaces are shown in Figure 2.8.

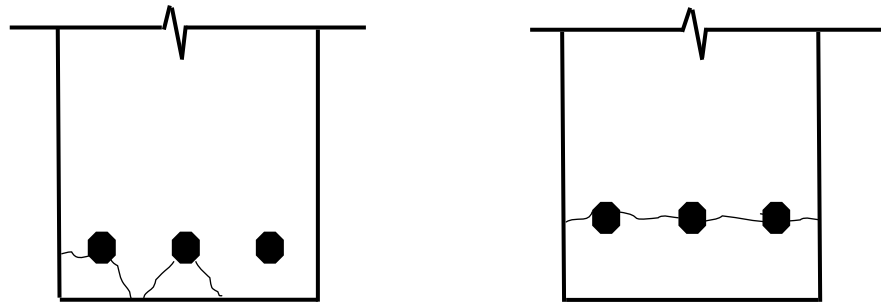


Figure 2.8(a): V-notch failure

Figure (2.8b): Split failure

Figure 2.8: Potential Splitting Surfaces (Warner et al., 1998)

Bond behaviour of concrete and reinforcing bars and the influence of different parameters on bond are generally based on empirical investigation because of the many problems involved in theoretical study. A variety of test specimen configurations have been used to study the bond between reinforcing bars and concrete, namely the pull-out test, beam-anchorage test and beam test. Beam tests are used to obtain the bond strength values for structural design purpose due to the realistic stress-state in the vicinity of bars and relative simplicity of fabrication and set-up. A typical set-up of the beam test to measure the development and splice strength directly in a full-scale member is shown in Figure 2.9:

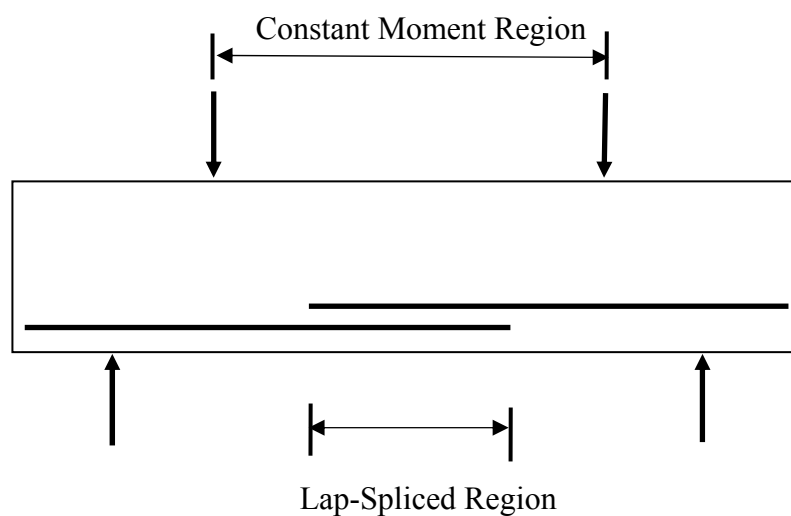


Figure 2.9: Beam Tests to Measure Bond Strength

For reinforced concrete design, it is important that the reinforcing bars are long enough to fully develop the steel stress. The minimum length of tensile reinforcing bars necessary to fully develop the yield stress, f_{sy} , is called the development length. From simple equilibrium considerations, the average bond stress u over the length L_s is given by

$$u = \frac{A_b f_{sy}}{\pi d_b L_s} \quad (2.90)$$

where A_b is the cross-sectional area of a bar and d_b is the bar diameter.

For the design of reinforced concrete structures, the lap splice of reinforcing bars is one of the practical aspects of the bond between concrete and reinforcing bars. Given the use of reinforcing bars in most reinforced concrete structures, study of the strength of lap splices is important. From test data on the calculation of development length of bars in tension (ACI408R-03, Warner et al., 1998, Orangun et al., 1977, Darwin et al., 1992, Esfahani and Rangan, 1998), the major factors that affect the development length include bar diameter and geometry, concrete cover, tensile strength of concrete, proximity of other bars, confinement by stirrups, surface coating on bars, bar casting position, yield stress of bar and concrete compressive strength.

Expressions for bond strength have been developed based on comparisons with test results using non-linear regression analysis. Recently, a theory-based analysis of the calculation of lap-spliced strength has been developed by Canbay and Frosch (2005). Some commonly used modelling approaches for predicting the bond strength of lap splices in Portland cement concrete beams are presented in the next section.

2.3.2 Modelling Approaches for Bond Strength of Lap-Spliced Bars in Beams

2.3.2.1 Canbay and Frosch (2005)

The analytical expression proposed by Canbay and Frosch is based on a physical model of the tension cracking of concrete in the lap-spliced region. The expression has been

verified using 203 unconfined test data with the splice region subjected to constant moment.

The tensile strength of concrete surrounding the bar is a major parameter that affects the development of the reinforcement for a splitting failure mode. In this model, two different splitting failure planes are assumed: side splitting and face splitting. Side splitting occurs when a horizontal split develops at the level of the bars, as shown in Figure 2.10. Face splitting occurs when a vertical split develops below the bars, as shown in Figure 2.11. A bond model to calculate the bond strength has been developed considering the two splitting failure modes. For simplicity, the tensile stresses are assumed to be uniformly distributed along the splice length and failure is assumed to occur when the concrete in the entire splice region reaches its tensile capacity.

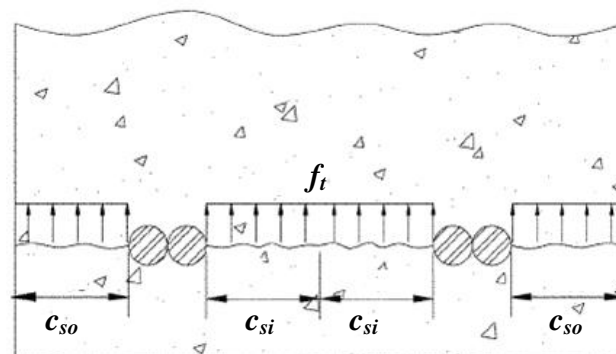


Figure 2.10: Side Splitting Failure (Canbay and Frosch, 2005)

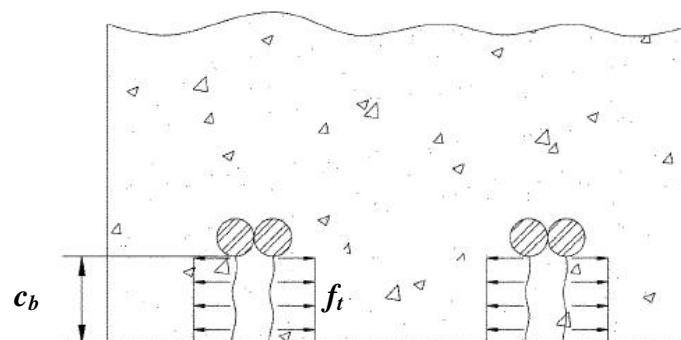


Figure 2.11: Face Splitting Failure (Canbay and Frosch, 2005)

For side splitting failure, the force required to cause splitting can be calculated by the following equation:

$$F_{splitting} = L_s [2c_{so} + (n-1)2c_{si}] f'_{ct} \quad (2.91)$$

where

n = numbers of bars being spliced

L_s = lap-spliced length

f'_{ct} = concrete tensile strength

$$= 6\sqrt{f'_c} \text{ (psi)}$$

In the case of face splitting failure, the force to cause splitting is given by using Equation 2.92:

$$F_{splitting} = L_s (2c_b n) f'_{ct} \quad (2.92)$$

In this model, the splitting force is the radial component of the force applied on the concrete by the reinforcing bars. These radial forces are generated by the longitudinal bar forces as below:

$$F_{long} = \sum A_b f_b \quad (2.93)$$

The geometrical relationship between the radial force, $F_{splitting}$, and the longitudinal force, F_{long} , can be found in Figure 2.12.

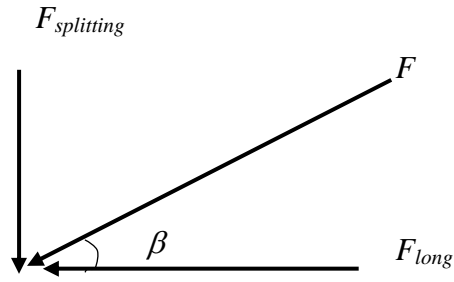


Figure 2.12: Relationship between longitudinal and splitting forces

The angle β can be calculated by

$$\tan \beta = \frac{F_{splitting}}{F_{long}} \quad (2.94)$$

The steel stress at splitting failure can be calculated using Equation 2.95:

$$f_b = \frac{F_{splitting}}{\sum A_b \tan \beta} \quad (2.95)$$

The bond stress is then calculated by

$$u = \frac{f_b d_b}{4L_s} \quad (2.96)$$

A detailed analysis incorporating the effect of primary variables affecting stress distribution was carried out by Canbay and Frosch to improve the model. It was found that the concrete cover, splice length, tensile strength of concrete and the inclination of cracks significantly affect splice behaviour. By incorporating the effect of variables

determined from the detailed analysis, the bond strength can be estimated using the following calculation steps and equations.

Calculation Steps:

Step 1: Calculating the effective cover by using Equation 2.97:

$$c_b^* = c_b \frac{0.77}{\sqrt{c_b/d_b}} ; c_{so}^* = c_{so} \frac{0.77}{\sqrt{c_{so}/d_b}} ; c_{si}^* = c_{si} \frac{0.77}{\sqrt{c_{si}/d_b}} \quad (2.97)$$

where

$$\frac{0.77}{\sqrt{c/d_b}} \leq 1.0$$

Step 2: Calculating the effective length by using Equation 2.98:

$$L_s^* = L_s \frac{33}{\sqrt{L_s/d_b} \times \sqrt[4]{f'_c}} \quad (2.98)$$

where

$$\frac{33}{\sqrt{L_s/d_b} \times \sqrt[4]{f'_c}} \leq 1.0$$

Step 3: Calculating the splitting force.

For side splitting failure, the splitting force is calculated using Equation 2.99:

$$F_{splitting} = L_s^* [2c_{so}^* + (n-1)2c_{si}^*] \times 6\sqrt{f'_c} \quad (2.99)$$

For face splitting failure, the splitting force is calculated using Equation 2.100:

$$F_{splitting} = L_s \left[2c_b^* \left(0.1 \frac{c_{so}}{c_b} + 0.9 \right) + 2c_b^* (n-1) \left(0.1 \frac{c_{si}}{c_b} + 0.9 \right) \right] \times 6\sqrt{f'_c} \quad (2.100)$$

where

$$\left(0.1 \frac{c_s}{c_b} + 0.9 \right) \geq 1.0$$

Step 4: Calculating the steel stress

$$f_b = \frac{F_{splitting}}{nA_b \tan \beta} \quad (2.101)$$

For the splitting force, the lower value of splitting force from side or face splitting should be used. The angle β is assumed to be 20 degrees to provide the optimal result from model calibration.

Step 5: Calculating the bond stress using Equation 2.96 as mentioned previously.

2.3.2.2 Esfahani and Rangan (1998)

Esfahani and Rangan (1998) conducted studies on local bond and bond strength of splices in normal strength concrete (NSC) and high strength concrete (HSC). For local bond, Tepfers (1973) partly cracked thick cylinder theory was used and modified to account for the variation of bursting angle and tensile plastic deformation of the concrete cylinder. The bond strength of splices was studied by using displacement theory based on the linear relationship between bond stress and slip. The influences of the length and different ratios between the bottom cover, side cover, and spacing between spliced bars and concrete

strength on the bond stress distribution and the bond strength were accounted for. By analysing past test results of splices in normal strength concrete, an analytical model was developed to predict the splice strength in NSC and HSC using a modified local bond theory and displacement theory.

The bond strength of splice in beams, u_m , can be determined using the following equation:

$$u_m = u_c \left(\frac{1 + 1/M}{1.85 + 0.024\sqrt{M}} \right) (0.88 + 0.12 \frac{c_{med}}{c_{min}}) \quad (2.102)$$

where

For $f'_c < 50\text{MPa}$, average bond stress u_c can be calculated using Equation 2.103:

$$u_c = 2.7 \frac{c_{min}/d_b + 0.5}{c_{min}/d_b + 3.6} \sqrt{f'_{ct}} \quad (2.103)$$

For $f'_c > 50\text{MPa}$,

$$u_c = 4.7 \frac{c_{min}/d_b + 0.5}{c_{min}/d_b + 5.69} \sqrt{f'_{ct}} \quad (2.104)$$

$$M = \cosh(0.0022L_s \sqrt{3 \frac{f'_c}{d_b}}) \quad (2.105)$$

where

- u_c = average bond stress
- f'_c = concrete compressive strength
- c_{min} = minimum ($c_b, c_{so}, c_{si} + d_b/2$)

c_{med}	=	median ($c_b, c_{so}, c_{si} + d_b/2$)
c_b	=	bottom cover
c_{so}	=	clear side cover
c_{si}	=	half of the clear spacing between bars
d_b	=	bar diameter
L_s	=	development or splice length.

2.3.2.3 Orangun et al (1977)

By using nonlinear regression analysis of test results, Orangun et al. (1977) developed expressions to describe the bond strength of bars with and without confining transverse reinforcement, as given in Equation 2.106 (in SI units). The regression analysis is based on 62 beams, including 57 with bottom-cast bars, 1 with top-cast bars and 4 with side-cast bars. This expression reflects the effect of concrete strength, cover, bar diameter, splice length and the transverse reinforcement on the strength of anchored bars. This expression also forms the basis for the bond requirement of the current ACI318 Building Code.

$$u = 0.084\sqrt{f'_c} \left(1.22 + 3.23 \frac{c_{min}}{d_b} + 53 \frac{d_b}{L_s} \right) \quad (2.106)$$

where

u	=	average bond stress
f'_c	=	concrete compressive strength
c_{min}	=	smaller of minimum concrete cover or half of the clear spacing between bars
L_s	=	development or splice length
d_b	=	bar diameter

2.3.2.4 Zuo and Darwin (2000)

Zuo and Darwin propose a new expression that represents the development or splice strength of bottom-cast uncoated bars as a function of concrete strength, member geometry, bar size, relative rib area and confinement provided by both concrete and transverse reinforcement. They expand the work of Darwin et al. (1996a) by evaluating the effects of concrete strength, reinforcing bar geometry, coarse aggregate quantity and type on splice strength. This design recommendation applies to both conventional and high relative rib area reinforcement. The database used for regression analysis includes 171 bottom-cast unconfined test specimens. The expression is given by using the following equation:

$$\frac{A_b \times f_s}{\sqrt[4]{f'_c}} = [59.8L_s(c_{\min} + 0.5d_b) + 2350A_b] \left(0.1 \frac{c_{\max}}{c_{\min}} + 0.9\right) \quad (2.107)$$

where

A_b	=	area of bar (in ²)
c_{\min}, c_{\max}	=	minimum or maximum value of c_s or c_b (in)
c_s	=	$\min(c_{si}+0.25, c_{so})$ (in)
c_{si}	=	half of the clear spacing between bars (in)
c_{so}	=	clear side cover of the reinforcing bars (in)

2.3.2.5 ACI Committee 408

The Committee has updated the expression by Zuo and Darwin (2000) with only minor changes using ACI 408 Database 10-2001 which consists of 478 bottom-cast tests as given in Equation 2.108:

$$\frac{A_b \times f_s}{\sqrt[4]{f'_c}} = [59.9L_s(c_{\min} + 0.5d_b) + 2400A_b] \left(0.1 \frac{c_{\max}}{c_{\min}} + 0.9\right) \quad (2.108)$$

with the same notation used for Zuo and Darwin (2000).

2.3.3 Code Provisions

2.3.3.1 Australian Standard AS3600-01 (2001)

The equation for the development length of a deformed bar in tension in the AS3600-01 was developed in the early 1980s. It is based on the bond strength of test beams provided with lap splices for bars in tension, and on the assumption that the development stress in tension is the same as the bond stress that develops in lap splices. This is in contrast to other codes and standards such as ACI 318, where the basic value for development length in tension must be multiplied by a factor greater than unity to obtain the required splice length (Warner et al., 1998).

According to AS3600-01, a check must be made for each cross section in bending to ensure that the yield strength f_{sy} can be developed on each side of that cross section. The development length $L_{sy,t}$ required to develop the yield stress of a deformed bar in tension is given by using Equation 2.109:

$$L_{sy,t} = \frac{k_1 k_2 f_{sy} A_b}{(2c + d_b) \sqrt{f'_c}} \geq 25k_1 d_b \quad (2.109)$$

where the factor k_1 accounts for the bar location, with $k_1 = 1.25$ for the horizontal bar with more than 300 mm of concrete cast below it, and $k_1 = 1.0$ for all other bars. The factor k_2 depends on the type of concrete member in which the bar is used for reinforcing, and also on the resulting mode of bond failure. For bars in slabs and walls, the common mode of failure is a “V-notch failure” (Figure 2.8a) and the value of k_2 is 1.7, provided that the clear spacing of the bars is not less than 150 mm. The value of k_2 is taken as 2.4 for closer spacings where a “splitting failure” (Figure 2.8b) may occur. For the case of beams and columns, the common mode of failure is a “splitting failure” type. Depending on the

presence of transverse reinforcement, the value of k_2 is 2.2 when transverse reinforcement is present and 2.4 when it is not.

The minimum value of $25k_1d_b$ at the right hand side of Equation 2.109 ensures that premature pull-out failure of the bar is prevented.

Rearranging the above formula with the value of k_1 and k_2 yields

$$L_{sy,t} = \frac{A_b f_{sy}}{\pi d_b u} = \frac{2.4 f_{sy} A_b}{(2c + d_b) \sqrt{f'_c}} \quad (2.110)$$

$$u_{AS3600-01} = 0.265(c/d_b + 0.5) \sqrt{f'_c} \quad (2.111)$$

2.3.3.2 Draft Australian Standard AS3600 (2005)

A simplified and a refined approach is proposed to calculate the development length in tension in the draft AS3600 (2005). In the simplified approach, the development length in tension $L_{st,t}$ is taken to as the basic development length $L_{st,db}$ as given by the following equation:

$$L_{st,db} = \frac{0.5k_1 f_{sy} d_b}{\sqrt{f'_c}} \quad (2.112)$$

The factor k_1 accounts for the bar location where $k_1 = 1.3$ for horizontal bar with more than 300 mm of concrete cast below the bar or $k_1 = 1.0$ for all other bars.

The refined approach is similar to the approach used in Eurocode 2 as given by the following equation:

$$L_{sy,t} = k_2 k_3 k_4 L_{st.tb} \quad (\geq 300 \text{ mm}) \quad (2.113)$$

The parameters k_2 , k_3 and k_4 are the modification factors that account for confinement, taken from Eurocode 2. The parameter k_2 can be determined from the following equation:

$$k_2 = 1.0 - \frac{0.15(c_d - d_b)}{d_b} \quad 0.7 \leq k_2 \leq 1.0 \quad (2.114)$$

where c_d is the smaller of the concrete cover to the deformed bar or half the clear distance to the next parallel bar, provided at least 3 transverse bars are located within the development length.

Factors k_3 and $k_4 = 1.0$ for bars without confinement by transverse reinforcement.

Rearranging the formula with appropriate k values lead to the following expression for bond strength:

$$u = \frac{d_b f_{sy}}{4L_s} = \frac{d_b f_{sy}}{4 \left(\frac{0.5 k_2 f_{sy} d_b}{\sqrt{f'_c}} \right)} \quad (2.115)$$

$$u_{AS3600 \text{ Draft}} = \frac{\sqrt{f'_c}}{2k_2} \quad (2.116)$$

2.3.3.3 American Concrete Institute Building Code ACI318-08 (2008)

The design provisions in ACI318-08 for development and splices are based on the bond stress equation developed by Orangun et al. (1977). The ACI provision is also applicable for concrete strengths up to 70MPa. A two-tiered approach is adopted with the refined approach, including the beneficial effects of transverse reinforcement.

In the refined method, the development length for deformed bars is given by

$$L_d = \left(\frac{3}{40} \frac{f_{sy}}{\lambda \sqrt{f'_c}} \frac{\alpha \beta \gamma}{\left(\frac{c_b + K_{tr}}{d_b} \right)} \right) d_b \quad (2.117)$$

with the confinement term $\left(\frac{c_b + K_{tr}}{d_b} \right) < 2.5$

Rearranging the above, the average bond stress (MPa) at ultimate is given by

$$u_{ACI318-08} = \frac{0.277 \sqrt{f'_c}}{\alpha \beta \gamma \lambda} \left(\frac{c + K_{tr}}{d_b} \right) \quad (2.118)$$

where

$\alpha = 1.0$ for bottom bar casting

$\beta = 1.0$ for uncoated reinforcement

$\gamma = 0.8$ for $d_b \leq 20$ mm and $\gamma = 1.0$ for $d_b > 20$ mm;

$\lambda = 1.0$ for normal weight concrete

c = smaller of the distance from the centre of the bar to the nearest concrete surface and one half of the centre-to-centre spacing of bars being developed.

The term K_{tr} is the transverse reinforcement index (in mm) and is calculated from

$$K_{tr} = \frac{A_{sv} f_{svy}}{10.34 s n_b} \quad (2.119)$$

where

A_{sv} = the total cross-sectional area of all transverse reinforcement within the spacing

s = the maximum spacing of the transverse reinforcement within L_s

n_b = the number of bars being developed along the plane of splitting.

2.3.4 Summary

The geopolymer technology has shown considerable promise for application in the concrete industry as an alternative binder to Portland cement. The low calcium fly ash-based geopolymer concrete has excellent engineering properties and is suitable for structural applications. However, to date, there has been limited research conducted on full-scale structural members using fly ash-based geopolymer concrete.

In the following chapters, the shear and bond behaviour of full-scale geopolymer concrete beams is studied. The analytical models and code provisions used for Portland cement concrete as described in Section 2.2 and Section 2.3 will be used to calculate the shear and bond strength of geopolymer concrete beams in this study.

SECTION ONE
SHEAR BEHAVIOUR OF REINFORCED
FLY ASH-BASED GEOPOLYMER
CONCRETE BEAMS

CHAPTER 3

MANUFACTURE AND TESTING OF BEAMS FOR SHEAR STUDY

This chapter describes the details of the experimental work designed to investigate the behaviour of reinforced fly ash-based geopolymer concrete beams failing in shear. Details of the test beams, materials, the manufacture of specimens, test set-up, instrumentation and test procedure are presented.

3.1 Experimental Aims

The experimental program was developed to study the shear behaviour of geopolymer concrete beams. The aims of the study were to:

- investigate the failure modes and crack patterns of geopolymer concrete beams
- study the effect of longitudinal tensile reinforcement ratio on the shear strength of geopolymer concrete beams
- compare the test shear strength of geopolymer concrete beams with predictions made using analytical models for Portland cement concrete beams
- obtain the load-deflection curves of the beams

3.2 Design of Test Specimens

A total of nine beams, each with a rectangular cross section of 200 mm x 300 mm and length of 2000 mm, were cast. The size of test specimen was selected to suit the capacity of the testing machine in the laboratory. The beams were designed to fail in shear according to draft Australian Standards AS3600 (2005). Initial strength calculations were performed by varying reinforcement ratios to obtain shear failures instead of flexural failures.

The beams were divided into three series according to the longitudinal tensile reinforcement ratio:

- Series 1 with longitudinal reinforcement of two N24mm bars ($p_{sl} = 1.74\%$);
- Series 2 with longitudinal reinforcement of two N28mm bars ($p_{sl} = 2.32\%$);
- Series 3 with longitudinal reinforcement of two N32mm bars ($p_{sl} = 3.14\%$).

Three transverse reinforcement ratios were obtained by varying the stirrup spacing, which were 125mm, 100mm and 75mm, giving transverse reinforcement ratios, p_{sv} of 0.10%, 0.13% and 0.17% respectively.

All the longitudinal reinforcements were deformed bars, used in Australian practice with the designation “N”, designed to provide minimum yield strength of 500MPa. Lateral reinforcement consisted of smooth wire (nominal diameter 4mm) with the designation “W”, according to Australian practice, and designed to achieve a minimum yield strength of 500MPa.

The concrete clear cover to reinforcement was 25mm for all faces. The beam details are given in Table 3.1. The cross-section and elevation view of beams for Series 1, Series 2 and Series 3 are shown in Figure 3.1, Figure 3.2 and Figure 3.3 respectively.

Table 3.1: Details of the Test Beams for Shear Study

Series	Beam Mark	b (mm)	d (mm)	Longitudinal Reinforcement		p_{sl} Ratio (%)	Transverse Reinforcement Spacing (mm)	p_{sv} Ratio (%)
				Top	Bottom			
1	S1-1	200	259	2N12	2N24	1.74	125	0.10
	S1-2	200	259	2N12	2N24	1.74	100	0.13
	S1-3	200	259	2N12	2N24	1.74	75	0.17
2	S2-1	200	257	2N12	2N28	2.32	125	0.10
	S2-2	200	257	2N12	2N28	2.32	100	0.13
	S2-3	200	257	2N12	2N28	2.32	75	0.17
3	S3-1	200	255	2N16	2N32	3.14	125	0.10
	S3-2	200	255	2N16	2N32	3.14	100	0.13
	S3-3	200	255	2N16	2N32	3.14	75	0.17

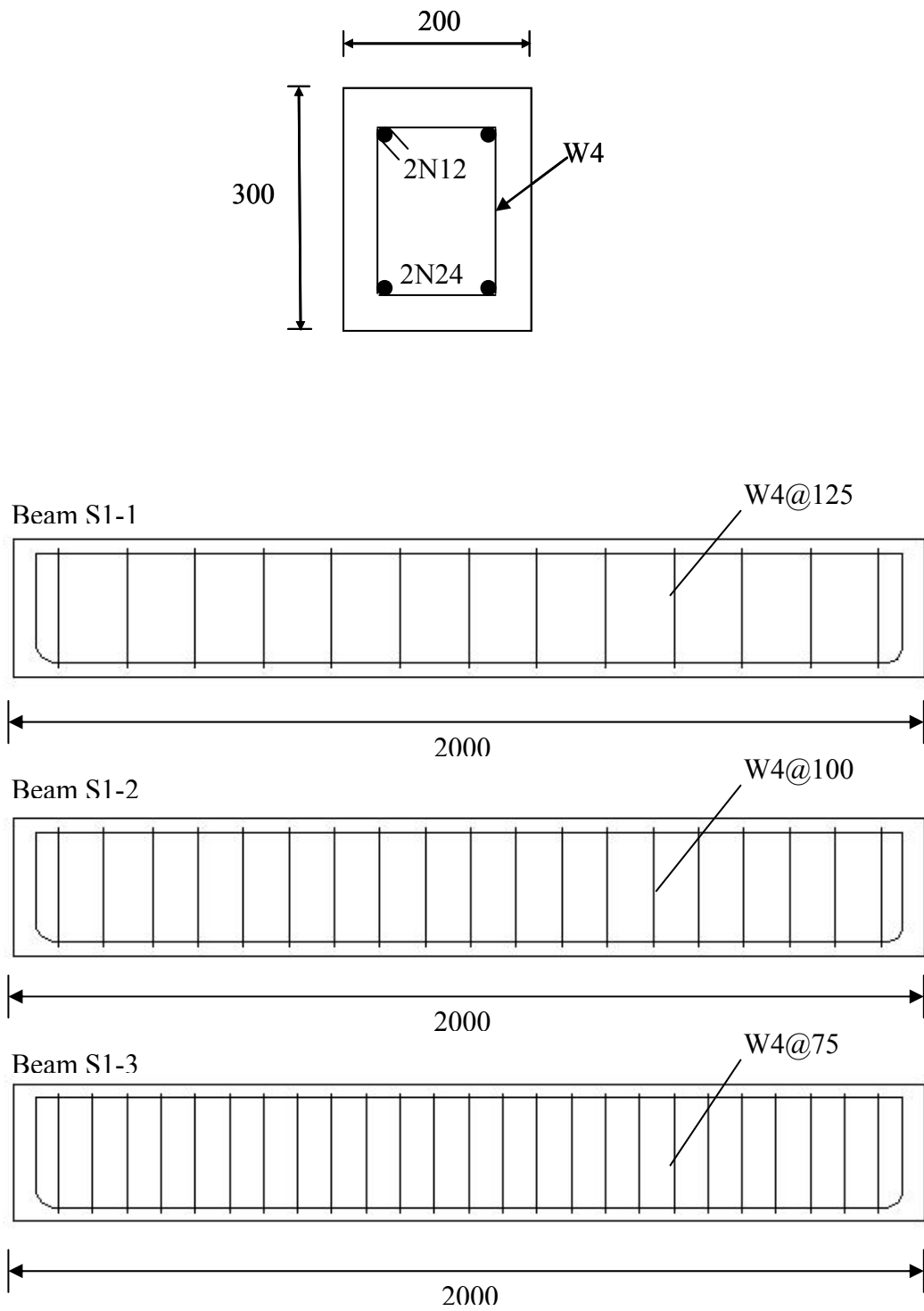


Figure 3.1: Cross-section and Elevation View of Beams for Series 1

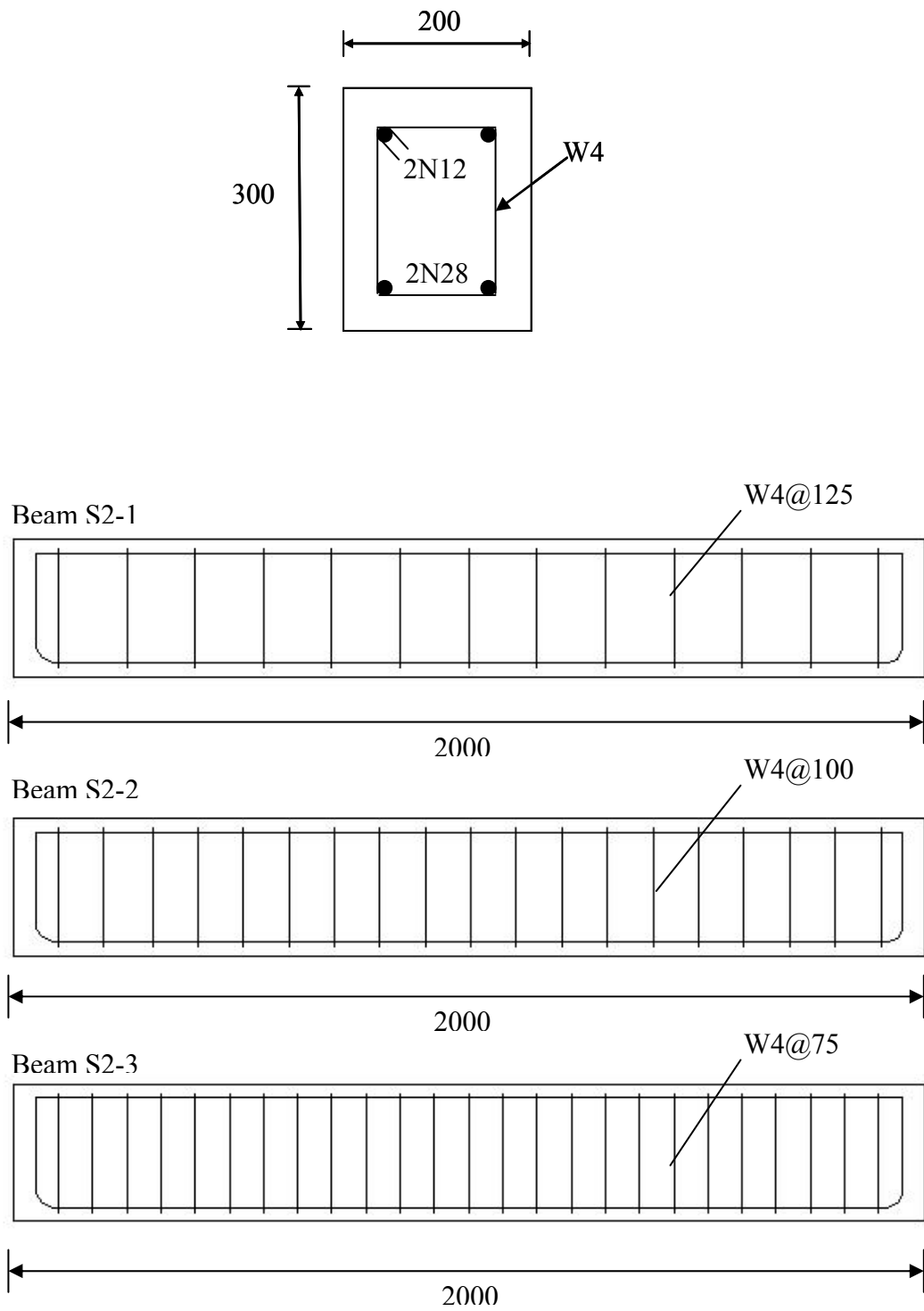


Figure 3.2: Cross-section and Elevation View of Beams for Series 2

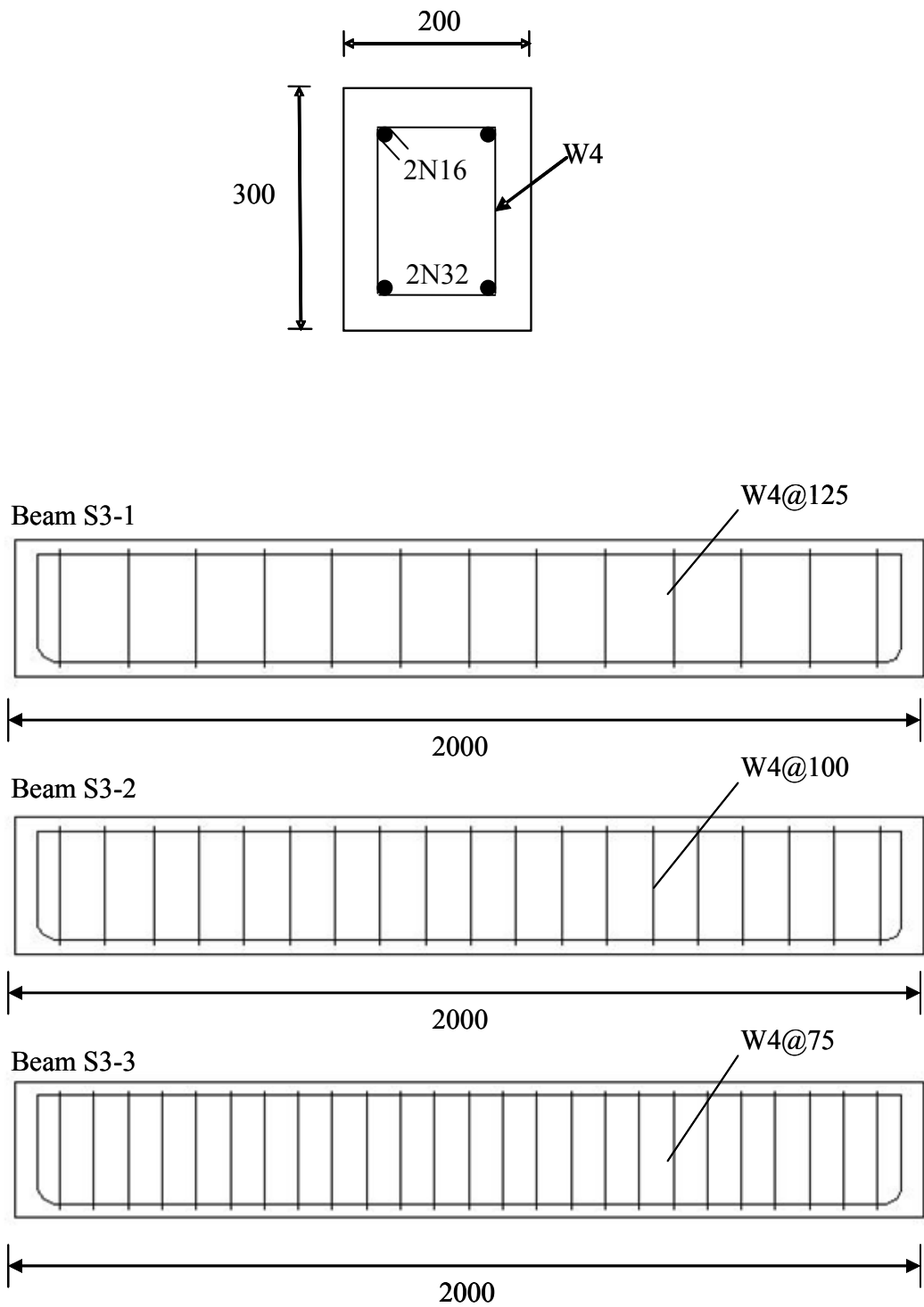


Figure 3.3: Cross-section and Elevation View of Beams for Series 3

3.3 Materials

3.3.1 Aggregates

The aggregates used in this study comprised three locally available aggregates used by the concrete industry in Western Australia. For the coarse aggregates, sizes of both 10mm and 7mm were used. They were classified as single sized, which denotes relatively few sizes of particles (Ryan and Samarin, 1992), crushed, granite type; and they were supplied by BGC Concrete and Asphalt. The fine aggregate was supplied by Rocla, and termed “concrete sand” in uncrushed form.

According to Australian Standards AS 1141.5-2000 and AS 1141.6.1-2000, the aggregates are to be soaked for 24 hours and left to drain until they reach Saturated Surface Dry (SSD) condition. Due to the large quantity of aggregates are needed for each concrete pour, it was not viable to use this method. As a result, the aggregates were sprayed with water at the stockpile outside the laboratory and transferred onto trays to allow the excess water to evaporate. Samples of the aggregates were taken from trays and placed into an oven for 24 hours to determine moisture content. Once the moisture content was determined, the water content of the wet mix could be adjusted to the appropriate design mix.

The moisture content (*M.C.*) of the aggregates was calculated using the following equation:

$$M.C. = \frac{M_{water}}{M_{sample}} \times 100 \quad (3.1)$$

Where

M_{water} = Mass of water obtained from a sample after being left in an oven for 24 hours (grams)

M_{sample} = Mass of the sample of aggregate before placing into the oven (grams)

The moisture content of the aggregates obtained was then compared to the moisture content of the samples of aggregates prepared for SSD moisture conditions. From samples of aggregates prepared, the SSD moisture conditions for aggregates were obtained and summarised in Table 3.2. These values were used to adjust the added water content in all the mix designs. Further information on calculation of the moisture content of aggregates and adjusted added water content of the mix design for each pour can be found in Appendix A1.

Table 3.2: SSD Moisture Conditions for Aggregates

Aggregate	Moisture Content (%)
10 mm Aggregate	0.3 % ± 0.04
7 mm Aggregate	0.5 % ± 0.05
Sand	0.7 % ± 0.09

The grading combination of the aggregates is shown in Table 3.3. The fineness modulus of the combined aggregates was 4.5.

Table 3.3: Grading Combination of Aggregates

Sieve Size	Aggregates			Combination* (% Passing)	BS 882:1992
	10mm	7mm	Fine Sand		
14	100	100	100	100.00	100
10	74.86	99.9	100	92.42	95-100
5	9.32	20.1	100	44.83	30.65
2.36	3.68	3.66	100	37.39	20-50
1.18	2.08	2.05	99.99	36.34	15-40
No. 600	1.47	1.52	79.58	28.83	10-30
No. 300	1.01	1.08	16.53	6.47	5-15
No. 150	0.55	0.62	1.11	0.77	0-18

* 30% (10mm) + 35% (7mm) + 35% (fine sand)

3.3.2 Fly Ash

All of the fly ash used in this study was low calcium, Class F (ASTM C618) dry fly ash obtained from the Collie Power Station, Western Australia. An X-Ray Fluorescence (XRF) Analysis was performed to determine the chemical composition of the fly ash. The test was carried out at the Department of Applied Chemistry, Curtin University of Technology, Perth, Western Australia.

The chemical composition of the fly ash is given in Table 3.4. The fly ash had low calcium oxide content and very low carbon content, as indicated by the Loss on Ignition (LOI) values.

The test for determining particle size distribution of the fly ash was carried out by CSIRO Minerals, Waterford, Western Australia, using the Malvern Instrument

Mastersizer MS2000. The particle size distribution of the fly ash is given in Figure 3.4. The particle size distribution in percentage by volume in interval is shown in graph A; graph B shows the particle size distribution in percentage by volume passing size.

Table 3.4: Chemical Composition of Fly Ash (mass %)

SiO ₂	Al ₂ O ₃	Fe ₂ O ₃	CaO	Na ₂ O	K ₂ O	TiO ₂	MgO	P ₂ O ₅	SO ₃	H ₂ O	LOI*
48.0	29.0	12.7	1.76	0.39	0.55	1.67	0.89	1.69	0.5	-	1.61

* Loss on ignition

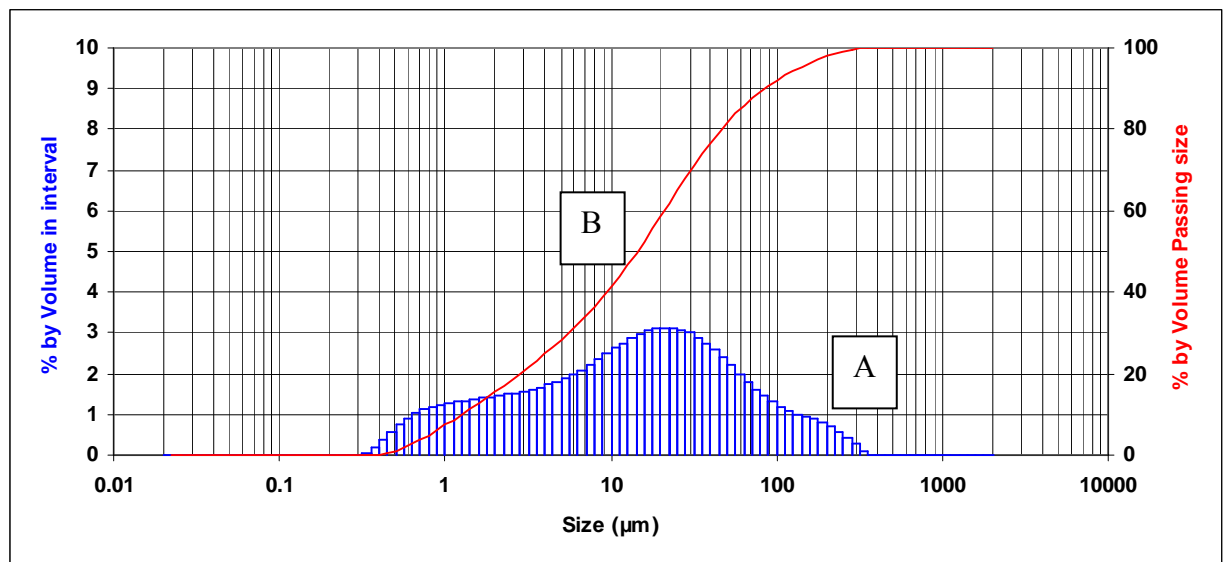


Figure 3.4: Particle Size Distributions of Fly Ash

3.3.3 Alkaline Liquid

The alkaline liquid used was a combination of sodium hydroxide and sodium silicate solution. The sodium hydroxide (NaOH) solution was made by dissolving NaOH solids (pellet form) in water. The NaOH pellets were commercial grade with 97% purity obtained from Lomb Scientific, Australia. The amount of NaOH solids in a solution can vary depending on the concentration of solution needed. The

concentration of the solution is expressed in terms of Molarity, M. In this study, only a concentration of 14M is used. For a 14M concentration, 560 grams of sodium hydroxide pellets are needed for one litre of solution, which is equivalent to 404 grams of NaOH solids per kg of the solution.

The NaOH solution was prepared by dissolving the NaOH pellets into distilled water and stirring under the fume hood until the solution became clear. The NaOH solution was prepared at the chemistry laboratory at Curtin University. As heat is generated when dissolving NaOH pellets, the NaOH solution is prepared at least one day prior to use.

The sodium silicate solution used was Grade A53 obtained from Swift & Company Limited, Australia. The chemical composition consisted of 14.7% Na₂O, 29.4% SiO₂ and 55.9% H₂O by mass. The specific gravity was 1.53g/cc and the viscosity at 20°C was 300cp. The ratio of SiO₂ to Na₂O was 2.0.

3.3.4 Superplasticiser

A naphthalene sulphonate superplasticiser was used to improve the workability of the fresh geopolymer concrete. It was supplied by Degussa, Perth, Australia, with the brand name of RHEOBUILD 1000.

3.4 Mixture Proportions for Geopolymer Concrete

Several trial mixes were conducted using the mixture proportions given by Sumajouw and Rangan (2006). The aims of conducting the trial mixes were:

- to become familiar with the preparation of materials, equipment and manufacturing processes involved in making geopolymer concrete
- to observe the workability of fresh geopolymer concrete for its suitability in casting structural members

- to obtain the mean compressive strength of 40MPa for this study
- to check the number of rest days needed to achieve the desired compressive strength
- to ensure consistency of results prior to casting the beam specimens

From the trial mixes, the mixture designated GP1 was selected. The details of the mixture's proportions are given in Table 3.5. It was found that good consistency of workability was achieved as indicated from slump tests. The average slump was 250mm. A compressive strength of 40MPa was obtained with steam curing for 24 hours at 60°C and no rest days prior to curing. Further details of the trial mixes are given in Appendix B1.

Table 3.5: Mixture Proportions of Geopolymer Concrete (GP1)

Material	Mass (kg/m ³)
Aggregate 10mm	551
Aggregate 7mm	643
Sand	643
Fly Ash	406
Sodium Hydroxide Solution (14M)	41
Sodium Silicate Solution	103
Superplasticiser	6.1
Extra added water	25.6

3.5 Properties of Reinforcement

All the reinforcement used in this study was standard deformed bar with a minimum yield strength of 500MPa. In order to obtain the actual yield strength and ultimate strength of the reinforcement, three sample bars from the same batch of steel were tested for each bar size in the laboratory. It was found that the yield strength was more than 500MPa for all the bars. A summary of the test results is given in Table 3.6 and Table 3.7, and shows the mean value with the range. These results will be used in the calculation and analysis of the beams presented in Chapter 4 and Chapter 5.

Table 3.6: Longitudinal Reinforcement Properties

Nominal Diameter (mm)	Nominal Area (mm ²)	Yield Strength (MPa)	Ultimate Strength (MPa)
12	110	570 ± 6	699 ± 7
16	200	563 ± 5	669 ± 5
24	450	559 ± 5	651 ± 3
28	620	560 ± 3	662 ± 4
32	800	571 ± 6	664 ± 5

Table 3.7: Transverse Reinforcement Properties

Nominal Diameter (mm)	Nominal Area (mm ²)	Yield Strength (MPa)	Ultimate Strength (MPa)
4	12.6	597 ± 2	658 ± 2

3.6 Manufacture of Test Specimens

The manufacturing process of all the test specimens was based on a study by Sumajouw and Rangan (2006). The following section describes the manufacturing process, including mould preparation, mixing, casting, steam curing and the de-moulding of test specimens.

3.6.1 Mould Preparation

The steel moulds for the beam specimens were designed specifically for the manufacture of the test specimens. It was fabricated externally and supplied to the laboratory. Silicon was placed along all joints to ensure imperviousness of the mould. A water-based release agent with the brand name of VALSOF PE-40 was applied to the surfaces of the mould and to all the cylinder moulds to assist in de-moulding the specimens. Figure 3.5 shows the assembled mould ready to cast the beam specimens.



Figure 3.5: Mould for Beam Specimens

3.6.2 Reinforcement Cage

A typical reinforcement cage is shown in Figure 3.6. The longitudinal reinforcement bars were supplied with 90° cogs at each end. The transverse reinforcements were two-legged vertical stirrups anchored in the compression zone by 135° hooks. Both the longitudinal reinforcement and transverse reinforcement were tied using 2mm diameter twisted wire. Bar chairs of 25mm were used to secure the steel cages to the sides and bottom of the moulds.



Figure 3.6: Reinforcement Cage

3.6.3 Mixing

The materials used for making geopolymer concrete have been described in Section 3.3. The fly ash, coarse and fine aggregates were prepared and stored in bins until the day of casting. Figure 3.7 shows the materials prepared in bins ready to make a batch of fly ash-based geopolymer concrete.



Figure 3.7: Materials for making Fly Ash- Based Geopolymer Concrete

For mixing, a rotating pan mixer of 70 litres' capacity with fixed blades, as shown in Figure 3.8, was used. Because of the limited capacity of pan mixer, four batches of concrete were prepared to cast two beam specimens.

The fly ash, coarse aggregates (10mm and 7mm) and sand were first mixed dry in the laboratory pan mixer for about three minutes. At the end of this mixing, the alkaline liquid, together with the superplasticiser and the extra water, were mixed together and added to the dry mixture. The mixing continued for another four minutes. After mixing, a slump test was used to measure the workability of every batch of geopolymer concrete. The slump test readings indicated that consistency was achieved for the different batches of concrete mixture. The summary of the average slump values with the range from four batches is given in Table 3.8.



Figure 3.8: Pan Mixer

The fresh geopolymer concrete was dark in colour and cohesive, as shown in Figure 3.9, and similar to what was observed in trial mixes in the study by Hardjito and Rangan (2005).



Figure 3.9: Fresh Geopolymer Concrete

Once the geopolymer concrete was completely mixed, it was immediately cast into the moulds for beam specimens and cylinder test specimens. The fresh geopolymer concrete was placed into the mould in layers. A stick internal vibrator was used to compact the fresh geopolymer concrete in the mould as shown in Figure 3.10.



Figure 3.10: Casting and Compacting Geopolymer Concrete

For each batch of concrete, three 100mm x 200mm diameter cylinders were also cast. All the cylinders were compacted and cured in the same manner as the beams, and were tested at the same time as the beam tests. The cylinders were tested in accordance to Australian Standards 1012.9 (1999) using a 2000kN capacity Farnell hydraulic testing machine in the laboratory. They were loaded until failure at a loading rate of 160kN/min. The average cylinder compressive strength with the range and age of the hardened concrete are given in Table 3.8.

Table 3.8: Concrete Properties of Geopolymer Concrete

Series	Beam Mark	Slump (mm)	Compressive Strength (MPa)	Age (Days)
1	S1-1	255 ± 5	45 ± 4	47
	S1-2	255 ± 5	45 ± 4	50
	S1-3	257 ± 6	44 ± 4	39
2	S2-1	250 ± 4	56 ± 6	72
	S2-2	255 ± 6	50 ± 4	56
	S2-3	255 ± 6	50 ± 4	56
3	S3-1	240 ± 5	49 ± 5	63
	S3-2	240 ± 5	49 ± 5	64
	S3-3	250 ± 4	56 ± 6	72

3.6.4 Steam Curing

After casting, both the beam specimens and the cylinders were covered with plastic sheeting to avoid condensation over the concrete. Figure 3.11 shows a typical set-up for the steam curing chamber. The steam hose and digital thermocouple were securely tied to the frame using twist wire.



Figure 3.11: Typical Set-up of Steam Curing Chamber

A steam boiler system with digital temperature control and thermocouple was used to deliver steam and maintain the temperature inside the steam curing chamber. Steam was automatically delivered through the solenoid valve controlled by the digital controller to obtain the desired temperature set. The steam boiler system is shown in Figure 3.12.



Figure 3.12: Steam boiler system

Figure 3.13 shows a complete set-up of the steam curing chamber. All specimens were cured for 24 hours at 60°C.



Figure 3.13: Complete Set-Up of Steam Curing Chamber

After curing, all specimens were removed from the chamber, de-moulded, and left in ambient conditions in the laboratory until the time of testing, as shown in Figure 3.14.



Figure 3.14: De-moulded Beams in Laboratory

3.7 Test Set-up and Instrumentation

All beams were simply supported over a span of 1680mm. The beams were tested and loaded to failure by a 2500 kN capacity Universal test machine in the laboratory. Figures 3.15 and 3.16 show the loading configuration and a typical test set-up for each test specimen.

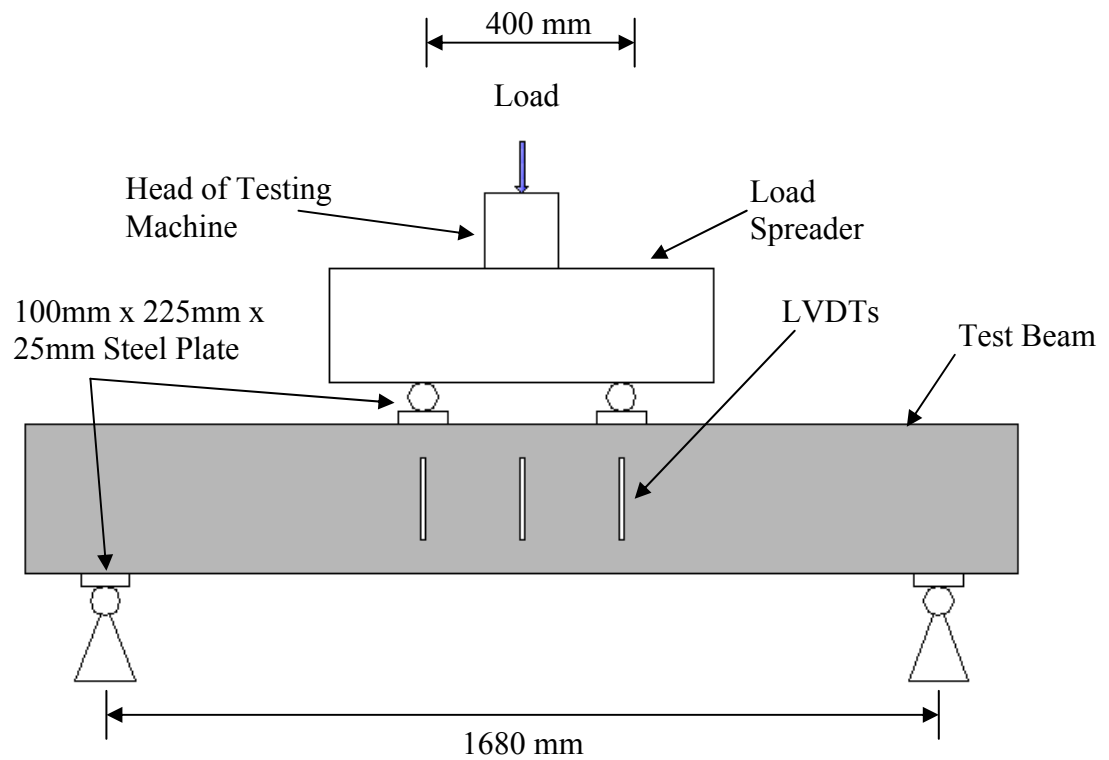


Figure 3.15: Loading Arrangement for Beam Tests



Figure 3.16: Typical Test Set-Up for Beam Tests

Three Linear Variable Differential Transducers (LVDTs) were used to measure the vertical deflections of test beams. A 100mm plunger travel LVDT was located at the mid-span, while two 50mm plunger travel LVDTs were placed at the centre of shear spans, as shown in Figure 3.17.



Figure 3.17: LVDTs for Vertical Displacement Measurement

Prior to testing, all LVDTs were calibrated using a milling machine. A dial gauge was used to measure the movement of LVDT that attached to the milling machine. The output of the LVDTs' movement was expressed in milli-volts (mV) and correlated to the measured change of the dial gauge in mm.

3.8 Testing Procedure

Prior to testing, all the beams were whitewashed in order to facilitate the marking of cracks. A preload of 20kN was applied to ensure test set-up and instrumentation worked properly. The beam was then unloaded and datum readings were taken.

The test was conducted by moving the test machine platen at a ram rate of 0.3mm per minute, which provided sufficient time of crack observation and marking during beam tests. Locations of cracks were marked during the process of testing until failure.

The rate of data captured was 10 samples per second. All loads and deflection data were electronically recorded using an automatic data acquisition system.

CHAPTER 4
PRESENTATION AND DISCUSSION OF TEST RESULTS FOR
SHEAR STUDY

This chapter presents the results from the experimental program described in Chapter 3. Observations on the behaviour of individual beams failing in shear, such as failure modes and crack patterns, are presented. This chapter also includes a summary of test results, including shear cracking load, shear strength, load-deflection characteristics and the effect of the longitudinal tensile reinforcement ratio on the shear strength of test beams.

4.1 Behaviour of Test Beams Failing in Shear

All of the beams were tested under monotonically increasing load until failure. The expected failure modes of a beam can be determined by its slenderness: that is, the shear span-to-depth ratio according to Nawy (2005) as presented in Table 4.1. The shear span-to-depth ratio for this study was 2.5 for all the test beams. From Table 4.1, it can be seen that either diagonal tension or shear compression failure could be expected at a span-to-depth ratio of 2.5.

Table 4.1: Effect of Beam Slenderness on Mode of Failure (Nawy, 2005)

Beam Category	Failure Mode	Shear Span-to-Depth (a/d) Ratio
Deep	Shear-Compression (S-C)	1-2.5
Intermediate	Diagonal-Tension (D-T)	2.5-5.5
Slender	Flexure (F)	> 5.5

As expected, for all the test beams two modes of failure were observed: diagonal tension failure and shear compression failure. The modes of failure and the crack patterns generally agreed with descriptions in the literature for Portland cement

beams (Choi and Park, 2007; Bresler and Scordelis, 1963; Ahmad and et al, 1986; Pendyala and Mendis, 2000; Vecchio and Shim, 2004).

The principal characteristics of the failure mechanism observed are described below:

- Diagonal Tension Failure

This type of failure occurred in Beams S1-3, S2-1, S3-1, S3-2 and S3-3. Flexural cracks first appeared in the centre portion of the beam, and gradually spread towards the supports at early load stages. At later load stages, two or three diagonal cracks developed at about $1.5d$ to $2d$ from the face of the support. As they stabilised, one of the diagonal cracks widened into a principal diagonal tension crack and extensively developed toward the loading point. The failure was brittle. The failure occurred as a result of longitudinal splitting in the compression zone near the load point, and of horizontal splitting along the tensile reinforcement near the end of the beam. No concrete spalling at the compression zone was observed after the ultimate load.

- Shear Compression Failure

This type of failure occurred in Beams S1-1, S1-2 S2-2 and S2-3. At early load stages, flexural cracks appeared in the centre portion of the beam, and gradually spread towards the supports. At later load stages, flexural-shear cracks formed near the supports. These cracks propagated towards the compression zone under increasing load. The failure occurred by the crushing of concrete in the compression zone, notably beneath and adjacent to the loading plates. Concrete spalling at the compression zone was observed after the ultimate load.

The behaviour of each beam failing in shear and the observed load at first crack, failure modes and overall crack patterns, are presented in the following:

Beam S1-1

Observations:

At early load stages, flexural cracks appeared in the centre portion of the beam and gradually spread towards the supports. The first flexural crack appeared at 81 kN. At later load stages, flexural-shear cracks formed near the supports. These cracks propagated towards the compression zone under increasing load. The failure occurred by the crushing of concrete in the compression zone, notably beneath and adjacent to the loading plates, as shown in Figure 4.1. The ultimate load was 415 kN. The mid-span deflection at ultimate load was 10.5 mm. Concrete spalling at the compression zone was observed after the ultimate load. The overall crack pattern of Beam S1-1 is given in Figures 4.2 and 4.3.



Figure 4.1: Concrete Crushing in Compression Zone for Beam S1-1

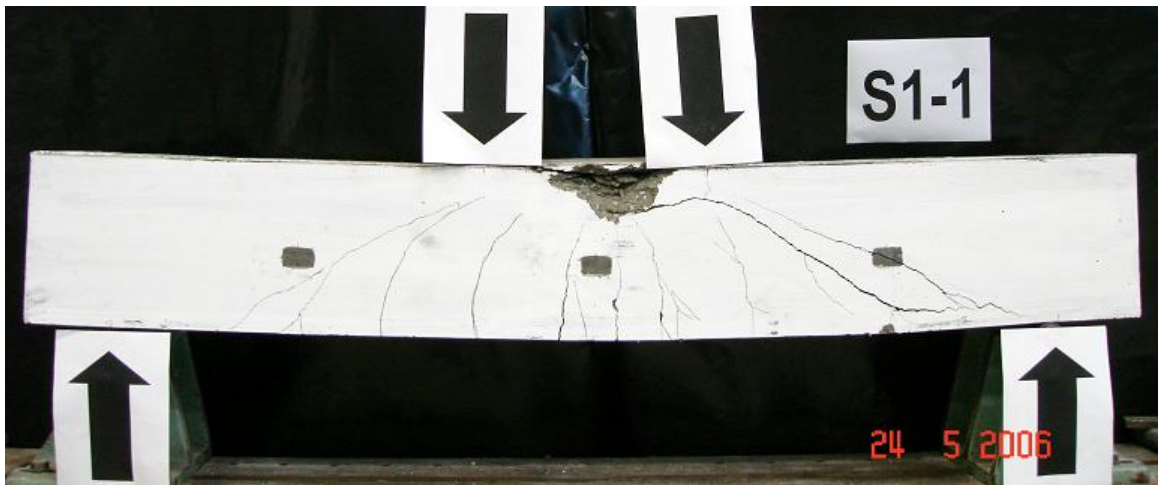


Figure 4.2: Overall Crack Pattern for Beam S1-1 (Front Face)



Figure 4.3: Overall Crack Pattern for Beam S1-1 (Back Face)

Beam S1-2

Observations:

At early load stages, flexural cracks appeared in the centre portion of the beam and gradually spread towards the supports. The first flexural crack appeared at 81 kN. At later load stages, flexural-shear cracks formed near the supports. These cracks propagated towards the compression zone under increasing load. The failure occurred by the crushing of concrete in the compression zone, notably beneath and adjacent to the loading plates, as shown in Figure 4.4. The ultimate load was 404 kN. The mid-span deflection at ultimate load was 12.2 mm. Concrete spalling at the compression zone was observed after the ultimate load. The overall crack pattern of Beam S1-2 is given in Figures 4.5 and 4.6.



Figure 4.4: Concrete Crushing in Compression Zone for Beam S1-2



Figure 4.5: Overall Crack Pattern for Beam S1-2 (Front Face)

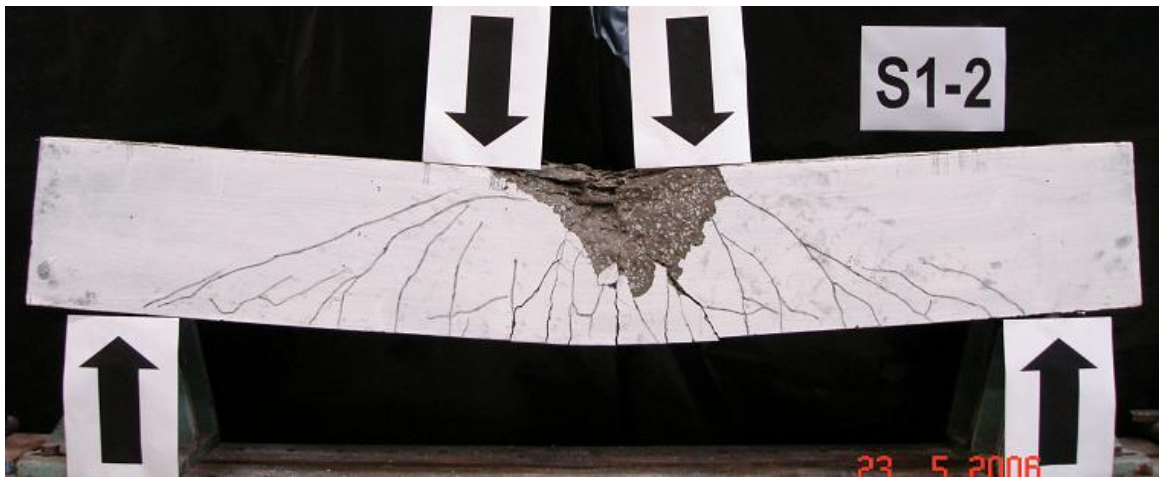


Figure 4.6: Overall Crack Pattern for Beam S1-2 (Back Face)

Beam S1-3

Observations:

Flexural cracks appeared in the centre portion of the beam and gradually spread towards the supports at early load stages. The first flexural crack appeared at 78 kN. At later load stages, two diagonal cracks developed at about $1.5d$ to $2d$ from the face of the support. As they stabilised, one of the diagonal cracks widened into a principal diagonal tension crack and extensively developed toward the loading point, as shown in Figure 4.7. The ultimate load was 370 kN. The mid-span deflection at ultimate load was 9.1 mm. The failure was brittle. No concrete spalling at the compression zone was observed after the ultimate load. The overall crack pattern of Beam S1-3 is given in Figures 4.8 and 4.9.



Figure 4.7: Principal Diagonal Crack Near Loading Point for Beam S1-3

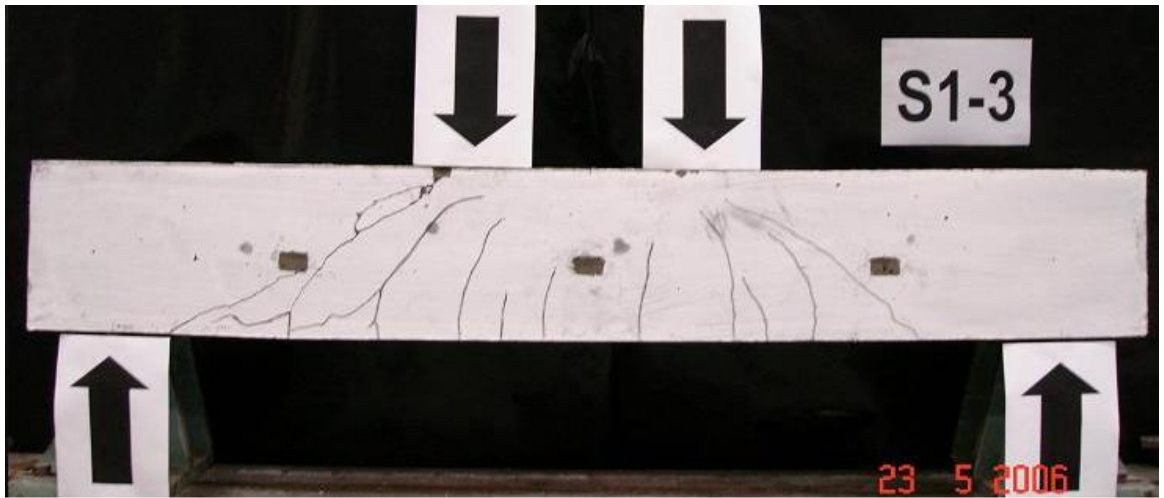


Figure 4.8: Overall Crack Pattern for Beam S1-3 (Front Face)

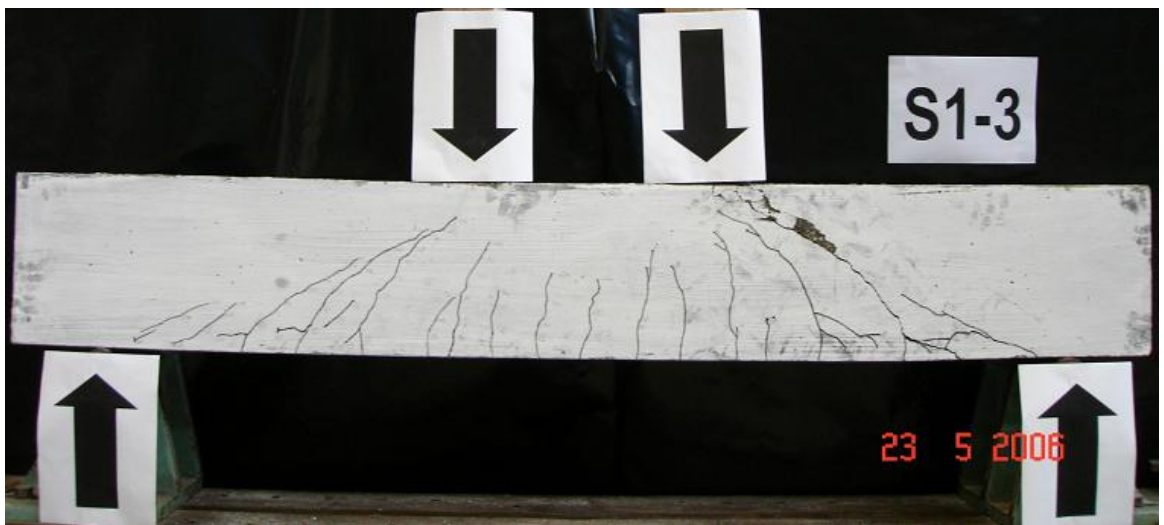


Figure 4.9: Overall Crack Pattern for Beam S1-3 (Back Face)

Beam S2-1

Observations:

Flexural cracks appeared in the centre portion of the beam, and gradually spread towards the supports at early load stages. The first flexural crack appeared at 99 kN. At later load stages, a principal diagonal tension crack developed near the support and extensively progressed toward the loading point, as shown in Figure 4.10. The ultimate load was 511 kN. The mid-span deflection at ultimate load was 9.9 mm. The failure was brittle. The principal diagonal crack divided the beam into two pieces. The overall crack pattern of Beam S2-1 is given in Figures 4.11 and 4.12.



Figure 4.10: Principal Diagonal Crack for Beam S2-1

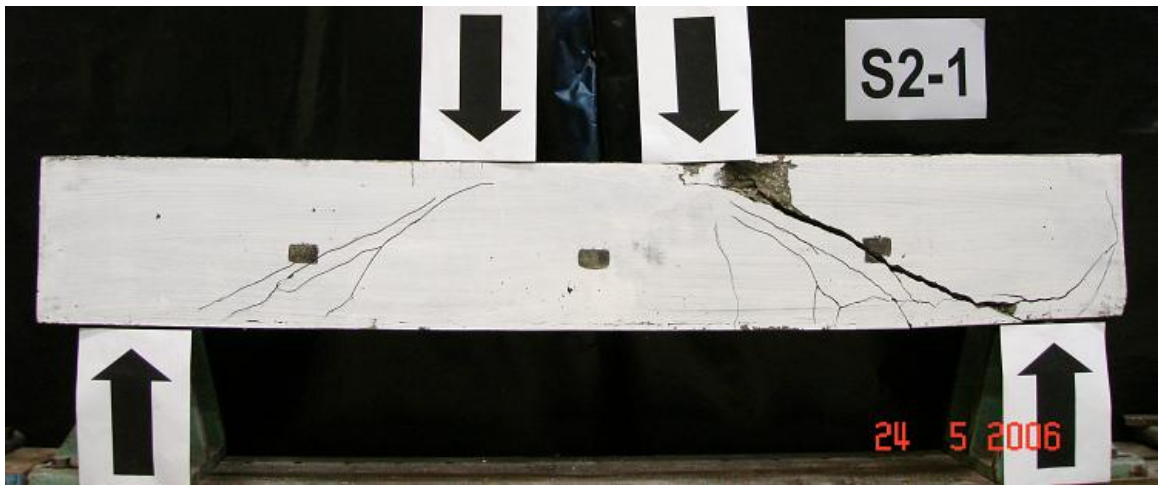


Figure 4.11: Overall Crack Pattern for Beam S2-1 (Front Face)

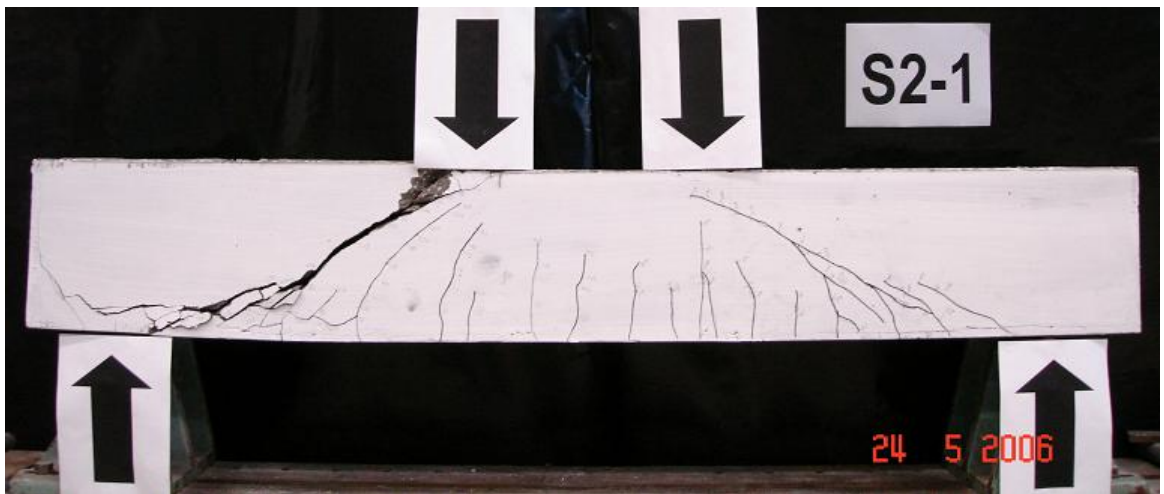


Figure 4.12: Overall Crack Pattern for Beam S2-1 (Back Face)

Beam S2-2

Observations:

At early load stages, flexural cracks appeared in the centre portion of the beam, and gradually spread towards the supports. The first flexural crack appeared at 101 kN. At later load stages, flexural-shear cracks formed near the supports. These cracks propagated towards the compression zone under increasing load. The failure occurred by the crushing of concrete in the compression zone, notably beneath and adjacent to the loading plates, as shown in Figure 4.13. The ultimate load was 519 kN. The mid-span deflection at ultimate load was 10.8 mm. Concrete spalling at the compression zone was observed after the ultimate load. The overall crack pattern of Beam S2-2 is given in Figures 4.14 and 4.15.



Figure 4.13: Concrete Crushing in Compression Zone for Beam S2-2

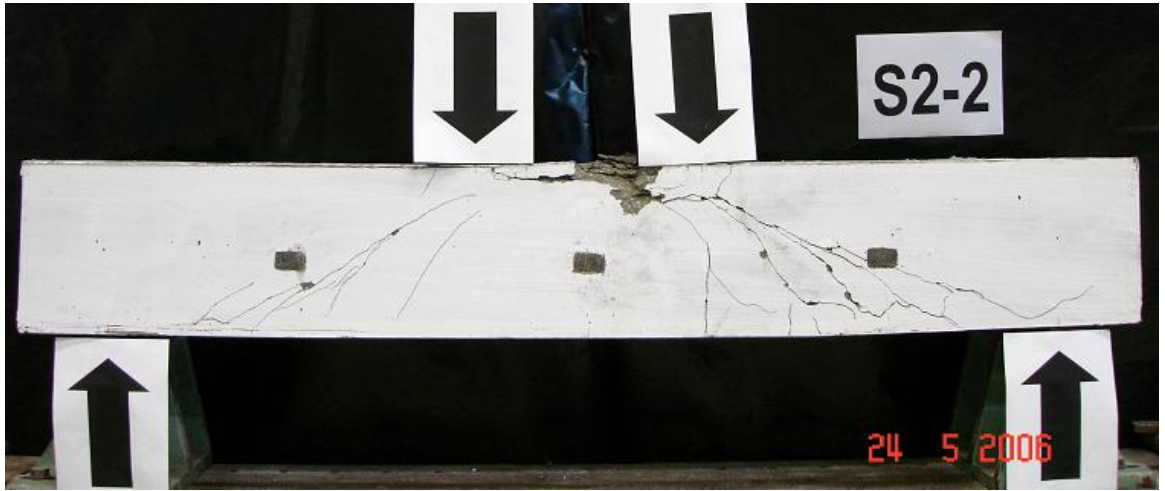


Figure 4.14: Overall Crack Pattern for Beam S2-2 (Front Face)

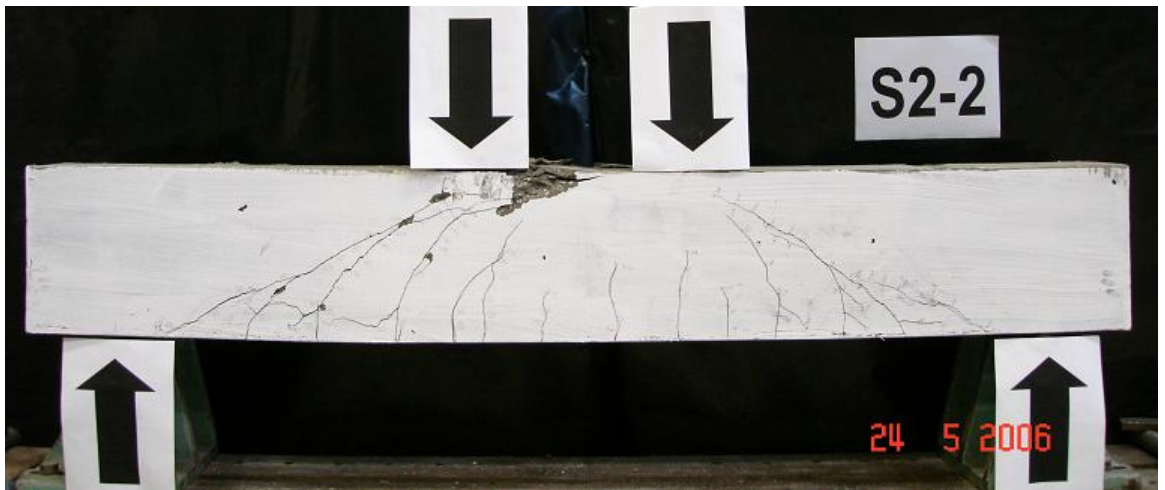


Figure 4.15: Overall Crack Pattern for Beam S2-2 (Back Face)

Beam S2-3

Observations:

At early load stages, flexural cracks appeared in the centre portion of the beam and gradually spread towards the supports. The first flexural crack appeared at 102 kN. At later load stages, flexural-shear cracks formed near the supports. These cracks propagated towards the compression zone under increasing load. The failure occurred by the crushing of concrete in the compression zone, notably beneath and adjacent to the loading plates, as shown in Figure 4.16. The ultimate load was 516 kN. The mid-span deflection at ultimate load was 11.8 mm. Concrete spalling at the compression zone was observed after the ultimate load. The overall crack pattern of Beam S2-3 is given in Figures 4.17 and 4.18.



Figure 4.16: Concrete Crushing in Compression Zone for Beam S2-3



Figure 4.17: Overall Crack Pattern for Beam S2-3 (Front Face)

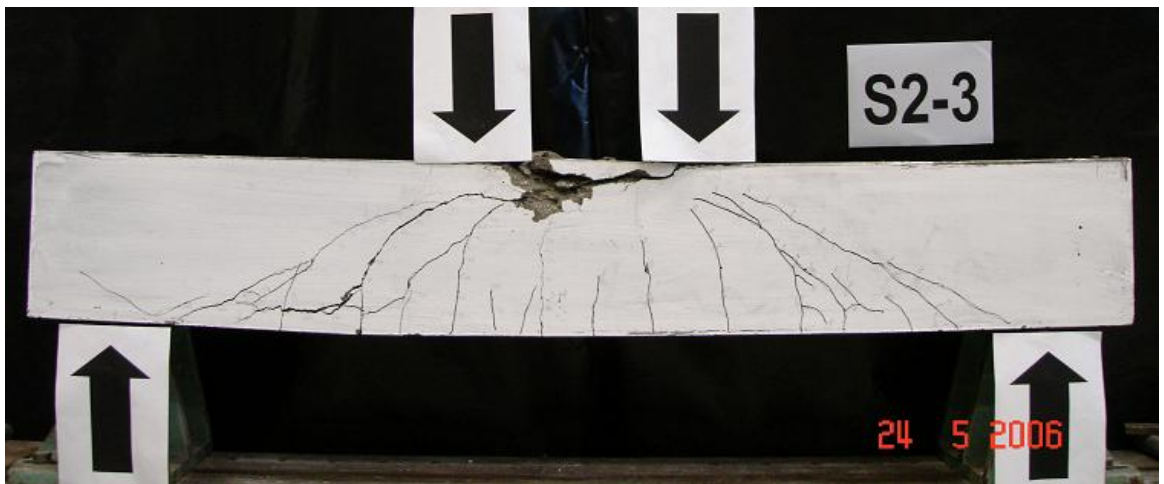


Figure 4.18: Overall Crack Pattern for Beam S2-3 (Back Face)

Beam S3-1

Observations:

Flexural cracks appeared in the centre portion of the beam and gradually spread towards the supports at early load stages. The first flexural crack appeared at 114 kN. At later load stages, a principal diagonal tension crack developed near the support and extensively progressed toward the loading point, as shown in Figure 4.19. The ultimate load was 523 kN. The mid-span deflection at ultimate load was 10.7 mm. The failure was brittle. The overall crack pattern of Beam S3-1 is given in Figures 4.20 and 4.21.



Figure 4.19: Principal Diagonal Crack for Beam S3-1

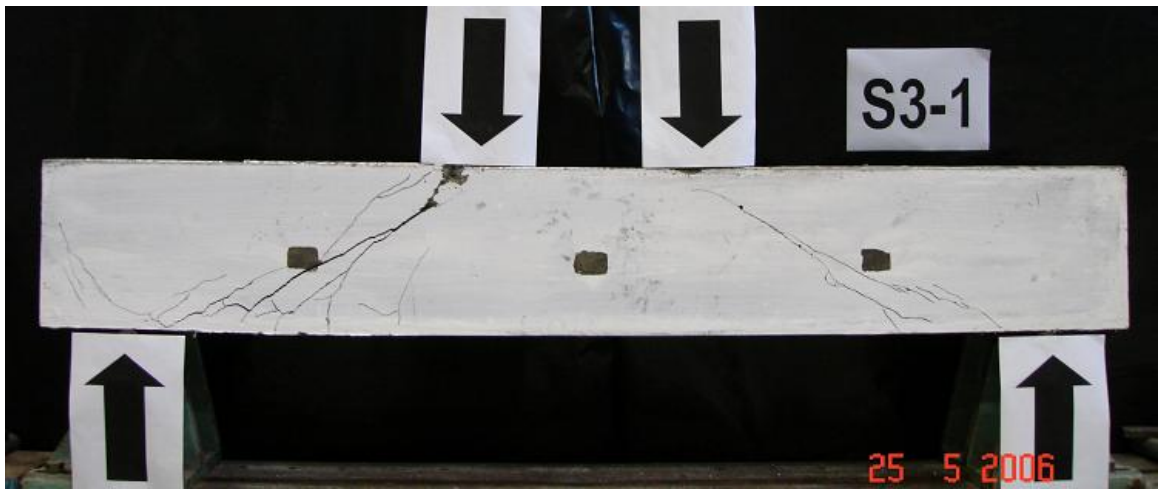


Figure 4.20: Overall Crack Pattern for Beam 3-1 (Front Face)

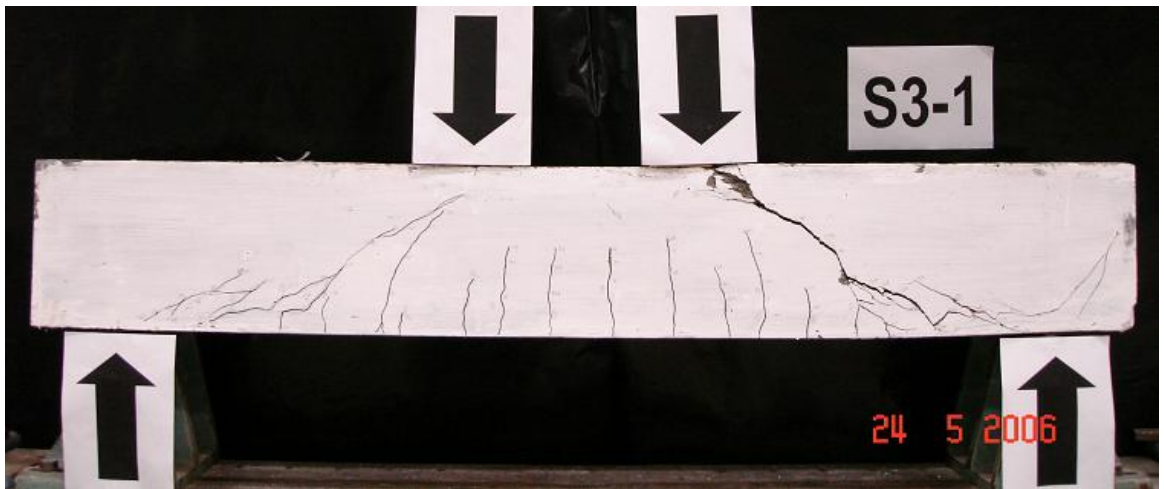


Figure 4.21: Overall Crack Pattern for Beam 3-1 (Back Face)

Beam S3-2

Observations:

Flexural cracks appeared in the centre portion of the beam and gradually spread towards the supports at early load stages. The first flexural crack appeared at 99 kN. At later load stages, a principal diagonal tension crack developed near the support and extensively progressed toward the loading point as shown in Figure 4.22. The ultimate load was 552.4 kN. The mid-span deflection at ultimate load was 12.2 mm. The failure was brittle. The overall crack pattern of Beam S3-2 is given in Figures 4.23 and 4.24.



Figure 4.22: Principal Diagonal Crack for Beam S3-2

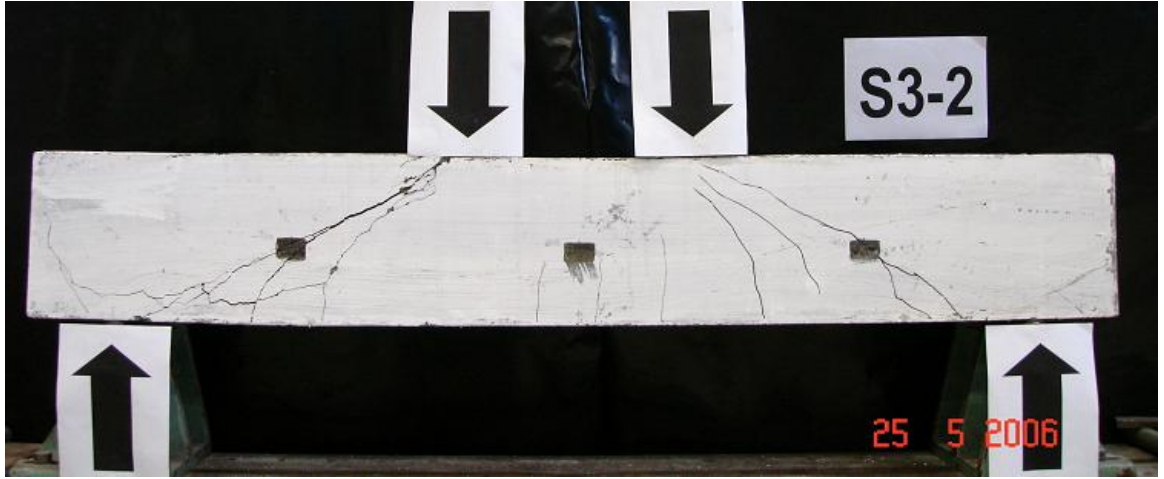


Figure 4.23: Overall Crack Pattern for Beam 3-2 (Front Face)

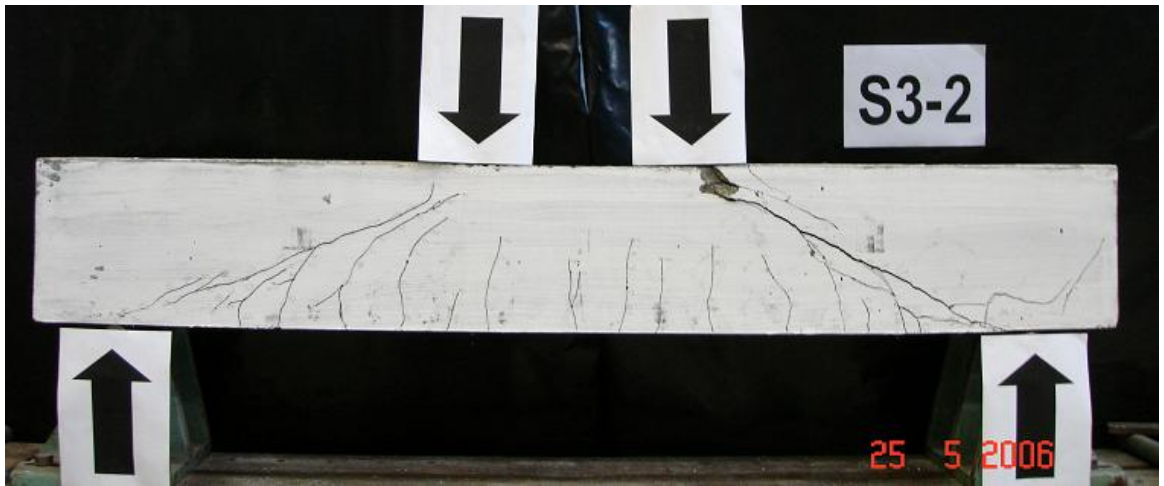


Figure 4.24: Overall Crack Pattern for Beam 3-2 (Back Face)

Beam S3-3

Observations:

Flexural cracks appeared in the centre portion of the beam and gradually spread towards the supports at early load stages. The first flexural crack appeared at 100 kN. At later load stages, a principal diagonal tension crack developed near the support and extensively progressed toward the loading point, as shown in Figure 4.25. The ultimate load was 660.8 kN. The mid-span deflection at ultimate load was 11.6 mm. The failure was brittle. The principal diagonal crack divided the beam into two pieces. The overall crack pattern of Beam S3-3 is given in Figures 4.26 and 4.27.



Figure 4.25: Principal Diagonal Crack for Beam S3-3

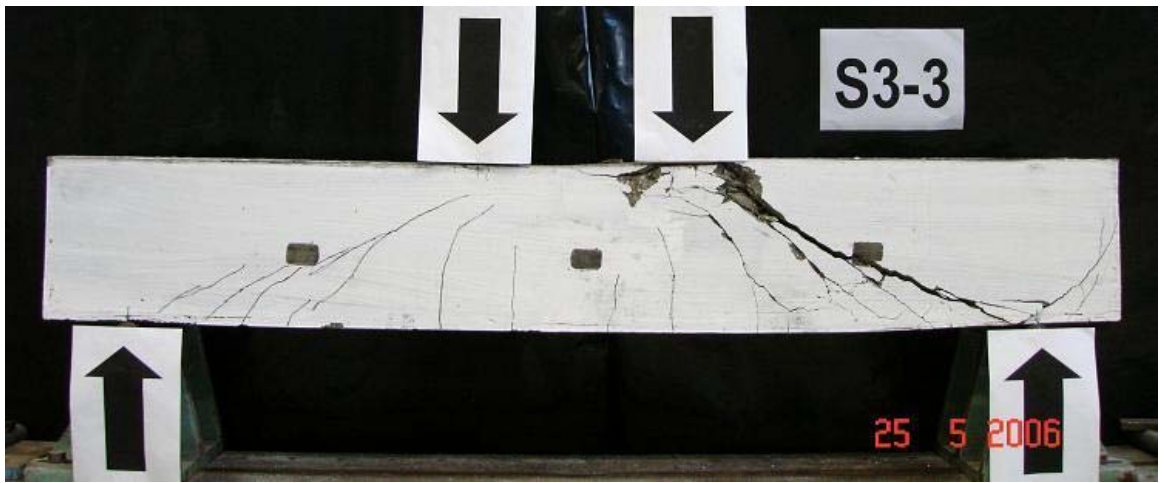


Figure 4.26: Overall Crack Pattern for Beam 3-3 (Front Face)

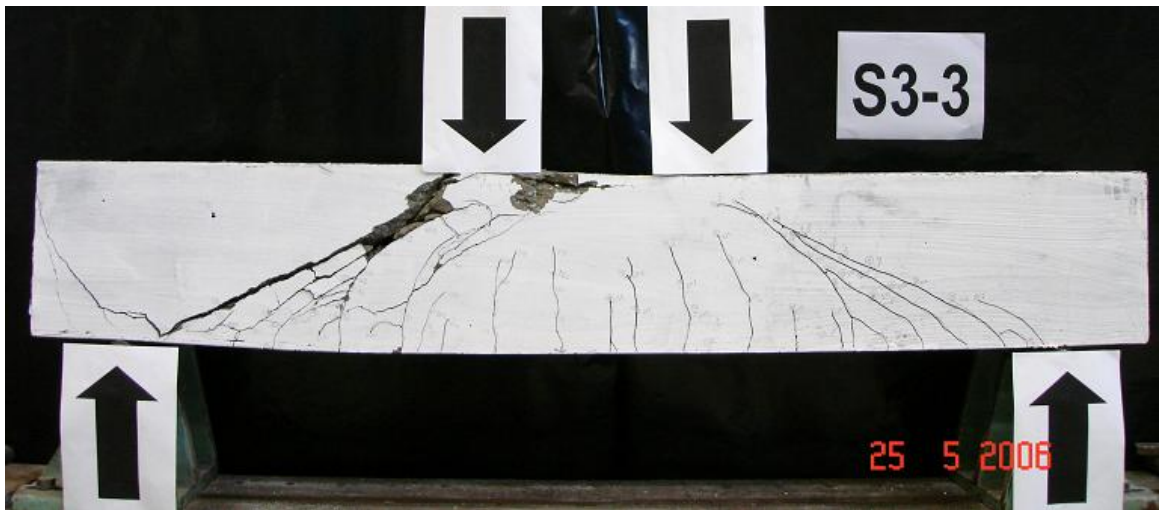


Figure 4.27: Overall Crack Pattern for Beam 3-3 (Back Face)

4.2 Load-Deflection Curves

The load-deflection curves of the test beams are given in Figures 4.28 to 4.36. The graphs highlight the behaviour and failure modes of the test beams.

Generally, the following features were observed for the beams:

- As the load increased, loss of stiffness was observed for all the beams due to propagation of flexure and shear cracks during load stages
- The test beams that failed in diagonal-tension were Beams S1-3, S2-1, S3-1, S3-2 and S3-3. The failures were sudden, with a sharp drop-off after peak load, as indicated in Figures 4.30, 4.31, 4.34, 4.35 and 4.36.
- The test beams that failed in shear-compression were Beams S1-1, S1-2, S2-2 and S2-3. The failures were less sudden and exhibited post-peak ductility, as indicated in Figures 4.28, 4.29, 4.32 and 4.33.
- Formation of first flexural crack and diagonal crack were evident from the load deflection curves, as reflected by the change of slope in the plot shown in Figures 4.28 to 4.36. These are similar to what is described in the literature for Portland cement concrete beams (Pendyala and Mendis, 2000; Tompos and Frosch, 2002).
- Observations on events of crack formation, widening of crack width and concrete spalling observed for individual test beam were recorded and are shown in Figures 4.28 to 4.36.

The complete load-deflection data for each beam are given in Appendix C.

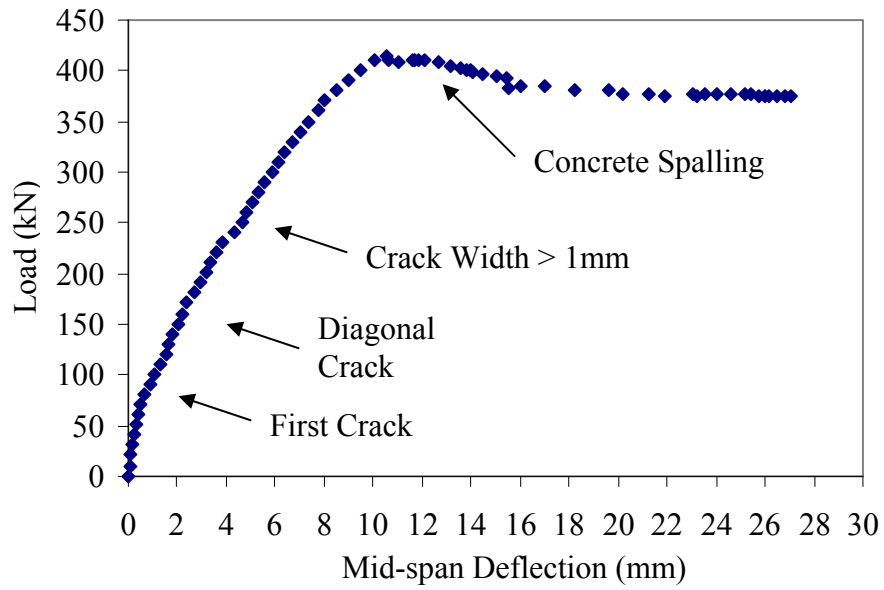


Figure 4.28: Load versus Mid-span Deflection for Beam S1-1

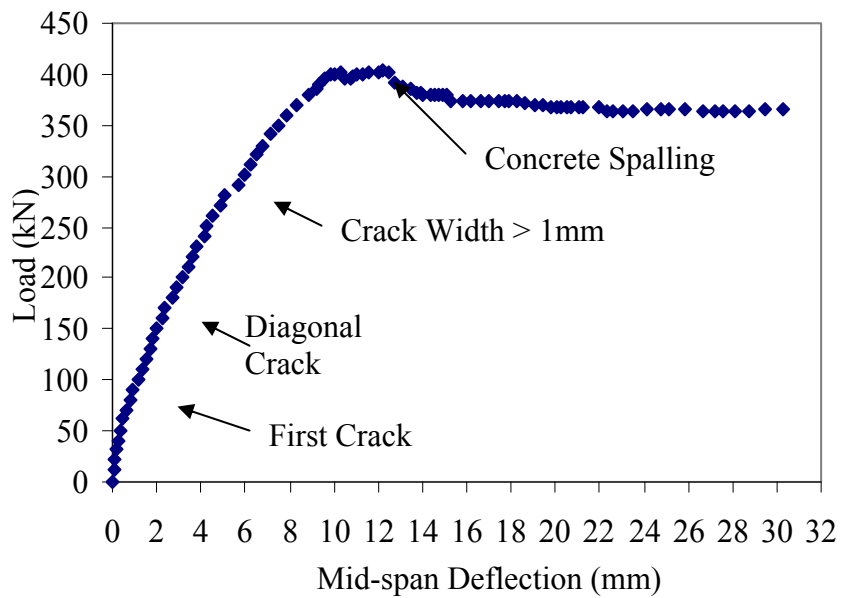


Figure 4.29: Load versus Mid-span Deflection for Beam S1-2

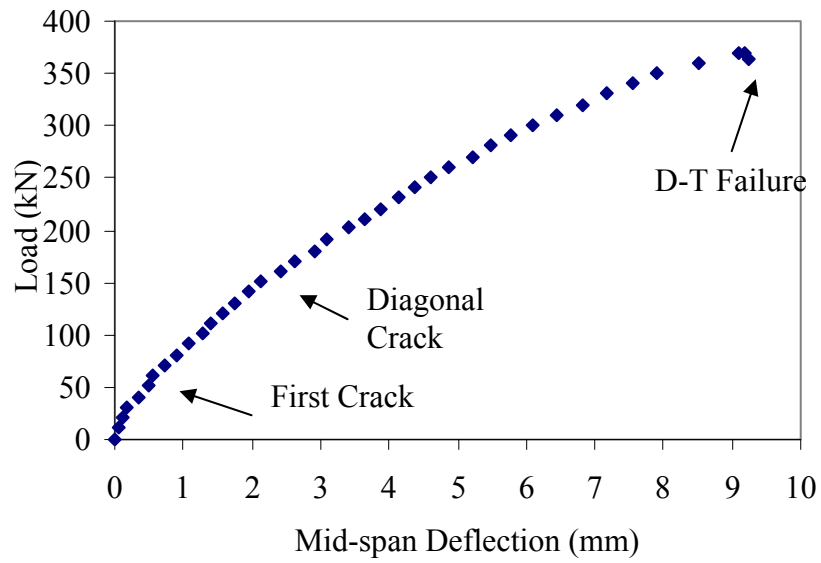


Figure 4.30: Load versus Mid-span Deflection for Beam S1-3

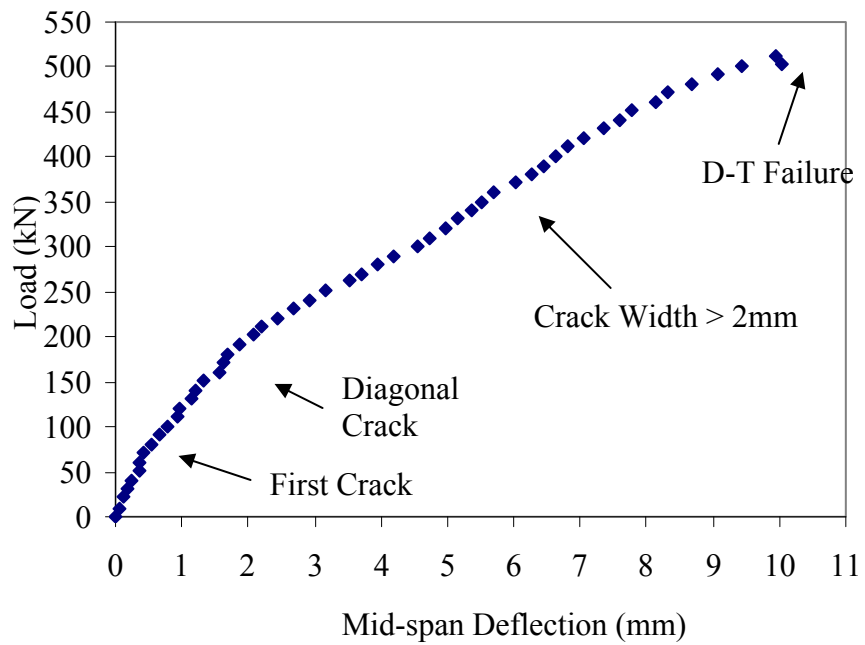


Figure 4.31: Load versus Mid-span Deflection for Beam S2-1

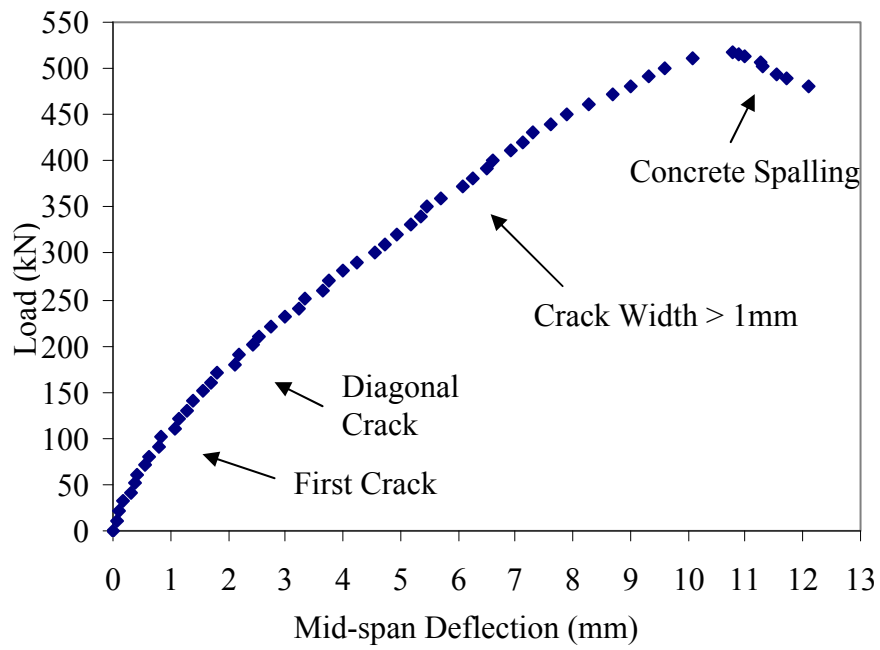


Figure 4.32: Load versus Mid-span Deflection for Beam S2-2

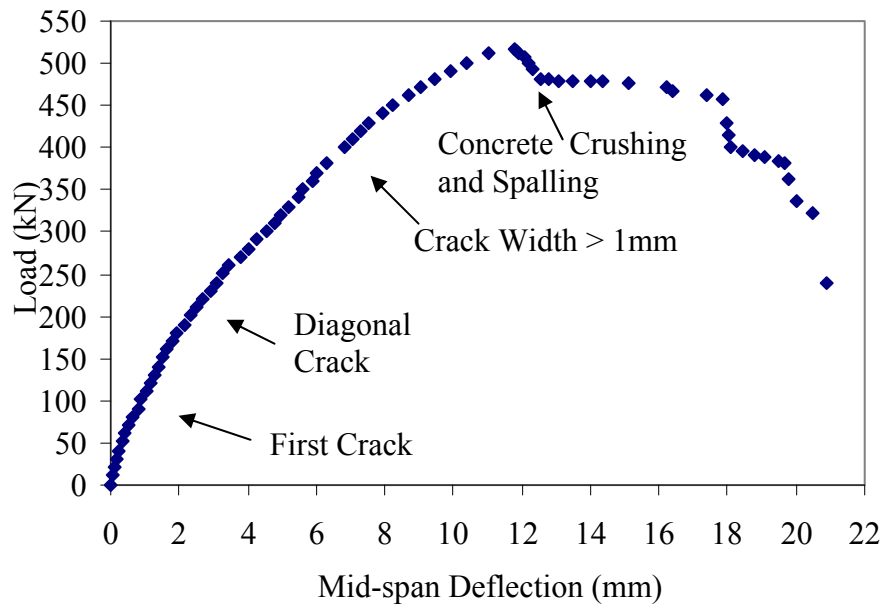


Figure 4.33: Load versus Mid-span Deflection for Beam S2-3

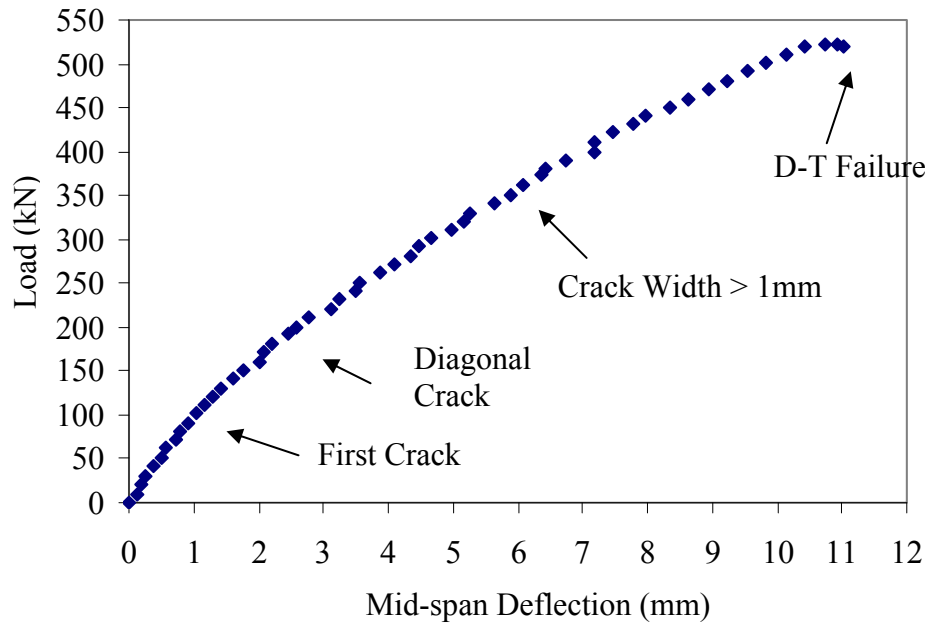


Figure 4.34: Load versus Mid-span Deflection for Beam S3-1

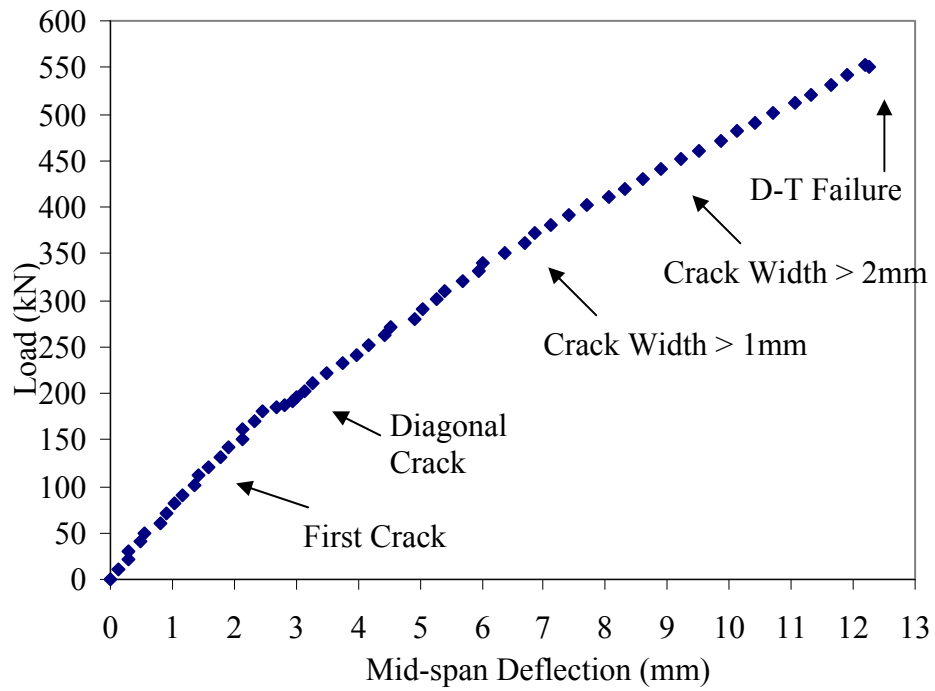


Figure 4.35: Load versus Mid-span Deflection for Beam S3-2

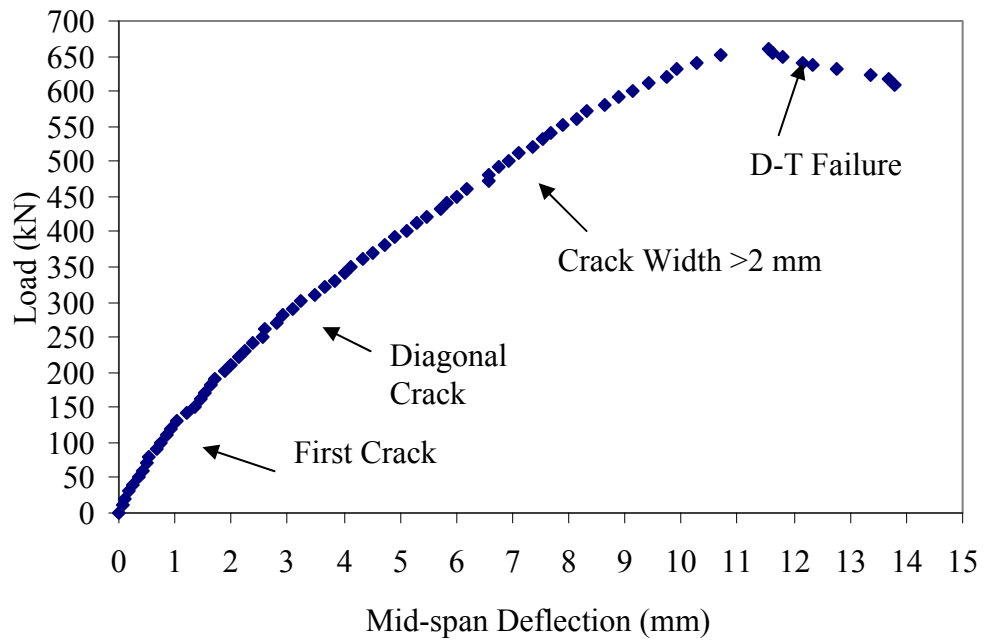


Figure 4.36: Load versus Mid-span Deflection for Beam S3-3

4.3 Shear Cracking Load

In this study, the shear cracking load (inclined cracking load) is defined as the load at the time that the main diagonal crack (the one which caused failure) crossed the mid-height of the beam (Zsutty, 1968; Pendyala and Mendis, 2000).

The observed shear cracking load for all beams is given in Table 4.2.

Table 4.2: Test Results for Shear Cracking Load

Series	Beam Mark	p_{sl} (%)	p_{sv} (%)	f'_c (MPa)	Shear Cracking Load (kN)
1	S1-1	1.74	0.10	45	86
	S1-2	1.74	0.13	45	85
	S1-3	1.74	0.17	44	82
2	S2-1	2.32	0.10	56	80
	S2-2	2.32	0.13	50	88
	S2-3	2.32	0.17	50	98
3	S3-1	3.14	0.10	49	80
	S3-2	3.14	0.13	49	94
	S3-3	3.14	0.17	56	112

4.4 Shear Strength of Test Beams

4.4.1 General

The ultimate shear resisted by the beam was half of the total imposed load on the beam. A summary of the test results is given in Table 4.3.

Table 4.3: Test Results for Shear Strength, V_{uTEST}

Series	Beam Mark	p_{sl} (%)	p_{sv} (%)	f'_c (MPa)	Peak Load (kN)	Test Shear Strength* (kN)
1	S1-1	1.74	0.10	45	415	210.3
	S1-2	1.74	0.13	45	404	204.8
	S1-3	1.74	0.17	44	370	187.8
2	S2-1	2.32	0.10	56	511	258.3
	S2-2	2.32	0.13	50	519	262.3
	S2-3	2.32	0.17	50	516	260.8
3	S3-1	3.14	0.10	49	523	261.5
	S3-2	3.14	0.13	49	552	276.2
	S3-3	3.14	0.17	56	661	333.3

**including the self-weight of the beam*

4.4.2 Influence of the Longitudinal Tensile Reinforcement Ratio on Shear Strength of Test Beams

Figures 4.37 to 4.39 show the effect of the longitudinal tensile reinforcement ratio on the shear capacity for beams with same shear reinforcement ratios. As expected, the shear capacity of the beams increased with the increase of the longitudinal reinforcement ratio. This trend is similar to what has been observed for Portland cement concrete beams (Kong and Rangan, 1998; Tompos and Frosch, 2002).

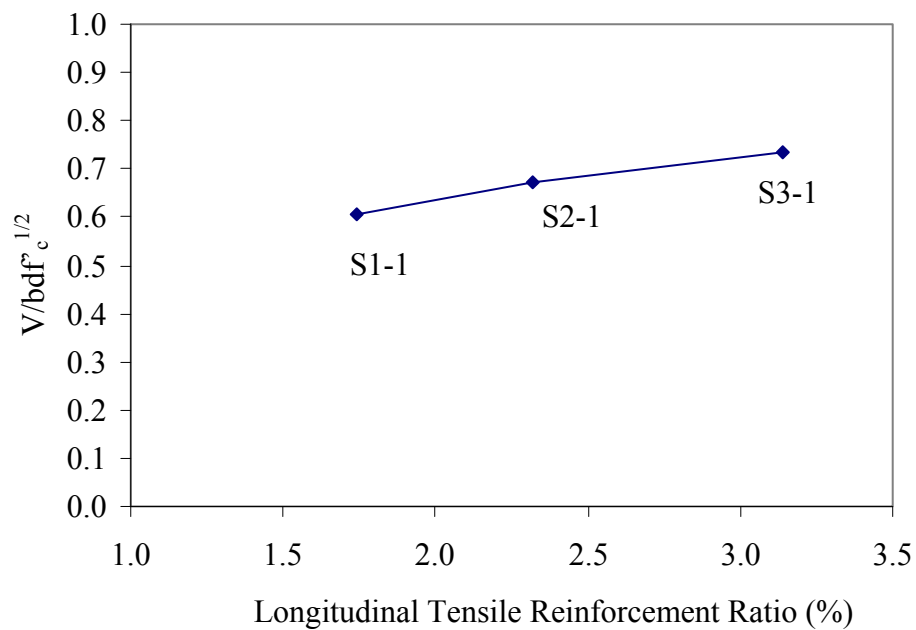


Figure 4.37: Effect of Longitudinal Tensile Reinforcement Ratio on the Shear Capacity of Beams for Shear Reinforcement Ratio of 0.10%

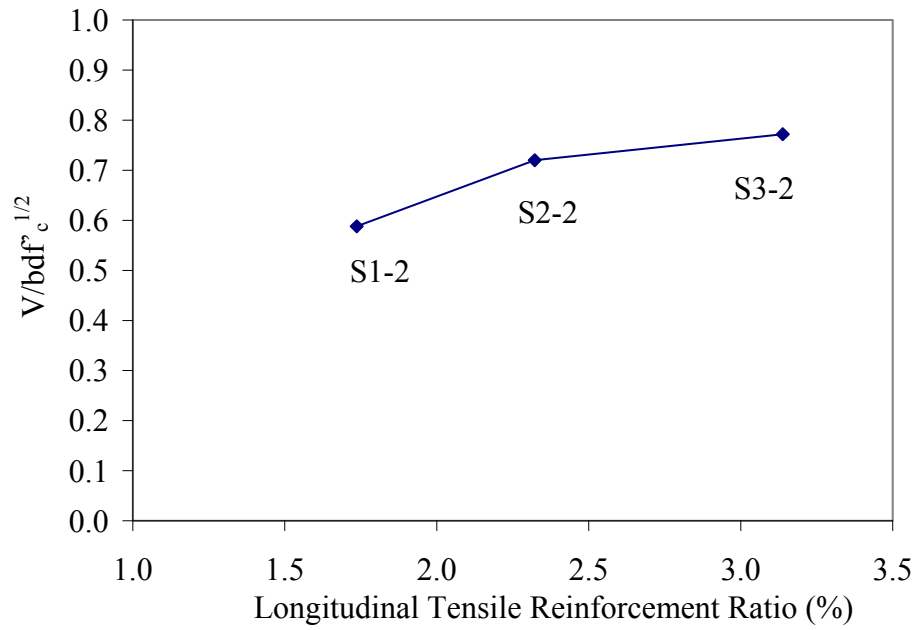


Figure 4.38: Effect of Longitudinal Tensile Reinforcement Ratio on the Shear Capacity of Beams for Shear Reinforcement Ratio of 0.13%

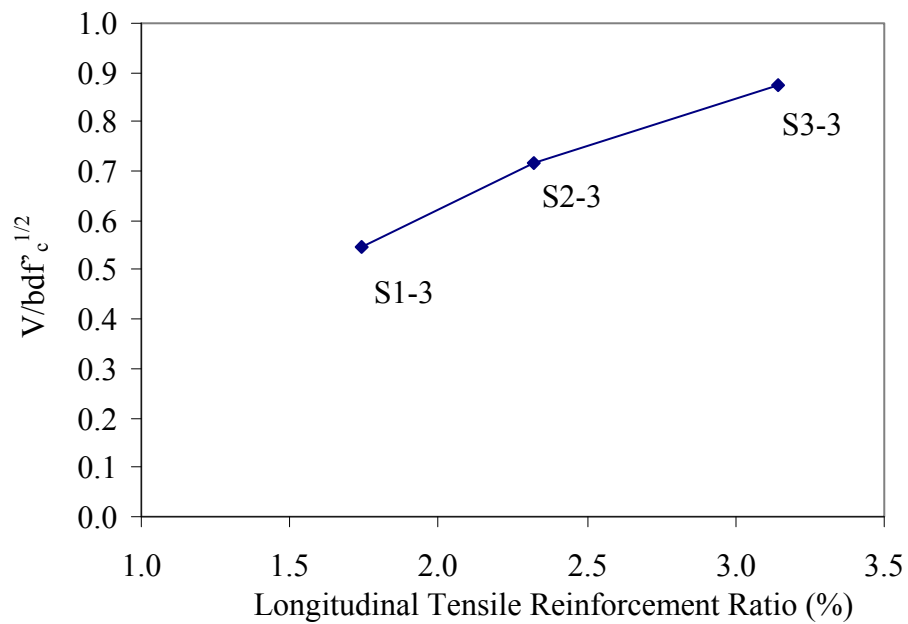


Figure 4.39: Effect of Longitudinal Tensile Reinforcement Ratio on the Shear Capacity of Beams for Shear Reinforcement Ratio of 0.17%

CHAPTER 5

ANALYTICAL MODELLING OF BEAMS IN SHEAR STUDY

5.1 Introduction

Two computer programs were used in this study to calculate the shear strength of geopolymer concrete beams. The first program, *ShearCalculator*, was written using C++ programming for analysis of the test beams by the method used by Kong and Rangan (1998), as presented in Section 2.2.2.2. The second program, *VecTor2*, is a non-linear finite element program developed by Vector Analysis Group at the University of Toronto, incorporating the behaviour models and constitutive relations of the Disturbed Stress Field Model (DSFM) from Vecchio (2000), as described in Section 2.2.2.3.

The calculation procedures including input and output information of these programs are presented in the following sections.

5.2 *ShearCalculator*

A computer program, *ShearCalculator*, was developed using Microsoft Visual C++ for the iterative calculation of the average stresses and average strains in the d - r coordinates of the shear element and in the concrete and steel, according to Kong and Rangan (1998). The calculation steps, input and output for the program are presented next.

5.2.1 Calculation Steps

The program was written using the following calculation steps. The equations given in Section 2.2.2.2 were used.

- Step 1: Input beam data (including sectional, geometrical, material properties).
- Step 2: Assume a value for shear strength, V_u (An initial value is selected from the initial stress analysis).
- Step 3: Select a value of ε_d (ε_d varies from 0 to -0.0035; a reasonable starting value is -1.0×10^{-5}).
- Step 4: Assume a value of ε_r (a reasonable starting value is 1.0×10^{-5}).
- Step 5: Calculate σ_l using Equation 2.37.
- Step 6: Calculate σ_d using Equations 2.30, 2.31 or 2.32.
- Step 7: Calculate σ_r using Equations 2.33 or 2.34.
- Step 8: Calculate A_{sIM} and A_{sIV} using Equations 2.39 and 2.40 respectively, and determine p_l using A_{sIV} .
- Step 9: Calculate ε_l using Equations 2.41 or 2.42.
- Step 10: Calculate ε_t using Equation 2.43 or 2.44.
- Step 11: Calculate ε_r using Equation 2.45.
- Step 12: Calculate θ using Equation 2.46. Hence, calculate ν_{lt} and γ_{lt} by using Equations 2.26 and 2.29, respectively. Calculate $V = \nu_{lt}(b_v d_v)$.
- Step 13: Repeat Steps 3 to 12 for other values of ε_d in the range of $-0.0035 < \varepsilon_d < 0$; plot the $V - \gamma_{lt}$ curve. The peak of the curve gives the ultimate shear strength V_u .
- Step 14: Compare the calculated V_u in Step 13 with the assumed value in Step 2. The solution is accepted when there is a convergence; otherwise, return to Step 2 and iterate.

5.2.2 Input Data for Beam

Input data is requested for each beam and a sample of the input dialogue for Beam S1-1 is shown in Figure 5.1. The input data includes:

- Beam cross section
- Concrete compressive strength
- Area of shear reinforcement
- Area of longitudinal reinforcement
- Shear reinforcement ratio
- Yield stress of reinforcement (longitudinal and transverse)
- Effective depth of beam
- Modulus of elasticity of steel
- Shear span

The screenshot shows the 'ShearCalculator' software window with a menu bar (Data, Report, Graph) and a main area containing input fields and buttons. The main text reads: 'This program calculates the maximum shear strength of concrete. Specify your parameters below and click on the [Start Calculations] button.'

Input fields include:

- fc: 45
- d: 259
- RDt: 0.001
- dv: 233.1
- fsty: 597
- a: 640
- Es: 200000
- a_: 381
- L: 1680
- N: 0
- b: 200
- Pf: 101460
- D: 300
- Ec: 0
- for: 0

Reinforcement table:

	Ast	fslv	vs	ORIENT
1	220	570	35	T
2	0	0	0	0
3	900	559	259	B

Other fields: n loop: 3, Ed: -0.000005, Filter Data: , DED: -0.000025, DED1: -0.000005, DED2: -0.000005, DED3: -0.00025.

Buttons: Start Calculations, Reset.

Modification checkboxes (1-8): Modification - 1, Modification - 2, Modification - 3, Modification - 4, Modification - 5, Modification - 6, Modification - 7, Modification - 8.

Output area: No modifications

Figure 5.1: Input Dialog of ShearCalculator Program for Beam S1-1

5.2.3 Numerical Example

A numerical example for Beam S1-1 tested in this study is given below to illustrate the solution algorithm described previously.

Step 1: Input Beam Data

The data used for the calculation is as below:

f'_c	= 45 MPa
a	= 640 mm
b	= 200 mm
D	= 300 mm
d	= 259 mm
d_v	= 0.9 x d = 233.1 mm
A_{sl}	= 900 mm ²
f_{sty}	= 559 MPa
A_{sv}	= 25 mm ²
f_{sty}	= 597 MPa
p_{sv}	= 0.001
E_s	= 200 x 103 MPa
N	= 0
a_-	= a - d = 381 mm

Step 2: Assume V_u

An initial stress analysis is performed by varying ε_d from 0 to -0.0035. The peak shear force from the preliminary analysis is taken as the initial guess of V_u . From the preliminary analysis, $V_u = 101.5$ kN.

Step 3: Select ε_d

For this example, the value of ε_d is the strain at the peak shear capacity V_u , which is:

$$\varepsilon_d = -2.105 \times 10^{-3}$$

Step 4: Assume ε_r

The value of ε_r is taken as 0.04 from the initial analysis.

Step 5: Determine σ_l

$$\sigma_l = 0 \text{ (as } N = 0\text{)}.$$

Step 6: Calculate σ_d

$$n' = 0.8 + \frac{45}{17} = 3.45$$

$$E_c = 3320\sqrt{45} + 6900 = 29171 \text{ MPa}$$

$$\varepsilon_o = -\frac{45}{29171} \left(\frac{3.45}{3.45-1} \right) = -2.17 \times 10^{-3}$$

$$K_f = 0.1825\sqrt{45} = 1.224 > 1.0$$

$$K_c = 0.35 \left(\frac{0.04}{0.002105} - 0.28 \right)^{0.8} = 3.65 > 0$$

$$\zeta = \frac{1}{1.0 + 1.224 \times 3.65} = 0.183$$

As $\varepsilon_d < \varepsilon_o$, using Equation 2.32 yields:

$$\sigma_d = -8.23 \text{ MPa.}$$

Step 7: Calculate σ_r

$$f_{cr} = 0.33\sqrt{45} = 2.21 \text{ MPa}$$

$$\varepsilon_{cr} = \frac{2.21}{29171} = 0.0758 \times 10^{-3}$$

Since $\varepsilon_r > \varepsilon_{cr}$, Equation 2.34 is used:

$$\sigma_r = \frac{2.21}{1 + \sqrt{500 \times 0.04}} = 0.404 \text{ MPa.}$$

Step 8: Calculate $A_{s\ell M}$, A_{sIV} and ρ_l

$$\text{From Equation 2.40: } A_{s\ell M} = \frac{101500 \times 381}{233.1 \times 559} = 296.66 \text{ mm}^2$$

$$A_{sIV} = A_{s\ell} - A_{s\ell M} = 900 - 296.66 = 603.34 \text{ mm}^2$$

$$\rho_l = \frac{A_{sIV}}{b_v d_v} = \frac{603.34}{200 \times 233.1} = 0.0129.$$

Step 9: Calculate ε_ℓ

Assume $\varepsilon_\ell \leq f_{s\ell y} / E_s$

From Equation 2.41: ε_ℓ

$$\begin{aligned} &= \frac{0.04(-8.23 - 0.404) + (0 - 0.404)(-0.002105 - 0.04)}{-8.23 - 0.404 + 0.0129 \times 200000(-0.002105 - 0.04)} \\ &= 0.00279 \end{aligned}$$

$$f_{s\ell y} / E_s = 0.002795$$

Since $\varepsilon_\ell < f_{s\ell y} / E_s$, the assumption is satisfactory.

Step 10: Calculate ε_t

Assume $\varepsilon_t > f_{svy} / E_s$

$$\begin{aligned} \text{From Equation 2.44: } \varepsilon_t &= \left(\frac{-0.404 - 0.001 \times 597}{-8.23 - 0.404} \right) (-0.002105 - 0.04) + 0.04 \\ &= 0.0352 \end{aligned}$$

$$f_{svy} / E_s = 0.002985$$

Since $\varepsilon_t > f_{svy} / E_s$, the assumption is satisfactory.

Step 11: Calculate ε_r

$$\begin{aligned}\text{From Equation 2.45: } \varepsilon_r &= 0.00279 + 0.0352 + 0.002105 \\ &= 0.04.\end{aligned}$$

Step 12: Calculate θ , v_{lt} , γ_{lt} and V

$$\begin{aligned}\text{From Equation 2.46: } \theta &= \tan^{-1}\left(\sqrt{\frac{0.00279 + 0.002105}{0.0352 + 0.002105}}\right) \\ &= 19.9^\circ\end{aligned}$$

$$\text{From Equation 2.26: } v_{lt} = -(-8.23 - 0.404)\sin 19.9^\circ \cos 19.9^\circ = 2.765 \text{ MPa}$$

$$\text{From Equation 2.29: } \gamma_{lt} = -2(-0.002105 - 0.04)\sin 19.9^\circ \cos 19.9^\circ = 0.0269$$

Therefore,

$$V = v_{lt}(b_v d_v) = 2.765 \times 200 \times 233.1 = 128.8 \text{ kN.}$$

Step 13: Repeat Step 3 to Step 12 for other values of ε_d and plot V - γ_{lt} curve

A graph of V - γ_{lt} ; the curve of beam S1-1 is also plotted, as shown in Figure 5.2.

The peak of the curve gives the ultimate shear strength V_u .

Step 14: Check V_u .

From Figure 5.2, the peak of the V - γ_{lt} curve is 128.8 kN. This value agrees with the assumed V_u value in Step 2. Thus, the solution is acceptable.

A report of the analysis is generated after the program is completed. A typical report of analysis for Beam S1-1 is given in Appendix D.

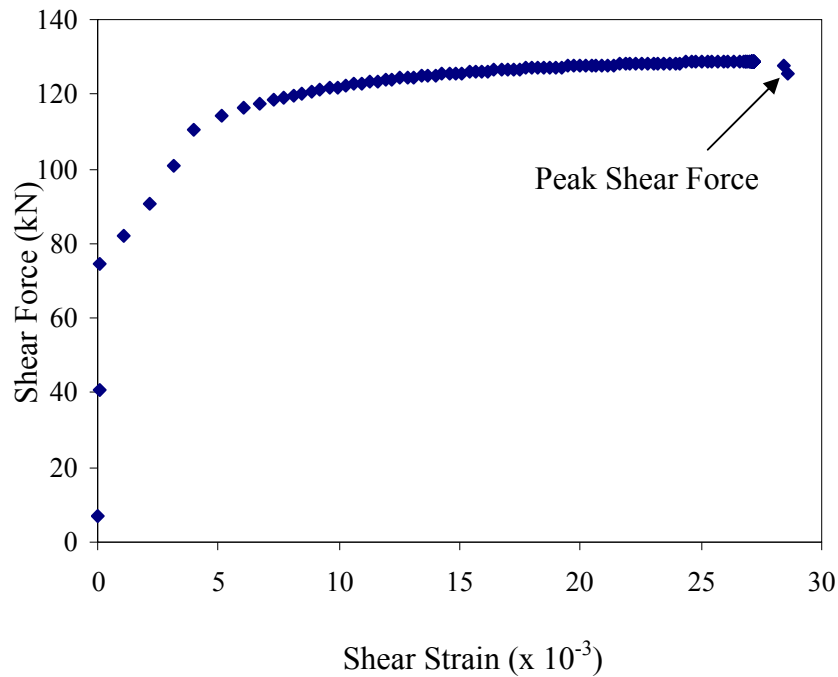


Figure 5.2: V - γ_h curve for Beam S1-1

5.3 *VecTor2*

Bundle analysis software available from the University of Toronto for the prediction of reinforced concrete elements was used to predict the shear strength and behaviour of geopolymer concrete beams failing in shear. In the following section, a brief description of this software is presented. A more detailed description of the software can be found in the *VecTor2 and FormWorks User's Manual* (Wong and Vecchio, 2002).

5.3.1 Calculation Procedure

1. Run *Formworks* – creating the model
2. Run *VecTor2* – Finite Element Analysis through *Formworks*

3. Run *Augustus* through *Formworks* to view the results

5.3.1.1 Input using *Formworks* Program

In order to model the nine geopolymer concrete beams for finite element analysis using *VecTor2*, a graphics-based pre-processor program *Formworks*, specially formulated for use with *VecTor2*, was used to construct the finite element mesh for all the beam analysis. *FormWorks* includes facilities for automatic mesh generation, bandwidth reduction and data visualisation and input, as well as specialised features such as automatic inclusion of bond link elements with rebar elements. In addition, the modelling of structural details, reinforcement details, and variable material properties is greatly facilitated by *FormWorks*. A typical *FormWorks* application window is shown in Figure 5.3.

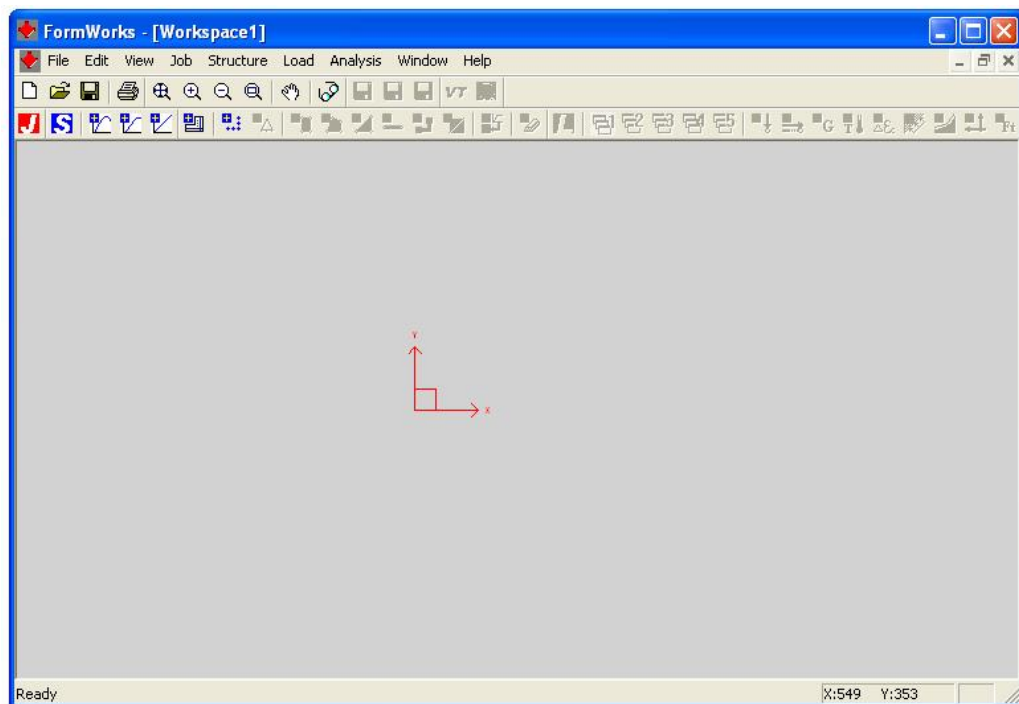


Figure 5.3: A Typical *FormWorks* Application Window

In *FormWorks*, three different types of ASCII files, job files, structure file and load case files, are created as input data files for *VecTor2*. The job file allows the user to define the analysis to be performed. The structure file allows the user to input data

relating to the structure mesh geometry and material properties. The load case files allow the user to input data related to applied loads.

The first step is to define the job data and select the material properties and behaviour models. The job control property page and models property page are shown in Figures 5.4 and 5.5.

Define Job

Job Control | Models

Job Data

Job file name: S3-1
 Job title: S3-1
 Date: 12 Jan 2007

Structure Data

Structure file name: S3-1
 Structure title: Enter Structure Title
 Structure type: Plane Membrane (2-D)

Loading Data

Load series ID: S3-1 Starting load stage no.: 1 No. of load stages: 161

Activate: Case 1 Case 2 Case 3 Case 4 Case 5

	Case 1	Case 2	Case 3	Case 4	Case 5
Load file name:	S3-1	NULL	NULL	NULL	NULL
Load case title:	Enter load case title	Enter load case title	Enter load case title	Enter load case title	Enter load case title
Initial factor:	0	0	0	0	0
Final factor:	40	0	0	0	0
Inc. factor:	0.25	0	0	0	0
Load type:	Monotonic	Monotonic	Monotonic	Monotonic	Monotonic
Repetitions:	1	1	1	1	1
Cyclic Inc. factor:	0	0	0	0	0

Analysis Parameters

Seed file name: NULL Convergence criteria: Displacements - Weighted Average
 Max. no. of iterations: 60 Analysis Mode: Nonlinear - Load Step
 Dynamic Averaging factor: 0.5 Results files: ASCII Files Only
 Convergence limit: 1.00001 Output format: To Computer

OK Cancel Apply

Figure 5.4: Job Control Property Page Display

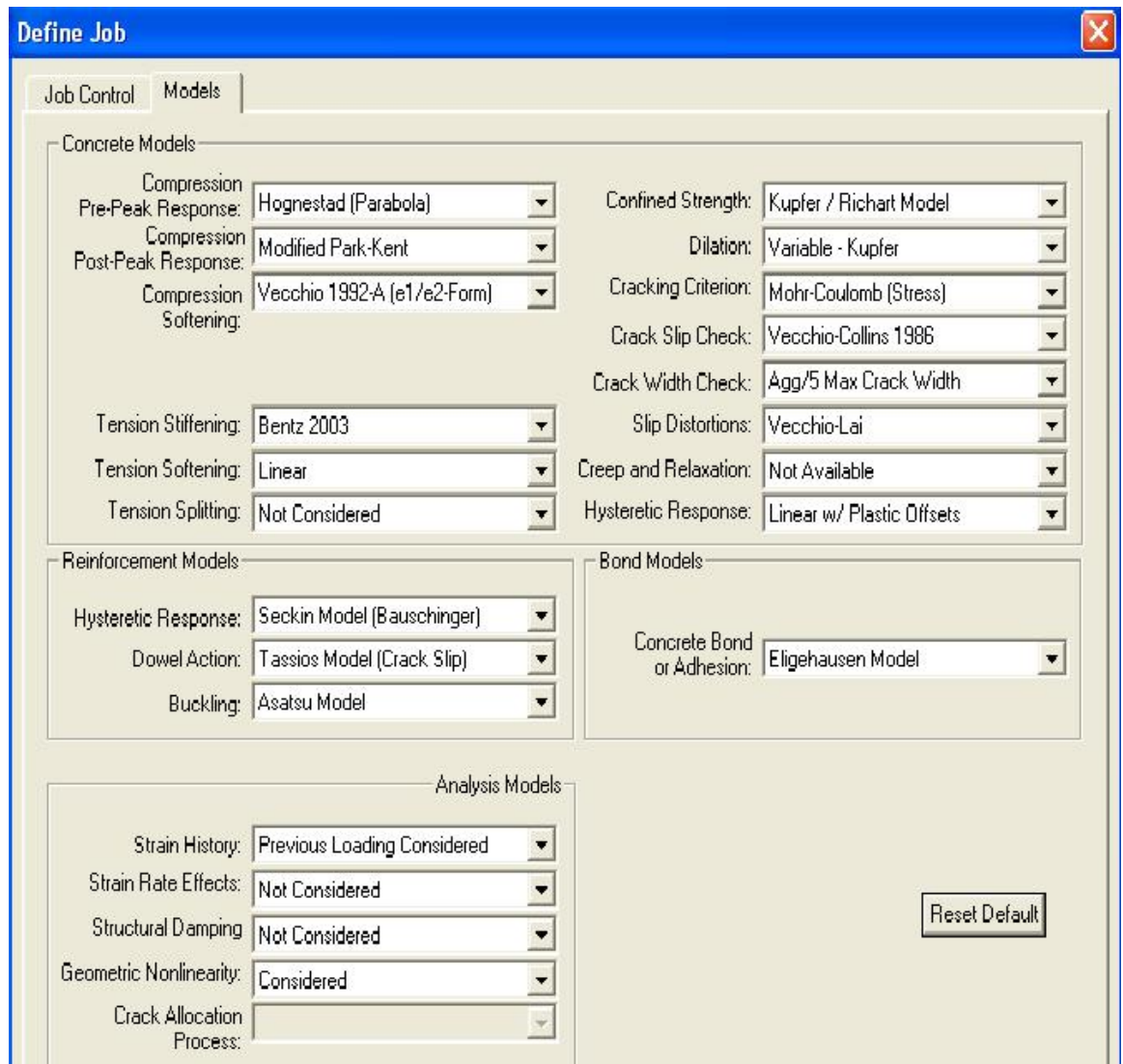


Figure 5.5: Models Property Page Display

The second step is to define the structure data which describe the finite element model itself. The finite element mesh is created by specifying the numbering and location of nodes, elements, nodal restraints, material types and properties. The structure information dialog box as shown in Figure 5.6 is updated when the model is constructed.

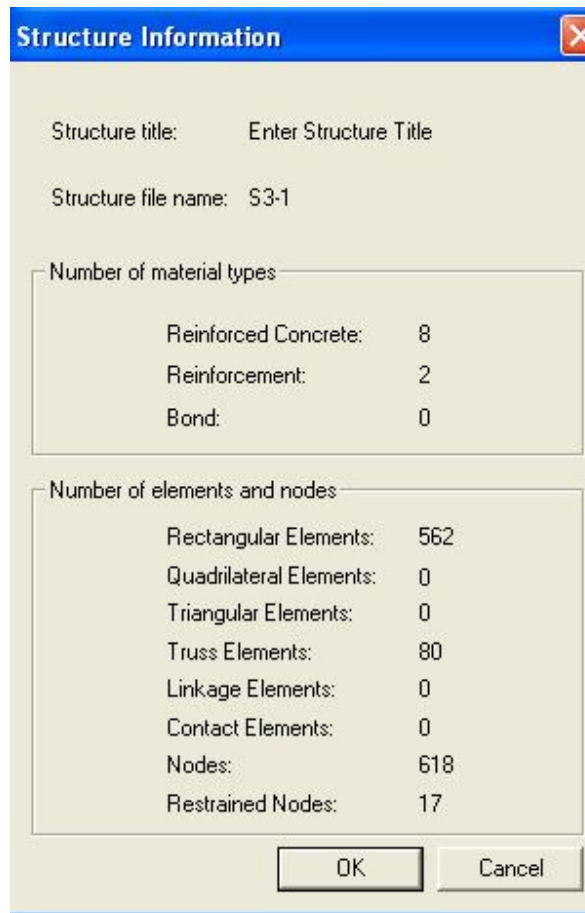


Figure 5.6: The Structure Information Dialog

The reinforced concrete material types and reinforcement properties can be defined using the dialog boxes shown in Figures 5.7 and 5.8.

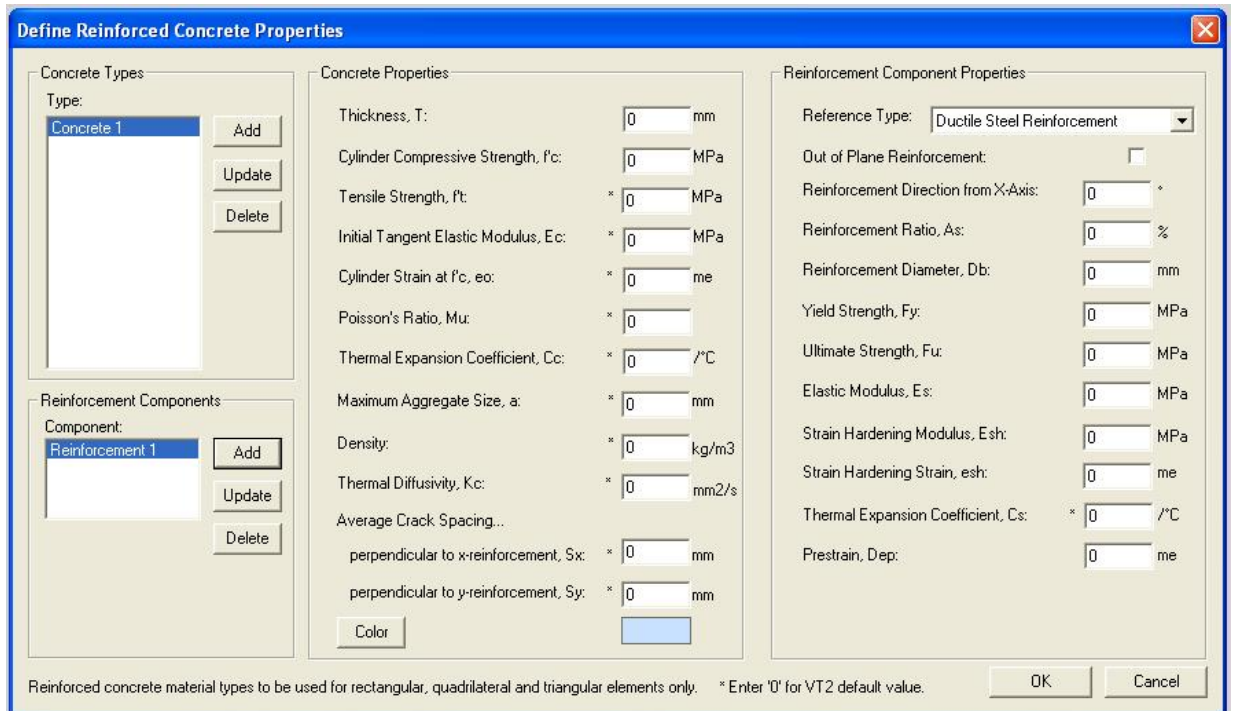


Figure 5.7: Reinforced Concrete Materials Property Dialog Box

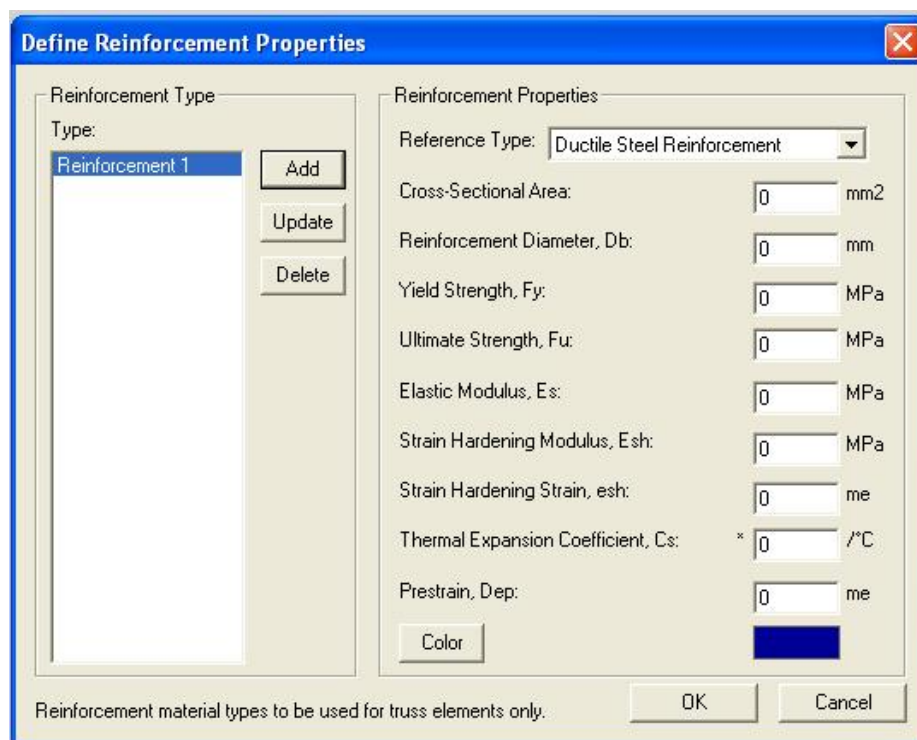


Figure 5.8: Reinforcement Material Properties Dialog Box

The third step is to define the load case. A load information dialog box is shown in Figure 5.9.

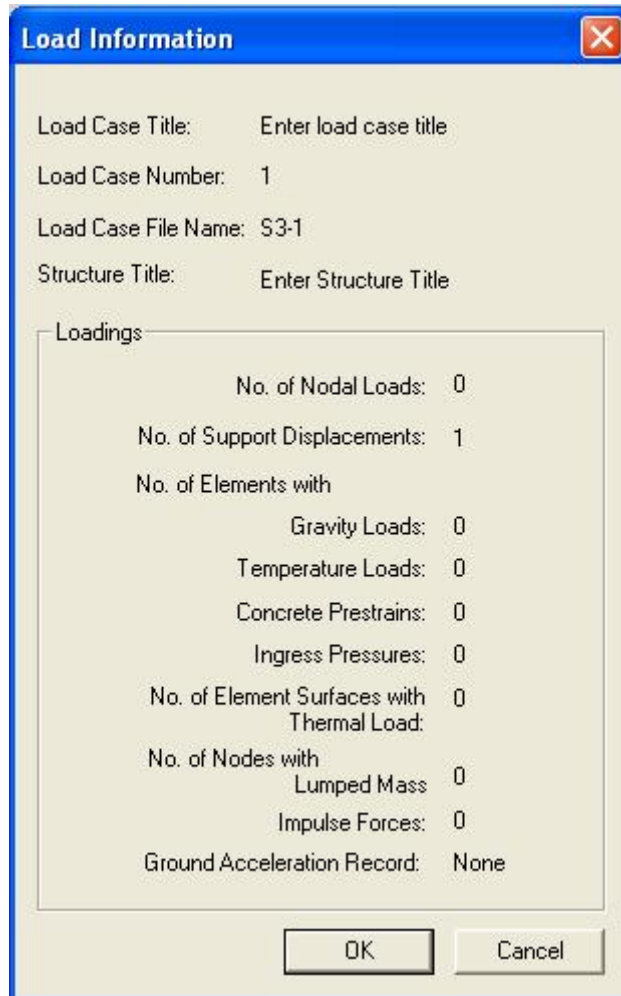


Figure 5.9: Load Information Dialog Box

All the nine beams tested were symmetrical; thus, only half of each beam was modelled. Meshes of 14 x 40, eight-degree-of-freedom rectangular elements were used for the beam. The longitudinal reinforcements (top and bottom) were modelled using truss bar elements, and the transverse reinforcement were modelled as smeared reinforcement. A typical finite element mesh used for modelling one of the geopolymer concrete beams is shown in Figure 5.10.

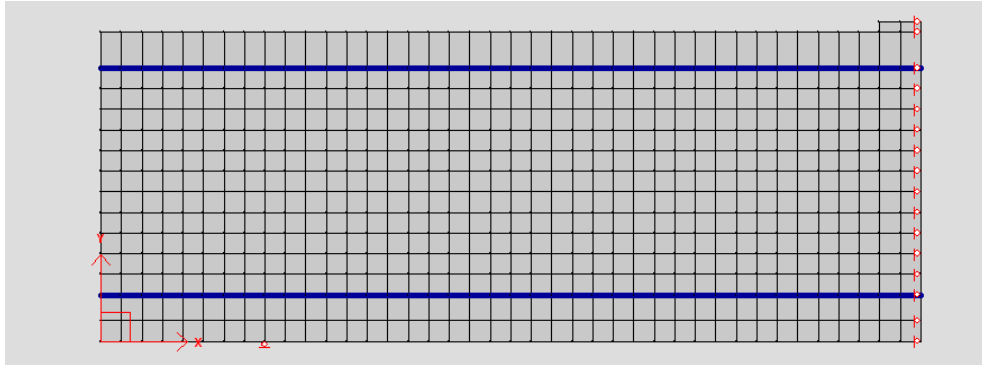


Figure 5.10: Typical Finite Element Meshes For Beam S3-1

For loading, a displacement-control mode with a typical step size of 0.25mm was used for all beams. The end support was restrained in Y-direction only, to simulate the condition of a roller support. The nodes at the beam centreline were restrained in the X-direction only, allowing downward movement at the centre of the beams.

For material properties specifications, the actual concrete compressive strength from the cylinder tests was used for all the beams. The actual yield strength and ultimate strength of both longitudinal and shear reinforcement obtained from laboratory tests were used. The modulus of elasticity for geopolymer concrete was taken from data measured by Hardjito and Rangan (2005), and interpolated to suit the concrete compressive strength for the beams in this study. For the tensile strength of geopolymer concrete, the recommendation by Neville (2000) was used, as below:

$$f'_{ct} = 0.3 f'_c \frac{2}{3}$$

All the constitutive modelling was done according to the default models of the DSFM. All input data files, namely job file, structure file and load case file for each beam, are given in Appendix E.

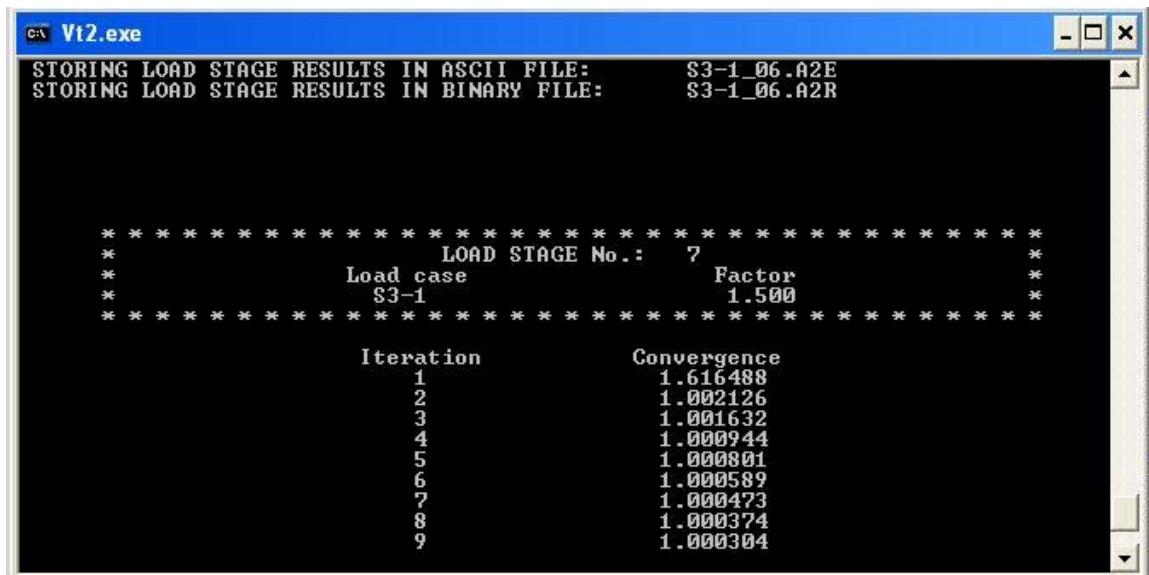
Once the Job, Structure and Load Case Data have been defined, the *VecTor2* analysis can be started.

5.3.1.2 VecTor2

VecTor2 is a two-dimensional non-linear finite element program for the analysis of reinforced concrete structures. *VecTor2* reads its input data files— the job file, structure file and load case files generated in *FormWorks*.

The computation algorithm involves using a modified secant stiffness formulation in an iterative manner, where the calculated material stiffness matrices are modified to reflect the current state of each element. Iterations are performed until the convergence of the material stiffness matrices is achieved. A typical *VecTor2* analysis dialog is shown in Figure 5.11.

The size of the result files from *VecTor2* is normally massive, and needs a post-processor program to allow fast inspection of the finite element analysis results. In this case, *Augustus* is used to retrieve the files and plot various kinds of graphs using information created from the analysis.



```

C:\> Vt2.exe
STORING LOAD STAGE RESULTS IN ASCII FILE:      S3-1_06.A2E
STORING LOAD STAGE RESULTS IN BINARY FILE:    S3-1_06.A2R

*****
*                                LOAD STAGE No.: 7                                *
*                                Load case      Factor                               *
*                                S3-1          1.500                                *
*****

      Iteration      Convergence
      1              1.616488
      2              1.002126
      3              1.001632
      4              1.000944
      5              1.000801
      6              1.000589
      7              1.000473
      8              1.000374
      9              1.000304

```

Figure 5.11: *VecTor2* Analysis Dialog

5.3.1.3 Augustus Program

A program called *Augustus* developed by University of Toronto is used as a post-processor for the data generated by *VecTor2*. It provides comprehensive post-analysis visualisation, such as global and local load-deformation response, element stress and strain conditions, deflection and crack patterns.

Figure 5.12 shows the crack pattern of Beam S3-1 generated by *Augustus*.

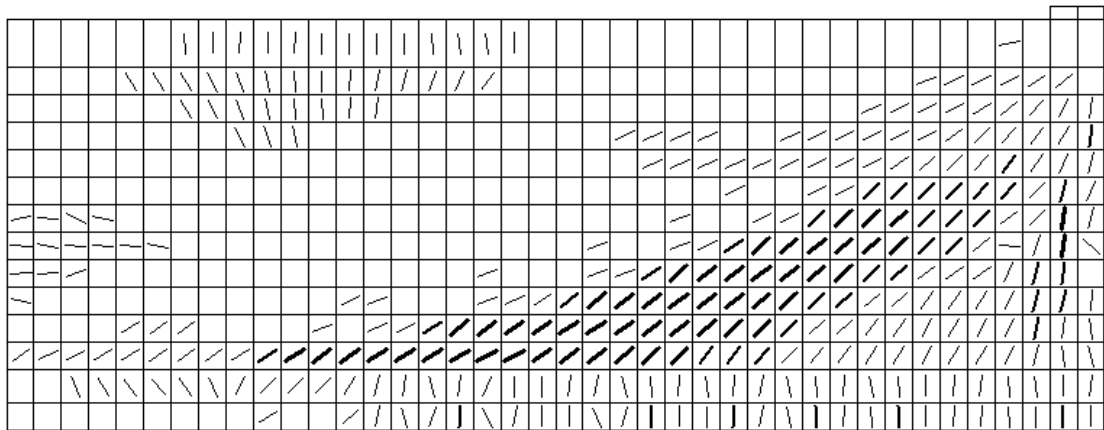


Figure 5.12: Crack Pattern of Beam S3-1 at Failure

All the results obtained from the analytical modelling using these computer programs are presented and compared with the test results in the next chapter.

CHAPTER 6

DISCUSSION AND CORRELATION OF TEST AND CALCULATED RESULTS FOR SHEAR STUDY

This chapter describes the correlation between test and calculated results for shear at diagonal cracking and also the shear strength of geopolymer concrete beams. The shear strength of the geopolymer concrete beams was calculated using the computer programs *ShearCalculator* and *VecTor2*, based on the theories of Kong and Rangan (1998) and Vecchio (2000), described in Chapter 5. The results calculated using the model proposed by von Ramin (2004) described in Chapter 2, to predict the shear strength of geopolymer concrete beams, are discussed. Comparison of shear strength between geopolymer concrete and Portland cement concrete beams using analytical models are presented. Correlation of test shear strength with the predictions by Codes is also given.

6.1 Shear at Diagonal Cracking

The prediction for the shear at diagonal cracking is calculated using the expression proposed by Zsutty (1968) and using the V_c term of the AS3600. It is usual practice to equate V_c from AS3600 to the shear force at initial diagonal cracking as no generally accepted and simple analytical method is available. This approach has no rational justification but provides a reasonable correlation with available test data and has been used in the ACI Code and Australian Standard for many years; it forms the basis for the shear provisions in AS3600 (Warner et al., 1998).

An expression derived by Zsutty (1968) reflecting some important parameters governing diagonal cracking strength using dimensional and statistical regression analysis also is used in many studies. The shear cracking load is given by Equation 6.1 below:

$$V_{cr} = 59bd \left(f'_c \rho \frac{d}{a} \right)^{\frac{1}{3}} \quad (6.1)$$

where

$$\rho = \left(\frac{A_{st}}{bd} \right)$$

The V_c term from draft AS3600 (2005), as given by Equation 2.82 in Section 2 previously:

$$V_c = \beta_1 \beta_2 \beta_3 b_v d_o \left[\frac{A_{st}}{b_v d_o \times f'_c} \right]^{1/3}$$

The results show good correlation between test and calculated values (Table 6.1). The average ratio of test/prediction value is 1.08 and 1.14 with Zsutty's expression and draft AS3600-05 respectively. The coefficient of variation (COV) using these two methods are similar, both giving 11.6%.

Table 6.1: Correlation of Test and Predicted Shear Cracking Load

Beam Mark	f'_c (MPa)	Test Shear Cracking Load (kN)	Prediction by Z_{suty} (Equation 6.1) (kN)	Test/Prediction (Z_{suty})	Prediction by AS3600 V_c Term (kN)	Test/Prediction (AS3600)
S1-1	45	87	75	1.16	70	1.23
S1-2	45	79	75	1.05	70	1.12
S1-3	44	82	75	1.09	70	1.17
S2-1	56	115	88	1.31	84	1.37
S2-2	50	92	85	1.08	81	1.14
S2-3	50	83	85	0.98	81	1.03
S3-1	49	79	92	0.86	87	0.91
S3-2	49	95	92	1.03	87	1.09
S3-3	56	112	97	1.15	91	1.23
			Average	1.08		1.14
			COV (%)	11.6		11.6

6.2 Shear Strength of Test Beams

6.2.1 Comparison with Prediction using Analytical Models

The calculated shear strength using the analytical models proposed by von Ramin (2004), Kong and Rangan (1998) and Vecchio (2000), described previously, are compared with the test values in Tables 6.2 and 6.3.

Table 6.2: Summary of Predicted Shear Strength using Analytical Models

Series	Beam Mark	p_{st} (%)	p_{sv} (%)	f'_c (MPa)	Test Shear Strength (kN)	Predicted Shear Strength (kN)		
						von Ramin (2004)	Kong and Rangan (1998)	Vecchio (2000)
1	S1-1	1.74	0.10	45	210.3	148.7	128.8	206.5
	S1-2	1.74	0.13	45	204.8	163.8	141.5	203.5
	S1-3	1.74	0.17	44	187.8	184.1	153.4	205.2
2	S2-1	2.32	0.10	56	258.3	167.2	142.3	234.4
	S2-2	2.32	0.13	50	262.3	173.8	154.2	231.6
	S2-3	2.32	0.17	50	260.8	193.7	173.0	250.9
3	S3-1	3.14	0.10	49	261.5	166.2	142.8	225.8
	S3-2	3.14	0.13	49	276.2	182.6	156.8	239.6
	S3-3	3.14	0.17	56	333.3	205.5	183.4	275.9

Table 6.3: Summary of Test-to-Predicted Ratio using Analytical Models

Series	Beam Mark	p_{sl} (%)	p_{sv} (%)	f'_c (MPa)	Test Shear Strength (kN)	Test / Predicted Ratio		
						von Ramin (2004)	Kong and Rangan (1998)	Vecchio (2000)
1	S1-1	1.74	0.10	45	210.3	1.41	1.63	1.02
	S1-2	1.74	0.13	45	204.8	1.25	1.45	1.01
	S1-3	1.74	0.17	44	187.8	1.02	1.22	0.92
2	S2-1	2.32	0.10	56	258.3	1.54	1.81	1.10
	S2-2	2.32	0.13	50	262.3	1.51	1.70	1.13
	S2-3	2.32	0.17	50	260.8	1.35	1.51	1.04
3	S3-1	3.14	0.10	49	229.8	1.57	1.83	1.16
	S3-2	3.14	0.13	49	261.5	1.51	1.76	1.15
	S3-3	3.14	0.17	56	276.2	1.62	1.82	1.21
					Average	1.42	1.64	1.08
					COV (%)	13.4	12.7	8.3

From Table 6.3, it can be seen that the mean value of test-to-predicted shear strength using the model proposed by von Ramin (2004) is 1.42 with a coefficient of variation of 13.4%. The mean value of test-to-predicted shear strength using Kong and Rangan (1998) is 1.64 with a coefficient of variation of 12.7%. The prediction

from *VecTor2* using the DSFM by Vecchio (2000) yields a mean test-to-predicted ratio of 1.08 and a coefficient of variation of 8.3%.

The test and calculated values using *VecTor2* incorporating the DSFM by Vecchio (2000) agree well, whereas values calculated by von Ramin (2004) and Kong and Rangan (1998) are conservative. This is because the *VecTor2* program allows greater facilitation and control for the user in terms of input. In addition, comprehensive finite element analysis for the test beams including material properties contributes to the production of better simulation of beams.

6.2.2 Comparison with Prediction using Code Provisions

The calculated shear strength using the code provisions are compared with the test values, presented in Tables 6.4 and 6.5.

Both the code provisions draft AS3600-05 and ACI318-08 give conservative results of shear strength prediction for geopolymer concrete beams. Draft AS3600-05 gives an average test-to-predicted ratio of 1.70 with a coefficient of variation of 12.9%; and ACI318-08 yields a test-to-predicted ratio of 2.55 with a coefficient of variation of 16.1%.

Table 6.4: Summary of Predicted Shear Strength using Code Provisions

Series	Beam Mark	p_{st} (%)	p_{sv} (%)	f'_c (MPa)	Test Shear Strength (kN)	Predicted Shear Strength (kN)	
						Draft AS3600-2005 (kN)	ACI318-08 (kN)
1	S1-1	1.74	0.10	45	210.3	123.7	87.4
	S1-2	1.74	0.13	45	204.8	126.2	94.8
	S1-3	1.74	0.17	44	187.8	155.8	106.6
2	S2-1	2.32	0.10	56	258.3	137.0	93.3
	S2-2	2.32	0.13	50	262.3	146.3	97.2
	S2-3	2.32	0.17	50	260.8	166.7	109.5
3	S3-1	3.14	0.10	49	261.5	139.8	88.5
	S3-2	3.14	0.13	49	276.2	152.2	95.8
	S3-3	3.14	0.17	56	333.3	176.6	112.1

Table 6.5: Summary of Test-to-Predicted Ratio using Code Provisions

Series	Beam Mark	p_{sl} (%)	p_{sv} (%)	f'_c (MPa)	Test Shear Strength (kN)	Test / Predicted Ratio	
						Draft AS3600-2005 (kN)	ACI318-08 (kN)
1	S1-1	1.74	0.10	45	210.3	1.70	2.41
	S1-2	1.74	0.13	45	204.8	1.62	2.16
	S1-3	1.74	0.17	44	187.8	1.21	1.76
2	S2-1	2.32	0.10	56	258.3	1.88	2.77
	S2-2	2.32	0.13	50	262.3	1.79	2.70
	S2-3	2.32	0.17	50	260.8	1.56	2.38
3	S3-1	3.14	0.10	49	261.5	1.87	2.95
	S3-2	3.14	0.13	49	276.2	1.82	2.88
	S3-3	3.14	0.17	56	333.3	1.89	2.97
					Average	1.70	2.55
					COV (%)	12.9	16.1

6.3 Cracking/Crushing Patterns and Failure Modes

Cracking and crushing patterns from analytical modelling using *VecTor2* were compared to the test beams. As all the beams were symmetrical about the centre point, only half of each beam (the left shear span) was modelled. The comparisons are shown in Figures 6.1 to 6.9. It was found that the modelling produced reasonably accurate results, especially for the beams which failed in diagonal tension: Beams S1-3, S2-1, S3-1, S3-2 and S3-3, as shown in Figures 6.3, 6.4, 6.7, 6.8 and 6.9 respectively. The crushing patterns near the loading plate were also simulated correctly for the beams which failed in shear-compression: Beams S1-1, S1-2, S2-2 and S2-3, as shown in Figures 6.1, 6.2, 6.5 and 6.6 respectively.

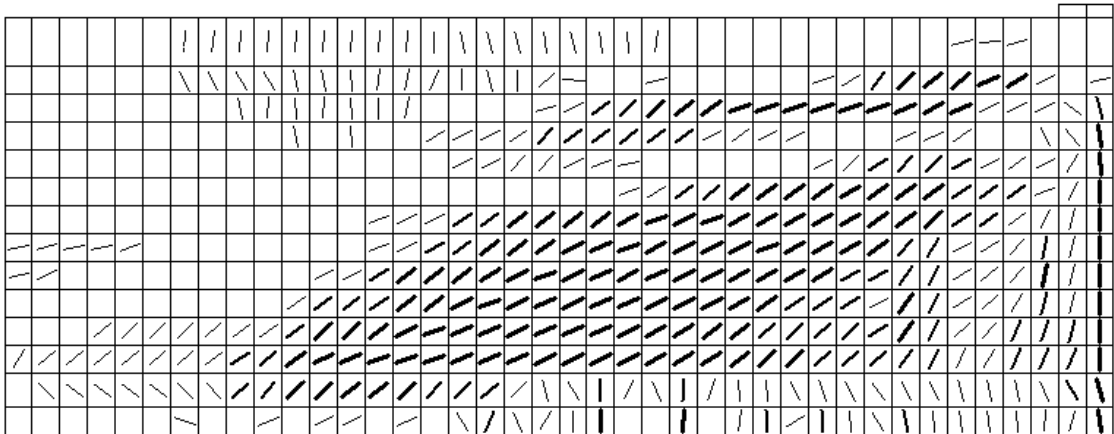


Figure 6.1: Comparison of Crack Patterns for Beam S1-1

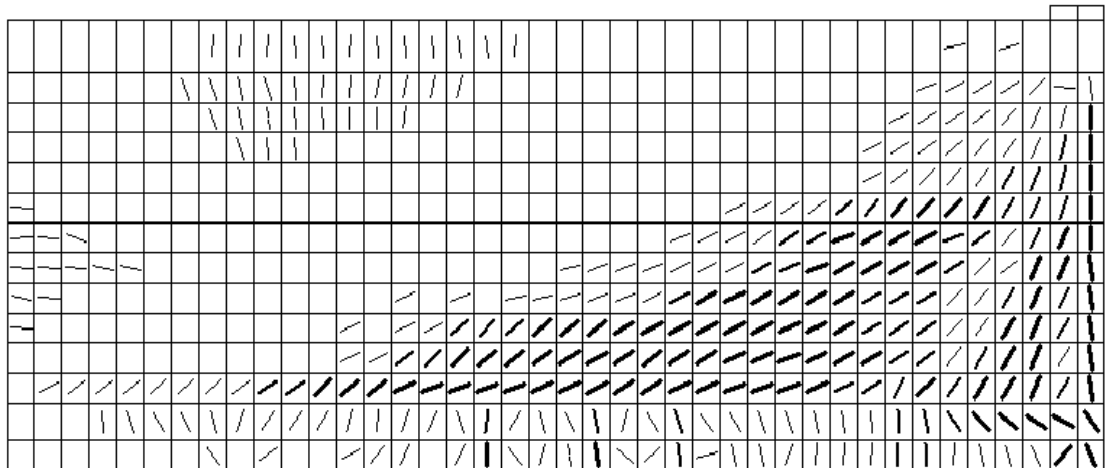
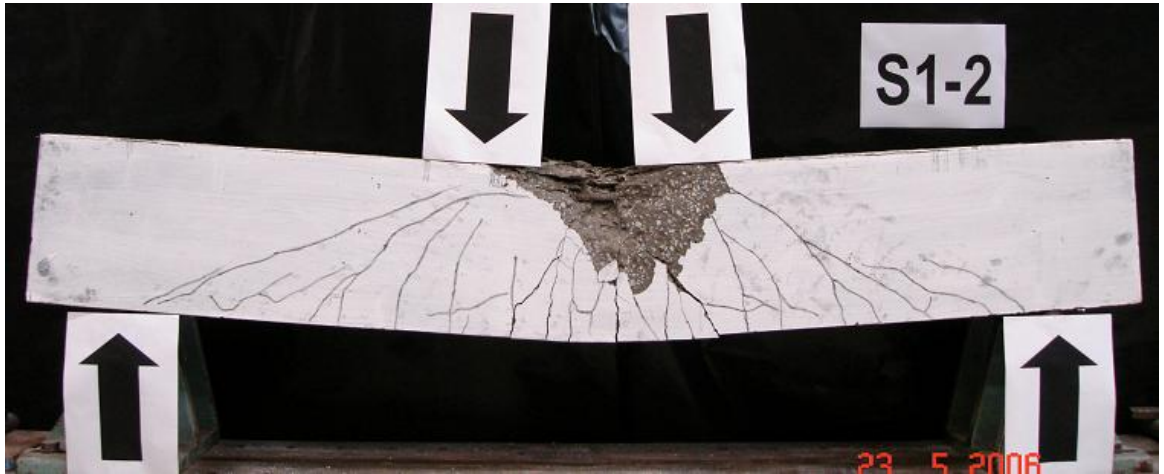


Figure 6.2: Comparison of Crack Patterns for Beam S1-2

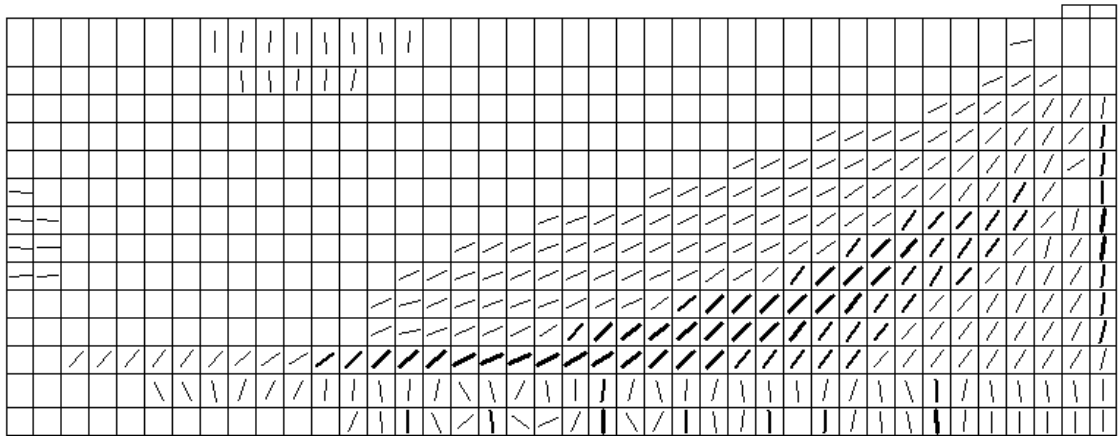
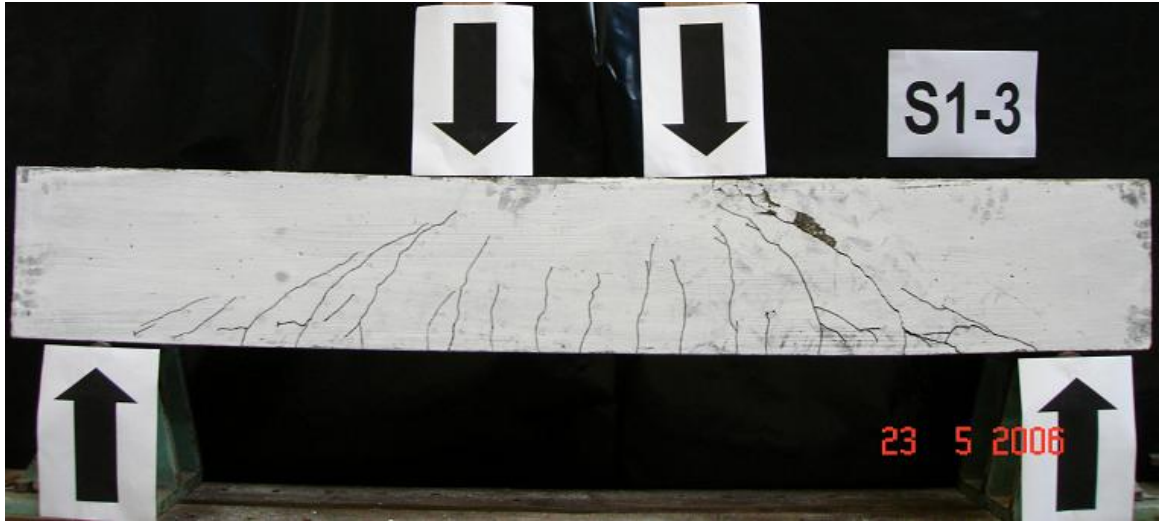


Figure 6.3: Comparison of Crack Patterns for Beam S1-3

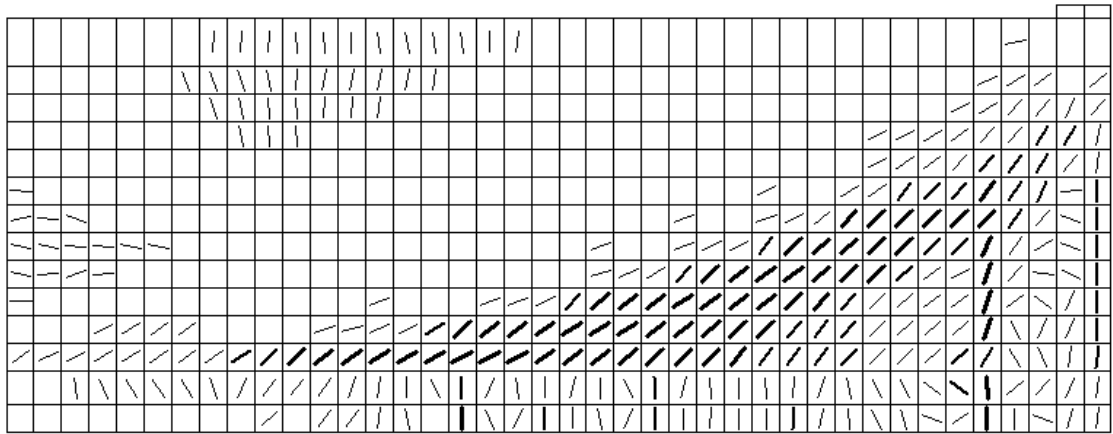
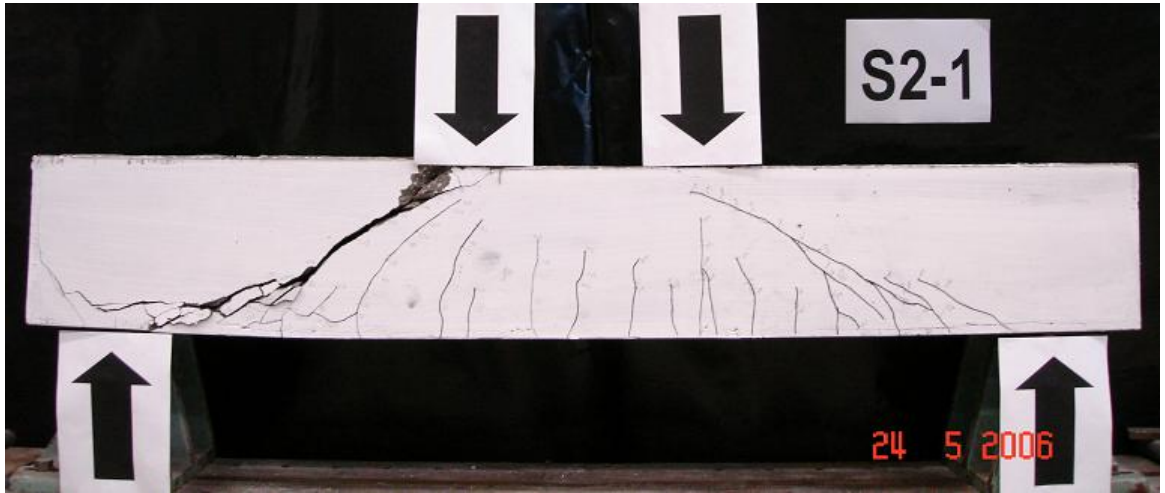


Figure 6.4: Comparison of Crack Patterns for Beam S2-1

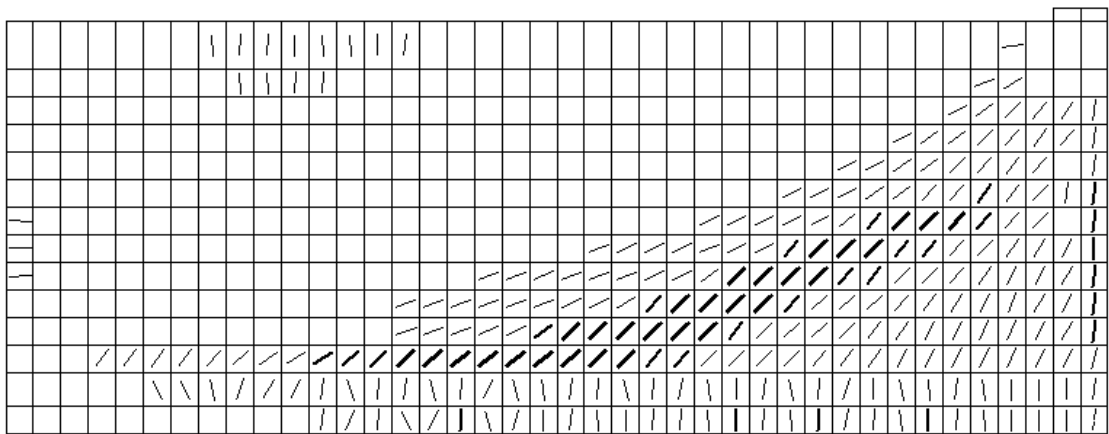


Figure 6.5: Comparison of Crack Patterns for Beam S2-2

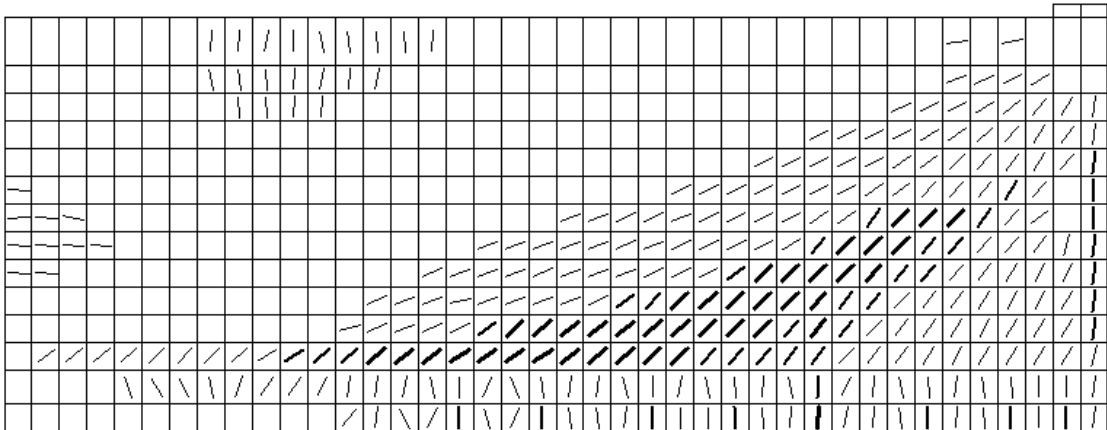
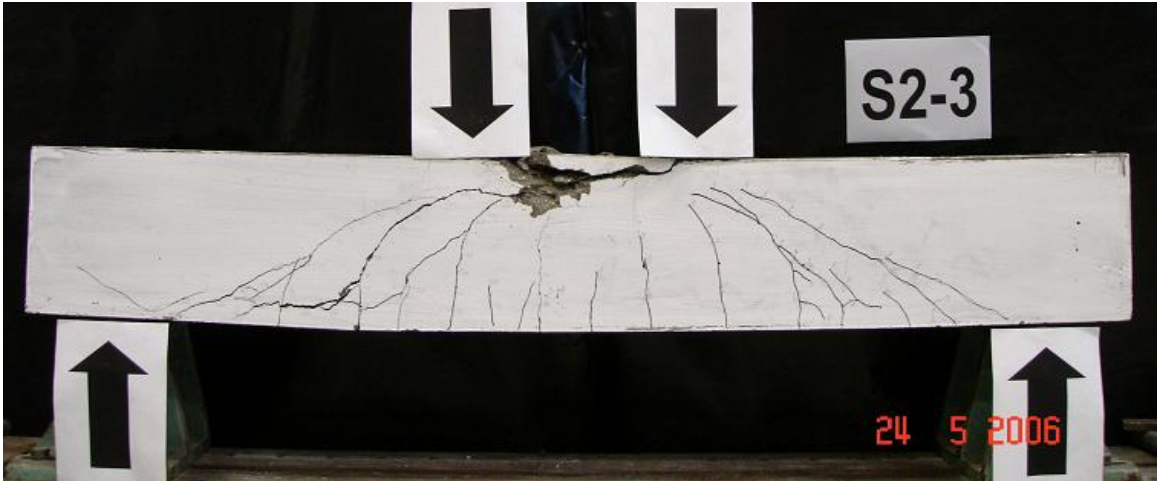


Figure 6.6: Comparison of Crack Patterns for Beam S2-3

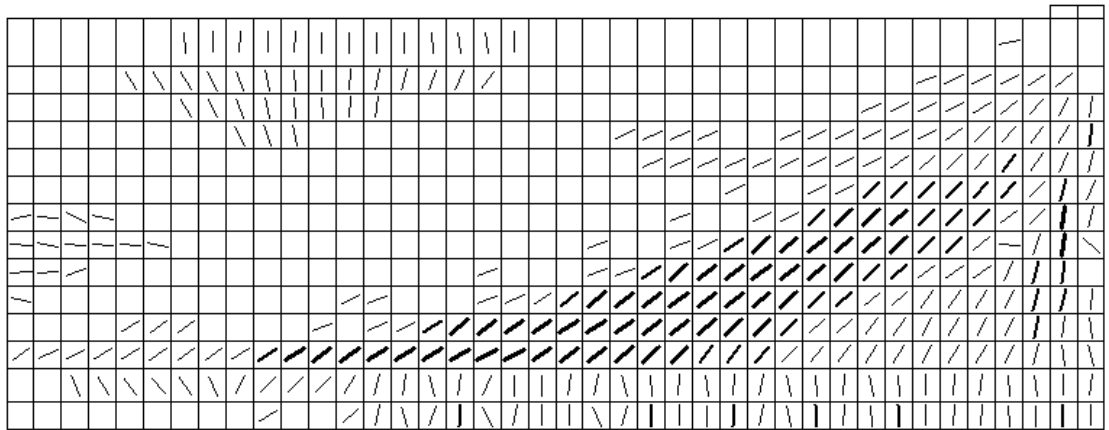
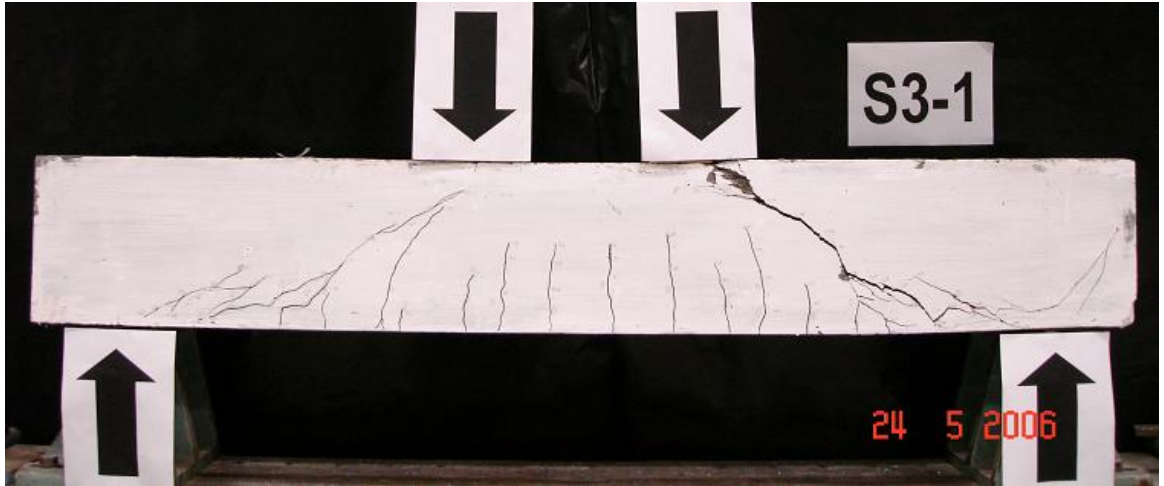


Figure 6.7: Comparison of Crack Patterns for Beam S3-1

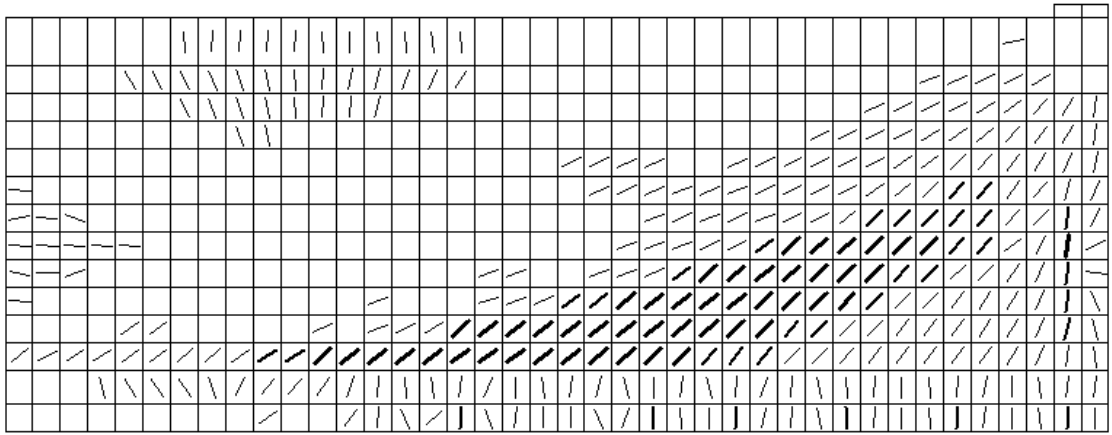
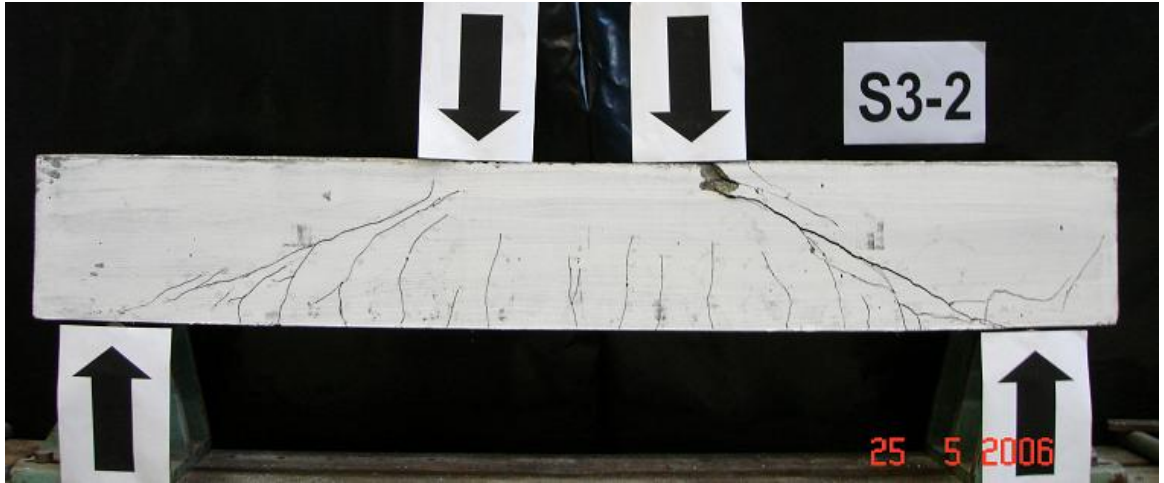


Figure 6.8: Comparison of Crack Patterns for Beam S3-2

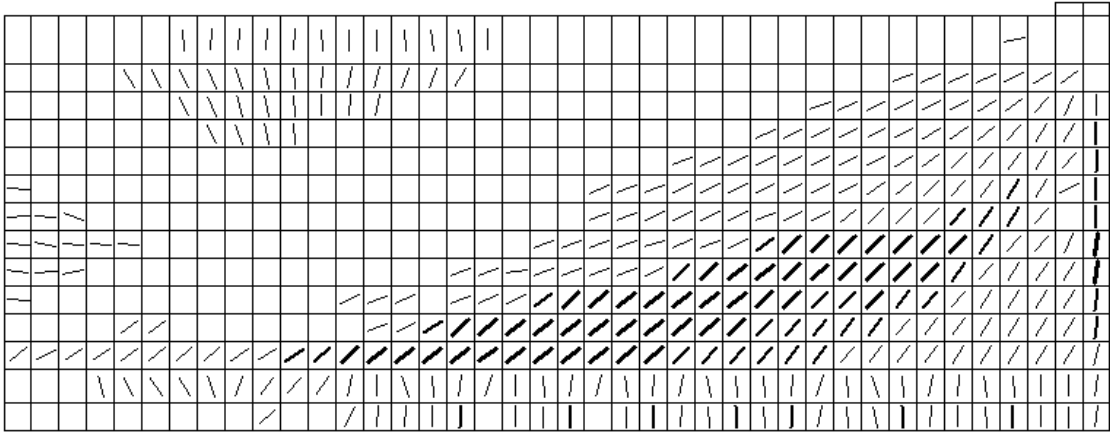
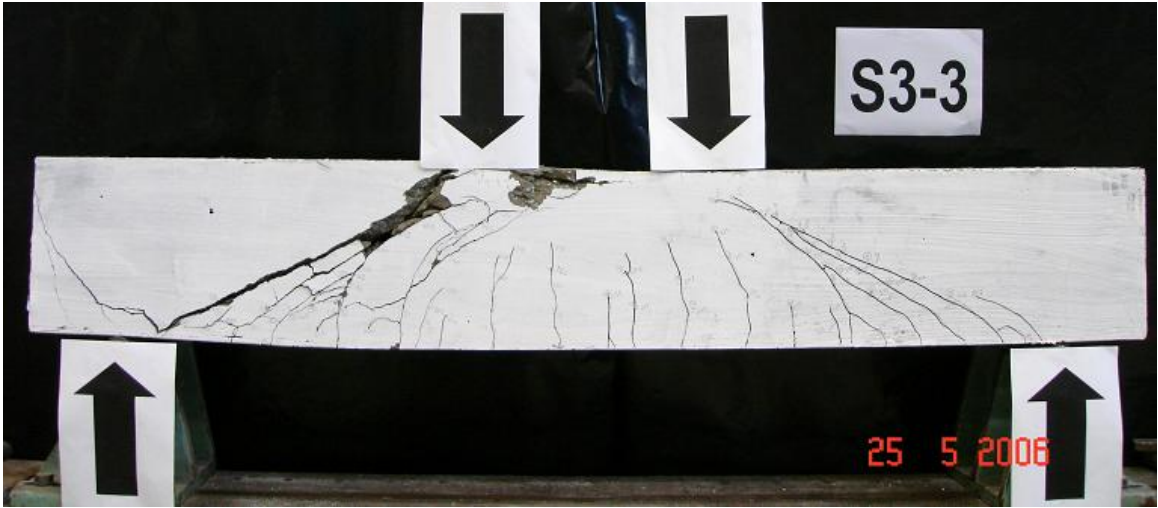


Figure 6.9: Comparison of Crack Patterns for Beam S3-3

6.4 Comparison of Shear Strength Between Geopolymer Concrete and Portland Cement Concrete Beams

In order to compare the shear strength of geopolymer concrete beams and Portland cement concrete beams, a summary of results from studies conducted by von Ramin (2004), Kong and Rangan (1998) and Vecchio (2000) for the validation of their analytical models for Portland cement concrete beams was used.

The model proposed by von Ramin (2004) was evaluated with 168 beams from the database of experimental results in the literature. It was found that the ratio of test to predicted shear capacity has a mean of 1.14 and a COV of 15.0%.

A total of 147 beams from literature were selected and calculated using theory by Kong and Rangan (1998). The test shear strength of the beams was compared to the prediction by theory and it was found that the ratio of test to predicted shear capacity of these 147 beams is 1.23 and a COV of 32.8%.

In support of the theoretical formations of the DSFM, experimental data from several series of test specimens were examined by Vecchio et al. (2001). Three series of beams were considered for model collaborations. The first set was 12 beams tested by Bresler and Scordelis (1963); the second set was 18 beams tested by Stanik (1998) and the third set was 24 beams tested by Gupta (1998). It was found that the ratio of test to predicted shear capacity of these 52 beams using DSFM has a mean of 1.00 and a coefficient of variation of 20.3%.

The results of model collaborations for Portland cement concrete beams by Vecchio (2000), Kong and Rangan (1998) and von Ramin (2004) are given in Table 6.6. The results are compared to the shear strength of geopolymer concrete beams obtained from these models.

Table 6.6: Comparison of Shear Strength of Geopolymer Concrete and Portland Cement Concrete Beams using Analytical Models

Models	Geopolymer Concrete Beams		Portland Cement Concrete Beams	
	Test/Predicted Ratio	COV (%)	Test/Predicted Ratio	COV (%)
Von Ramin (2004)	1.42	13.4	1.14	15.0
Kong and Rangan (1998)	1.64	12.7	1.23	32.8
Vecchio (2000)	1.08	8.3	1.00	20.3

From Table 6.6, it can be seen that the DSFM model proposed by Vecchio (2000) incorporating finite element analysis gives the best prediction of shear capacity for both geopolymer concrete and Portland cement concrete beams.

According to Vecchio et al. (2001), for beams containing shear reinforcement ratio less than 0.2%, the DSFM shows improved correlation with test results. For the behaviour of beams typically dominated by the formation of a principal diagonal crack, the DSFM shows better modelling in delaying the rotation of the cracks, resulting in improved predictions of strength. This explains the good correlation of results for the geopolymer concrete beams in this study, most of which failed in diagonal tension dominated by the formation of principal cracks, and with shear reinforcement ratio ranged from 0.10% to 0.17%.

The comparison of the results demonstrates that the methods of calculations used for reinforced Portland cement concrete beams are applicable for predicting the shear

strength of reinforced geopolymer concrete beams. Code provisions are safe to predict the shear strength of geopolymer concrete beams.

SECTION TWO
BOND BEHAVIOUR OF REINFORCED FLY
ASH-BASED GEOPOLYMER CONCRETE
BEAMS

CHAPTER 7

MANUFACTURE AND TESTING OF BEAMS FOR BOND STUDY

This chapter describes the details of the test program prepared to investigate the bond strength of lap-spliced bars in fly ash-based geopolymer concrete beams. Details of the test beams, materials, manufacturing of specimens, test set-up, instrumentation and test procedure are presented.

7.1 Experimental Aims

The experimental program was developed to study the bond behaviour of geopolymer concrete beams. The aims of the study included:

- Investigating the failure modes and crack patterns of the geopolymer concrete beams failing in bond
- Investigating the steel-geopolymer concrete interface at splice region after failure
- Studying the effect of concrete cover, bar diameter, splice length and concrete compressive strength on bond strength of geopolymer concrete
- Comparing the test bond strength of geopolymer concrete beams with predictions using analytical models and code provisions for Portland cement concrete beams
- Obtaining the load-deflection curves of the beams

7.2 Design of Test Specimens

The test program consisted of twelve lap-spliced beam specimens with a cross section of 200 mm x 300 mm. All beam specimens were 2500 mm long. The size of test specimen was selected to suit the capacity of the testing machine in the laboratory.

The beams were designed to study the influence of concrete compressive strength, bar diameter and splice length on the strength of splices in geopolymer concrete beams. All the beams were designed with tensile lap-splices in the constant moment zone. The design splice length was calculated based on draft AS3600 (2005), as described in Chapter 2. In order to obtain a bond splitting mode of failure, all splice lengths were chosen to develop steel stress less than yield at failure. No transverse reinforcement was provided in the splice region.

The beams were divided into two series:

- Series D: three bar sizes of 16 mm, 20 mm and 24 mm diameter were selected, giving three C/d_b ratios (where C is the minimum cover) of 1.0, 1.5 and 2.2 respectively. The L_s/d_b ratio for all the test beams in this series was fixed at 15.
- Series L: three splice lengths of 300 mm, 450 mm and 720 mm were selected, giving three ratios L_s/d_b of 12.5, 18.8 and 30.0 respectively. The C/d_b ratio for all the test beams in this series was fixed at 1.0.

In each series, two identical companion beams using normal strength geopolymer concrete and high strength geopolymer concrete were cast. Nominal concrete compressive strengths of 30 MPa – 35 MPa for normal strength geopolymer concrete and 50 MPa to 55 MPa for high strength geopolymer concrete were selected.

For the beam mark, a two-part notation was used to indicate the parameters in each beam. The first part of notation indicates the concrete strength (N for normal strength geopolymer concrete or H for high strength geopolymer concrete). The second part indicates whether D (bar diameter) or L (splice length) is the parameter, with the associated ratios of C/d_b or L_s/d_b values.

The complete details of the beams are given in Table 7.1.

Table 7.1: Details of the Test Beams for Bond Study

Series	Beam Mark	C/d_b Ratio	L_s/d_b Ratio	Bar Diameter d_b (mm)	Splice Length L_s (mm)	Bottom cover c_b (mm)	Side Cover c_{so} (mm)	Half of Spacing Between Spliced Bars c_{si} (mm)
D	N-D-1.0	1.0	15.0	24	360	25	25	27
	N-D-1.5	1.5	15.0	20	300	30	30	30
	N-D-2.2	2.2	15.0	16	240	35	35	33
	H-D-1.0	1.0	15.0	24	360	25	25	27
	H-D-1.5	1.5	15.0	20	300	30	30	30
	H-D-2.2	2.2	15.0	16	240	35	35	33
L	N-L-12.5	1.0	12.5	24	300	25	25	27
	N-L-18.8	1.0	18.8	24	450	25	25	27
	N-L-30.0	1.0	30.0	24	720	25	25	27
	H-L-12.5	1.0	12.5	24	300	25	25	27
	H-L-18.8	1.0	18.8	24	450	25	25	27
	H-L-30.0	1.0	30.0	24	720	25	25	27

All the longitudinal reinforcements were deformed bars used in Australian practice with the designation “N”, which is designed to give a minimum yield strength of 500MPa. Transverse reinforcement was provided at the shear spans using size 10 mm deformed bars to prevent shear failures. The geometry and details of the beams are shown in Figures 7.1 to 7.6.

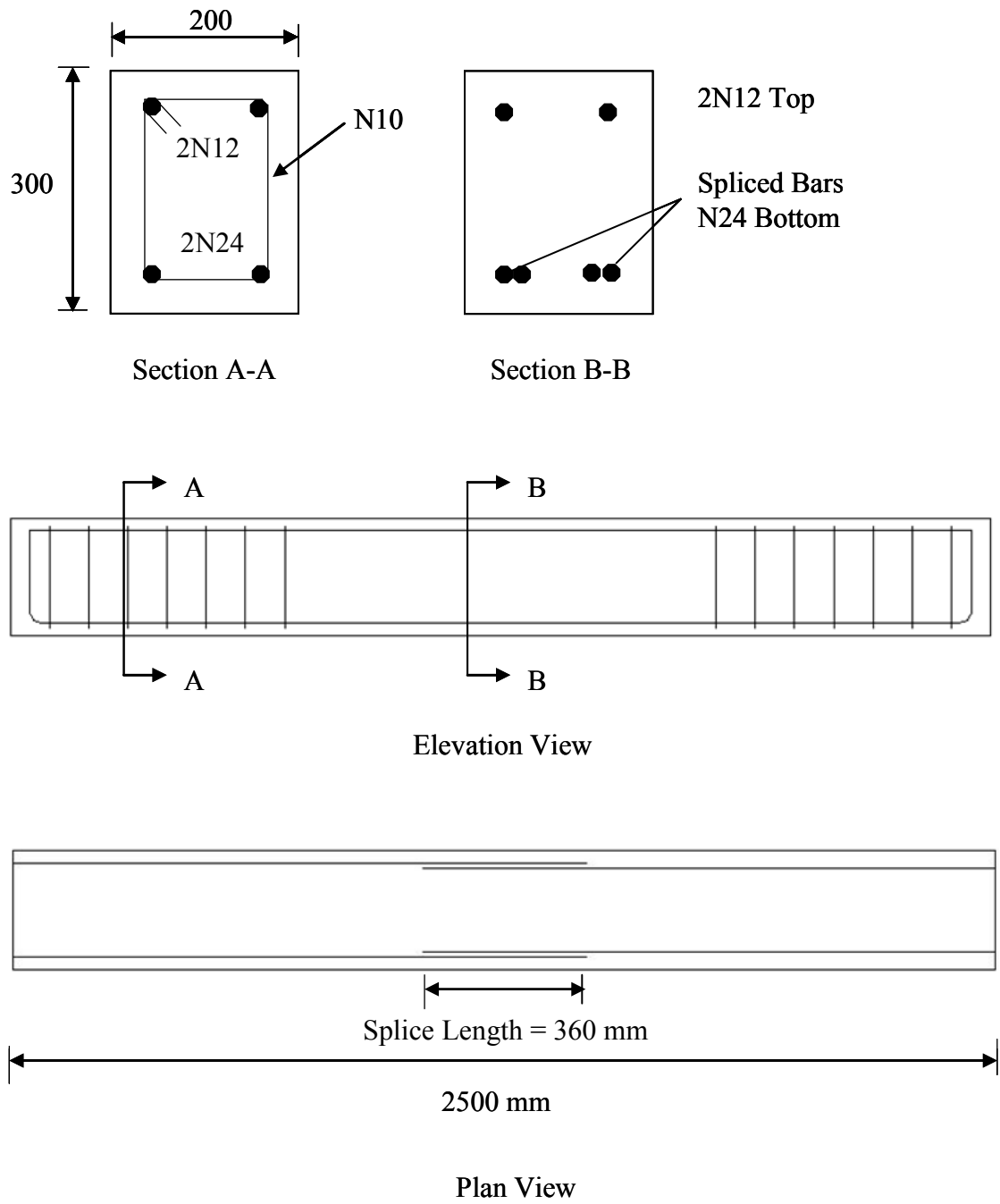


Figure 7.1: Geometry and Reinforcement Arrangement for Beams N-D-1.0 and H-D-1.0

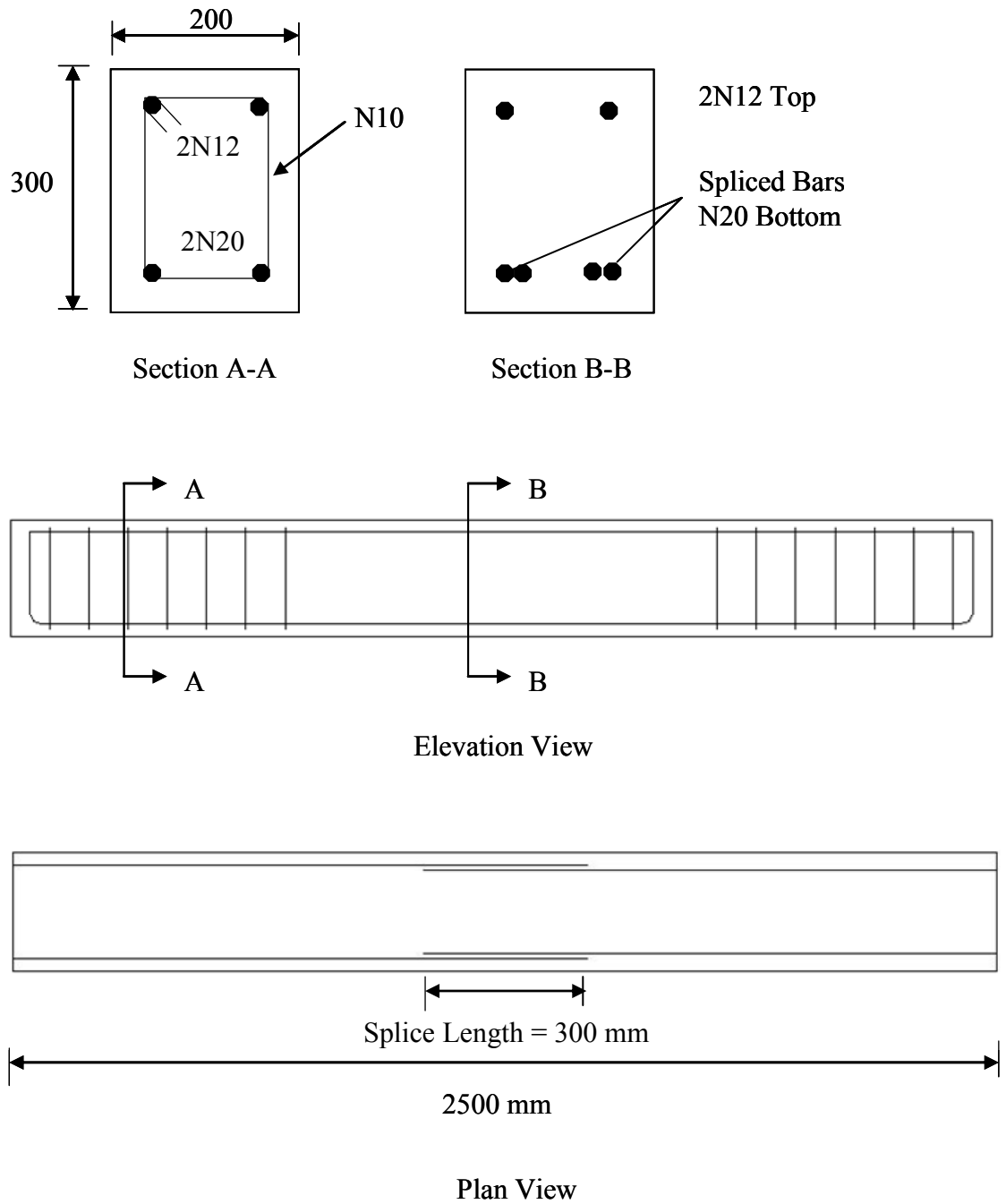


Figure 7.2: Geometry and Reinforcement Arrangement for Beams N-D-1.5 and H-D-1.5

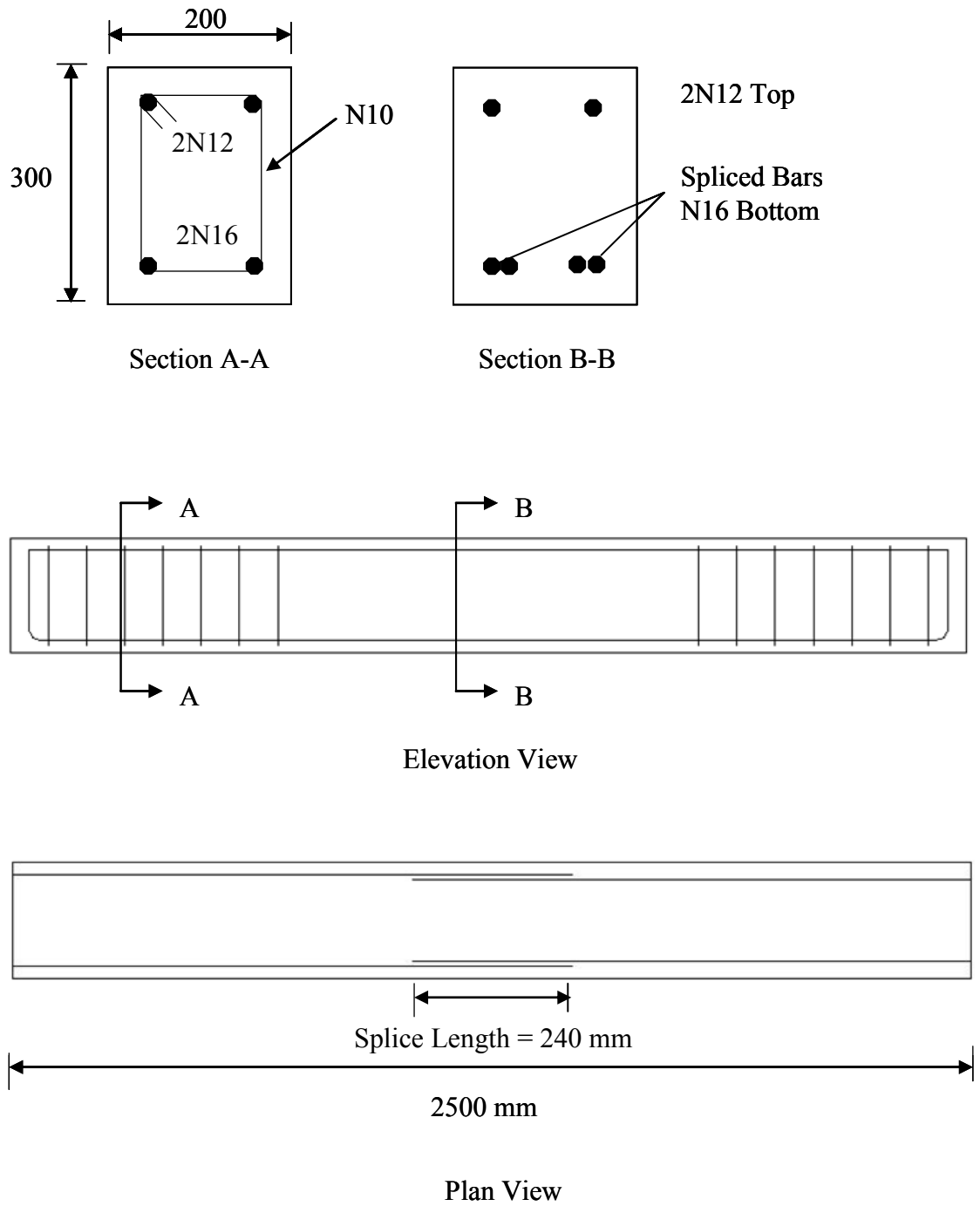


Figure 7.3: Geometry and Reinforcement Arrangement for Beams N-D-2.2 and H-D-2.2

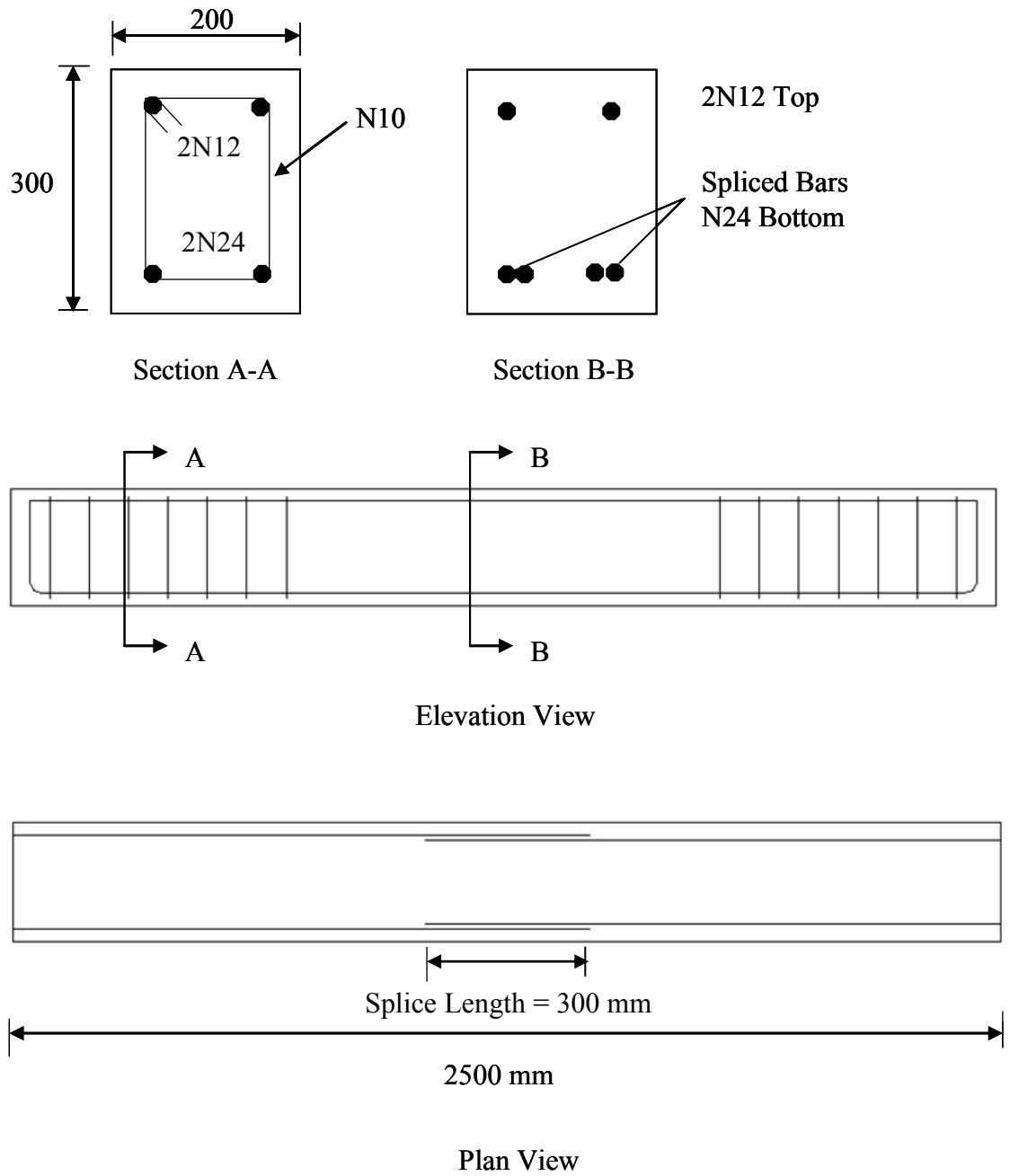


Figure 7.4: Geometry and Reinforcement Arrangement for Beams N-L-12.5 and H-L-12.5

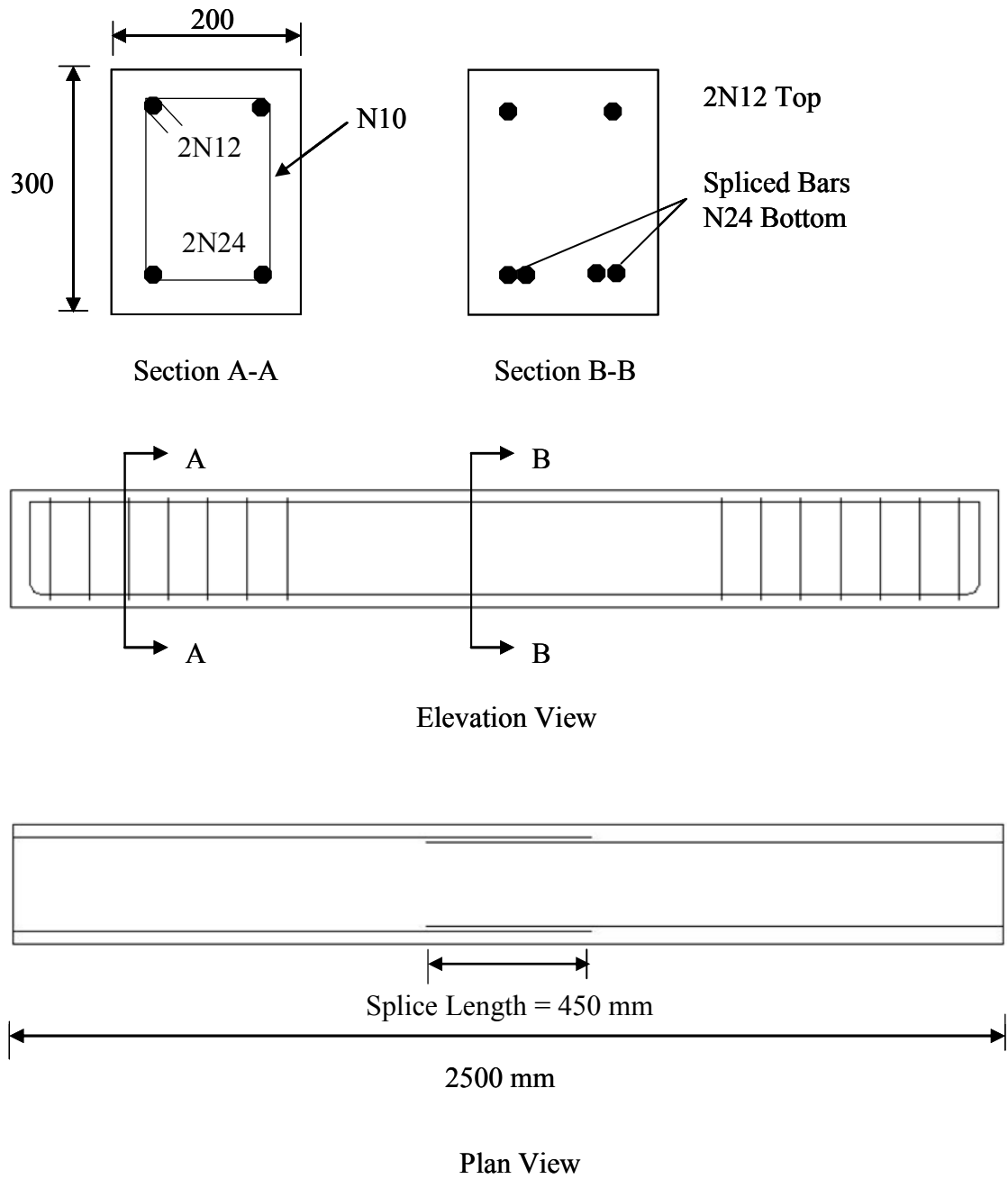
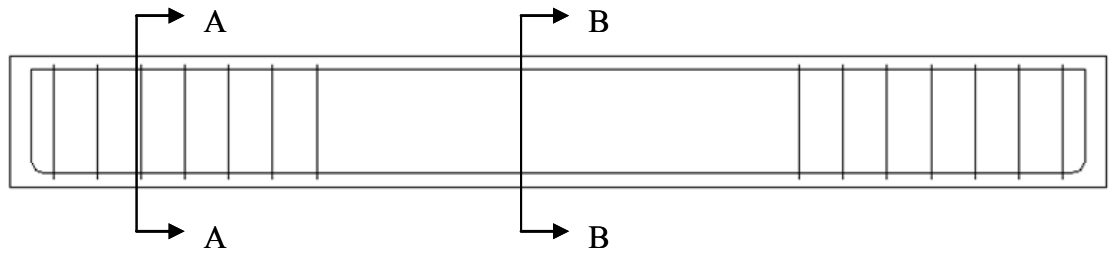
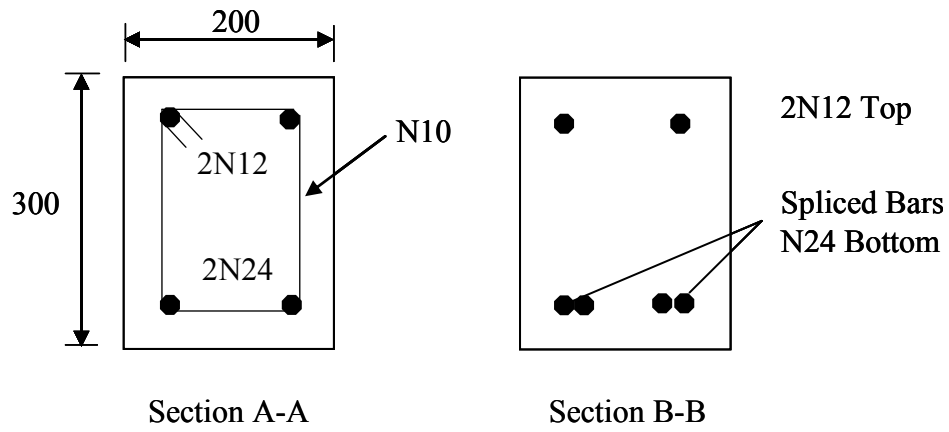
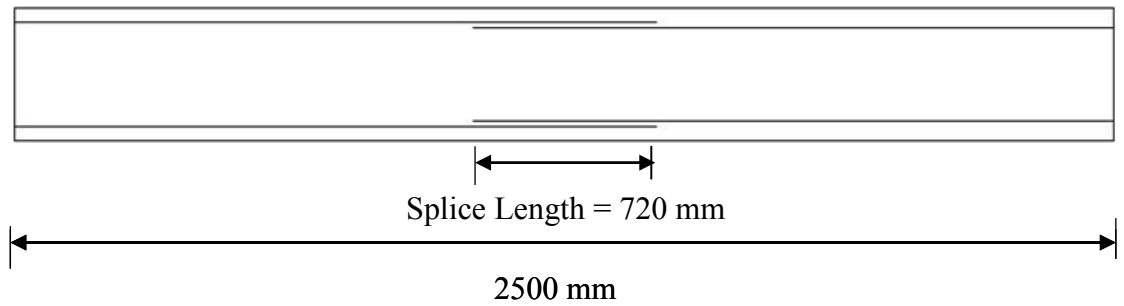


Figure 7.5: Geometry and Reinforcement Arrangement for Beams N-L-18.8 and H-L-18.8



Elevation View



Plan View

Figure 7.6: Geometry and Reinforcement Arrangement for Beams N-L-30.0 and H-L-30.0

7.3 Materials

The aggregates, alkaline liquid and superplasticiser used in manufacturing geopolymer concrete beams for the study of bond behaviour of geopolymer concrete beams were the same as those used for studying the shear behaviour of beams, as described in Section 3.3.

Information on the calculation of the moisture content of the aggregates and the adjusted added water content of the mix design for each pour is given in Appendix A2.

The low-calcium fly ash was from a different batch obtained from Collie Power Station than the batch described in Section 3.3.2. The chemical composition of the fly ash as determined by X-Ray Fluorescence (XRF) analysis is shown in Table 7.2, and the particle size distribution is shown in Figure 7.7. Graph A shows the particle size distribution in percentage by volume in interval; whereas graph B shows the particle size distribution in percentage by volume passing size (Figure 7.7).

Table 7.2: Chemical composition of fly ash (mass %)

SiO ₂	Al ₂ O ₃	Fe ₂ O ₃	CaO	Na ₂ O	K ₂ O	TiO ₂	MgO	P ₂ O ₅	SO ₃	H ₂ O	LOI*
50.8	26.9	13.5	2.05	0.33	0.57	1.57	1.33	1.46	0.31	-	1.42

* *Loss on ignition*

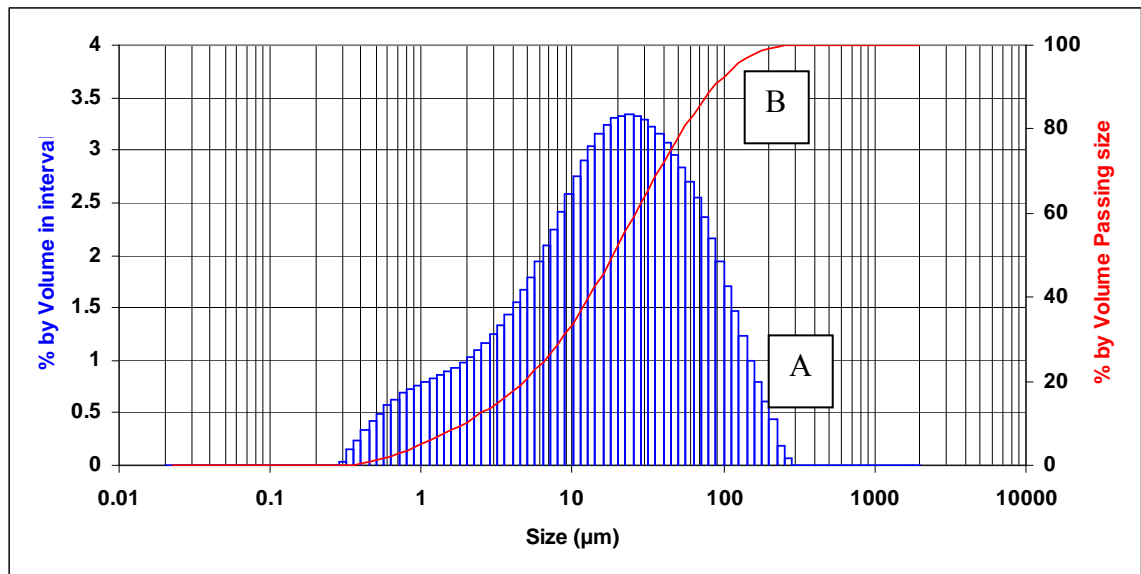


Figure 7.7: Particle Size Distributions of Fly Ash

7.4 Mixture Proportions for Geopolymer Concrete

The mixture proportion with the designation GP1, developed previously for the geopolymer concrete beams in Section 3.4, was used to obtain a mean compressive strength of 30 MPa to 35 MPa for six beams in this study. These beams are N-D-1.0, N-D-1.5, N-D-2.2, N-L-12.5, N-L-18.8 and N-L-30.0.

Several trial mixes were prepared according to mixture proportions developed by Sumajouw and Rangan (2006) to obtain mean compressive strengths of 50 MPa to 55 MPa. From these trial mixes, the mixture proportion with the designation GP2 was selected. The compressive strength was obtained with steam curing of 24 hours at 60°C and three rest days prior to curing. It was found that a good consistency of workability was achieved, as indicated from slump tests. The average slump was 210 mm. Further details of the trial mix for GP2 are given in Appendix B2. GP2 was used to manufacture six geopolymer concrete beams with concrete compressive strengths of 50 MPa to 55 MPa. These beams are H-D-1.0, H-D-1.5, H-D-2.2, H-L-12.5, H-L-18.8 and H-L-30.0.

The details of the mixture proportion for GP1 and GP2 are given in Table 7.3. It can be seen that the only difference between the two mixtures is the mass of extra water added.

Table 7.3: Mixture Proportions of Geopolymer Concrete

Material	GP1	GP2
	Mass (kg/m ³)	Mass (kg/m ³)
Aggregate 10mm	551	556
Aggregate 7mm	643	650
Sand	643	650
Fly Ash	406	410
Sodium Hydroxide Solution (14M)	41	41
Sodium Silicate Solution	103	103
Superplasticiser	6.1	6.1
Extra added water	25.6	16.5
Rest Period (days)	None	3 days

7.5 Properties of Reinforcement

All the reinforcement used in this study was standard deformed bar designed to give a minimum yield strength of 500MPa. In order to obtain the actual yield strength and ultimate strength of the reinforcement, three sample bars of each size, from the same batch of steel production, were tested in the laboratory. It was found that the yield strength was more than 500MPa for all bars. The summary of the test results is given in Table 7.4 and Table 7.5, and shows the mean value and range. These results will be used in the calculation and analysis of the beams in Chapter 8 and Chapter 9.

Table 7.4: Longitudinal Reinforcement Properties

Nominal Diameter (mm)	Nominal Area (mm ²)	Yield Strength (MPa)	Ultimate Strength (MPa)
16	200	539 ± 5	638 ± 5
20	310	564 ± 3	653 ± 5
24	450	563 ± 3	655 ± 4

Table 7.5: Transverse Reinforcement Properties

Nominal Diameter (mm)	Nominal Area (mm ²)	Yield Strength (MPa)	Ultimate Strength (MPa)
10	78.5	554 ± 3	637 ± 2

7.6 Manufacture of Test Specimens

The manufacture of all test specimens was similar to that described in Section 3.6. Due to the limited capacity of pan mixer, five batches of geopolymer concrete were prepared to cast two beam specimens for each pour. Further information on the calculation of the moisture content of aggregates and the adjusted added water content of the mix design for each pour are given in Appendix A2.

The fly ash, coarse aggregates (10mm and 7mm) and sand were first mixed dry in the laboratory pan mixer (70-litre capacity) for about three minutes. Next the

alkaline liquid, together with the super plasticiser and the extra water, were mixed together and added into the dry mixture. The mixing continued for another four minutes. After mixing, a slump test was used to measure the workability of every batch of geopolymer concrete. The slump test readings indicated that consistency was achieved for the different batches of concrete mixtures. The summary of the average slump values and the range from five batches is given in Table 7.6.

Once the mixing of the geopolymer concrete was complete, it was immediately cast into the moulds for beam specimens and cylinder test specimens. The fresh geopolymer concrete was placed into the mould in layers. A stick internal vibrator was used to compact the fresh geopolymer concrete in the mould.

For each batch of concrete, at least three 100mm x 200mm diameter cylinders were cast. A total of six 150mm x 300mm diameter cylinders were also cast for splitting tensile tests, to obtain the tensile strength of geopolymer concrete. All the cylinders were compacted and cured in the same manner as the beams, and were tested at the same time as the beam tests. The cylinders were tested in accordance to Australian Standards 1012.9 (1999) to obtain the concrete compressive strength. The cylinder splitting tests to obtain the tensile strength of geopolymer concrete were done according to Australian Standard 1012:10-2000 (2000). The mean concrete compressive strength and the range, mean concrete tensile strength and the range, and the age of testing of the hardened concrete are given in Table 7.6.

Table 7.6: Concrete Properties

Series	Beam Mark	Slump (mm)	Mean Concrete Compressive Strength f'_c (MPa)	Mean Tensile Strength of Concrete f'_{ct} (MPa)	Age (days)
D	N-D-1.0	261 ± 5	37 ± 4	3.62 ± 0.3	21
	N-D-1.5	261 ± 5	37 ± 4	3.62 ± 0.3	21
	N-D-2.2	265 ± 4	30 ± 5	2.96 ± 0.5	19
	H-D-1.0	210 ± 5	55 ± 4	4.06 ± 1.0	32
	H-D-1.5	210 ± 5	55 ± 4	4.06 ± 1.0	32
	H-D-2.2	240 ± 5	48 ± 6	4.48 ± 0.7	66
L	N-L-12.5	265 ± 4	30 ± 5	2.96 ± 0.5	19
	N-L-18.8	268 ± 4	29 ± 4	2.93 ± 0.4	18
	N-L-30.0	268 ± 4	29 ± 4	2.93 ± 0.4	18
	H-L-12.5	240 ± 5	48 ± 6	4.48 ± 0.7	66
	H-L-18.8	235 ± 5	51 ± 6	4.65 ± 0.4	46
	H-L-30.0	235 ± 5	51 ± 6	4.65 ± 0.4	46

For each pour to cast two beam specimens, three 100mm x 150mm concrete cylinders were used to determine the modulus of elasticity, E_c and Poisson's ratio. The tests were carried out according to Australian Standard AS 1012.17 (1997),

where E_c was determined as the secant modulus measured at the stress level equal to 40 percent of the average compressive strength of concrete cylinders. One LVDT (Linear Voltage Differential Transducer) was used to measure the lateral deformation of the test cylinder at mid-height, while two LVDTs were used to measure the axial deformation of the cylinders. The typical set-up can be found in Figure 7.8. The test results of the mean modulus of elasticity and the range, and the Poisson's ratio and the range are given in Table 7.7.



Figure 7.8: Typical Test Set-Up for Modulus of Elasticity of Concrete and Poisson Ratio

Table 7.7: Modulus of Elasticity and Poisson's Ratio

Mixture Proportion	Average Concrete Compressive Strength (MPa)	Modulus of Elasticity E_c (GPa)	Poisson's Ratio
GP1	29	19.5 ± 0.9	0.138 ± 0.01
GP1	30	19.5 ± 0.9	0.138 ± 0.01
GP1	37	21.0 ± 0.7	0.138 ± 0.02
GP2	48	23.5 ± 0.5	0.140 ± 0.02
GP2	51	24.0 ± 0.9	0.140 ± 0.01
GP2	55	26.0 ± 0.5	0.145 ± 0.02

7.7 Steam Curing

The steam curing set-up for the beams was similar to that described in Section 3.6.4. For the high strength geopolymer concrete beams using mixture proportion GP2, all six beams were placed inside the steam curing room for three rest days before curing for 24 hours at 60°C. After curing, all specimens were removed from the chamber, de-moulded, and left in ambient conditions in the laboratory until the time of testing.

7.8 Test Set-up and Instrumentation

All beams were simply supported over a span of 2300mm. The beams were tested and loaded to failure by a 2500 kN-capacity Universal test machine in the laboratory. Figures 7.9 and 7.10 and show the loading configuration and a typical test set-up for the test specimens.

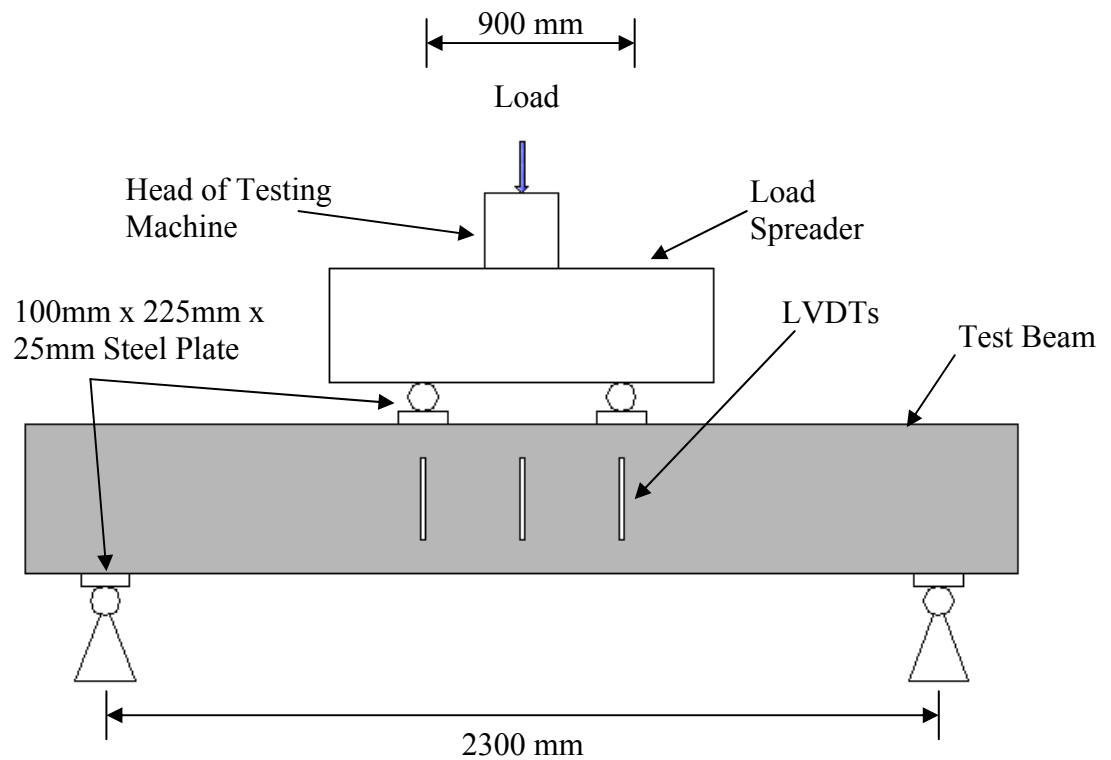


Figure 7.9: Loading Arrangement for Beam Tests



Figure 7.10: Typical Test Set-Up for Beam Tests

Three LVDTs were used to measure the vertical deflections of test beams. A 50mm plunger travel LVDT was located at the mid-span, while two 50mm plunger travel LVDTs were placed under the applied concentrated loads. Prior to tests, all LVDTs were calibrated using a milling machine. A dial gauge was used to measure the movement of the LVDT that was attached to the milling machine. The output of the LVDT's movement was expressed in milli-volts (mV) and correlated to the measured change of the dial gauge in mm.

7.9 Testing Procedure

Prior to testing, all beams were whitewashed to facilitate the marking of cracks. A preload of 20kN was applied to ensure that the test set-up and instrumentation worked properly. The beam was then unloaded and datum readings were taken.

The failure load of each beam was predicted prior to testing using draft AS3600-2005, as knowing the approximate failure load gave the advantage of control, especially when the specimen was near failure. The test was conducted by moving

the test machine platen at a ram rate of 0.3mm per minute, which provided sufficient time of crack observation and marking during beam tests. The locations of cracks were marked during the process of testing, until failure. The duration of each test was 20 to 30 minutes.

The rate of data captured was 10 samples per second. All loads and deflection data were electronically recorded using an automatic data acquisition system.

CHAPTER 8

PRESENTATION AND DISCUSSION OF TEST RESULTS FOR BOND STUDY

This chapter presents the results of the test beams from the experimental program described in Chapter 7. Observations on the bond behaviour of individual beams, such as failure modes, crack patterns and steel-geopolymer concrete interface at splice regions after failure, are presented. This chapter also includes a summary of test results, including the average bond stress, the effect of parameters on bond strength and the load-deflection characteristics of test beams.

8.1 General Behaviour of Test Specimens

Twelve beams were tested under monotonically increasing load until failure. The behaviour of all test beams was similar. All beams failed by splitting of the concrete at the tension face within the splice region. In general, the first flexural cracks for all beams formed initially on the tension face in the constant moment region. As the load increased, cracks formed along the entire length of the constant moment zone including the splice region. Failure occurred just after the longitudinal splitting cracks formed in the bottom cover on the tension side of beam at the splice region, and in the side cover at the levels of the splice. It was observed that when compared to normal strength geopolymer concrete beams, the high strength geopolymer concrete beams failed in a more brittle manner. Generally, this is expected and is similar to what is observed in Portland cement concrete specimens reported in the literature (Hamad and Mike, 2003; Hamad and Itani, 1998; Esfahani and Rangan, 1998; Zuo and Darwin, 2000).

Typical crack patterns at the splice region at both the side face and bottom face of Beam N-D-1.0 are shown in Figures 8.1 and 8.2.

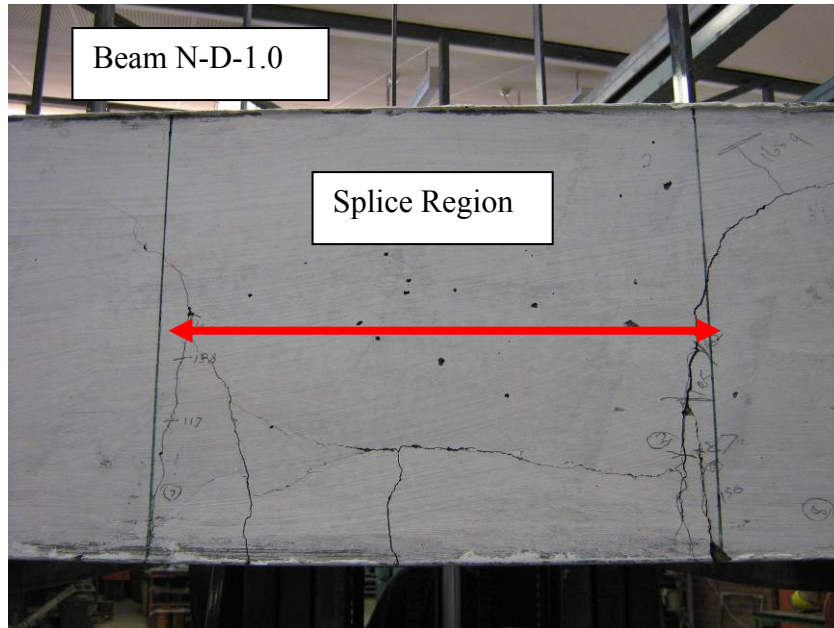


Figure 8.1: Crack Pattern of Beam N-D-1.0 over the Splice Region After Failure (Side Face)

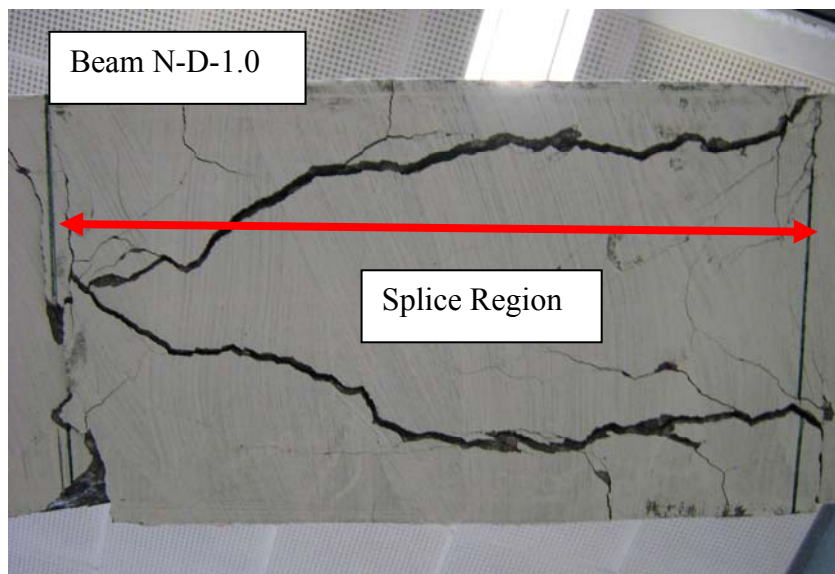


Figure 8.2: Crack Pattern of Beam N-D-1.0 over the Splice Region After Failure (Bottom Face)

8.2 Failure Modes and Crack Patterns

The observed cracking patterns on the side and bottom face of all beam specimens were similar regardless of C/d_b and L_s/d_b ratios. Figure 8.3 shows the crack patterns at the splice region of three normal strength geopolymer concrete beams in D-series, with C/d_b ratios of 1.0, 1.5 and 2.2. The crack patterns at the splice region of three high strength geopolymer concrete beams in D-series, with C/d_b ratios of 1.0, 1.5 and 2.2, are given in Figure 8.4. It can be seen that the crack patterns were similar for all beams.

Figure 8.5 shows the crack patterns at the splice region of three normal strength geopolymer concrete beams in L-series, with L_s/d_b ratios of 12.5, 18.8 and 30.0. The crack patterns at the splice region of three high strength geopolymer concrete beams in L-series, with L_s/d_b ratios of 12.5, 18.8 and 30.0, are given in Figure 8.6. It can be seen that crack patterns were similar for all beams, but with a greater extent of concrete spalling of cover in the splice region when $L_s/d_b = 30$.

All flexural cracks outside the splice region were tiny hairline cracks. In the splice region, it was observed that the crack widths for normal strength geopolymer concrete (typically 0.5mm to 1mm) were smaller than for higher strength geopolymer concrete (typically 1.5mm to 2mm), for all beams. Figure 8.7 shows the comparison between the crack widths of Beams N-D-1.0 and H-D-1.0. The only difference between the two beams is in the concrete compressive strength. It can be seen from Figure 8.7 that the crack width in the splice region for Beam H-D-1.0 is greater than that for Beam N-D-1.0. Photographs showing the splitting crack pattern (side and bottom view) for each pair of geopolymer concrete beams (normal and high strength) in the splice region for D-series and L-series are given in Figure F.1 to Figure F.12 in Appendix F.

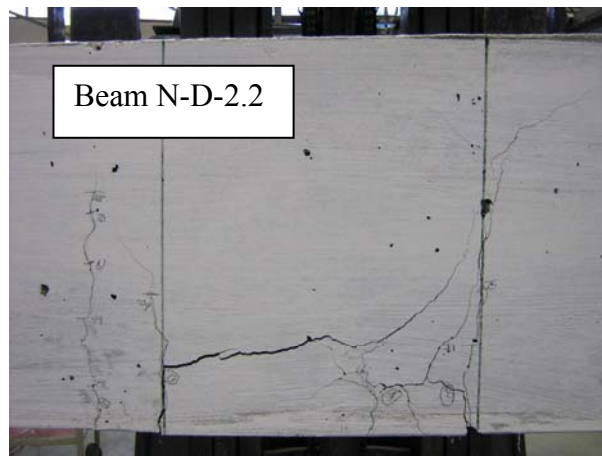
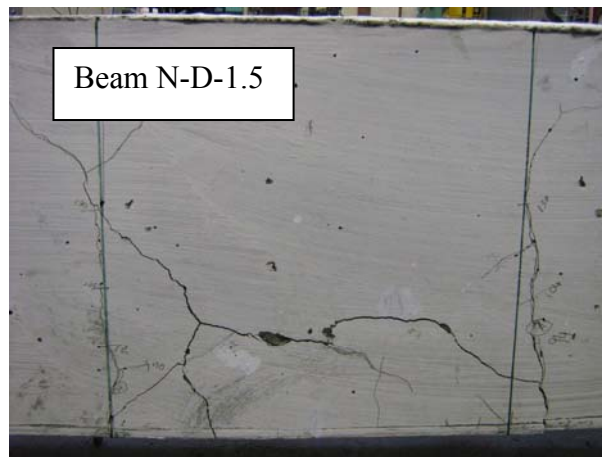
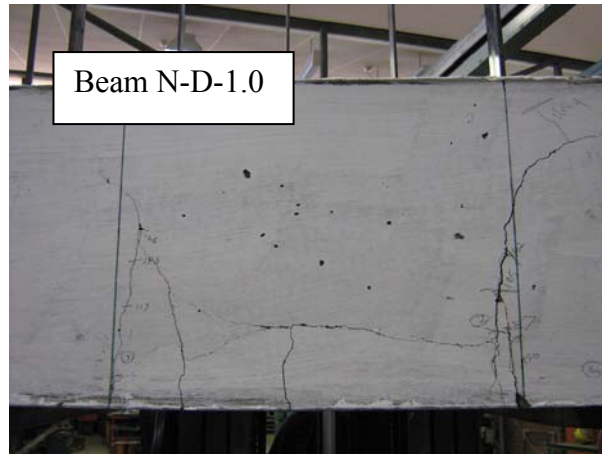


Figure 8.3 : Crack Pattern of Normal Strength Geopolymer Concrete Beams over the Splice Region After Failure (D-Series)

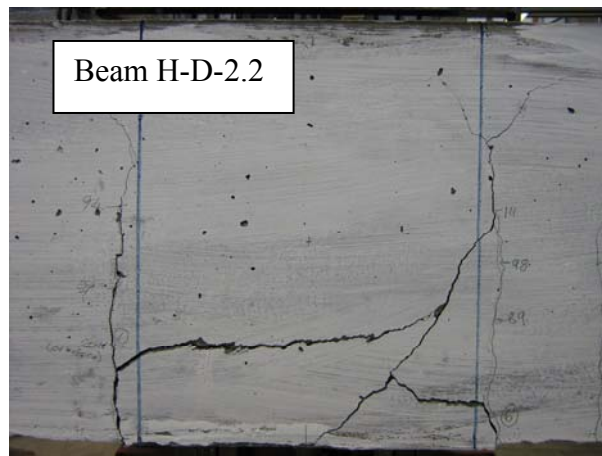
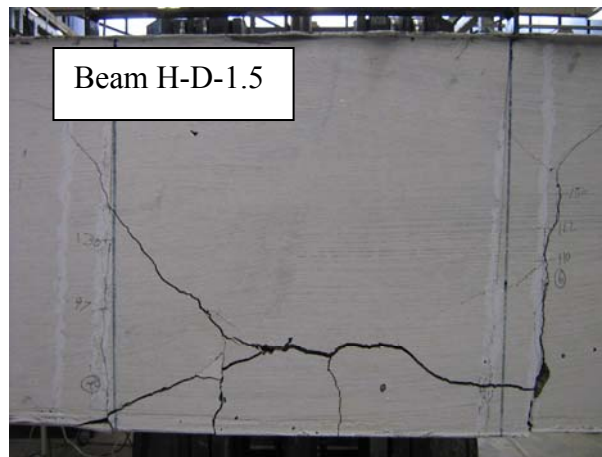
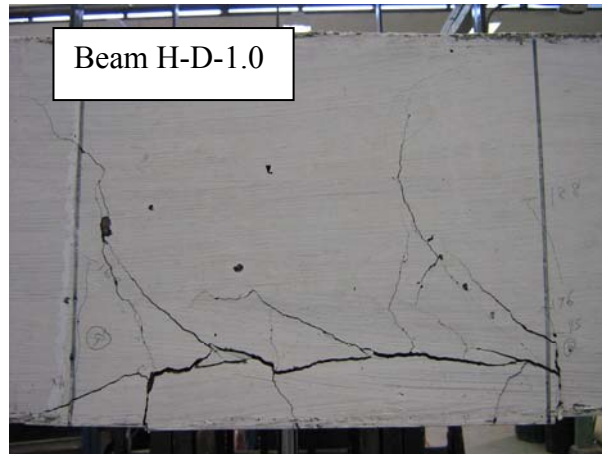


Figure 8.4 : Crack Pattern of High Strength Geopolymer Concrete Beams over the Splice Region After Failure (D-Series)

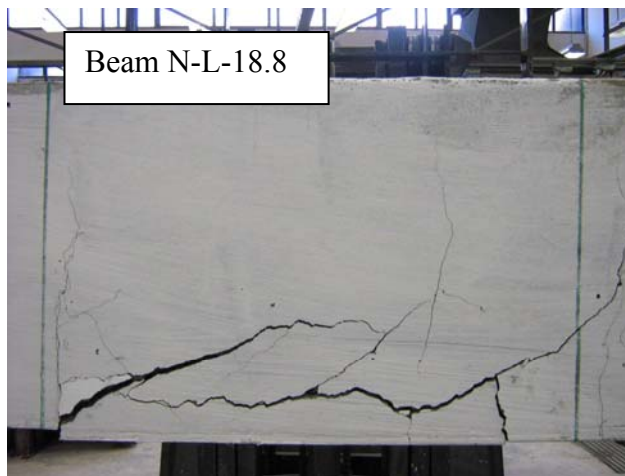
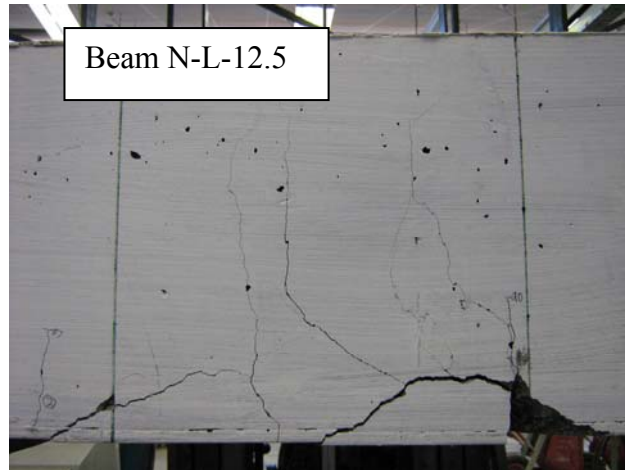


Figure 8.5 : Crack Pattern of Normal Strength Geopolymer Concrete Beams over the Splice Region After Failure (L-Series)

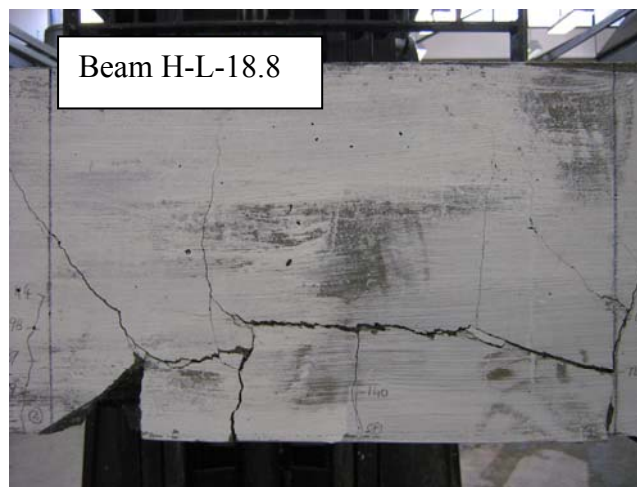
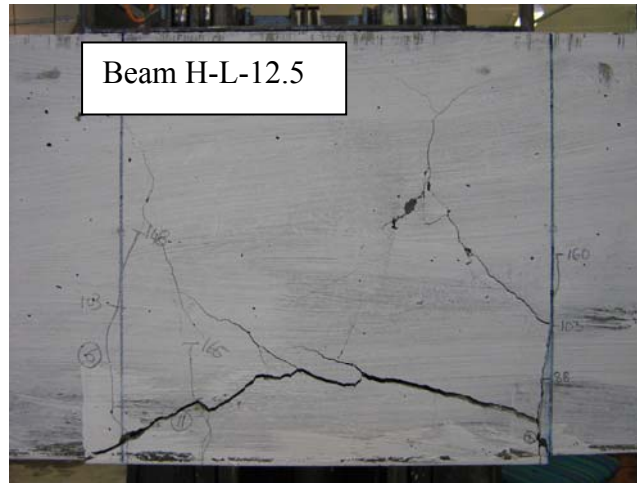


Figure 8.6 : Crack Pattern of High Strength Geopolymer Concrete Beams over the Splice Region After Failure (L-Series)

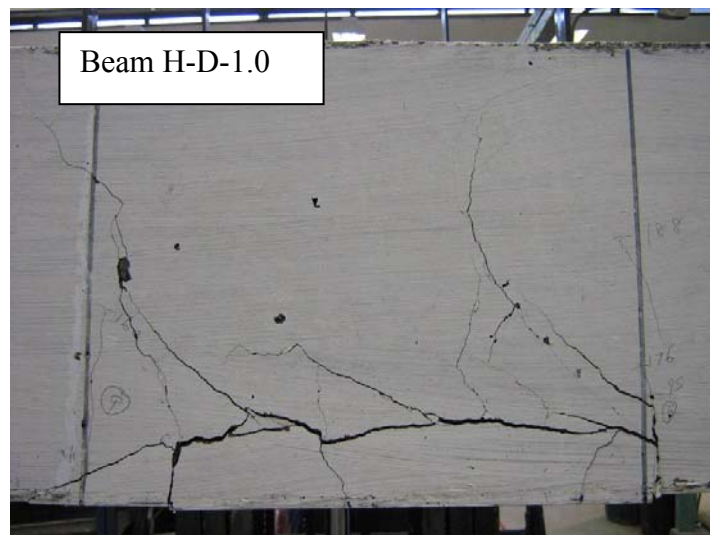
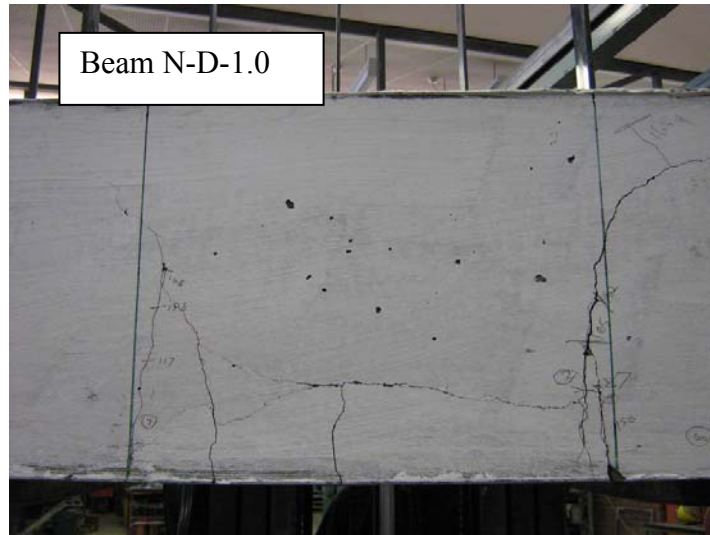


Figure 8.7 : Comparison of Crack Width In Splice Region for Beam N-D-1.0 and Beam H-D-1.0

8.3 Observation on Steel-Geopolymer Concrete Interface at Splice Region After Failure

Following the tests, the concrete cover was removed to study the nature of the interaction at the steel-geopolymer concrete interface. It was observed that the concrete between the ribs at the geopolymer concrete-steel interface showed no signs of crushing for both normal strength and high strength geopolymer concrete. Figure 8.8 shows the geopolymer concrete-steel interface for Beam N-L-30, where no concrete crushing in front of the ribs was observed. Figure 8.9 shows the clear rib pattern of the bar on the geopolymer concrete for Beam N-L-30. This is contrary to what is observed for normal strength Portland cement concrete, where the concrete between the ribs at the concrete-steel interface shows signs of crushing. It has reported that the extent of concrete damage at the steel-concrete interface depends on the concrete strength for Portland cement concrete (Azizinamini et al., 1993; Esfahani and Rangan, 1998).



**Figure 8.8: Surface Condition of Reinforcing Bars After Failure
(Normal Strength Concrete – Beam N-L-30)**



**Figure 8.9: Rib Patterns of Bar on Geopolymer Concrete
(Normal Strength Concrete – Beam N-L-30)**

Photographs showing the steel-geopolymer concrete interface at the splice region after failure for each beam are given in Figures G.1 to G.12 in Appendix G.

8.4 Test Results

The actual details of the test beams, including the side cover, bottom cover, spacing between spliced bars and spliced length, are given in Table 8.1.

Table 8.1: Actual Details of Test Beams

Series	Beam Mark	Compressive Strength f'_c (MPa)	Bar Diameter d_b (mm)	Splice Length L_s (mm)	Bottom Cover c_b (mm)	Side Cover c_{so} (mm)	Half of Spacing Between Spliced Bars c_{si} (mm)	C/d_b Ratio	L_s/d_b Ratio
D	N-D-1.0	37	24	355	30	32	20	1.1	14.8
	N-D-1.5	37	20	303	30	32	28	1.5	15.2
	N-D-2.2	30	16	240	40	38	29	2.2	15.0
	H-D-1.0	55	24	356	25	28	25	1.0	14.8
	H-D-1.5	55	20	301	30	38	24	1.5	15.1
	H-D-2.2	48	16	243	40	39	28	2.2	15.2
L	N-L-12.5	30	24	300	31	27	25	1.1	12.5
	N-L-18.8	29	24	452	25	27	23	1.0	18.8
	N-L-30.0	29	24	723	25	28	25	1.0	30.1
	H-L-12.5	48	24	300	27	27	24	1.1	12.5
	H-L-18.8	51	24	455	25	30	22	1.0	19.0
	H-L-30.0	51	24	722	25	30	24	1.0	30.1

8.4.1 Failure Loads and Moments

The failure loads and the maximum bending moments of all test beams are given in Table 8.2.

Table 8.2: Failure Loads and Moments

Series	Beam Mark	Compressive Strength f'_c (MPa)	C/d_b Ratio	L_s/d_b Ratio	Failure Load P_{max} (kN)	Maximum Bending Moment M_{max}^* (kNm)
D	N-D-1.0	37	1.1	14.8	165.2	58.7
	N-D-1.5	37	1.5	15.2	145.5	51.8
	N-D-2.2	30	2.2	15.0	111.0	39.7
	H-D-1.0	55	1.0	14.8	194.8	69.1
	H-D-1.5	55	1.5	15.1	172.6	61.3
	H-D-2.2	48	2.2	15.2	135.7	48.4
L	N-L-12.5	30	1.1	12.5	135.7	48.4
	N-L-18.8	29	1.0	18.8	194.8	69.1
	N-L-30.0	29	1.0	30.1	249.1	88.1
	H-L-12.5	48	1.1	12.5	167.7	59.6
	H-L-18.8	51	1.0	19.0	251.6	88.9
	H-L-30.0	51	1.0	30.1	323.1	114.0

Note: * including the moment due to self-weight of the beam and loading system

8.4.2 Test Bond Strength

The average bond stress was calculated using Equation 8.1, obtained by evaluating the total force developed in the bar, $A_b f_s$ divided by the bar surface area over the splice length given by

$$u = \frac{A_b f_s}{\pi d_b L_s} = \frac{f_s d_b}{4L_s} \quad (8.1)$$

where

u = Average bond stress (MPa)

A_b = Area of one bar

d_b = Diameter of bar

L_s = Splice length

f_s = Stress in the tensile steel

All the beams were designed as under-reinforced beams and all the splice lengths were designed to develop steel stress less than yield stress at failure, as mentioned in Section 7.2. The steel stress, f_s , was determined based on elastic cracked section analysis by using the transformed section analysis as given in Equation 8.2.

$$f_s = \frac{M_{\max}}{A_{st} jd} \quad (8.2)$$

where

M_{\max} = Maximum bending moment when bond failure occurred

A_{st} = Area of tensile steel

jd = Lever arm; the lever arm coefficient was calculated by performing a conventional elastic analysis of a fully cracked transformed section.

The calculated steel stress and average bond stress are presented in Table 8.3.

Table 8.3: Summary of Test Results for Steel Stress and Average Bond Stress

Series	Beam Mark	Compressive Strength f'_c (MPa)	Bar Diameter d_b (mm)	Steel Stress f_s (MPa)	Average Bond Stress u (MPa)
D	N-D-1.0	37	24	292.5	4.94
	N-D-1.5	37	20	365.6	6.03
	N-D-2.2	30	16	440.5	7.34
	H-D-1.0	55	24	334.2	5.63
	H-D-1.5	55	20	429.5	7.13
	H-D-2.2	48	16	532.6	8.77
L	N-L-12.5	30	24	242.5	4.85
	N-L-18.8	29	24	339.2	4.50
	N-L-30.0	29	24	432.5	3.59
	H-L-12.5	48	24	292.1	5.84
	H-L-18.8	51	24	432.5	5.70
	H-L-30.0	51	24	554.2	4.61

From the test results of the sample bars used for the test specimens (Section 7.5), the yield stresses of bars of 24mm, 20mm, and 16mm were 563 MPa, 564 MPa and 539 MPa respectively. It can be seen that the calculated steel stress values from Table 8.3 were less than the yield stresses of the steel tested. Therefore, the method based

on elastic analysis to determine the steel stress was considered to be acceptable to calculate the average bond stress of the test specimens.

8.4.3 Effect of Parameters on Bond Stress

8.4.3.1 Effect of C/d_b

Three C/d_b ratios, 1.0, 1.5 and 2.2 (for bar diameters of 24 mm, 20 mm and 16 mm respectively), were used in six geopolymer concrete beams. For each C/d_b ratio, two companion beams with different concrete strengths were tested; these were Beams N-D-1.0 and H-D-1.0; N-D-1.5 and H-D-1.5; N-D-2.2 and H-D-2.2.

The effect of C/d_b ratio on bond strength for each pair of geopolymer concrete beams is presented in Figure 8.10. It can be seen that the bond stress increases as C/d_b increases (or bar size decreases) for both normal strength (represented by N-series) and high strength (represented by H-series) geopolymer concrete. This trend is similar to what is observed for Portland cement concrete beams and reported in the literature (Canbay and Frosch, 2005).

Sofi et al. (2007) observe that the normalised bond strength increases with a reduction in bar size for low calcium fly ash geopolymer mortar and concrete beam-end specimens. The trend of test results observed in their study is similar to what is observed in this study.

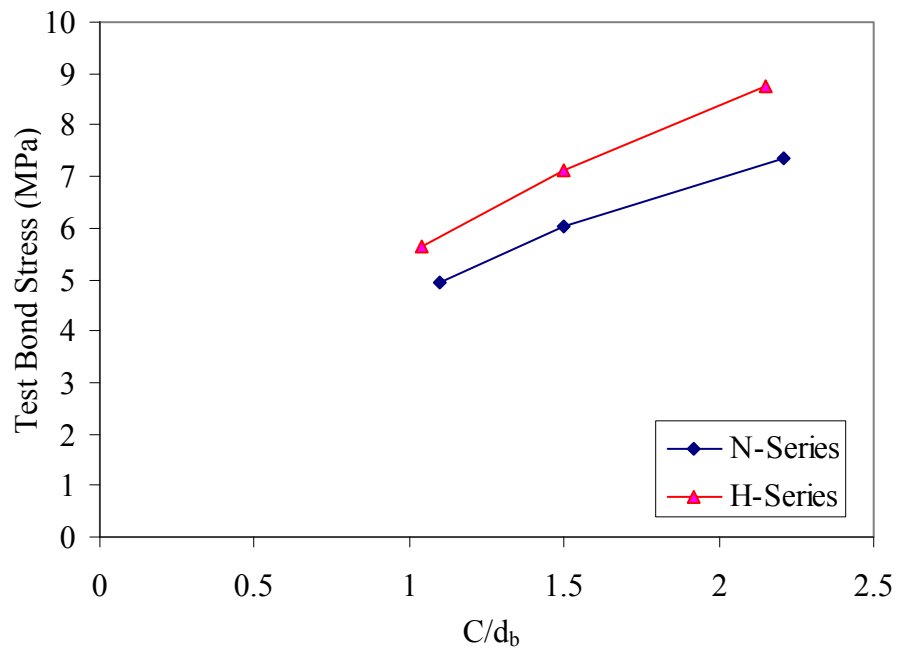


Figure 8.10: Effect of C/d_b on Bond Stress

8.4.3.2 Effect of L_s/d_b

Three L_s/d_b ratios, 12.5, 18.8 and 30.0, were used in six geopolymer concrete beams. For each L_s/d_b ratio, two companion beams with different concrete strengths were tested; these were Beams N-L-12.5 and H-L-12.5; N-L-18.8 and H-L-18.8; N-L-30.0 and H-L-30.0.

The effect of L_s/d_b on bond strength for each pair of geopolymer concrete beams is presented in Figure 8.11. As L_s/d_b increases, the bond stress decreases for both normal strength (represented by N-series) and high strength (represented by H-series) geopolymer concrete. This observation is found to be similar to the reported literature from Azizinamini et al. (1993) for Portland cement concrete beams.

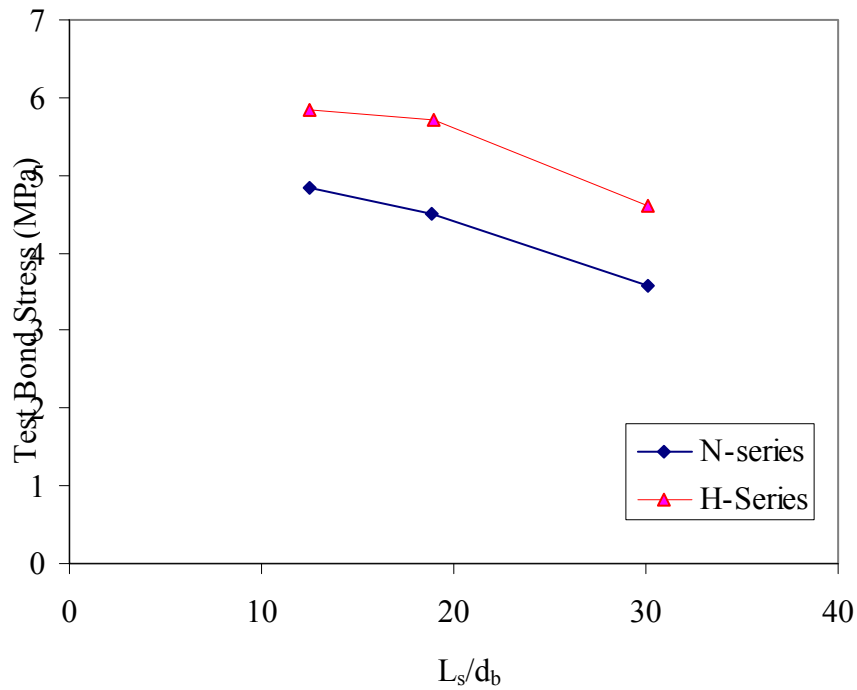


Figure 8.11: Effect of L_s/d_b on Bond Stress

8.4.3.3 Effect of Concrete Compressive Strength

Two types of concrete compressive strength, represented by normal strength and high strength given by the mix designs GP1 and GP2 respectively, were used in this study. For D-Series with C/d_b ratios as the parameter, it can be seen from Figure 8.12 that bond stress increased with the increase in compressive strength for the same C/d_b ratio in all cases. This trend is similar to what was observed by Sarker et al. (2007) on the effect of compressive strength on bond strength for geopolymer concrete beam-end specimens with C/d_b ratios ranging from 1.8 to 3.2.

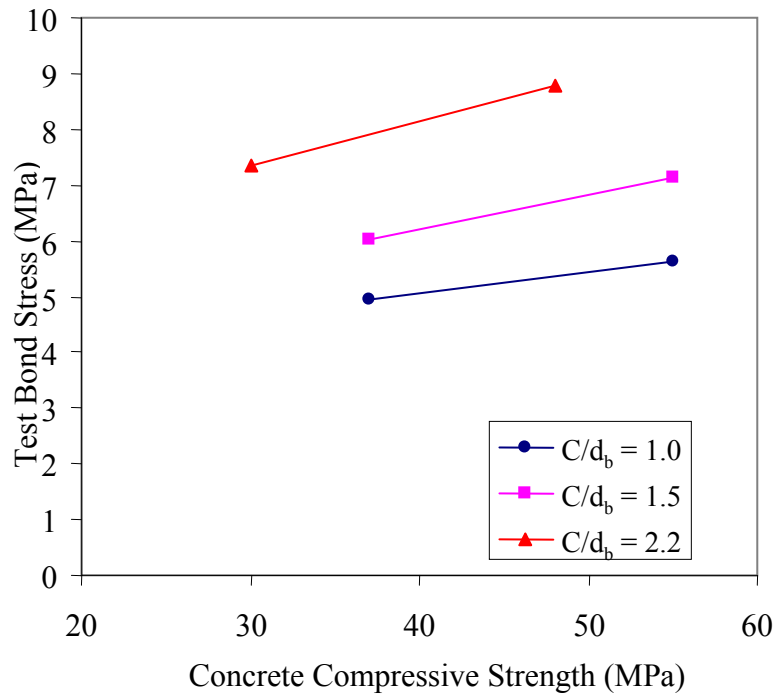


Figure 8.12: Effect of Concrete Compressive Strength on Bond Stress (D-Series)

For L-Series with L_s/d_b ratios as parameter, it can be seen from Figure 8.13 that bond stress increases with the increase in compressive strength for the same L_s/d_b ratio in all cases.

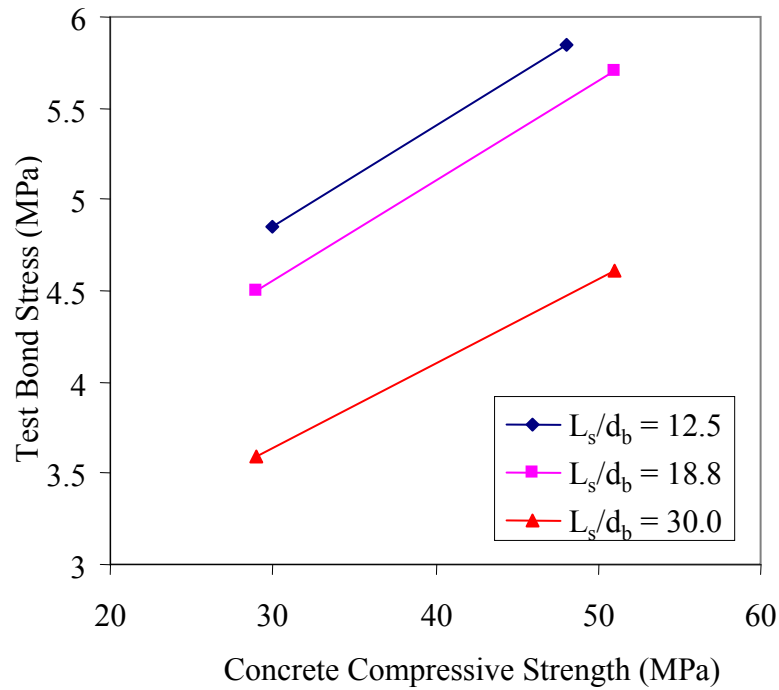


Figure 8.13: Effect of Concrete Compressive Strength on Bond Stress (L-Series)

8.5 Load-Deflection Curves

Figures 8.14 to 8.19 illustrate the load-deflection relation at mid-span for geopolymer concrete beams. Geopolymer concrete beams with the same design parameters were paired for comparison purposes. The graphs highlight the behaviour and stiffness of the beams.

Generally, the following features were observed:

- As the load increased, loss of stiffness was observed for all beams with the propagation of cracks during load stages
- Mid-span deflection increases linearly with load until flexural cracking occurs.

- After the development of flexural cracks, the slope of the load-deflection relationship decreases.
- When comparing the beams in pairs, the beams display similar stiffness up to the cracking load.
- For the same applied load, the beam with the higher concrete strength (H-series) has a smaller deflection as the bending stiffness is proportional to the concrete strength in the linear elastic range.
- Observation on formation of the first flexural crack was evident from the load deflection curves, as reflected by the change of slope in the plots shown in Figures 8.14 to 8.19. These are similar to those described in the literature for Portland cement concrete beams (Esfahani and Rangan, 1998).
- Other observations on events of crack formation and crack width at splice region for each test beam were also recorded, and are shown in Figures 8.14 to 8.19.

The complete load-deflection data for each beam are given in Appendix H.

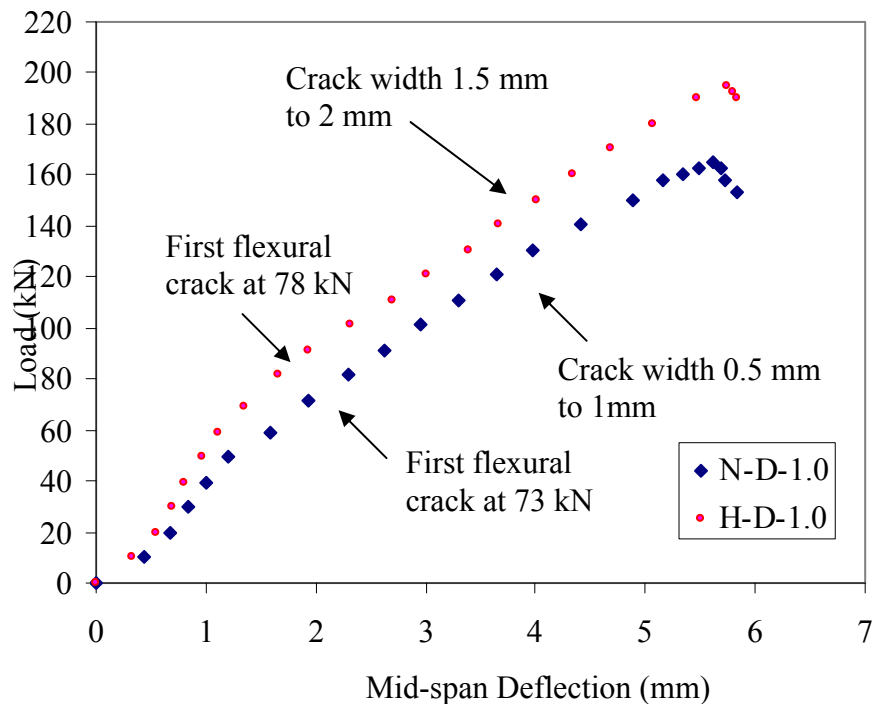


Figure 8.14: Load versus Mid-span Deflection for Beams N-D-1.0 and H-D-1.0

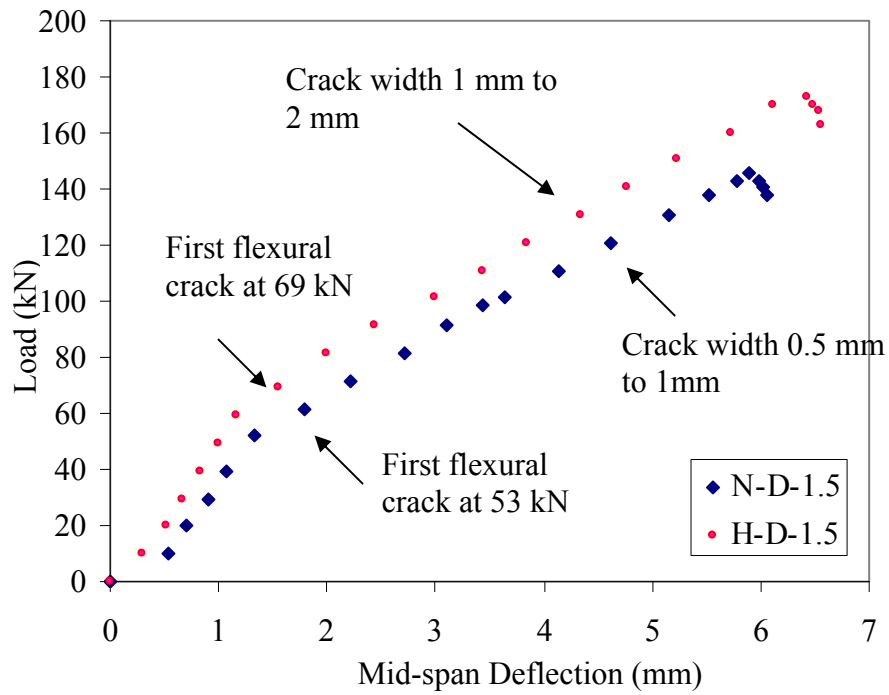


Figure 8.15: Load versus Mid-span Deflection for Beams N-D-1.5 and H-D-1.5

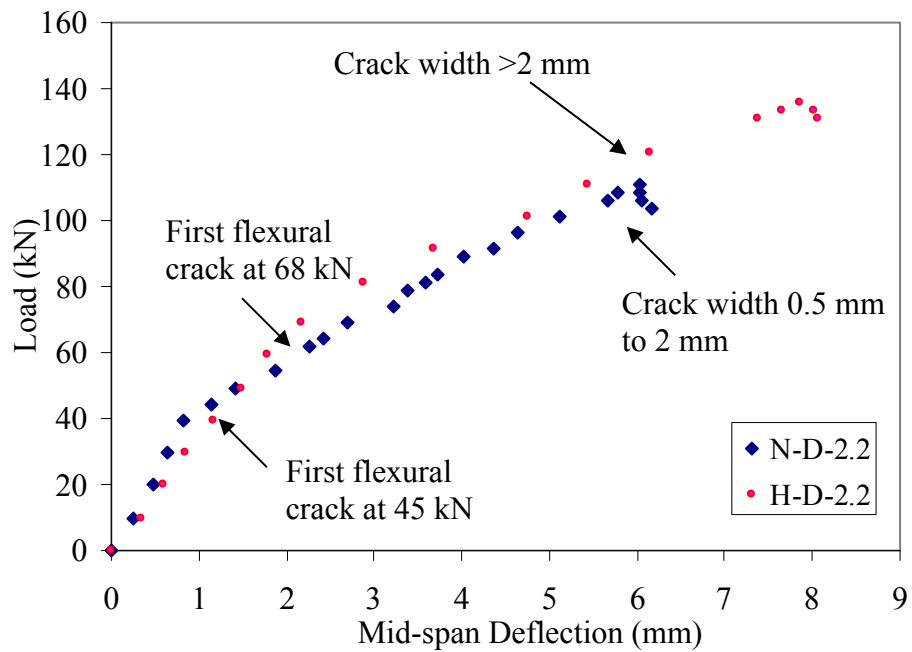


Figure 8.16: Load versus Mid-span Deflection for Beams N-D-2.2 and H-D-2.2

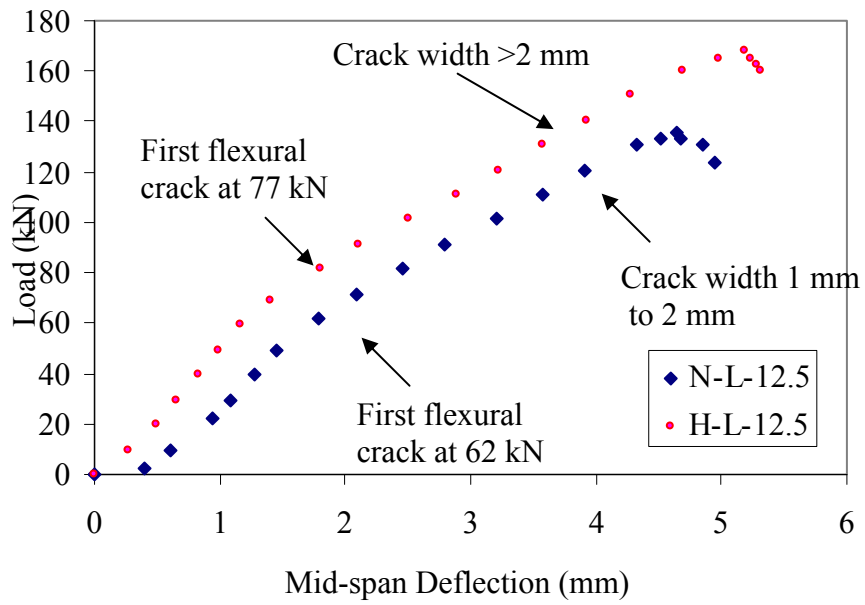


Figure 8.17: Load versus Mid-span Deflection for Beams N-L-12.5 and H-L-12.5

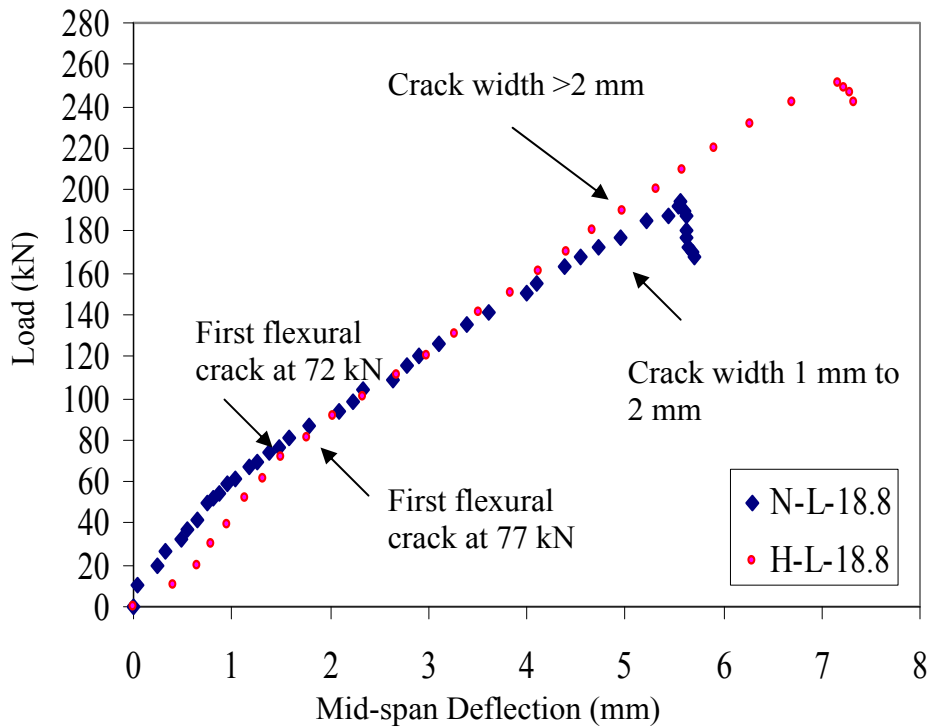


Figure 8.18: Load versus Mid-span Deflection for Beams N-L-18.8 and H-L-18.8

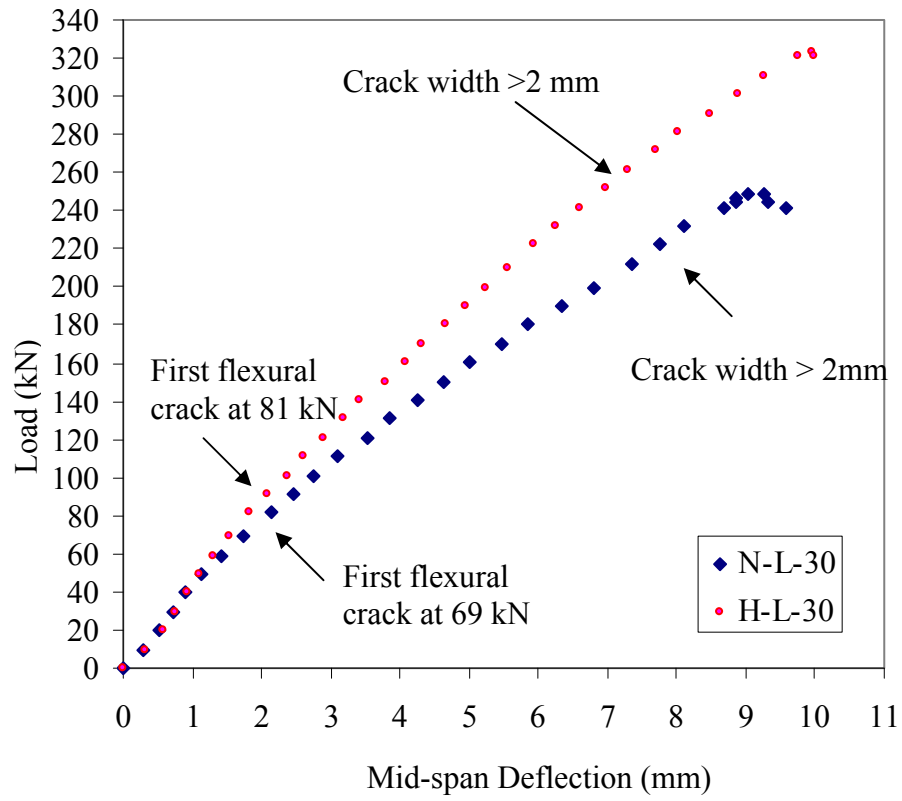


Figure 8.19: Load versus Mid-span Deflection for Beams N-L-30.0 and H-L-30.0

CHAPTER 9

DISCUSSION AND CORRELATION OF TEST RESULTS AND CALCULATED RESULTS FOR BOND STUDY

This chapter describes the correlation between the test and calculated bond strengths using the analytical models and code provisions presented in Section 2.3. The analytical models include Orangun et al. (1977), Zuo and Darwin (2000), ACI408R-03 (2003), Esfahani and Rangan (1998) and Canbay & Frosch (2005). Code provisions such as AS3600-01 (2001), draft AS3600 (2005) and ACI318-08 are used to predict the bond strength of geopolymer concrete beams. Comparison between the bond strength of geopolymer concrete and Portland cement concrete using analytical models are also presented.

9.1 Bond strength of Lap Splices in Geopolymer Concrete Beams

9.1.1 Comparison with Prediction using Analytical Models

The calculated bond strength of lap splices in geopolymer concrete beams using the analytical models is compared with the test values presented in Tables 9.1 and 9.2.

From Table 9.2, it can be seen that the analytical model proposed by Canbay & Frosch (2005) predicts the bond strength of tensile splices of geopolymer concrete beams most accurately, with an average test-to-prediction ratio of 1.17 and coefficient of variation of 11.97%. Other models, proposed by Orangun et al. (1977), Zuo and Darwin (2000), ACI 408R-03 and Esfahani and Rangan (1998), yielded similar predictions for the bond strength of all beams, with an average test-to-prediction ratio of 1.25 to 1.30.

Table 9.1: Summary of Predicted Bond Strength using Analytical Models

Series	Beam Mark	Test Bond Strength (MPa)	Predicted Bond Strength (MPa)				
			Orangun	Zuo & Darwin	ACI 408R-03	Esfahani & Rangan	Canbay & Frosch
D	N-D-1.0	4.94	3.83	4.38	4.43	4.26	4.23
	N-D-1.5	6.03	4.72	4.76	4.82	5.01	4.99
	N-D-2.2	7.34	4.88	5.12	5.17	6.92	5.31
	H-D-1.0	5.63	5.08	4.87	4.93	4.22	5.23
	H-D-1.5	7.13	5.37	5.20	5.26	5.67	6.14
	H-D-2.2	8.77	6.03	5.67	5.73	7.80	6.71
L	N-L-12.5	4.85	4.06	4.60	4.66	4.03	3.83
	N-L-18.8	4.50	3.23	3.64	3.68	3.16	3.70
	N-L-30.0	3.59	2.87	2.99	3.01	2.64	3.80
	H-L-12.5	5.84	5.06	5.17	5.24	4.55	4.79
	H-L-18.8	5.70	4.19	4.22	4.27	3.77	4.99
	H-L-30.0	4.61	3.73	3.51	3.55	3.26	5.08

Table 9.2: Summary of Test-to-Predicted Ratio using Analytical Models

Beam Mark	Test/Prediction Ratio				
	Orangun	Zuo & Darwin	ACI408R-03	Esfahani & Rangan	Canbay & Frosch
N-D-1.0	1.29	1.13	1.11	1.16	1.17
N-D-1.5	1.28	1.27	1.25	1.20	1.21
N-D-2.2	1.50	1.43	1.42	1.06	1.38
H-D-1.0	1.11	1.16	1.14	1.33	1.08
H-D-1.5	1.33	1.37	1.36	1.26	1.16
H-D-2.2	1.45	1.55	1.53	1.12	1.31
N-L-12.5	1.19	1.06	1.04	1.21	1.27
N-L-18.8	1.40	1.24	1.22	1.42	1.22
N-L-30.0	1.25	1.20	1.19	1.36	0.94
H-L-12.5	1.16	1.13	1.12	1.28	1.22
H-L-18.8	1.36	1.35	1.34	1.51	1.14
H-L-30.0	1.24	1.31	1.30	1.41	0.91
Average	1.30	1.27	1.25	1.28	1.17
S.D.	0.12	0.14	0.14	0.13	0.14
COV (%)	9.23	11.02	11.20	10.16	11.97

In this study, splitting tensile cylinders were made during the manufacture of all beams and tested on the same day as the beam tests. The measured tensile strength of geopolymer concrete is given in Table 7.6 in Section 7.6.

Crack development is a function of the tensile strength of concrete in the beam web (Nawy, 2005). Concrete cracks when the principal tensile stresses exceed the tensile strength of concrete. For bond failures involving the splitting of the concrete, the peak load is governed by the tensile response of the concrete (ACI 408R-03). The analytical expression proposed by Canbay and Frosch (2005) is based on a physical model of tension cracking of concrete in the lap-spliced region. In this model, the tensile strength of concrete surrounding the bar is a major parameter that affects the development of the reinforcement for a splitting failure. The bond strength predicted by the Canbay and Frosch model in Table 9.1 was calculated using the expression for tensile strength of concrete originally proposed in this model and described in Section 2.3.

The bond strength of lap splices of all beams was re-calculated based on the measured tensile strength of geopolymer concrete using the Canbay and Frosch model. It was found that when using the measured tensile strength of geopolymer concrete from the splitting tensile cylinders tested, an improved correlation of test and calculated bond strength for geopolymer concrete beams was obtained. From Table 9.3, it can be seen that the average test-to-prediction ratio is 1.0 with coefficient of variation of 15.21%.

Table 9.3: Predicted Bond Strength from Canbay and Frosch Model using Actual Tensile Strength Results

Beam Mark	Test Bond Strength (MPa)	Predicted Bond Strength (MPa) (Canbay & Frosch Model using actual f'_{ct} from test)	Test/Prediction Ratio
N-D-1.0	4.94	5.06	0.98
N-D-1.5	6.03	5.96	1.01
N-D-2.2	7.34	4.15	1.28
H-D-1.0	5.63	5.75	0.98
H-D-1.5	7.13	6.75	1.06
H-D-2.2	8.77	8.71	1.01
N-L-12.5	4.85	4.15	1.17
N-L-18.8	4.50	4.04	1.12
N-L-30.0	3.59	4.15	0.86
H-L-12.5	5.84	6.22	0.94
H-L-18.8	5.70	6.52	0.87
H-L-30.0	4.61	6.64	0.69
Average			1.00
S.D			0.15
COV (%)			15.21

9.1.2 Comparison of Bond Strength using Code Provisions

The bond strength of lap splices was calculated using standard design provisions contained in AS3600-01 (2001), draft AS3600 (2005) and ACI318-08 (2008). The test and calculated bond strength are compared in Table 9.4. The code provisions are found to be conservative in predicting the bond strength of geopolymer concrete beams. From Table 9.4, it can be seen that the average test-to-prediction ratio by AS3600-01 is 2.03 with a coefficient of variation of 10.84%. Both draft AS3600 (2005) and ACI 318-08 (2008) predict similar average test-to-prediction ratios, of 1.74 and 1.70 respectively, with a smaller coefficient of variation of 8.82% given by ACI 318-08 (2008).

Sofi et al. (2007) performed bond strength tests using beam-end specimens. Comparison of bond stress values from their study with AS 3600 and ACI 318 recommendations show that the provisions are conservative in predicting the development length of geopolymer concrete. From the bond strength of geopolymer concrete using beam-end specimens investigated by Sarker et al. (2007), a similar trend of results is also obtained, as observed in this study.

Table 9.4: Bond Strength: Summary of Results by Code Provisions

Beam Mark	Test Bond Strength (MPa)	Predicted Bond Strength (MPa)			Test/Prediction Ratio		
		AS3600-01	AS3600-05 Draft	ACI 318-08	AS3600-01	AS3600-05 Draft	ACI 318-08
N-D-1.0	4.94	2.15	2.97	2.98	2.30	1.67	1.66
N-D-1.5	6.03	3.06	3.24	3.41	1.97	1.86	1.77
N-D-2.2	7.34	3.36	3.12	4.60	2.19	2.35	1.60
H-D-1.0	5.63	3.03	3.73	3.20	1.86	1.51	1.76
H-D-1.5	7.13	3.34	3.82	4.15	2.14	1.87	1.72
H-D-2.2	8.77	4.13	3.90	5.82	2.12	2.25	1.51
N-L-12.5	4.85	2.24	2.76	2.75	2.17	1.76	1.77
N-L-18.8	4.50	2.08	2.68	2.33	2.16	1.68	1.94
N-L-30.0	3.59	2.20	2.71	2.33	1.63	1.32	1.54
H-L-12.5	5.84	2.75	3.47	3.15	2.12	1.69	1.85
H-L-18.8	5.70	2.68	3.53	3.08	2.13	1.62	1.85
H-L-30.0	4.61	2.84	3.57	3.08	1.62	1.29	1.49
				Average	2.03	1.74	1.70
				S.D.	0.22	0.32	0.15
				COV(%)	10.84	18.39	8.82

9.2 Comparison of Bond Strength between Geopolymer Concrete and Portland Cement Concrete Beams

In order to compare the bond strength of geopolymer concrete beams to Portland cement concrete beams, 20 beams tested by Esfahani and Rangan (1998) were selected. These Portland cement concrete beams were chosen due to their similar specimen size and also because they used a similar test set-up at the Curtin University Laboratory. The summary of Esfahani and Rangan's test results using current code provisions and analytical models is presented in Table 9.5. It can be seen that the Canbay and Frosch (2005) model yields the best result, giving a test-prediction ratio of 1.00 with a standard deviation value of 0.20.

The correlation of test results and predictions using Orangun et al. (1977), Zuo and Darwin (2000), ACI408R-03 (2003) and Esfahani and Rangan (1998) for bars not confined by transverse reinforcements were performed using ACI 408 Database 10-2001 for Portland cement concrete specimens as reported in ACI 408R-03 (2003). The summary of these results' correlation in the form of test-prediction ratios is given in Table 9.6. For the purposes of direct comparison, the summary of results for geopolymer concrete beams using the same predictions is also given in Table 9.6. It can be seen that, in general, the bond strength of geopolymer concrete beams is about 20% more than that of Portland cement concrete specimens using the same prediction methods.

Table 9.5: Summary of Test-to-Predicted Ratio for Bond Strength of Portland Cement Concrete Beams

Beam Mark	Test/Prediction Ratio							
	Orangun	Zuo & Darwin	ACI 408R-03	Esfahani & Rangan	Canbay & Frosch	AS3600-01	Draft AS3600-05	ACI318-08
1	0.82	1.37	0.89	1.08	1.06	1.79	1.45	1.70
2	0.65	1.41	0.78	0.93	0.85	1.44	1.16	1.37
3	0.83	1.18	0.95	1.05	0.88	1.49	1.20	1.41
4	0.69	1.28	0.87	0.95	0.74	1.25	1.01	1.18
5	0.86	1.05	1.03	1.08	0.80	1.36	1.10	1.28
6	0.69	1.39	0.90	0.93	0.66	1.11	0.90	1.05
7	0.71	1.87	0.85	0.98	0.87	1.46	1.18	1.39
8	0.97	1.90	0.97	1.11	1.06	1.98	1.60	1.87
9	0.98	1.31	0.97	1.07	0.98	2.01	1.62	1.90
10	0.74	1.82	0.81	0.92	0.82	1.38	1.12	1.31
11	1.02	1.95	1.05	1.16	1.03	1.92	1.55	1.82
12	1.09	1.84	1.00	1.09	1.01	2.06	1.67	1.95
13	1.16	2.05	1.25	0.97	1.19	2.31	1.85	1.84
14	1.36	1.82	1.42	1.10	1.32	2.88	2.11	2.05
15	1.36	1.58	1.29	1.06	1.17	3.31	1.96	1.82
16	1.11	1.00	1.44	1.11	1.36	1.86	2.16	1.58
17	1.34	0.89	1.26	1.01	1.31	2.67	2.16	1.00
18	0.97	1.33	1.12	0.91	1.14	1.63	1.80	0.89
19	1.00	1.52	1.14	1.10	0.75	1.40	1.13	1.33
20	0.89	1.51	1.00	0.97	0.99	1.61	1.58	1.52
Average	0.96	0.34	1.05	1.03	1.00	1.85	1.52	1.51
S.D	0.22	22.52	0.19	0.08	0.20	0.57	0.40	0.34
COV (%)	22.92	18.87	18.10	7.77	20.00	27.33	26.31	22.52

Table 9.6: Comparison of Test/Prediction Ratio between Geopolymer Concrete and Portland Cement Concrete Beams using Same Prediction Methods

Models	Geopolymer Concrete Beams		Portland Cement Concrete Beams	
	Test/ Predicted Ratio	COV (%)	Test/ Predicted Ratio	COV (%)
Orangun	1.30	9.23	1.03	20.19
Zuo and Darwin	1.27	11.02	1.01	11.19
ACI408R-03	1.25	11.20	1.00	11.10
Esfahani and Rangan	1.28	10.16	0.94	20.21

9.2.1 Relationship between Splitting Tensile Strength and Bond Strength of Geopolymer Concrete

Hardjito and Rangan (2005) measured the tensile strength of fly ash-based geopolymer concrete by performing cylinder splitting tests on 150 mm x 300 mm concrete cylinders and comparing the results to the calculated values, using the draft Australian Standards for Concrete Structures AS3600 (2005) and expression by Neville (2000). It was observed that the measured indirect tensile strength of fly ash-based geopolymer concrete is larger than the values recommended by the draft AS3600 (2005) and Neville (2000) for Portland cement concrete.

Gourley and Johnson (2005) observe that the limiting factor in strength for both Portland cement concrete and geopolymer concrete is the aggregate's strength. However, they found that corresponding tensile strengths are higher in geopolymer concrete because the tensile strength of the matrix is greater and there is a chemical bond to any silica-containing aggregate particles. They suggest that in Portland cement concrete, the matrix-aggregate bond is predominantly the result of physical

interlock and the bond zone being weaker than the matrix through the puddling effect during mixing and compaction. The Portland cement matrix strength is dominated by physical interlock effects.

Sofi et al. (2007) performed indirect tensile tests geopolymer mortar and concrete specimens using low calcium fly ash. From the test results of beam-end specimens used to measure the bond performance of geopolymer mortar and concrete, they find that the tensile strength of geopolymer concrete relates closely to bond strength, where the bond stress behaviour of geopolymer concrete abides by the variances of the tensile strength of geopolymer concrete.

All the above show that the tensile strength of geopolymer concrete is larger than that of Portland cement concrete, and that there is a close relationship between the splitting tensile strength and the bond strength of geopolymer concrete. As shown earlier in the re-calculation of bond strength of lap splices in geopolymer concrete beams using actual measured tensile strength of concrete in the model proposed by Canbay and Forsch (2005) (see Section 9.1), an improved correlation of test and calculated bond strength for geopolymer concrete beams is obtained. The average test-to-prediction ratio improves from 1.17 to 1.00. This indicates that that higher tensile strength of geopolymer concrete contributes to the higher bond strength of geopolymer concrete when compared to Portland cement concrete.

CHAPTER 10

CONCLUSIONS AND RECOMMENDATIONS

This chapter presents the conclusions of the research program and recommendations for future research. The shear behaviour of reinforced fly ash-based geopolymer concrete beams and the bond behaviour of lap splices in geopolymer concrete beams were investigated in the experimental programs. The experimental results were compared with prediction methods currently used for reinforced Portland cement concrete structural members, including code provisions and analytical models. Correlation of test results with predictions from various models was conducted and the evaluation of the suitability of these methods of prediction for geopolymer concrete was carried out.

10.1 Conclusions

10.1.1 Shear Behaviour of Reinforced Fly Ash-Based Geopolymer Concrete Beams

A total of nine beams were cast, all 2000 mm in length and with rectangular cross sections of 200 mm x 300 mm. All the beams were designed to fail in shear. All beams were simply supported over a span of 1680mm and subjected to two symmetrically-placed concentrated loads. The shear span-to-depth ratio was 2.5 for all beams. The test parameter was the longitudinal reinforcement ratio. From the experimental program and the analytical modelling of test beams using current models for Portland cement members, the following conclusions are made:

- For the test beams, two modes of failure were observed: diagonal tension failure and shear compression failure. The modes of failure and crack patterns were generally similar to those described in the literature for Portland cement concrete beams.

- From the load-deflection curves, the formation of first flexural crack and diagonal crack were evident. These points were reflected by the change in slope of the graphs. These were similar to what was described in the literature for Portland cement concrete beams.
- Good correlation between test and calculated values of shear cracking load was obtained. The average ratio of test/prediction value was 1.08 and 1.14 with Zsutty's expression and draft AS3600-05 respectively. The coefficients of variation using these two methods were similar, both giving 11.6%.
- The shear strength of the beams was influenced by the longitudinal tensile reinforcement ratio. As expected, the shear strength of the beams increased with the increase of the longitudinal tensile reinforcement ratio.
- Conservative results of shear strength prediction for geopolymer concrete beams are found by using the design provisions contained in the draft Australian Standard for Concrete Structures AS3600-05 and American Concrete Institute Building Code ACI 318-08. The draft AS3600 (2005) gave an average test-prediction ratio of 1.70 with a coefficient of variation of 12.9%. The ACI318-08 yielded a test-prediction ratio of 2.55 with a coefficient of variation of 16.1%.
- Comparison was made between the test shear strength of beams with predictions, using three analytical models based on different theories and approaches to shear design for reinforced concrete beams. Good correlation of test-to-prediction value was obtained by using the Finite Element Analysis program *VecTor2* incorporating the Disturbed Stress Field Model by Vecchio (2000). A mean test-prediction ratio of 1.08 with a coefficient of variation of 8.3% was found.
- The cracking and crushing patterns derived from analytical modelling using *VecTor2* were compared to the test beams. It was found that the modelling produced reasonably accurate results, especially for beams failed in diagonal tension. The crushing patterns near the loading plate were also simulated correctly for beams failed in shear-compression.
- Comparison of shear strength of geopolymer concrete beams to Portland cement concrete beams was conducted using results from studies conducted

by von Ramin (2004), Kong and Rangan (1998) and Vecchio (2000) to validate their analytical models for Portland cement concrete beams. The DSFM model proposed by Vecchio (2000) gave the best prediction of shear capacity for both geopolymer concrete and Portland cement concrete beams.

- Overall, this study demonstrated that the methods of calculations used in the case of reinforced Portland cement concrete beams are applicable in predicting the shear strength of reinforced geopolymer concrete beams. Code provisions are generally conservative and are safe to predict the shear strength of geopolymer concrete beams.

10.1.2 Bond Behaviour of Reinforced Fly Ash-Based Geopolymer Concrete Beams

The experimental program included manufacturing and testing twelve lap-spliced beam specimens. All the beams were 200 mm wide, 300 mm deep and 2500 mm long. The beams were reinforced with bars spliced in a constant moment region and designed to fail in a bond-splitting mode. No transverse reinforcement was provided in the splice region. The beams were divided into two series to investigate the test parameters of bond strength: concrete cover, bar diameter, splice length and concrete compressive strength. From the experimental work and analysis of the test beams using current models for Portland cement concrete members, the following conclusions were drawn:

- The failure modes and crack patterns observed for reinforced geopolymer concrete beams were similar to those reported in the literature for reinforced Portland cement concrete beams. All beams failed by a splitting of the concrete at the tension face within the splice region.
- Observations on the geopolymer concrete-steel interface showed no signs of concrete crushing in front of the ribs in either normal strength or high strength geopolymer concrete. This is contrary to what is reported for Portland cement normal strength concrete, where signs of concrete crushing in front of the ribs has been observed.

- The bond strength was influenced by the concrete cover and bar diameter represented by the C/d_b ratio. The bond stress increases as C/d_b increases (or bar size decreases) for both normal strength and high strength geopolymer concrete. This trend is similar to what is reported of Portland cement concrete beams.
- For the effect of L_s/d_b on bond strength, it was observed that as L_s/d_b increases, the bond stress decreases for both normal and high strength geopolymer concrete. This observation is found to be similar to reports in the literature of Portland cement concrete beams.
- The bond stress increased with the increase in compressive strength for the same C/d_b ratio. This trend is similar to what has been reported of geopolymer concrete beam-end specimens. It was observed that the bond stress increased with the increase in compressive strength for the same L_s/d_b ratio in all cases.
- Observation on formation of the first flexural crack was evident from the load deflection curves, as reflected by the change of slope in the graphs. These were similar to what is described in the literature for Portland cement concrete beams.
- The design provisions contained in the Australian Standard for Concrete Structures AS3600-01, draft AS 3600 (2005) and American Concrete Institute Building Code ACI 318-08 are conservative and are safe to predict the development length and lap-spliced length of geopolymer concrete.
- The correlation of test bond strength with predictions from analytical models show that the analytical model proposed by Canbay & Frosch (2005) predicts the bond strength of tensile lap splices of geopolymer concrete beams with an average test-to-prediction ratio of 1.17 and coefficient of variation of 11.97%. All other models yield similar prediction for bond strength of all beams with an average test-to-prediction ratio of 1.25 to 1.30.
- The higher bond strength of geopolymer concrete is found to be closely related to the tensile strength of geopolymer concrete.

- An improved correlation of test and calculated bond strength for lap splices in geopolymer concrete was obtained with an average test-to-prediction ratio of 1.0 and a coefficient of variation of 15.21% when using the measured tensile strength of geopolymer concrete obtained from the testing of splitting tensile cylinders in the model proposed by Canbay and Frosch.
- Overall, this study demonstrates that the design provisions and analytical models used for the prediction of bond strength of lap-splices in reinforced Portland cement concrete beams are applicable to reinforced geopolymer concrete beams.

10.2 Recommendations for Future Research

There exists very limited information on geopolymer concrete in the areas of bond and shear. Further research needs are highlighted and presented next.

10.2.1 Shear behaviour of Reinforced Fly Ash-Based Geopolymer Concrete

With respect to shear behaviour of geopolymer concrete, further research is recommended to include the following:

- Investigation of the mechanism of shear transfer such as aggregate interlock and dowel action in geopolymer concrete.
- Investigation of the effect of shear reinforcement on shear capacity, with a wider range of shear reinforcement ratios.
- Further investigation of the effect of concrete compressive strength on shear capacity, including the full range of concrete compressive strength currently used in practice.

10.2.2 Bond Behaviour of Lap Splices in Geopolymer Concrete

With respect to bond strength of lap splices in geopolymer concrete, further research is recommended to include the following:

- Investigation of the effect of concrete properties on the bond strength of geopolymer concrete. This can include the full range of concrete compressive strengths currently used in practice. In addition, the tensile properties of geopolymer concrete should be further studied. This should include the study of fracture energy, which is the capacity of the concrete to dissipate energy as a crack opens.
- Study of the effect of bar properties on bond strength. This should include a wider range of bar sizes currently in use. The effect of the geometry of the bar, such as deformation, height and face angle on bond strength, should also be investigated.
- Investigation into the effect of confinement on bond strength by using transverse reinforcement in the splice region.

REFERENCES

- ACI Committee 318 (2008). *Building Code Requirements for Structural Concrete, ACI 318–08*, American Concrete Institute, Farmington Hills, MI.
- ACI Committee 408 (2003). *408R–03: Bond Development of Straight Reinforcing Bars in Tension*, American Concrete Institute, Farmington Hills, MI.
- Ahmad, S.H., Khaloo, A.R. and Poveda, A. (1986). “Shear Capacity of Reinforced High-Strength Concrete Beams”, *ACI Journal*, March–April, 297–305.
- Anderson, J.E. (2007). “Green Cement: Finding a Solution for a Sustainable Cement Industry”, Green Cities Competition, Bears Breaking Boundaries, Department of Civil and Environmental Engineering, University of California, Berkeley.
- Andini, S., Cioffi, R., Colangelo, F., Grieco, T., Montagnaro, F. and Santoro, L. (2008). “Coal Fly Ash as Raw Material for the Manufacture of Geopolymer-based Products”, *Waste Management*, 28, 416–423.
- Aoyama, H. (1993). “Design Philosophy for Shear in Earthquake Resistance in Japan”, *Earthquake Resistance of Reinforced Concrete Structures*, T. Okayed, ed., Department of Architecture, Faculty of Engineering, University of Tokyo, Tokyo, 407–418.
- ASCE–ACI Committee 445 (1998). “Recent Approaches to Shear Design for Structural Concrete”, *Journal of Structural Engineering*, ASCE, 124 (12), Dec, 1375–1471.

- Azizinamini, A., Chisala, M. and Ghosh, S.K. (1995). “Tension Development Length of Reinforcing Bars Embedded In High-Strength Concrete”, *Engineering Structures*, 17(7), 512–522.
- Azizinamini, A., Stark, M., Roller, J.J. and Ghosh, S.K. (1993). “Bond Performance of Reinforcing Bars Embedded in High-Strength Concrete”, *ACI Structural Journal*, 90 (5), Sept–Oct., 554–561.
- Bakharev, T. (2005a). “Resistance of Geopolymers Materials to Acid Attack”, *Cement and Concrete Research*, 35 (6), 658–670.
- Bakharev, T. (2005b). “Geopolymeric Materials Prepared Using Class F Fly Ash and Elevated Temperature Curing”, *Cement and Concrete Research*, 35(6), 1224–1232.
- Bakharev, T. (2005c). “Durability of Geopolymer Materials in Sodium and Magnesium Sulfate Solutions”, *Cement and Concrete Research*, 35 (6), 1233–1246.
- Barbosa, V.F.F., MacKenzie, K.J.D. and Thaumaturgo, C. (2000). “Synthesis and Characterization of Materials Based on Inorganic Polymers of Alumina and Silica: Sodium Polysialate Polymers”, *International Journal of Inorganic Material*, 2 (4), 309–317.
- Bazant, Z.P. and Kim, J.K. (1984). “Size Effect In Shear Failure of Longitudinal Reinforced Beams”, *ACI Journal*, 81(5), 456–468.
- Bentz, E.C., Vecchio, F.J. and Collins, M.P. (2006). “Simplified Compression Field Theory for Calculating Shear Strength of Reinforced Concrete Elements”, *ACI Structural Journal*, 103 (4), July–Aug, 614–624.
- Bresler, B. and Scordelis, A.C. (1963). “Shear Strength of Reinforced Concrete Beams”, *Journal of American Concrete Institute*, January, 51–72.

- Canbay, E. and Frosch, R.J. (2005). “Bond Strength of Lap-Spliced Bars”, *ACI Structural Journal*, 102 (4), July–Aug, 605–614.
- Carrasquillo, R.L., Nilson, A.H. and Slate, F.O. (1981). “Properties of High Strength Concrete Subject to Short-Term Loads”, *ACI Journal*, 23(2), 145–155.
- Chang, E.H., Sarker, P., Lloyd, N. and Rangan, B.V. (2007). “Shear Behaviour of Reinforced Fly Ash-Based Geopolymer Concrete Beams”, *Proceedings of the 23rd Biennial Conference of the Concrete Institute of Australia*, Adelaide, Australia, 679–688.
- Choi, K.K. and Park, H.G. (2007). “Unified Shear Strength Model for Reinforced Concrete Beams – Part II: Verification and Simplified Method”, *ACI Structural Journal*, 104 (2), Mar–Apr, 153–161.
- Collins, M.P. and Mitchell, D. (1997). *Prestressed Concrete Structures*, 1st ed., Response Publications, Canada.
- Collins, M.P., Mitchell, D., Adebar, P. and Vecchio, F.J. (1996). “A General Shear Design Method”, *ACI Structural Journal*, 93 (1), 36–45.
- Committee BD-002 Standards Australia (2005). *Concrete Structures: Draft Australian Standard AS3600-2005*, Standards Australia.
- Damtoft, J.S., Lukasik, J., Herfort, D., Sorrentino, D. and Gartner, E.M. (2007). “Sustainable Development and Climate Change Initiatives”, *Cement and Concrete Research*, 38, 115–127.
- Darwin, D., McCabe, S.L., Idun, E.K. and Schoenekase, S.P. (1992). “Development Length Criteria: Bars Not Confined by Transverse Reinforcement” *ACI Structural Journal*, 89(6), Nov–Dec., 709–720.

- Darwin, D., Tholen, M. L., Idun, E. K. and Zuo, J. (1996a). “Splice Strength of High Relative Rib Area Reinforcing Bars,” *ACI Structural Journal*, 93 (1), Jan.–Feb., 95–107.
- Darwin, D., Tholen, M. L., Idun, E. K. and Zuo, J. (1996b). “Development Length Criteria for Conventional and High Relative Rib Area Reinforcing Bars,” *ACI Structural Journal*, 93 (1), May–June, 347–359.
- Davidovits, J. (1991). “Properties of Geopolymer Cements”, *Journal of Thermal Analysis*, 37, 1633–1656.
- Davidovits, J. (1994). “High-Alkali Cements for 21st Century Concretes in Concrete Technology, Past, Present and Future”, *Proceedings of V. Mohan Malhotra Symposium*. Editor: P. Kumar Mehta, ACI SP-144, 383-397.
- Davidovits, J. (1999). “Chemistry of Geopolymeric Systems, Terminology”, *Proceedings of the Geopolymer 2005 World Congress*, Saint-Quentin, France.
- Duxson, P., Fernández-Jiménez, A., Provis, J.L., Lukey, G.C., Palomo, A. and van Deventer, J.S.J. (2007a). “Geopolymer Technology: The Current State of the Art”, *Journal of Material Science*, 42, 2917–2933.
- Duxson, P., Provis, J.L., Lukey, G.C., Palomo, A. and van Deventer, J.S.J. (2007b). “The Role of Inorganic Polymer Technology in the Development of Green Concrete”, *Cement and Concrete Research*, 37, 1590–1597.
- Esfahani, M.R. (1995). *Bond between High Strength Concrete and Reinforcing Bars in Splices*, PhD Thesis, School of Civil Engineering, Curtin University of Technology, Western Australia.
- Esfahani, M.R. and Rangan, B.V. (1998). “Bond between Normal Strength and High Strength Concrete (HSC) and Reinforcing Bars in Splices in Beams”, *ACI Structural Journal*, 95 (3), 272–280.

- Fernandez-Jimenez, A., Palomo, A. and Criado, M. (2004). “Microstructure Development of Alkali-activated Fly Ash Cement: A Descriptive Model”, *Cement and Concrete Research*, 35(6), 1204–1209.
- Fernández-Jiménez, A., Palomo, A. and López-Hambrados, C. (2006). “Engineering Properties of Alkali-Activated Fly Ash Concrete”, *ACI Materials Journal*, 103(2), Mar–Apr, 106–112.
- García-Lodeiro, I., Palomo, A. and Fernández-Jiménez, A. (2007). “Alkali-aggregate Reaction in Activated Fly Ash Systems”, *Cement and Concrete Research*, 37, 175–183.
- Gilbert, R.I. (2007). “The New Anchorage and Splice Length Provisions in AS3600 – A Comparison with Other Codes and Experimental Data”, *Proceedings of the 23rd Biennial Conference of the Concrete Institute of Australia*, Adelaide.
- Grigg, A. and Sarker, P.K. (2006). “Bond Strength of Geopolymer Concrete”, Final Year Research Report, Civil Engineering Department, Curtin University of Technology, Western Australia.
- Gourley, J.T. (2003). “Geopolymers: Opportunities for Environmentally Friendly Construction Materials”, *Materials 2003 Conference: Adaptive Materials for a Modern Society*, Institute of Materials Engineering Australasia, October, Sydney.
- Gourley, J.T. and Johnson, G.B. (2005). “Developments in Geopolymer Precast Concrete”, *Proceedings of the Geopolymer 2005 World Congress*, Saint-Quentin, France, 139–143.
- Gupta, P.R. (1998). *Shear Design of Reinforced Concrete Members under Axial Compression*, PhD Thesis, Department of Civil Engineering, University of Toronto, Canada.

- Hadley, D.N. (2005). *The Nature of Paste-aggregate Interphase*, PhD thesis, School of Civil Engineering, Purdue University, IN. 1972.
- Hamad, B.S. and Itani, M.S. (1998). “Bond Strength of Reinforcement in High-Performance Concrete: The Role of Silica Fume, Casting Position, and Superplasticizer Dosage”, *ACI Structural Journal*, September–October, 499–511.
- Hamad, B.S. and Mike, J.A. (2003). “Experimental Investigation of Bond Strength of Hot-Dip Galvanized Reinforcement in Normal- and High-Strength Concrete”, *ACI Structural Journal*, July–August, 465–470.
- Hardjito, D. and Rangan, B.V. (2005). “Development and Properties of Low-Calcium Fly Ash-Based Geopolymer Concrete”, Research Report GC1, Faculty of Engineering, Curtin University of Technology, available at espace@curtin or www.geopolymer.org
- Hoang, C.L. and Nielsen M.P. (1998). “Plasticity Approach to Shear Design”, *Cement and Concrete Composites*, 20, 437–453.
- Hsu, T.T.C. (1988). “Softened Truss Model Theory for Shear and Torsion”, *ACI Structural Journal*, 85(6), Nov–Dec., 624–635.
- Hsu, T.T.C. (1993). *Unified Theory of Reinforced Concrete*, CRC Press, FL.
- Kani, M.W., Huggins, M.W. and Wiltkopp, P.F. (1979). *Kani on Shear in Reinforced Concrete*, University of Toronto, Canada.
- Kong, P.Y.L. (1996). *Shear Strength of High Performance Concrete Beams*, PhD Thesis, School of Civil Engineering, Curtin University of Technology, Western Australia.
- Kong, P.Y.L. and Rangan, B.V. (1998). “Shear Strength of High-Performance Concrete Beams”, *ACI Structural Journal*, 95 (6), Nov–Dec, 677 – 688.

- Komnitsas, K. and Zaharaki, D. (2007). "Geopolymerisation: A Review and Prospects for the Minerals Industry", *Minerals Engineering*, 20, 1261–1277.
- Kumar S., Kumar, R., Alex, T.C., Bandopadhyay, A. and Mehrotra, S.P. (2005). "Effect of Mechanically Activated Fly Ash on the Properties of Geopolymer Cement", *Proceedings of the Geopolymer 2005 World Congress*, Saint-Quentin, France.
- Kumar, R., Kumar, S. and Mehrotra, S.P. (2007). "Towards Sustainable Solutions for Fly Ash Through Mechanical Activation", *Resources, Conservation and Recycling*, 52, 157–159.
- Kupfer, H. (1964). "Erweiterung der Morsch'schen Fachwerkanalogie mit Hilfe des Prinzips vom Minimum der Formänderungsarbeit (Generalization of Mörsch's truss analogy using the principle of minimum strain energy)", *Comite Euro-International du Beton, Bulletin d'Information, No.40*, CEB, Paris, 44-57.
- Lee, W.K.W. and van Deventer, J.S.J. (2002). "The Effect of Ionic Contaminants on the Early-Age Properties of Alkali-Activated Fly Ash-Based Cements", *Cement and Concrete Research*, 32(4), 577–584.
- Lee, W.K.W. and van Deventer, J.S.J. (2004). "The Interface Between Natural Siliceous Aggregates and Geopolymers", *Cement and Concrete Research*, 34(2), 95–206.
- MacGregor, J.G. and Bartlett, F.M. (2000). *Reinforced Concrete: Mechanics and Design*, Prentice Hall Canada, Ontario.
- Magnusson, G. (2000). "Bond and Anchorage of Ribbed Bars in High-Strength Concrete", Research Report, Division of Concrete Structures, Department of Structural Engineering, Chalmers University of Technology, Sweden.

- Malhotra, V.M. (1998). “Role of Supplementary Cementing Materials in Reducing Greenhouse Gas Emission”, MTL Division Report MTL 98–03 (OP&J), Natural resources Canada, Ottawa.
- Manz, O. E. (1998). “Coal Fly Ash: A Retrospective and Future Look”, *Energieia*, 9 (2), 1–6.
- Mehta, P.K. (2001). “Reducing the Environmental Impact of Concrete”, *ACI Concrete International*, 23(10), 61–66.
- Mehta, P.K. (2008). “Coal Fly Ash: The Most Powerful Tool for Sustainability of the Concrete Industry”, *Ash at Work*, 1, 38–43.
- Mörsch, E. (1920). *Der Eisenbetonbau-Seine Theorie und Anwendung (Reinforced Concrete Construction – Theory and Application*, 5th Ed., Wittwer, Stuttgart, Vol.1, Part.1.
- Nawy, E.G. (2005). *Reinforced Concrete: A Fundamental Approach*, Pearson Prentice Hall, NJ.
- Neville, A.M. (2000). *Properties of Concrete*, Longman, NY.
- Orangun, C. O., Jirsa, J. O. and Breen, J. E. (1975). “The Strength of Anchored Bars: A Reevaluation of Test Data on Development Length and Splices,” Research Report No.154–3F, Center of Highway Research, The University of Texas.
- Orangun, C. O., Jirsa, J. O. and Breen, J. E. (1977). “A Reevaluation of Test Data on Development Length and Splices”, *ACI Journal*, 74 (3), 114–122.
- Palomo A., Grutzeck, M.W. and Blanco, M.T. (1999). “Alkali-activated Fly Ashes: A Cement for the Future”, *Cement and Concrete Research*, 29, 1323–1329.
- Park, R. and Paulay, T. (1975). *Reinforced Concrete Structures*, John Wiley, Chichester, UK.

- Phair, J.W. (2006). "Green Chemistry for Sustainable Cement Production and Use", *Green Chemistry*, 8, 763–780.
- Pendyala, R.S. and Mendis, P. "Experimental Study on Shear Strength of High-Strength Concrete Beams", *ACI Structural Journal*, 2000, 97(4), 564–571.
- Rangan, B.V. (2008a). "Fly Ash-Based Geopolymer Concrete", Research Report GC4, Faculty of Engineering, Curtin University of Technology, WA, available at espace@curtin or www.geopolymer.org.
- Rangan, B.V. (2008b). "Studies on Fly Ash-Based Geopolymer Concrete", *Malaysia Construction Research Journal*, 3 (2), 1–20.
- Regan, P.E. (1993). "Research on Shear: A Benefit to Humanity or a Waste of Time?", *The Structural Engineer*, 71(19), 337–347.
- Reineck, K.H. (1991). "Ultimate Shear Force of Structural Concrete Members Without Transverse Reinforcement Derived From a Mechanical Model", *ACI Structural Journal*, 88(5), 592–602.
- Ritter, W. (1899). "Die bauweise hennebique", *Schweizerische Bauzeitung*, 33(7), 59-61.
- Ryan, W.G. and Samarin, A. (1992). *Australian Concrete Technology*, Longman Cheshire, Victoria.
- Sarker, P.K., Grigg, A. and Chang, E.H. (2007). "Bond Strength of Fly Ash-Based Geopolymer Concrete With Reinforcing Bars", *Proceedings of Recent Developments in Structural Engineering, Mechanics and Computation*, CD ROM, Ed. A. Zingoni, Millpress, Netherlands.

- Sindhunata, van Deventer, J.S.J., Lukey, G.C. and Xu, H. (2006). “Effect of Curing Temperature and Silicate Concentration on Fly Ash-Based Geopolymerization”, *Industrial and Engineering Chemistry Research*, 47, 2991–2999.
- Standards Australia (1997). “Methods of Testing Concrete – Method 17: Determination of the Static Chord Modulus of Elasticity and Poisson’s Ratio of Concrete Specimens.”
- Standards Australia (1999). “Methods of Testing Concrete – Method 9: Determination of the Compressive Strength of Concrete Specimens.”
- Standards Australia (2000): “Methods of Testing Concrete – Method 10: Determination of Indirect Tensile Strength of Concrete Cylinders.”
- Standards Australia (2000): “Method for Sampling and Testing Aggregates – Method 5: Particle Density and Water Absorption of Fine Aggregates.”
- Standards Australia (2000): “Method for Sampling and Testing Aggregates – Method 6.1: Particle Density and Water Absorption of Coarse Aggregates – Weighing-in-water Method.”
- Standards Australia (2001). “Concrete Structures, AS3600–2001.”
- Škvára, F., Kopecký, L., Němeček, J. and Bittnar, A. (2006). “Microstructure of Geopolymer Materials Based on Fly Ash”, *Ceramics – Silikáty* 50(4), 208–215.
- Sofi, M., van Deventer, J.S.J., Mendis, P. and Lukey, G.C. (2007a). “Engineering Properties of Inorganic Polymer Concretes (IPCs)”, *Cement and Concrete Research*, 37 (2), 251–257.

- Sofi, M., van Deventer, J.S.J., Mendis, P. and Lukey, G.C. (2007b). “Bond Performance of Reinforcing Bars in Inorganic Polymer Concrete (IPC)”, *Journal of Materials Science*, 42 (9), 3007–3016.
- Song, X. J., Marosszeky, M., Brungs, M. and Chang, Z.T. (2005). “Response of Geopolymer Concrete to Sulphuric Acid Attack”, *Proceedings of the Geopolymer 2005 World Congress*, Saint-Quentin, France, 157–160.
- Stanik, B. (1998). “The Influence of Concrete Strength, Distribution of Longitudinal Reinforcement, Amount of Transverse Reinforcement, and Member Size on Shear Strength of Reinforced Concrete Members”, MSc Thesis, Department of Civil Engineering, University of Toronto.
- Struble, L., Skalny, J. and Mindess, S. (1980). “A Review of the Cement-Aggregate Bond”, *Cement and Concrete Research*, 10, 277–286.
- Sumajouw, M.D.J. and Rangan, B.V. (2006). “Low-Calcium Fly Ash-Based Geopolymer Concrete: Reinforced Beams and Columns”, Research Report GC3, Faculty of Engineering, Curtin University of Technology, Western Australia, available at espace@curtin or www.geopolymer.org
- Swanepoel, J.C. and Strydom, C.A. (2002). “Utilisation of Fly Ash in a Geopolymeric Material”, *Applied Chemistry*, 17 (8), 1143–1148.
- Tepfers, R. (1973). “A Theory of Bond Applied to Over-lapping Tensile Reinforcement Splices for Deformed Bars”, Publication 73:2, Division of Concrete Structures, Chalmers University of Technology, Sweden.
- Tompos, E.J. and Frosch, R.J. (2002). “Influence of Beam Size, Longitudinal Reinforcement, and Stirrup Effectiveness on Concrete Shear Strength”, *ACI Structural Journal*, 99 (5), 559–567.

- van Jaarsveld, J.G.S., van Deventer, J.S.J. and Lukey, G.C. (2002). “The Effect of Composition and Temperature on the Properties of Fly-ash and Kaolinite-based Geopolymers”, *Chemical Engineering Journal*, 89 (1–3), 63–73.
- van Jaarsveld, J.G.S., Van Deventer, J.S.J. and Lukey, G.C. (2003). “The Characterisation of Source Materials in Fly Ash-based geopolymers”, *Materials Letters*, 57(7), 1272–1280.
- Vecchio, F.J. (2000). “Disturbed Stress Field Model for Reinforced Concrete: Formulation”, *Journal of Structural Engineering*, 126(9), 1070–1077.
- Vecchio, F.J. (2001). “Disturbed Stress Field Model for Reinforced Concrete: Implementation”, *Journal of Structural Engineering*, 127(1), 12–20.
- Vecchio, F.J. and Collins, M.P. (1982). “The Response of Reinforced Concrete to In-plane Shear and Normal Stresses”, Publication No. 82–03, Department of Civil Engineering, University of Toronto.
- Vecchio, F.J. and Collins, M.P. (1986). “The Modified Compression Field Theory for Reinforced Concrete Elements Subjected to Shear”, *ACI Journal*, 83(2), 219–231.
- Vecchio, F.J. and Collins, M.P. (1993). “Compression Response of Crack Reinforced Concrete”, *Journal of Structural Engineering*, 119 (12), Nov–Dec, 3590–3610.
- Vecchio, F.J., Lai, D., Shim, W. and Ng, J. (2001). “Disturbed Stress Field Model for Reinforced Concrete: Validation”, *Journal of Structural Engineering*, April, 350–358.
- Vecchio, F.J. and Shim, W. (2004). “Experimental and Analytical Reexamination of Classic Concrete Beam Tests”, *ASCE Journal of Structural Engineering*, 130 (3), 460–469.

- von Ramin, M. (2004). *Shear Strength of Reinforced Concrete Members Subjected to Monotonic and Cyclic Loads*, PhD Thesis, Department of Civil, Environmental, and Architectural Engineering, University of Kansas.
- von Ramin, M. and Matamoros, A. B. (2006). “Shear Strength of Reinforced Concrete Members Subjected to Monotonic Loads”, *ACI Structural Journal*, 103(1), 83–92.
- Wallah, S.E. and Rangan, B.V. (2006). “Low-calcium Fly Ash-based Geopolymer Concrete: Long Term Properties”, Research Report GC2, Faculty of Engineering, Curtin University of Technology, Western Australia, available at espace@curtin or www.geopolymer.org
- Walraven, J.C. (1981). “The Fundamental Analysis of Aggregate Interlock”, *Journal of Structural Division*, ASCE, 108, 2245–2270.
- Warner, R. F., Rangan, B.V., Hall, A.S. and Faulkes, K.A. (1998). *Concrete Structures*, Addison Wesley Longman, Melbourne.
- Watanabe, F., and Ichinose, T. (1991). “Strength and Ductility Design of RC Members Subjected to Combined Bending and Shear”, *Preliminary Proceedings*, International Workshop on Concrete Shear in Earthquake, University of Houston, TX, IV4–1–IV4–10.
- Wong, P.S. and Vecchio, F.J. (2002). *VecTor2 and Formworks User’s Manual*, University of Toronto, Canada.
- Xu, H. and van Deventer, J.S.J. (2000). “The Geopolymerisation of Alumino-Silicate Minerals”, *International Journal of Mineral Processing*, 59(3), 247–266.

Xu, H. and van Deventer, J.S.J. (2002). “Microstructural Characterisation of Geopolymers Synthesized from Kaolinite/Stilbite Mixtures Using XRD, MAS-NMR, SEM/EDX, TEM/EDX and HREM ”, *Cement and Concrete Research*, 32, 1705–1716.

Zsutty, T.C. (1968). “Beam Shear Strength Prediction by Analysis of Existing Data”, *ACI Journal*, 65(11), 943–951.

Zuo, J. and Darwin, D., (2000). “Splice Strength of Conventional and High Relative Rib Area Bars in Normal and High Strength Concrete”, *ACI Structural Journal*, 97 (4), July–Aug, 630–641.

Every reasonable effort has been made to acknowledge the owners of copyright material. I would be pleased to hear from any copyright owner who has been omitted or incorrectly acknowledged.

APPENDICES

APPENDIX A1

WATER ADJUSTED FOR THE MIX ACCORDING TO MOISTURE CONDITIONS OF AGGREGATES (SHEAR STUDY)

Shear Stage	Pour#4	Beam S1-1 and Beam S1-2			Symbols						
Mix Design	GP1	Per Pour	Per Batch		A =	weight of test portion before put into oven					
Material		Weight (g)	Weight (g)	SSD (%)	B =	weight of test portion after taken out from oven					
Aggregate 10mm	554	155922	38980	0.3	C =	weight of tray					
Aggregate 7mm	647	181910	45477	0.5	D =	weight of test portion before put into oven (without tray) (A - C)					
Sand	647	181910	45477	0.7	E =	weight of test portion after taken out from oven (without tray) (B - C)					
Fly Ash	408	114748	28687		F =	mass of water of test portion (D - E)					
NaOH Solution (14M)	41	11542	2885		G =	water content of test portion (%) (F/D) x 100					
Sodium silicate Solution	103	28957	7239		H =	mass of water in bin (G/100) x weight of aggregate					
Superplasticizer	6.1	1721	430		I =	mass of water SSD SSD (%) x weight of aggregate					
Added Water	25.8	7262	1815		J =	difference between mass of water of bin & SSD (H - I)					
Bin No.	Aggregate	A	B	C	D	E	F	G	H	I	J
1	10 mm	1117.6	1114.2	313	804.6	801.2	3.4	0.42	180.3	116.9	63.4
2	10 mm	995.5	993.3	313	682.5	680.3	2.2	0.32	137.5	116.9	20.6
3	10 mm	1084.2	1082.4	313	771.2	769.4	1.8	0.23	99.6	116.9	-17.4
4	10 mm	900.6	899.5	313	587.6	586.5	1.1	0.19	79.9	116.9	-37.1
5	7 mm	1038.8	1035.6	305	733.8	730.6	3.2	0.44	217.3	227.4	-10.1
6	7 mm	1055.7	1052.8	305	750.7	747.8	2.9	0.39	192.5	227.4	-34.9
7	7 mm	1285.6	1282.2	305	980.6	977.2	3.4	0.35	172.8	227.4	-54.6
8	7 mm	1009.9	1006.5	305	704.9	701.5	3.4	0.48	240.3	227.4	13.0
9	Sand	799.2	796.4	120	679.2	676.4	2.8	0.41	205.4	318.3	-112.9
10	Sand	870.7	865.6	120	750.7	745.6	5.1	0.68	338.5	318.3	20.2
11	Sand	922.4	918.5	120	802.4	798.5	3.9	0.49	242.2	318.3	-76.1
12	Sand	1002.3	998.4	120	882.3	878.4	3.9	0.44	220.3	318.3	-98.1
Batch No	Bin No.			water in	added						
	10mm	7mm	Sand	bins	water						
1	1	5	9	-59.6	1875						
2	2	6	10	5.9	1809						
3	3	7	11	-148.1	1963						
4	4	8	12	-122.2	1937						

APPENDIX A2

WATER ADJUSTED FOR THE MIX ACCORDING TO MOISTURE CONDITIONS OF AGGREGATES (BOND STUDY)

Bond Stage	Pour#5	Beam H-D-2.2 and Beam H-L-12.5			Symbols							
Mix Design	GP2	Per Pour	Per Batch		A =	weight of test portion before put into oven						
Material		Weight (g)	Weight (g)	SSD (%)	B =	weight of test portion after taken out from oven						
Aggregate 10mm	554	213336	42667	0.3	C =	weight of tray						
Aggregate 7mm	647	249149	49830	0.5	D =	weight of test portion before put into oven (without tray)						(A - C)
Sand	647	249149	49830	0.7	E =	weight of test portion after taken out from oven (without tray)						(B - C)
Fly Ash	408	157114	31423		F =	mass of water of test portion						(D - E)
NaOH Solution (14M)	41	15788	3158		G =	water content of test portion (%)						(F/D) x 100
Sodium silicate Solution	103	39664	7933		H =	mass of water in bin						(G/100) x weight of aggregate
Superplasticizer	6.1	2349	470		I =	mass of water SSD						SSD (%) x weight of aggregate
Added Water	16.5	6354	1271		J =	difference between mass of water of bin & SSD						(H - I)
Bin No.	Aggregate	A	B	C	D	E	F	G	H	I	J	
1	10 mm	1005.2	1001.6	313	692.2	688.6	3.6	0.52	221.9	128.0	93.9	
2	10 mm	1337.2	1334.9	313	1024.2	1021.9	2.3	0.22	95.8	128.0	-32.2	
3	10 mm	1209.7	1203.3	313	896.7	890.3	6.4	0.71	304.5	128.0	176.5	
4	10 mm	993.2	991.2	313	680.2	678.2	2	0.29	125.5	128.0	-2.5	
5	10 mm	1100.8	1099.2	313	787.8	786.2	1.6	0.20	86.7	128.0	-41.3	
6	7 mm	966.2	962.7	305	661.2	657.7	3.5	0.53	263.8	249.2	14.6	
7	7 mm	1089.2	1084	305	784.2	779	5.2	0.66	330.4	249.2	81.3	
8	7 mm	1122.6	1119.2	305	817.6	814.2	3.4	0.42	207.2	249.2	-41.9	
9	7 mm	1078.3	1073.2	305	773.3	768.2	5.1	0.66	328.6	249.2	79.5	
10	7 mm	1008.3	1003.2	305	703.3	698.2	5.1	0.73	361.3	249.2	112.2	
11	Sand	997.2	994.2	120	877.2	874.2	3	0.34	170.4	348.8	-178.4	
12	Sand	893.5	888.8	120	773.5	768.8	4.7	0.61	302.8	348.8	-46.0	
13	Sand	856.9	853.1	120	736.9	733.1	3.8	0.52	257.0	348.8	-91.8	
14	Sand	1033.6	1027.3	120	913.6	907.3	6.3	0.69	343.6	348.8	-5.2	
15	Sand	1009.5	1004	120	889.5	884	5.5	0.62	308.1	348.8	-40.7	
		Bin No.			water in	added						
Batch No	10mm	7mm	Sand	bins	water							
1	1	6	11	-69.9	1341							
2	2	7	12	3.1	1268							
3	3	8	13	42.7	1228							
4	4	9	14	71.7	1199							
5	5	10	15	30.1	1241							

Bond Stage	Pour#6	Beam H-L-18.8 and H-L-30.0		
Mix Design	GP2	Per Pour	Per Batch	
Material		Weight (g)	Weight (g)	SSD (%)
Aggregate 10mm	554	213336	42667	0.3
Aggregate 7mm	647	249149	49830	0.5
Sand	647	249149	49830	0.7
Fly Ash	408	157114	31423	
NaOH Solution (14M)	41	15788	3158	
Sodium silicate Solution	103	39664	7933	
Superplasticizer	6.1	2349	470	
Added Water	16.5	6354	1271	

Symbols

- A = weight of test portion before put into oven
- B = weight of test portion after taken out from oven
- C = weight of tray
- D = weight of test portion before put into oven (without tray) (A - C)
- E = weight of test portion after taken out from oven (without tray) (B - C)
- F = mass of water of test portion (D - E)
- G = water content of test portion (%) $(F/D) \times 100$
- H = mass of water in bin $(G/100) \times \text{weight of aggregate}$
- I = mass of water SSD $\text{SSD} (\%) \times \text{weight of aggregate}$
- J = difference between mass of water of bin & SSD (H - I)

Bin No.	Aggregate	A	B	C	D	E	F	G	H	I	J
1	10 mm	966.5	962.3	313	653.5	649.3	4.2	0.64	274.2	128.0	146.2
2	10 mm	1102.5	1099.2	313	789.5	786.2	3.3	0.42	178.3	128.0	50.3
3	10 mm	992.8	989.2	313	679.8	676.2	3.6	0.53	226.0	128.0	97.9
4	10 mm	1007.3	1004.5	313	694.3	691.5	2.8	0.40	172.1	128.0	44.1
5	10 mm	922.8	918.9	313	609.8	605.9	3.9	0.64	272.9	128.0	144.9
6	7 mm	1100.7	1097.2	305	795.7	792.2	3.5	0.44	219.2	249.2	-30.0
7	7 mm	1088.3	1085.3	305	783.3	780.3	3	0.38	190.8	249.2	-58.3
8	7 mm	1342.7	1339.2	305	1037.7	1034.2	3.5	0.34	168.1	249.2	-81.1
9	7 mm	1078.3	1073.2	305	773.3	768.2	5.1	0.66	328.6	249.2	79.5
10	7 mm	1227.9	1225.8	305	922.9	920.8	2.1	0.23	113.4	249.2	-135.8
11	Sand	1007.8	1002.5	120	887.8	882.5	5.3	0.60	297.5	348.8	-51.3
12	Sand	922.9	919.4	120	802.9	799.4	3.5	0.44	217.2	348.8	-131.6
13	Sand	898.5	892.3	120	778.5	772.3	6.2	0.80	396.8	348.8	48.0
14	Sand	1079.4	1074.3	120	959.4	954.3	5.1	0.53	264.9	348.8	-83.9
15	Sand	1189.2	1183.2	120	1069.2	1063.2	6	0.56	279.6	348.8	-69.2

Batch No	Bin No.			water in bins	added water
	10mm	7mm	Sand		
1	1	6	11	64.9	1206
2	2	7	12	-139.6	1411
3	3	8	13	64.9	1206
4	4	9	14	39.6	1231
5	5	10	15	-60.1	1331

APPENDIX B1
TRIAL MIX DATA FOR MIXTURE GP1

Table B1.1: Cylinder Compressive Strength Data for Trial Mix 1 (GP1)

Age after Casting	Load (kN)			Compressive Strength (MPa)			Average Compressive Strength
(days)	Cylinder 1	Cylinder 2	Cylinder 3	Cylinder 1	Cylinder 2	Cylinder 3	(MPa)
3	250.2	266.1	259.1	31.9	33.9	33.0	33
7	255	266.4	267.9	32.5	33.9	34.1	33
14	301.2	299.5	297	38.3	38.1	37.8	38
21	300.1	301	308.2	38.2	38.3	39.2	39
28	298.7	310.1	312	38.0	39.5	39.7	39
60	322.1	323.3	337	41.0	41.2	42.9	42
90	328	325.1	324.9	41.8	41.4	41.4	42

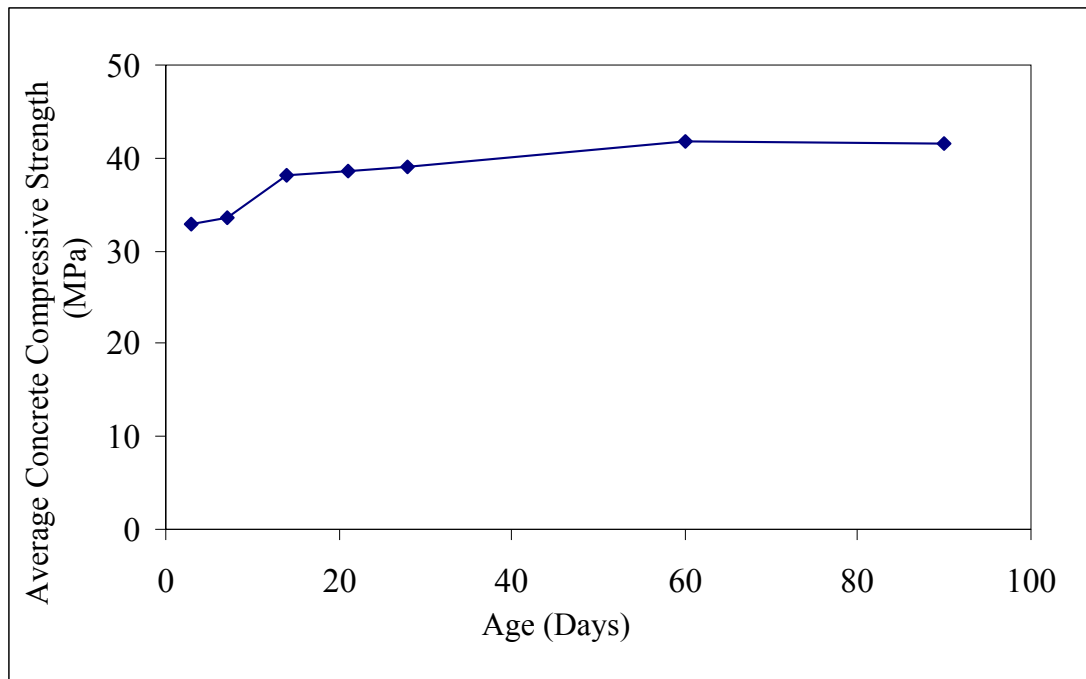


Figure B1.1: Concrete Compressive Strength Development for Trial Mix 1 (GP1)

APPENDIX B2
TRIAL MIX DATA FOR MIXTURE GP2

Table B2.1: Cylinder Compressive Strength Data for Trial Mix 1 (GP2)

Age after Casting	Load (kN)			Compressive Strength (MPa)			Average Compressive Strength
(Days)	Cylinder 1	Cylinder 2	Cylinder 3	Cylinder 1	Cylinder 2	Cylinder 3	(MPa)
3	399	401.2	389.2	50.8	51.1	49.6	50
7	388	421.1	423.8	49.4	53.6	54.0	52
14	445	465.3	449	56.7	59.2	57.2	58
21	466	442	458.3	59.3	56.3	58.4	58
28	477.2	459.4	455	60.8	58.5	57.9	59
60	499	471	482.3	63.5	60.0	61.4	62

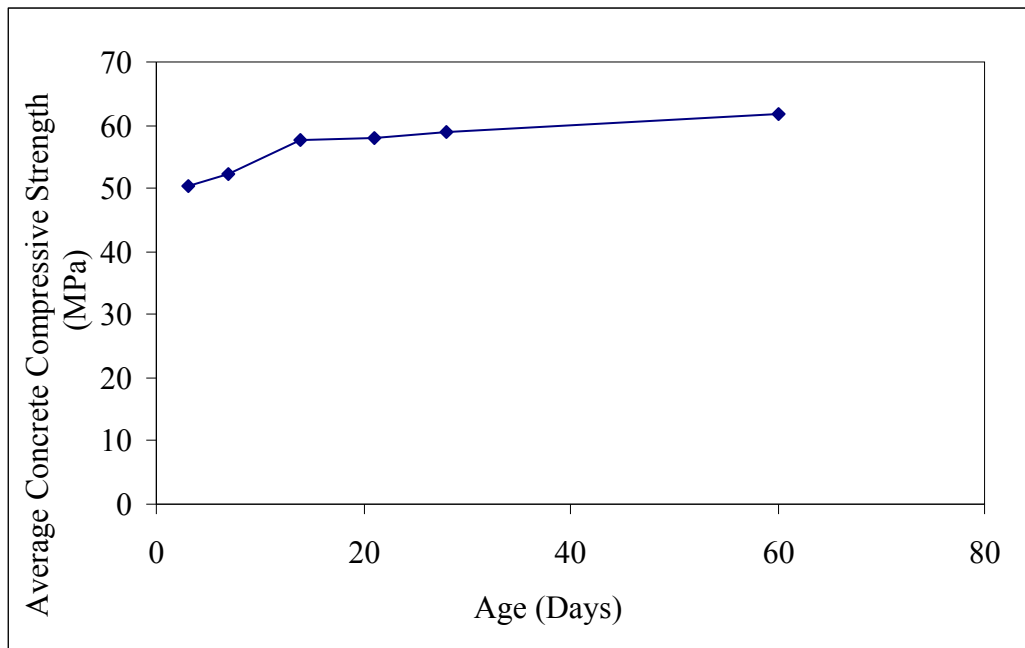


Figure B2.1: Concrete Compressive Strength Development for Trial Mix 1 (GP2)

APPENDIX C
TEST DATA FOR BEAMS (SHEAR STUDY)

Table C.1: Test Data for Beam S1-1

Load (kN)	Shear Force (kN)	Mid-span Deflection (mm)
0.00	0.00	0.00
9.97	4.99	0.06
21.19	10.60	0.12
31.16	15.58	0.18
41.14	20.57	0.24
51.11	25.56	0.37
61.08	30.54	0.43
71.06	35.53	0.49
81.03	40.52	0.67
91.00	45.50	0.91
100.97	50.49	1.03
110.95	55.48	1.28
120.92	60.46	1.52
130.89	65.45	1.64
140.86	70.43	1.82
150.84	75.42	2.01
160.81	80.41	2.19
170.78	85.39	2.37
180.75	90.38	2.68
190.73	95.37	2.92
200.69	100.35	3.16
210.67	105.34	3.34
220.65	110.33	3.59
230.62	115.31	3.83
240.59	120.30	4.32
250.56	125.28	4.62
260.54	130.27	4.80
270.51	135.26	5.05
280.48	140.24	5.29
290.45	145.23	5.59
300.43	150.22	5.90
310.40	155.20	6.14
320.37	160.19	6.38
330.34	165.17	6.69
340.32	170.16	6.99
350.29	175.15	7.36
360.26	180.13	7.78
370.24	185.12	8.02
380.21	190.11	8.51
390.18	195.09	9.00
400.15	200.08	9.48

410.13	205.06	10.03
415.11	207.56	10.52
410.13	205.06	10.64
407.63	203.82	11.06
410.13	205.07	11.64
410.13	205.07	11.67
411.37	205.69	11.85
411.37	205.69	12.10
407.63	203.82	12.71
403.89	201.95	13.13
402.65	201.32	13.56
401.40	200.70	13.80
400.15	200.08	13.98
398.90	199.45	14.10
397.66	198.83	14.47
395.17	197.59	15.08
392.67	196.34	15.44
385.19	192.60	16.05
383.95	191.98	17.02
382.70	191.35	15.57
381.45	190.73	18.24
380.21	190.11	19.64
377.71	188.86	20.18
376.47	188.23	21.22
375.22	187.61	21.89
376.47	188.23	23.04
375.22	187.61	23.22
376.47	188.23	23.53
376.47	188.23	24.01
376.47	188.23	24.62
376.47	188.23	25.17
377.71	188.86	25.40
375.22	187.61	25.78
375.22	187.61	26.02
375.22	187.61	26.14
375.22	187.61	26.51
375.22	187.61	26.81
375.22	187.61	27.05
320.37	160.19	27.72
310.39	155.20	28.02
225.63	112.82	29.06

Table C.2: Test Data for Beam S1-2

Load (kN)	Shear Force (kN)	Mid-pan Deflection (mm)
0.00	0.00	0.00
11.22	5.61	0.06
21.19	10.60	0.12
31.17	15.58	0.18
41.14	20.57	0.24
51.11	25.56	0.37
62.33	31.17	0.49
71.06	35.53	0.61
81.03	40.52	0.79
91.00	45.50	0.91
100.97	50.49	1.16
110.95	55.48	1.34
120.92	60.46	1.52
130.89	65.45	1.70
140.86	70.43	1.82
150.84	75.42	2.00
160.81	80.41	2.25
170.78	85.39	2.37
180.75	90.38	2.68
190.73	95.36	2.92
200.70	100.35	3.16
210.67	105.34	3.40
220.65	110.32	3.65
231.86	115.93	3.77
241.84	120.92	4.13
250.56	125.28	4.26
261.78	130.89	4.56
271.75	135.88	4.86
281.73	140.86	5.05
291.70	145.85	5.65
300.43	150.22	5.96
310.39	155.20	6.26
321.61	160.81	6.50
330.34	165.17	6.81
341.56	170.78	7.17
350.29	175.15	7.48
360.26	180.13	7.90
370.23	185.12	8.33
380.21	190.11	8.87
386.44	193.22	9.24
390.18	195.09	9.30

395.17	197.58	9.60
398.90	199.45	9.85
400.15	200.08	10.03
401.39	200.70	10.33
395.17	197.59	10.52
396.43	198.22	10.76
397.66	198.83	10.88
398.91	199.46	11.00
400.15	200.08	11.31
401.39	200.70	11.55
402.65	201.33	11.98
403.89	201.95	12.22
402.65	201.33	12.46
392.67	196.34	12.77
387.69	193.85	13.07
385.19	192.60	13.43
381.45	190.73	13.74
382.70	191.35	13.92
378.96	189.48	14.04
380.21	190.11	14.41
378.96	189.48	14.53
380.21	190.11	14.71
380.20	190.10	14.95
380.21	190.11	15.14
373.97	186.99	15.26
373.97	186.99	15.80
372.73	186.37	16.17
373.97	186.99	16.66
373.97	186.99	17.02
373.97	186.99	17.45
372.73	186.37	17.75
372.73	186.37	17.93
373.97	186.99	18.24
371.48	185.74	18.60
368.98	184.49	19.03
368.99	184.50	19.39
367.74	183.87	19.82
367.74	183.87	20.06
367.74	183.87	20.24
367.74	183.87	20.55
367.74	183.87	20.73
367.74	183.87	21.03
367.74	183.87	21.28
367.74	183.87	21.95

364.00	182.00	22.37
362.76	181.38	22.61
362.76	181.38	23.04
364.02	182.01	23.47
365.25	182.63	24.13
365.25	182.63	24.74
365.25	182.63	25.17
366.49	183.25	25.90
362.76	181.38	26.63

364.00	182.00	27.60
364.00	182.00	28.75
365.25	182.63	29.48
366.49	183.25	30.27
365.25	182.63	33.07
362.76	181.38	34.05
360.26	180.13	34.89
359.01	179.51	35.38
357.79	178.90	36.11

Table C.3: Test Data for Beam S1-3

Load (kN)	Shear Force (kN)	Mid-span Deflection (mm)
0.00	0.00	0.00
11.22	5.61	0.06
21.19	10.60	0.12
31.17	15.58	0.18
41.14	20.57	0.36
51.11	25.56	0.49
61.08	30.54	0.55
71.06	35.53	0.73
81.03	40.52	0.91
91.00	45.50	1.09
102.22	51.11	1.28
110.95	55.48	1.40
120.92	60.46	1.58
130.99	65.50	1.76
140.86	70.43	1.95
150.84	75.42	2.13
160.81	80.41	2.43
170.78	85.39	2.61
180.75	90.38	2.92
190.73	95.37	3.10
201.95	100.98	3.40
210.67	105.34	3.65
220.65	110.33	3.89
231.86	115.93	4.13
240.59	120.30	4.38
250.56	125.28	4.62
260.54	130.27	4.86
270.51	135.26	5.23
280.48	140.24	5.47
290.45	145.23	5.78
300.43	150.22	6.08
310.39	155.20	6.44
320.37	160.19	6.81
330.34	165.17	7.17
340.32	170.16	7.54
350.29	175.15	7.90
360.26	180.13	8.51
370.23	185.12	9.11
369.99	185.00	9.18
362.76	181.38	9.24
213.16	106.58	9.61
220.65	110.33	9.61
224.38	112.19	9.73

Table C.4: Test Data for Beam S2-1

Load (kN)	Shear Force (kN)	Mid-span Deflection (mm)
0.00	0.00	0.00
9.97	4.99	0.06
21.19	10.60	0.12
31.16	15.58	0.18
41.14	20.57	0.24
51.11	25.56	0.37
61.10	30.55	0.37
71.06	35.53	0.43
81.03	40.52	0.55
91.00	45.50	0.67
100.97	50.49	0.79
110.95	55.48	0.92
120.90	60.45	0.97
130.89	65.45	1.16
140.86	70.43	1.22
150.84	75.42	1.34
160.81	80.41	1.58
170.78	85.39	1.64
180.75	90.38	1.70
190.73	95.37	1.88
201.95	100.98	2.07
210.67	105.34	2.19
220.65	110.33	2.43
230.62	115.31	2.67
240.59	120.30	2.92
251.81	125.91	3.16

261.78	130.89	3.53
270.51	135.26	3.71
280.48	140.24	3.95
290.45	145.23	4.19
300.43	150.22	4.56
310.40	155.20	4.74
321.62	160.81	4.98
331.59	165.80	5.17
341.56	170.78	5.35
350.29	175.15	5.53
360.26	180.13	5.71
371.48	185.74	6.02
381.45	190.73	6.26
390.18	195.09	6.44
401.39	200.70	6.63
411.37	205.69	6.81
421.34	210.67	7.05
431.32	215.66	7.36
441.29	220.65	7.59
451.26	225.63	7.78
461.23	230.62	8.15
471.21	235.61	8.33
481.18	240.59	8.69
491.15	245.58	9.06
501.13	250.57	9.42
511.10	255.55	9.96
503.60	251.80	10.03

Table C.5: Test Data for Beam S2-2

Load (kN)	Shear Force (kN)	Mid-span Deflection (mm)
0.00	0.00	0.00
11.22	5.61	0.06
21.19	10.60	0.12
32.41	16.21	0.18
41.14	20.57	0.30
51.11	25.56	0.37
61.08	30.54	0.43
71.06	35.53	0.55
81.03	40.52	0.61
91.00	45.50	0.79
100.97	50.49	0.85
110.95	55.48	1.09
120.92	60.46	1.16
130.89	65.45	1.28
140.86	70.43	1.40
150.84	75.42	1.58
160.81	80.41	1.70
170.78	85.39	1.82
180.75	90.38	2.13
190.73	95.37	2.19
200.70	100.35	2.43
210.67	105.34	2.55
220.64	110.32	2.74
230.62	115.31	2.98
240.59	120.30	3.22
250.56	125.28	3.34
260.53	130.27	3.65
270.51	135.26	3.77
280.48	140.24	4.01
290.45	145.23	4.25

301.67	150.84	4.56
310.40	155.20	4.74
320.37	160.19	4.92
330.34	165.17	5.17
340.32	170.16	5.35
350.29	175.15	5.47
360.26	180.13	5.71
371.48	185.74	6.08
381.45	190.73	6.26
391.43	195.72	6.50
400.15	200.08	6.62
411.37	205.69	6.93
420.10	210.05	7.11
430.10	215.05	7.29
440.10	220.05	7.60
450.01	225.01	7.90
461.23	230.62	8.27
471.21	235.61	8.69
481.18	240.59	8.99
491.15	245.58	9.30
501.13	250.57	9.60
511.09	255.55	10.09
518.58	259.29	10.76
516.08	258.04	10.88
513.59	256.80	11.00
506.11	253.06	11.25
502.37	251.19	11.31
493.65	246.83	11.55
489.90	244.95	11.73
479.93	239.97	12.09
300.43	150.22	13.25

Table C.6: Test Data for Beam S2-3

Load (kN)	Shear Force (kN)	Mid-span Deflection (mm)
0.00	0.00	0.00
11.23	5.62	0.06
21.19	10.60	0.12
31.16	15.58	0.18
41.14	20.57	0.24
51.10	25.55	0.37
61.10	30.55	0.42
71.10	35.55	0.55
81.00	40.50	0.67
91.00	45.50	0.79
100.97	50.49	0.85
110.95	55.48	1.03
120.92	60.46	1.16
130.89	65.45	1.28
140.86	70.43	1.39
150.84	75.42	1.52
160.81	80.41	1.64
170.78	85.39	1.82
180.75	90.38	1.94
190.75	95.38	2.19
200.70	100.35	2.31
210.70	105.35	2.49
220.60	110.30	2.67
230.60	115.30	2.92
240.60	120.30	3.10
250.60	125.30	3.28
260.53	130.27	3.46
270.50	135.25	3.77
280.50	140.25	4.01
290.45	145.23	4.26
300.43	150.22	4.56
310.40	155.20	4.80
320.40	160.20	4.98
330.34	165.17	5.17
340.32	170.16	5.47
350.29	175.15	5.60
360.26	180.13	5.89

370.23	185.12	6.02
381.45	190.73	6.32
400.15	200.08	6.80
410.13	205.07	7.05
420.10	210.05	7.29
430.10	215.05	7.54
440.04	220.02	7.96
450.02	225.01	8.20
461.23	230.62	8.69
471.21	235.61	9.06
481.18	240.59	9.48
491.15	245.58	9.91
501.13	250.57	10.39
511.10	255.55	11.00
516.10	258.05	11.79
514.84	257.42	11.85
512.34	256.17	11.91
507.36	253.68	12.10
501.13	250.57	12.22
492.40	246.20	12.34
482.43	241.22	12.53
478.69	239.35	14.35
477.44	238.72	15.14
472.45	236.23	16.23
467.47	233.74	16.41
461.23	230.62	17.39
457.50	228.75	17.87
401.40	200.70	18.11
396.40	198.20	18.42
390.18	195.09	18.78
388.93	194.47	19.09
385.19	192.60	19.51
381.45	190.73	19.64
362.76	181.38	19.76
337.80	168.90	20.00
321.62	160.81	20.49
239.35	119.67	20.91

Table C.7: Test Data for Beam S3-1

Load (kN)	Shear Force (kN)	Mid-span Deflection (mm)
0.00	0.00	0.00
9.97	4.99	0.12
21.19	10.60	0.18
29.92	14.96	0.25
41.14	20.57	0.37
51.11	25.56	0.49
62.34	31.17	0.55
71.06	35.53	0.74
81.03	40.52	0.80
91.00	45.50	0.92
100.97	50.49	1.04
112.19	56.10	1.17
120.92	60.46	1.29
130.89	65.45	1.41
140.86	70.43	1.60
150.84	75.42	1.77
160.81	80.41	2.02
170.78	85.39	2.09
180.75	90.38	2.20
191.97	95.99	2.45
200.69	100.35	2.58
210.67	105.34	2.76
220.65	110.32	3.13
231.86	115.93	3.25
240.59	120.30	3.49
250.56	125.28	3.56
261.78	130.89	3.86

270.50	135.25	4.11
281.73	140.87	4.35
291.70	145.85	4.48
301.67	150.84	4.66
311.65	155.83	4.97
320.37	160.19	5.15
330.34	165.17	5.27
341.56	170.78	5.64
350.29	175.15	5.89
361.50	180.75	6.07
372.70	186.35	6.37
380.20	190.10	6.44
390.18	195.09	6.75
400.15	200.08	7.17
410.12	205.06	7.17
421.35	210.68	7.48
431.32	215.66	7.79
440.04	220.02	7.97
450.02	225.01	8.34
460.12	230.06	8.65
471.05	235.53	8.91
480.12	240.06	9.12
491.23	245.62	9.46
501.50	250.75	9.75
511.05	255.53	10.03
520.23	260.12	10.35
523.02	261.51	10.69
521.12	260.56	10.92
519.10	259.55	11.03

Table C.8: Test Data for Beam S3-2

Load (kN)	Shear Force (kN)	Mid-span Deflection (mm)
0.00	0.00	0.00
9.97	4.99	0.13
21.19	10.60	0.31
29.92	14.96	0.31
39.89	19.95	0.49
49.86	24.93	0.55
61.08	30.54	0.80
71.06	35.53	0.92
82.27	41.14	1.04
91.00	45.50	1.17
100.97	50.49	1.35
110.95	55.47	1.41
119.67	59.84	1.59
130.89	65.45	1.78
140.86	70.43	1.90
150.84	75.42	2.15
160.81	80.40	2.15
170.78	85.39	2.33
180.75	90.38	2.45
186.00	93.00	2.70
188.00	94.00	2.80
190.73	95.36	2.94
195.20	97.60	3.00
201.95	100.97	3.13
210.67	105.34	3.25
221.89	110.95	3.50
231.86	115.93	3.74
241.84	120.92	3.99
251.81	125.90	4.17

261.78	130.89	4.42
270.51	135.25	4.54
280.48	140.24	4.91
290.45	145.23	5.03
300.43	150.21	5.27
310.40	155.20	5.40
320.37	160.19	5.70
331.59	165.80	5.95
340.32	170.16	6.01
351.54	175.77	6.38
361.51	180.75	6.68
371.48	185.74	6.87
380.21	190.10	7.11
391.50	195.75	7.41
401.20	200.60	7.70
411.35	205.68	8.05
420.22	210.11	8.32
431.15	215.58	8.61
440.21	220.11	8.90
452.12	226.06	9.21
461.13	230.57	9.52
470.15	235.08	9.85
482.23	241.12	10.12
491.12	245.56	10.41
500.25	250.13	10.70
511.05	255.53	11.05
520.15	260.08	11.32
530.22	265.11	11.64
541.02	270.51	11.91
552.40	276.20	12.20
550.11	275.06	12.25

Table C.9: Test Data for Beam S3-3

Load (kN)	Shear Force (kN)	Mid-span Deflection (mm)
0.00	0.00	0.00
11.22	5.61	0.06
21.19	10.60	0.12
31.16	15.58	0.18
41.14	20.57	0.24
51.11	25.56	0.37
61.08	30.54	0.43
71.06	35.53	0.49
81.03	40.51	0.55
91.00	45.50	0.67
100.97	50.49	0.73
110.95	55.48	0.85
120.92	60.46	0.91
130.89	65.45	1.03
140.86	70.43	1.22
150.84	75.42	1.34
160.81	80.41	1.46
170.78	85.39	1.52
180.75	90.38	1.64
190.73	95.37	1.70
200.70	100.35	1.88
210.67	105.34	2.00
220.64	110.32	2.13
230.62	115.31	2.25
240.59	120.30	2.37
250.56	125.28	2.55
260.53	130.27	2.61
270.51	135.26	2.80
280.48	140.24	2.91
290.45	145.23	3.10
300.43	150.22	3.22
310.40	155.20	3.47
320.37	160.19	3.65
330.34	165.17	3.83
340.31	170.16	4.01
350.29	175.15	4.13
360.26	180.13	4.32
370.23	185.12	4.50
380.21	190.11	4.74
391.43	195.72	4.92
401.37	200.69	5.11
411.37	205.69	5.29
420.10	210.05	5.47
431.32	215.66	5.71

441.29	220.65	5.84
450.02	225.01	6.02
461.23	230.62	6.20
471.20	235.60	6.56
481.18	240.59	6.57
491.15	245.58	6.75
501.13	250.57	6.93
511.09	255.55	7.11
521.07	260.54	7.36
531.04	265.52	7.54
541.02	270.51	7.66
550.99	275.50	7.90
560.96	280.48	8.15
570.94	285.47	8.33
580.91	290.46	8.63
590.88	295.44	8.87
600.85	300.43	9.12
610.83	305.42	9.42
620.80	310.40	9.73
630.77	315.39	9.91
640.74	320.37	10.27
650.71	325.36	10.69
660.68	330.34	11.55
654.46	327.23	11.61
649.47	324.74	11.79
640.74	320.37	12.15
637.00	318.50	12.34
630.77	315.39	12.77
622.04	311.02	13.37
617.06	308.53	13.68
608.33	304.17	13.79

APPENDIX D
SAMPLE OF BEAM ANALYSIS REPORT USING *ShearCalculator*

Beam S1-1

```
*** Data *****
f'c, concrete compressive strength, MPa = 45
Ec, Modulus of Elasticity for concrete, MPa = 29171
f'cr, concrete cracking stress, MPa = 2.21
Rot, shear reinforcement ratio = 0.0010
fsty, yield stress of shear reinforcement, MPa = 597
Es, modulus of elasticity for steel = 200000
b, beam width, mm = 200
D, beam depth, mm = 300
d, effective depth, mm = 259
dv = 0.9d = 233.1
a, shear span, mm = 640
a/d = 2.50
a_ = a -d, mm = 381
N = 0
*****
```

```
#####StartAnalysis#####
```

```
Asl(1) = 220.000000 : fsly(1) = 570.000000 : ys(1) = 35.000000 : ORIENT(1) = T
Asl(2) = 0.000000 : fsly(2) = 0.000000 : ys(2) = 0.000000 : ORIENT(2) = 0
Asl(3) = 900.000000 : fsly(3) = 559.000000 : ys(3) = 259.000000 : ORIENT(3) =
B
Asl_M_V = 900.000000 : fsly_M_V = 559.000000
AslFLEX = 296.664618 : AslSHR = 603.335382 : ROl = 0.012942 : (AslSHR/Asl_M_V)
= 0.670373
Ig = 526925914.038182
lcr = 227718116.418906
Mcr = 14769586.059830
ed(0) = -0.000005 : V(0) = 6799.815323
ed(1) = -0.000030 : V(1) = 40798.792665
ed(2) = -0.000055 : V(2) = 74796.495315
ed(3) = -0.000080 : V(3) = 82198.333392
ed(4) = -0.000105 : V(4) = 90640.184924
ed(5) = -0.000130 : V(5) = 100652.499029
ed(6) = -0.000155 : V(6) = 110576.634292
ed(7) = -0.000180 : V(7) = 114020.494901
ed(8) = -0.000205 : V(8) = 116241.522213
ed(9) = -0.000230 : V(9) = 117679.218290
ed(10) = -0.000255 : V(10) = 118630.731353
ed(11) = -0.000280 : V(11) = 119284.069379
ed(12) = -0.000305 : V(12) = 119842.459524
ed(13) = -0.000330 : V(13) = 120349.972306
ed(14) = -0.000355 : V(14) = 120814.026430
ed(15) = -0.000380 : V(15) = 121240.548726
ed(16) = -0.000405 : V(16) = 121634.347950
ed(17) = -0.000430 : V(17) = 121999.378524
ed(18) = -0.000455 : V(18) = 122338.930943
ed(19) = -0.000480 : V(19) = 122655.771992
ed(20) = -0.000505 : V(20) = 122952.249859
ed(21) = -0.000530 : V(21) = 123230.374173
ed(22) = -0.000555 : V(22) = 123491.877811
ed(23) = -0.000580 : V(23) = 123738.265242
ed(24) = -0.000605 : V(24) = 123970.850775
ed(25) = -0.000630 : V(25) = 124190.789134
```

ed(26) = -0.000655 : V(26) = 124399.100141
ed(27) = -0.000680 : V(27) = 124596.688809
ed(28) = -0.000705 : V(28) = 124784.361843
ed(29) = -0.000730 : V(29) = 124962.841280
ed(30) = -0.000755 : V(30) = 125132.775852
ed(31) = -0.000780 : V(31) = 125294.750505
ed(32) = -0.000805 : V(32) = 125449.294431
ed(33) = -0.000830 : V(33) = 125596.887875
ed(34) = -0.000855 : V(34) = 125737.967933
ed(35) = -0.000880 : V(35) = 125872.933529
ed(36) = -0.000905 : V(36) = 126002.149683
ed(37) = -0.000930 : V(37) = 126125.951215
ed(38) = -0.000955 : V(38) = 126244.645945
ed(39) = -0.000980 : V(39) = 126358.517492
ed(40) = -0.001005 : V(40) = 126467.827715
ed(41) = -0.001030 : V(41) = 126572.818856
ed(42) = -0.001055 : V(42) = 126673.715428
ed(43) = -0.001080 : V(43) = 126770.725882
ed(44) = -0.001105 : V(44) = 126864.044081
ed(45) = -0.001130 : V(45) = 126953.850612
ed(46) = -0.001155 : V(46) = 127040.313951
ed(47) = -0.001180 : V(47) = 127123.591513
ed(48) = -0.001205 : V(48) = 127203.830576
ed(49) = -0.001230 : V(49) = 127281.169123
ed(50) = -0.001255 : V(50) = 127355.736596
ed(51) = -0.001280 : V(51) = 127427.654573
ed(52) = -0.001305 : V(52) = 127497.037382
ed(53) = -0.001330 : V(53) = 127563.992654
ed(54) = -0.001355 : V(54) = 127628.621828
ed(55) = -0.001380 : V(55) = 127691.020608
ed(56) = -0.001405 : V(56) = 127751.279377
ed(57) = -0.001430 : V(57) = 127809.483578
ed(58) = -0.001455 : V(58) = 127865.714058
ed(59) = -0.001480 : V(59) = 127920.047387
ed(60) = -0.001505 : V(60) = 127972.556148
ed(61) = -0.001530 : V(61) = 128023.309198
ed(62) = -0.001555 : V(62) = 128072.371919
ed(63) = -0.001580 : V(63) = 128119.806440
ed(64) = -0.001605 : V(64) = 128165.671842
ed(65) = -0.001630 : V(65) = 128210.024352
ed(66) = -0.001655 : V(66) = 128252.917517
ed(67) = -0.001680 : V(67) = 128294.402371
ed(68) = -0.001705 : V(68) = 128334.527580
ed(69) = -0.001730 : V(69) = 128373.339586
ed(70) = -0.001755 : V(70) = 128410.882736
ed(71) = -0.001780 : V(71) = 128447.199403
ed(72) = -0.001805 : V(72) = 128482.330097
ed(73) = -0.001830 : V(73) = 128516.313569
ed(74) = -0.001855 : V(74) = 128549.186910
ed(75) = -0.001880 : V(75) = 128580.985641
ed(76) = -0.001905 : V(76) = 128611.743796
ed(77) = -0.001930 : V(77) = 128641.494003
ed(78) = -0.001955 : V(78) = 128670.267557
ed(79) = -0.001980 : V(79) = 128698.094489
ed(80) = -0.002005 : V(80) = 128725.003633
ed(81) = -0.002030 : V(81) = 128751.022682
ed(82) = -0.002055 : V(82) = 128776.178251
ed(83) = -0.002080 : V(83) = 128800.495926
ed(84) = -0.002105 : V(84) = 128824.000314
ed(85) = -0.002130 : V(85) = 128807.614508
ed(86) = -0.002155 : V(86) = 128663.477912

ed(87) = -0.002180 : V(87) = 128545.482532
ed(88) = -0.002205 : V(88) = 128498.075866
ed(89) = -0.002230 : V(89) = 128462.970226
ed(90) = -0.002255 : V(90) = 128440.009541
ed(91) = -0.002280 : V(91) = 128429.042823
ed(92) = -0.002305 : V(92) = 128319.314663
ed(93) = -0.002330 : V(93) = 128172.465328
ed(94) = -0.002355 : V(94) = 128013.260375
ed(95) = -0.002380 : V(95) = 127841.873135
ed(96) = -0.002405 : V(96) = 127658.490016
ed(97) = -0.002430 : V(97) = 127463.309778
ed(98) = -0.002455 : V(98) = 127256.542760
ed(99) = -0.002480 : V(99) = 127038.410072
ed(100) = -0.002505 : V(100) = 126809.142748
ed(101) = -0.002530 : V(101) = 126568.980885
ed(102) = -0.002555 : V(102) = 126318.172760
ed(103) = -0.002580 : V(103) = 126056.973943
ed(104) = -0.002605 : V(104) = 125785.646405
ed(105) = -0.002630 : V(105) = 125504.457637
ed(106) = -0.002655 : V(106) = 125213.679773
ed(107) = -0.002680 : V(107) = 124913.588742
ed(108) = -0.002705 : V(108) = 124604.463427
ed(109) = -0.002730 : V(109) = 124286.584866
ed(110) = -0.002755 : V(110) = 123960.235471
ed(111) = -0.002780 : V(111) = 123625.698293
ed(112) = -0.002805 : V(112) = 123283.256311
ed(113) = -0.002830 : V(113) = 122933.191774
ed(114) = -0.002855 : V(114) = 122575.785569
ed(115) = -0.002880 : V(115) = 122211.316644
ed(116) = -0.002905 : V(116) = 121840.061463
ed(117) = -0.002930 : V(117) = 121462.293511
ed(118) = -0.002955 : V(118) = 121078.282839
ed(119) = -0.002980 : V(119) = 120688.295648
ed(120) = -0.003005 : V(120) = 120292.593920
ed(121) = -0.003030 : V(121) = 119891.435087
ed(122) = -0.003055 : V(122) = 119485.071735
ed(123) = -0.003080 : V(123) = 119073.751351
ed(124) = -0.003105 : V(124) = 118657.716105
ed(125) = -0.003130 : V(125) = 118237.202661
ed(126) = -0.003155 : V(126) = 117812.442027
ed(127) = -0.003180 : V(127) = 117383.659430
ed(128) = -0.003205 : V(128) = 116951.074224
ed(129) = -0.003230 : V(129) = 116514.899819
ed(130) = -0.003255 : V(130) = 116075.343636
ed(131) = -0.003280 : V(131) = 115632.607091
ed(132) = -0.003305 : V(132) = 115186.885589
ed(133) = -0.003330 : V(133) = 114738.368543
ed(134) = -0.003355 : V(134) = 114287.239411
ed(135) = -0.003380 : V(135) = 113833.675742
ed(136) = -0.003405 : V(136) = 113377.849245
ed(137) = -0.003430 : V(137) = 112919.925858
ed(138) = -0.003455 : V(138) = 112460.065841
ed(139) = -0.003480 : V(139) = 111998.423866
ed(140) = -0.003505 : V(140) = 111535.149126
Vmaxcyc1 = 84
ed(0) = -0.000005 : V(0) = 6799.815323
ed(1) = -0.000030 : V(1) = 40798.792665
ed(2) = -0.000055 : V(2) = 74796.495315
ed(3) = -0.000080 : V(3) = 82198.333392
ed(4) = -0.000105 : V(4) = 90640.184924
ed(5) = -0.000130 : V(5) = 100652.499029

ed(6) = -0.000155 : V(6) = 110576.634292
ed(7) = -0.000180 : V(7) = 114020.494901
ed(8) = -0.000205 : V(8) = 116241.522213
ed(9) = -0.000230 : V(9) = 117679.218290
ed(10) = -0.000255 : V(10) = 118630.731353
ed(11) = -0.000280 : V(11) = 119284.069379
ed(12) = -0.000305 : V(12) = 119842.459524
ed(13) = -0.000330 : V(13) = 120349.972306
ed(14) = -0.000355 : V(14) = 120814.026430
ed(15) = -0.000380 : V(15) = 121240.548726
ed(16) = -0.000405 : V(16) = 121634.347950
ed(17) = -0.000430 : V(17) = 121999.378524
ed(18) = -0.000455 : V(18) = 122338.930943
ed(19) = -0.000480 : V(19) = 122655.771992
ed(20) = -0.000505 : V(20) = 122952.249859
ed(21) = -0.000530 : V(21) = 123230.374173
ed(22) = -0.000555 : V(22) = 123491.877811
ed(23) = -0.000580 : V(23) = 123738.265242
ed(24) = -0.000605 : V(24) = 123970.850775
ed(25) = -0.000630 : V(25) = 124190.789134
ed(26) = -0.000655 : V(26) = 124399.100141
ed(27) = -0.000680 : V(27) = 124596.688809
ed(28) = -0.000705 : V(28) = 124784.361843
ed(29) = -0.000730 : V(29) = 124962.841280
ed(30) = -0.000755 : V(30) = 125132.775852
ed(31) = -0.000780 : V(31) = 125294.750505
ed(32) = -0.000805 : V(32) = 125449.294431
ed(33) = -0.000830 : V(33) = 125596.887875
ed(34) = -0.000855 : V(34) = 125737.967933
ed(35) = -0.000880 : V(35) = 125872.933529
ed(36) = -0.000905 : V(36) = 126002.149683
ed(37) = -0.000930 : V(37) = 126125.951215
ed(38) = -0.000955 : V(38) = 126244.645945
ed(39) = -0.000980 : V(39) = 126358.517492
ed(40) = -0.001005 : V(40) = 126467.827715
ed(41) = -0.001030 : V(41) = 126572.818856
ed(42) = -0.001055 : V(42) = 126673.715428
ed(43) = -0.001080 : V(43) = 126770.725882
ed(44) = -0.001105 : V(44) = 126864.044081
ed(45) = -0.001130 : V(45) = 126953.850612
ed(46) = -0.001155 : V(46) = 127040.313951
ed(47) = -0.001180 : V(47) = 127123.591513
ed(48) = -0.001205 : V(48) = 127203.830576
ed(49) = -0.001230 : V(49) = 127281.169123
ed(50) = -0.001255 : V(50) = 127355.736596
ed(51) = -0.001280 : V(51) = 127427.654573
ed(52) = -0.001305 : V(52) = 127497.037382
ed(53) = -0.001330 : V(53) = 127563.992654
ed(54) = -0.001355 : V(54) = 127628.621828
ed(55) = -0.001380 : V(55) = 127691.020608
ed(56) = -0.001405 : V(56) = 127751.279377
ed(57) = -0.001430 : V(57) = 127809.483578
ed(58) = -0.001455 : V(58) = 127865.714058
ed(59) = -0.001480 : V(59) = 127920.047387
ed(60) = -0.001505 : V(60) = 127972.556148
ed(61) = -0.001530 : V(61) = 128023.309198
ed(62) = -0.001555 : V(62) = 128072.371919
ed(63) = -0.001580 : V(63) = 128119.806440
ed(64) = -0.001605 : V(64) = 128165.671842
ed(65) = -0.001630 : V(65) = 128210.024352
ed(66) = -0.001655 : V(66) = 128252.917517

ed(67) = -0.001680 : V(67) = 128294.402371
ed(68) = -0.001705 : V(68) = 128334.527580
ed(69) = -0.001730 : V(69) = 128373.339586
ed(70) = -0.001755 : V(70) = 128410.882736
ed(71) = -0.001780 : V(71) = 128447.199403
ed(72) = -0.001805 : V(72) = 128482.330097
ed(73) = -0.001830 : V(73) = 128516.313569
ed(74) = -0.001855 : V(74) = 128549.186910
ed(75) = -0.001880 : V(75) = 128580.985641
ed(76) = -0.001905 : V(76) = 128611.743796
ed(77) = -0.001930 : V(77) = 128641.494003
ed(78) = -0.001955 : V(78) = 128670.267557
ed(79) = -0.001980 : V(79) = 128698.094489
ed(80) = -0.002005 : V(80) = 128725.003633
ed(81) = -0.002030 : V(81) = 128751.022682
ed(82) = -0.002055 : V(82) = 128776.178251
ed(83) = -0.002080 : V(83) = 128800.495926
ed(84) = -0.002085 : V(84) = 128805.261095
ed(85) = -0.002090 : V(85) = 128809.993929
ed(86) = -0.002095 : V(86) = 128814.694617
ed(87) = -0.002100 : V(87) = 128819.363350
ed(88) = -0.002105 : V(88) = 128824.000314
ed(89) = -0.002110 : V(89) = 128828.605697
ed(90) = -0.002115 : V(90) = 128833.179684
ed(91) = -0.002120 : V(91) = 128837.722458
ed(92) = -0.002125 : V(92) = 128836.702030
ed(90) = -0.002111 : V(90) = 128829.064506
ed(91) = -0.002111 : V(91) = 128829.523000
ed(92) = -0.002112 : V(92) = 128829.981181
ed(93) = -0.002112 : V(93) = 128830.439049
ed(94) = -0.002113 : V(94) = 128830.896604
ed(95) = -0.002113 : V(95) = 128831.353845
ed(96) = -0.002114 : V(96) = 128831.810774
ed(97) = -0.002114 : V(97) = 128832.267389
ed(98) = -0.002115 : V(98) = 128832.723693
ed(99) = -0.002115 : V(99) = 128833.179684
ed(100) = -0.002116 : V(100) = 128833.635363
ed(101) = -0.002116 : V(101) = 128834.090730
ed(102) = -0.002117 : V(102) = 128834.545785
ed(103) = -0.002117 : V(103) = 128835.000529
ed(104) = -0.002118 : V(104) = 128835.454961
ed(105) = -0.002118 : V(105) = 128835.909082
ed(106) = -0.002119 : V(106) = 128836.362892
ed(107) = -0.002119 : V(107) = 128836.816391
ed(108) = -0.002120 : V(108) = 128837.269580
ed(109) = -0.002120 : V(109) = 128837.722458
ed(110) = -0.002121 : V(110) = 128838.175026
ed(111) = -0.002121 : V(111) = 128838.627283
ed(112) = -0.002122 : V(112) = 128839.079231
ed(113) = -0.002122 : V(113) = 128839.530869
ed(114) = -0.002123 : V(114) = 128839.982197
ed(115) = -0.002123 : V(115) = 128840.433216
ed(116) = -0.002124 : V(116) = 128840.883926
ed(117) = -0.002124 : V(117) = 128841.334327
ed(118) = -0.002125 : V(118) = 128839.615603
ed(119) = -0.002375 : V(119) = 127880.614275
ed(120) = -0.002625 : V(120) = 125567.151470
ed(121) = -0.002875 : V(121) = 122292.091672
ed(122) = -0.003125 : V(122) = 118330.087999
ed(123) = -0.003375 : V(123) = 113933.659801
ed(124) = -0.003625 : V(124) = 109302.477512

```

Vmaxcycl = 117
CYCLE = 0 : No. of loops for er = 3
ed(0) = -0.000005 : er(0) = 0.000005 : el(0) = -0.000000 : et(0) = -0.000000
Xi(0) = 0.449590 : Sd(0) = -0.145856 : Sr(0) = 0.145856 : Sl(0) = 0.000000 :
St(0) = 0.000000
Slc(0) = 0.000000 : Stc(0) = 0.000000
fst(0) = -0.000000 : fsl(0) = -0.000000
ALPHA(0) = 45.000000degs : vlt(0) = 0.145856 : glt(0) = 0.000010 : V(0) =
6799.815323
*** Shear web in UNCRACKED state (er < ecr) ***
*** Shear r/f in ELASTIC state (fst < fsty) ***
*** Smeared long r/f in ELASTIC state (fsl < fsly_M_V) ***
Ie(0) = 526925914.038182 : dflex(0) = 0.080557 : dshear(0) = 0.003200 : dmax(0)
= 0.083757
esl(0) = 0.000017 : Curv(0) = 0.000000
*** Flexural cracking has NOT occurred (M < Mcr) ***
CYCLE = 1 : No. of loops for er = 4
ed(1) = -0.000030 : er(1) = 0.000030 : el(1) = -0.000000 : et(1) = -0.000000
Xi(1) = 0.449590 : Sd(1) = -0.875135 : Sr(1) = 0.875135 : Sl(1) = 0.000000 :
St(1) = 0.000000
Slc(1) = 0.000000 : Stc(1) = 0.000000
fst(1) = -0.000007 : fsl(1) = -0.000007
ALPHA(1) = 45.000001degs : vlt(1) = 0.875135 : glt(1) = 0.000060 : V(1) =
40798.792665
*** Shear web in UNCRACKED state (er < ecr) ***
*** Shear r/f in ELASTIC state (fst < fsty) ***
*** Smeared long r/f in ELASTIC state (fsl < fsly_M_V) ***
Ie(1) = 281867812.353019 : dflex(1) = 0.903566 : dshear(1) = 0.019200 : dmax(1)
= 0.922766
esl(1) = 0.000308 : Curv(1) = 0.000002
*** Flexural cracking has occurred (M >= Mcr) ***
CYCLE = 2 : No. of loops for er = 4
ed(2) = -0.000055 : er(2) = 0.000055 : el(2) = -0.000000 : et(2) = -0.000000
Xi(2) = 0.449590 : Sd(2) = -1.604386 : Sr(2) = 1.604387 : Sl(2) = 0.000000 :
St(2) = 0.000000
Slc(2) = 0.000001 : Stc(2) = 0.000000
fst(2) = -0.000110 : fsl(2) = -0.000102
ALPHA(2) = 45.000011degs : vlt(2) = 1.604386 : glt(2) = 0.000110 : V(2) =
74796.495315
*** Shear web in UNCRACKED state (er < ecr) ***
*** Shear r/f in ELASTIC state (fst < fsty) ***
*** Smeared long r/f in ELASTIC state (fsl < fsly_M_V) ***
Ie(2) = 236506200.630465 : dflex(2) = 1.974227 : dshear(2) = 0.035200 : dmax(2)
= 2.009426
esl(2) = 0.000672 : Curv(2) = 0.000004
*** Flexural cracking has occurred (M >= Mcr) ***
CYCLE = 3 : No. of loops for er = 207
ed(3) = -0.000080 : er(3) = 0.001046 : el(3) = 0.000358 : et(3) = 0.000608
Xi(3) = 0.233013 : Sd(3) = -2.332052 : Sr(3) = 1.284782 : Sl(3) = 0.000000 :
St(3) = 0.000000
Slc(3) = -0.925694 : Stc(3) = -0.121576
fst(3) = 121.575545 : fsl(3) = 71.528823
ALPHA(3) = 38.577135degs : vlt(3) = 1.763156 : glt(3) = 0.001097 : V(3) =
82198.333392
*** Shear web in CRACKED state (er >= ecr) ***
*** Shear r/f in ELASTIC state (fst < fsty) ***
*** Smeared long r/f in ELASTIC state (fsl < fsly_M_V) ***
Ie(3) = 234339502.633250 : dflex(3) = 2.189655 : dshear(3) = 0.351153 : dmax(3)
= 2.540808
esl(3) = 0.000746 : Curv(3) = 0.000005
*** Flexural cracking has occurred (M >= Mcr) ***

```

CYCLE = 4 : No. of loops for er = 131
 ed(4) = -0.000105 : er(4) = 0.002173 : el(4) = 0.000649 : et(4) = 0.001419
 Xi(4) = 0.172864 : Sd(4) = -3.047595 : Sr(4) = 1.083923 : Sl(4) = 0.000000 :
 St(4) = 0.000000
 Slc(4) = -1.679916 : Stc(4) = -0.283756
 fst(4) = 283.756040 : fsl(4) = 129.807837
 ALPHA(4) = 35.124629degs : vlt(4) = 1.944234 : glt(4) = 0.002144 : V(4) =
 90640.184924
 *** Shear web in CRACKED state (er >= ecr) ***
 *** Shear r/f in ELASTIC state (fst < fsty) ***
 *** Smeared long r/f in ELASTIC state (fsl < fsly_M_V) ***
 Ie(4) = 232656395.249761 : dflex(4) = 2.432003 : dshear(4) = 0.686022 : dmax(4)
 = 3.118025
 esl(4) = 0.000828 : Curv(4) = 0.000005
 *** Flexural cracking has occurred (M >= Mcr) ***
 CYCLE = 5 : No. of loops for er = 107
 ed(5) = -0.000130 : er(5) = 0.003259 : el(5) = 0.000893 : et(5) = 0.002236
 Xi(5) = 0.151771 : Sd(5) = -3.730676 : Sr(5) = 0.972427 : Sl(5) = 0.000000 :
 St(5) = 0.000000
 Slc(5) = -2.311070 : Stc(5) = -0.447180
 fst(5) = 447.179754 : fsl(5) = 178.577394
 ALPHA(5) = 33.326130degs : vlt(5) = 2.158998 : glt(5) = 0.003111 : V(5) =
 100652.499029
 *** Shear web in CRACKED state (er >= ecr) ***
 *** Shear r/f in ELASTIC state (fst < fsty) ***
 *** Smeared long r/f in ELASTIC state (fsl < fsly_M_V) ***
 Ie(5) = 231324436.500272 : dflex(5) = 2.716197 : dshear(5) = 0.995616 : dmax(5)
 = 3.711813
 esl(5) = 0.000925 : Curv(5) = 0.000006
 *** Flexural cracking has occurred (M >= Mcr) ***
 CYCLE = 6 : No. of loops for er = 141
 ed(6) = -0.000155 : er(6) = 0.004270 : el(6) = 0.001105 : et(6) = 0.003010
 Xi(6) = 0.142196 : Sd(6) = -4.356465 : Sr(6) = 0.899429 : Sl(6) = 0.000000 :
 St(6) = 0.000000
 Slc(6) = -2.860036 : Stc(6) = -0.597000
 fst(6) = 597.000000 : fsl(6) = 220.996267
 ALPHA(6) = 32.248097degs : vlt(6) = 2.371871 : glt(6) = 0.003994 : V(6) =
 110576.634292
 *** Shear web in CRACKED state (er >= ecr) ***
 *** Shear r/f in PLASTIC state (fst >= fsty) ***
 *** Smeared long r/f in ELASTIC state (fsl < fsly_M_V) ***
 Ie(6) = 230437984.598305 : dflex(6) = 2.995488 : dshear(6) = 1.278142 : dmax(6)
 = 4.273630
 esl(6) = 0.001020 : Curv(6) = 0.000006
 *** Flexural cracking has occurred (M >= Mcr) ***
 CYCLE = 7 : No. of loops for er = 124
 ed(7) = -0.000180 : er(7) = 0.005750 : el(7) = 0.001312 : et(7) = 0.004258
 Xi(7) = 0.128237 : Sd(7) = -4.814652 : Sr(7) = 0.821243 : Sl(7) = 0.000000 :
 St(7) = 0.000000
 Slc(7) = -3.396409 : Stc(7) = -0.597000
 fst(7) = 597.000000 : fsl(7) = 262.442056
 ALPHA(7) = 30.108692degs : vlt(7) = 2.445742 : glt(7) = 0.005147 : V(7) =
 114020.494901
 *** Shear web in CRACKED state (er >= ecr) ***
 *** Shear r/f in PLASTIC state (fst >= fsty) ***
 *** Smeared long r/f in ELASTIC state (fsl < fsly_M_V) ***
 Ie(7) = 230198901.785787 : dflex(7) = 3.091989 : dshear(7) = 1.646911 : dmax(7)
 = 4.738900
 esl(7) = 0.001053 : Curv(7) = 0.000006
 *** Flexural cracking has occurred (M >= Mcr) ***
 CYCLE = 8 : No. of loops for er = 102

```

ed(8) = -0.000205 : er(8) = 0.006957 : el(8) = 0.001455 : et(8) = 0.005297
Xi(8) = 0.122876 : Sd(8) = -5.136081 : Sr(8) = 0.772652 : Sl(8) = 0.000000 :
St(8) = 0.000000
Slc(8) = -3.766430 : Stc(8) = -0.597000
fst(8) = 597.000000 : fsl(8) = 291.033734
ALPHA(8) = 28.780631degs : vlt(8) = 2.493383 : glt(8) = 0.006045 : V(8) =
116241.522213
*** Shear web in CRACKED state (er >= ecr) ***
*** Shear r/f in PLASTIC state (fst >= fsty) ***
*** Smeared long r/f in ELASTIC state (fsl < fsly_M_V) ***
Ie(8) = 230059400.385647 : dflex(8) = 3.154130 : dshear(8) = 1.934243 : dmax(8)
= 5.088373
esl(8) = 0.001074 : Curv(8) = 0.000007
*** Flexural cracking has occurred (M >= Mcr) ***
CYCLE = 9 : No. of loops for er = 85
ed(9) = -0.000230 : er(9) = 0.007903 : el(9) = 0.001554 : et(9) = 0.006120
Xi(9) = 0.121797 : Sd(9) = -5.359469 : Sr(9) = 0.740897 : Sl(9) = 0.000000 :
St(9) = 0.000000
Slc(9) = -4.021572 : Stc(9) = -0.597000
fst(9) = 597.000000 : fsl(9) = 310.748681
ALPHA(9) = 27.924652degs : vlt(9) = 2.524222 : glt(9) = 0.006731 : V(9) =
117679.218290
*** Shear web in CRACKED state (er >= ecr) ***
*** Shear r/f in PLASTIC state (fst >= fsty) ***
*** Smeared long r/f in ELASTIC state (fsl < fsly_M_V) ***
Ie(9) = 229974633.535374 : dflex(9) = 3.194318 : dshear(9) = 2.153858 : dmax(9)
= 5.348176
esl(9) = 0.001088 : Curv(9) = 0.000007
*** Flexural cracking has occurred (M >= Mcr) ***
CYCLE = 10 : No. of loops for er = 74
ed(10) = -0.000255 : er(10) = 0.008648 : el(10) = 0.001623 : et(10) = 0.006770
Xi(10) = 0.122935 : Sd(10) = -5.517804 : Sr(10) = 0.718872 : Sl(10) =
0.000000 : St(10) = 0.000000
Slc(10) = -4.201932 : Stc(10) = -0.597000
fst(10) = 597.000000 : fsl(10) = 324.685171
ALPHA(10) = 27.344256degs : vlt(10) = 2.544632 : glt(10) = 0.007265 : V(10) =
118630.731353
*** Shear web in CRACKED state (er >= ecr) ***
*** Shear r/f in PLASTIC state (fst >= fsty) ***
*** Smeared long r/f in ELASTIC state (fsl < fsly_M_V) ***
Ie(10) = 229920770.677855 : dflex(10) = 3.220900 : dshear(10) = 2.324798 :
dmax(10) = 5.545698
esl(10) = 0.001097 : Curv(10) = 0.000007
*** Flexural cracking has occurred (M >= Mcr) ***
CYCLE = 11 : No. of loops for er = 69
ed(11) = -0.000280 : er(11) = 0.009252 : el(11) = 0.001675 : et(11) = 0.007298
Xi(11) = 0.125212 : Sd(11) = -5.634551 : Sr(11) = 0.702574 : Sl(11) =
0.000000 : St(11) = 0.000000
Slc(11) = -4.334978 : Stc(11) = -0.597000
fst(11) = 597.000000 : fsl(11) = 334.965692
ALPHA(11) = 26.926681degs : vlt(11) = 2.558646 : glt(11) = 0.007697 : V(11) =
119284.069379
*** Shear web in CRACKED state (er >= ecr) ***
*** Shear r/f in PLASTIC state (fst >= fsty) ***
*** Smeared long r/f in ELASTIC state (fsl < fsly_M_V) ***
Ie(11) = 229884775.675598 : dflex(11) = 3.239146 : dshear(11) = 2.463190 :
dmax(11) = 5.702336
esl(11) = 0.001103 : Curv(11) = 0.000007
*** Flexural cracking has occurred (M >= Mcr) ***
CYCLE = 12 : No. of loops for er = 70
ed(12) = -0.000305 : er(12) = 0.009821 : el(12) = 0.001720 : et(12) = 0.007796

```

```

Xi(12) = 0.127514 : Sd(12) = -5.738131 : Sr(12) = 0.688341 : Sl(12) =
0.000000 : St(12) = 0.000000
Slc(12) = -4.452791 : Stc(12) = -0.597000
fst(12) = 597.000000 : fsl(12) = 344.069159
ALPHA(12) = 26.565566degs : vlt(12) = 2.570623 : glt(12) = 0.008101 : V(12) =
119842.459524
*** Shear web in CRACKED state (er >= ecr) ***
*** Shear r/f in PLASTIC state (fst >= fsty) ***
*** Smeared long r/f in ELASTIC state (fsl < fsly_M_V) ***
Ie(12) = 229854630.779391 : dflex(12) = 3.254736 : dshear(12) = 2.592384 :
dmax(12) = 5.847120
esl(12) = 0.001109 : Curv(12) = 0.000007
*** Flexural cracking has occurred (M >= Mcr) ***
CYCLE = 13 : No. of loops for er = 72
ed(13) = -0.000330 : er(13) = 0.010377 : el(13) = 0.001763 : et(13) = 0.008285
Xi(13) = 0.129660 : Sd(13) = -5.834691 : Sr(13) = 0.675353 : Sl(13) =
0.000000 : St(13) = 0.000000
Slc(13) = -4.562338 : Stc(13) = -0.597000
fst(13) = 597.000000 : fsl(13) = 352.533969
ALPHA(13) = 26.237381degs : vlt(13) = 2.581509 : glt(13) = 0.008492 : V(13) =
120349.972306
*** Shear web in CRACKED state (er >= ecr) ***
*** Shear r/f in PLASTIC state (fst >= fsty) ***
*** Smeared long r/f in ELASTIC state (fsl < fsly_M_V) ***
Ie(13) = 229827715.718580 : dflex(13) = 3.268902 : dshear(13) = 2.717358 :
dmax(13) = 5.986260
esl(13) = 0.001113 : Curv(13) = 0.000007
*** Flexural cracking has occurred (M >= Mcr) ***
CYCLE = 14 : No. of loops for er = 74
ed(14) = -0.000355 : er(14) = 0.010921 : el(14) = 0.001802 : et(14) = 0.008764
Xi(14) = 0.131670 : Sd(14) = -5.925131 : Sr(14) = 0.663420 : Sl(14) =
0.000000 : St(14) = 0.000000
Slc(14) = -4.664711 : Stc(14) = -0.597000
fst(14) = 597.000000 : fsl(14) = 360.444327
ALPHA(14) = 25.937076degs : vlt(14) = 2.591463 : glt(14) = 0.008871 : V(14) =
120814.026430
*** Shear web in CRACKED state (er >= ecr) ***
*** Shear r/f in PLASTIC state (fst >= fsty) ***
*** Smeared long r/f in ELASTIC state (fsl < fsly_M_V) ***
Ie(14) = 229803499.669679 : dflex(14) = 3.281852 : dshear(14) = 2.838602 :
dmax(14) = 6.120454
esl(14) = 0.001118 : Curv(14) = 0.000007
*** Flexural cracking has occurred (M >= Mcr) ***
CYCLE = 15 : No. of loops for er = 75
ed(15) = -0.000380 : er(15) = 0.011455 : el(15) = 0.001839 : et(15) = 0.009236
Xi(15) = 0.133560 : Sd(15) = -6.010182 : Sr(15) = 0.652392 : Sl(15) =
0.000000 : St(15) = 0.000000
Slc(15) = -4.760790 : Stc(15) = -0.597000
fst(15) = 597.000000 : fsl(15) = 367.868419
ALPHA(15) = 25.660660degs : vlt(15) = 2.600612 : glt(15) = 0.009239 : V(15) =
121240.548726
*** Shear web in CRACKED state (er >= ecr) ***
*** Shear r/f in PLASTIC state (fst >= fsty) ***
*** Smeared long r/f in ELASTIC state (fsl < fsly_M_V) ***
Ie(15) = 229781567.972291 : dflex(15) = 3.293753 : dshear(15) = 2.956523 :
dmax(15) = 6.250275
esl(15) = 0.001122 : Curv(15) = 0.000007
*** Flexural cracking has occurred (M >= Mcr) ***
CYCLE = 16 : No. of loops for er = 77
ed(16) = -0.000405 : er(16) = 0.011979 : el(16) = 0.001874 : et(16) = 0.009700

```

Xi(16) = 0.135343 : Sd(16) = -6.090449 : Sr(16) = 0.642147 : Sl(16) =
 0.000000 : St(16) = 0.000000
 Slc(16) = -4.851302 : Stc(16) = -0.597000
 fst(16) = 597.000000 : fsl(16) = 374.862289
 ALPHA(16) = 25.404920degs : vlt(16) = 2.609059 : glt(16) = 0.009598 : V(16) =
 121634.347950
 *** Shear web in CRACKED state (er >= ecr) ***
 *** Shear r/f in PLASTIC state (fst >= fsty) ***
 *** Smeared long r/f in ELASTIC state (fsl < fsly_M_V) ***
 Ie(16) = 229761591.107045 : dflex(16) = 3.304738 : dshear(16) = 3.071459 :
 dmax(16) = 6.376198
 esl(16) = 0.001126 : Curv(16) = 0.000007
 *** Flexural cracking has occurred (M >= Mcr) ***
 CYCLE = 17 : No. of loops for er = 78
 ed(17) = -0.000430 : er(17) = 0.012494 : el(17) = 0.001907 : et(17) = 0.010157
 Xi(17) = 0.137032 : Sd(17) = -6.166437 : Sr(17) = 0.632587 : Sl(17) =
 0.000000 : St(17) = 0.000000
 Slc(17) = -4.936849 : Stc(17) = -0.597000
 fst(17) = 597.000000 : fsl(17) = 381.472600
 ALPHA(17) = 25.167238degs : vlt(17) = 2.616889 : glt(17) = 0.009949 : V(17) =
 121999.378524
 *** Shear web in CRACKED state (er >= ecr) ***
 *** Shear r/f in PLASTIC state (fst >= fsty) ***
 *** Smeared long r/f in ELASTIC state (fsl < fsly_M_V) ***
 Ie(17) = 229743303.282190 : dflex(17) = 3.314920 : dshear(17) = 3.183700 :
 dmax(17) = 6.498619
 esl(17) = 0.001129 : Curv(17) = 0.000007
 *** Flexural cracking has occurred (M >= Mcr) ***
 CYCLE = 18 : No. of loops for er = 79
 ed(18) = -0.000455 : er(18) = 0.013002 : el(18) = 0.001939 : et(18) = 0.010608
 Xi(18) = 0.138635 : Sd(18) = -6.238573 : Sr(18) = 0.623632 : Sl(18) =
 0.000000 : St(18) = 0.000000
 Slc(18) = -5.017942 : Stc(18) = -0.597000
 fst(18) = 597.000000 : fsl(18) = 387.738641
 ALPHA(18) = 24.945451degs : vlt(18) = 2.624173 : glt(18) = 0.010292 : V(18) =
 122338.930943
 *** Shear web in CRACKED state (er >= ecr) ***
 *** Shear r/f in PLASTIC state (fst >= fsty) ***
 *** Smeared long r/f in ELASTIC state (fsl < fsly_M_V) ***
 Ie(18) = 229726487.287595 : dflex(18) = 3.324389 : dshear(18) = 3.293489 :
 dmax(18) = 6.617879
 esl(18) = 0.001132 : Curv(18) = 0.000007
 *** Flexural cracking has occurred (M >= Mcr) ***
 CYCLE = 19 : No. of loops for er = 81
 ed(19) = -0.000480 : er(19) = 0.013502 : el(19) = 0.001968 : et(19) = 0.011054
 Xi(19) = 0.140161 : Sd(19) = -6.307223 : Sr(19) = 0.615212 : Sl(19) =
 0.000000 : St(19) = 0.000000
 Slc(19) = -5.095011 : Stc(19) = -0.597000
 fst(19) = 597.000000 : fsl(19) = 393.693825
 ALPHA(19) = 24.737754degs : vlt(19) = 2.630969 : glt(19) = 0.010628 : V(19) =
 122655.771992
 *** Shear web in CRACKED state (er >= ecr) ***
 *** Shear r/f in PLASTIC state (fst >= fsty) ***
 *** Smeared long r/f in ELASTIC state (fsl < fsly_M_V) ***
 Ie(19) = 229710963.550489 : dflex(19) = 3.333224 : dshear(19) = 3.401041 :
 dmax(19) = 6.734266
 esl(19) = 0.001135 : Curv(19) = 0.000007
 *** Flexural cracking has occurred (M >= Mcr) ***
 CYCLE = 20 : No. of loops for er = 81
 ed(20) = -0.000505 : er(20) = 0.013996 : el(20) = 0.001997 : et(20) = 0.011494

```

Xi(20) = 0.141616 : Sd(20) = -6.372699 : Sr(20) = 0.607270 : Sl(20) =
0.000000 : St(20) = 0.000000
Slc(20) = -5.168428 : Stc(20) = -0.597000
fst(20) = 597.000000 : fsl(20) = 399.366822
ALPHA(20) = 24.542625degs : vlt(20) = 2.637328 : glt(20) = 0.010958 : V(20) =
122952.249859
*** Shear web in CRACKED state (er >= ecr) ***
*** Shear r/f in PLASTIC state (fst >= fsty) ***
*** Smeared long r/f in ELASTIC state (fsl < fsly_M_V) ***
Ie(20) = 229696582.076762 : dflex(20) = 3.341490 : dshear(20) = 3.506540 :
dmax(20) = 6.848030
esl(20) = 0.001138 : Curv(20) = 0.000007
*** Flexural cracking has occurred (M >= Mcr) ***
CYCLE = 21 : No. of loops for er = 83
ed(21) = -0.000530 : er(21) = 0.014483 : el(21) = 0.002024 : et(21) = 0.011929
Xi(21) = 0.143006 : Sd(21) = -6.435273 : Sr(21) = 0.599759 : Sl(21) =
0.000000 : St(21) = 0.000000
Slc(21) = -5.238515 : Stc(21) = -0.597000
fst(21) = 597.000000 : fsl(21) = 404.782429
ALPHA(21) = 24.358769degs : vlt(21) = 2.643294 : glt(21) = 0.011282 : V(21) =
123230.374173
*** Shear web in CRACKED state (er >= ecr) ***
*** Shear r/f in PLASTIC state (fst >= fsty) ***
*** Smeared long r/f in ELASTIC state (fsl < fsly_M_V) ***
Ie(21) = 229683216.416659 : dflex(21) = 3.349244 : dshear(21) = 3.610147 :
dmax(21) = 6.959391
esl(21) = 0.001141 : Curv(21) = 0.000007
*** Flexural cracking has occurred (M >= Mcr) ***
CYCLE = 22 : No. of loops for er = 84
ed(22) = -0.000555 : er(22) = 0.014964 : el(22) = 0.002050 : et(22) = 0.012360
Xi(22) = 0.144337 : Sd(22) = -6.495185 : Sr(22) = 0.592635 : Sl(22) =
0.000000 : St(22) = 0.000000
Slc(22) = -5.305550 : Stc(22) = -0.597000
fst(22) = 597.000000 : fsl(22) = 409.962243
ALPHA(22) = 24.185079degs : vlt(22) = 2.648903 : glt(22) = 0.011600 : V(22) =
123491.877811
*** Shear web in CRACKED state (er >= ecr) ***
*** Shear r/f in PLASTIC state (fst >= fsty) ***
*** Smeared long r/f in ELASTIC state (fsl < fsly_M_V) ***
Ie(22) = 229670759.077945 : dflex(22) = 3.356533 : dshear(22) = 3.712005 :
dmax(22) = 7.068538
esl(22) = 0.001143 : Curv(22) = 0.000007
*** Flexural cracking has occurred (M >= Mcr) ***
CYCLE = 23 : No. of loops for er = 85
ed(23) = -0.000580 : er(23) = 0.015440 : el(23) = 0.002075 : et(23) = 0.012786
Xi(23) = 0.145614 : Sd(23) = -6.552642 : Sr(23) = 0.585864 : Sl(23) =
0.000000 : St(23) = 0.000000
Slc(23) = -5.369778 : Stc(23) = -0.597000
fst(23) = 597.000000 : fsl(23) = 414.925200
ALPHA(23) = 24.020596degs : vlt(23) = 2.654188 : glt(23) = 0.011913 : V(23) =
123738.265242
*** Shear web in CRACKED state (er >= ecr) ***
*** Shear r/f in PLASTIC state (fst >= fsty) ***
*** Smeared long r/f in ELASTIC state (fsl < fsly_M_V) ***
Ie(23) = 229659117.991860 : dflex(23) = 3.363401 : dshear(23) = 3.812239 :
dmax(23) = 7.175640
esl(23) = 0.001146 : Curv(23) = 0.000007
*** Flexural cracking has occurred (M >= Mcr) ***
CYCLE = 24 : No. of loops for er = 87
ed(24) = -0.000605 : er(24) = 0.015912 : el(24) = 0.002098 : et(24) = 0.013208

```



```

Xi(24) = 0.146841 : Sd(24) = -6.607830 : Sr(24) = 0.579414 : Sl(24) =
0.000000 : St(24) = 0.000000
Slc(24) = -5.431416 : Stc(24) = -0.597000
fst(24) = 597.000000 : fsl(24) = 419.688001
ALPHA(24) = 23.864488degs : vlt(24) = 2.659177 : glt(24) = 0.012222 : V(24) =
123970.850775
*** Shear web in CRACKED state (er >= ecr) ***
*** Shear r/f in PLASTIC state (fst >= fsty) ***
*** Smeared long r/f in ELASTIC state (fsl < fsly_M_V) ***
Ie(24) = 229648213.756669 : dflex(24) = 3.369883 : dshear(24) = 3.910964 :
dmax(24) = 7.280847
esl(24) = 0.001148 : Curv(24) = 0.000007
*** Flexural cracking has occurred (M >= Mcr) ***
CYCLE = 25 : No. of loops for er = 87
ed(25) = -0.000630 : er(25) = 0.016378 : el(25) = 0.002121 : et(25) = 0.013627
Xi(25) = 0.148020 : Sd(25) = -6.660913 : Sr(25) = 0.573257 : Sl(25) =
0.000000 : St(25) = 0.000000
Slc(25) = -5.490655 : Stc(25) = -0.597000
fst(25) = 597.000000 : fsl(25) = 424.265453
ALPHA(25) = 23.716029degs : vlt(25) = 2.663895 : glt(25) = 0.012526 : V(25) =
124190.789134
*** Shear web in CRACKED state (er >= ecr) ***
*** Shear r/f in PLASTIC state (fst >= fsty) ***
*** Smeared long r/f in ELASTIC state (fsl < fsly_M_V) ***
Ie(25) = 229637977.463627 : dflex(25) = 3.376012 : dshear(25) = 4.008280 :
dmax(25) = 7.384292
esl(25) = 0.001150 : Curv(25) = 0.000007
*** Flexural cracking has occurred (M >= Mcr) ***
CYCLE = 26 : No. of loops for er = 88
ed(26) = -0.000655 : er(26) = 0.016840 : el(26) = 0.002143 : et(26) = 0.014041
Xi(26) = 0.149156 : Sd(26) = -6.712037 : Sr(26) = 0.567370 : Sl(26) =
0.000000 : St(26) = 0.000000
Slc(26) = -5.547667 : Stc(26) = -0.597000
fst(26) = 597.000000 : fsl(26) = 428.670749
ALPHA(26) = 23.574579degs : vlt(26) = 2.668363 : glt(26) = 0.012826 : V(26) =
124399.100141
*** Shear web in CRACKED state (er >= ecr) ***
*** Shear r/f in PLASTIC state (fst >= fsty) ***
*** Smeared long r/f in ELASTIC state (fsl < fsly_M_V) ***
Ie(26) = 229628348.964746 : dflex(26) = 3.381816 : dshear(26) = 4.104277 :
dmax(26) = 7.486093
esl(26) = 0.001152 : Curv(26) = 0.000007
*** Flexural cracking has occurred (M >= Mcr) ***
CYCLE = 27 : No. of loops for er = 90
ed(27) = -0.000680 : er(27) = 0.017297 : el(27) = 0.002165 : et(27) = 0.014453
Xi(27) = 0.150252 : Sd(27) = -6.761333 : Sr(27) = 0.561730 : Sl(27) =
0.000000 : St(27) = 0.000000
Slc(27) = -5.602603 : Stc(27) = -0.597000
fst(27) = 597.000000 : fsl(27) = 432.915699
ALPHA(27) = 23.439573degs : vlt(27) = 2.672602 : glt(27) = 0.013122 : V(27) =
124596.688809
*** Shear web in CRACKED state (er >= ecr) ***
*** Shear r/f in PLASTIC state (fst >= fsty) ***
*** Smeared long r/f in ELASTIC state (fsl < fsly_M_V) ***
Ie(27) = 229619275.479643 : dflex(27) = 3.387322 : dshear(27) = 4.199038 :
dmax(27) = 7.586359
esl(27) = 0.001154 : Curv(27) = 0.000007
*** Flexural cracking has occurred (M >= Mcr) ***
CYCLE = 28 : No. of loops for er = 91
ed(28) = -0.000705 : er(28) = 0.017751 : el(28) = 0.002185 : et(28) = 0.014861

```

Xi(28) = 0.151309 : Sd(28) = -6.808922 : Sr(28) = 0.556320 : Sl(28) = 0.000000 : St(28) = 0.000000
Slc(28) = -5.655602 : Stc(28) = -0.597000
fst(28) = 597.000000 : fsl(28) = 437.010918
ALPHA(28) = 23.310511degs : vlt(28) = 2.676627 : glt(28) = 0.013414 : V(28) = 124784.361843
*** Shear web in CRACKED state (er >= ecr) ***
*** Shear r/f in PLASTIC state (fst >= fsty) ***
*** Smeared long r/f in ELASTIC state (fsl < fsly_M_V) ***
Ie(28) = 229610710.465423 : dflex(28) = 3.392550 : dshear(28) = 4.292636 : dmax(28) = 7.685187
esl(28) = 0.001155 : Curv(28) = 0.000007
*** Flexural cracking has occurred (M >= Mcr) ***
CYCLE = 29 : No. of loops for er = 92
ed(29) = -0.000730 : er(29) = 0.018201 : el(29) = 0.002205 : et(29) = 0.015266
Xi(29) = 0.152331 : Sd(29) = -6.854908 : Sr(29) = 0.551122 : Sl(29) = 0.000000 : St(29) = 0.000000
Slc(29) = -5.706786 : Stc(29) = -0.597000
fst(29) = 597.000000 : fsl(29) = 440.965987
ALPHA(29) = 23.186947degs : vlt(29) = 2.680456 : glt(29) = 0.013704 : V(29) = 124962.841280
*** Shear web in CRACKED state (er >= ecr) ***
*** Shear r/f in PLASTIC state (fst >= fsty) ***
*** Smeared long r/f in ELASTIC state (fsl < fsly_M_V) ***
Ie(29) = 229602612.692609 : dflex(29) = 3.397523 : dshear(29) = 4.385140 : dmax(29) = 7.782663
esl(29) = 0.001157 : Curv(29) = 0.000007
*** Flexural cracking has occurred (M >= Mcr) ***
CYCLE = 30 : No. of loops for er = 93
ed(30) = -0.000755 : er(30) = 0.018648 : el(30) = 0.002224 : et(30) = 0.015669
Xi(30) = 0.153320 : Sd(30) = -6.899391 : Sr(30) = 0.546121 : Sl(30) = 0.000000 : St(30) = 0.000000
Slc(30) = -5.756270 : Stc(30) = -0.597000
fst(30) = 597.000000 : fsl(30) = 444.789580
ALPHA(30) = 23.068481degs : vlt(30) = 2.684101 : glt(30) = 0.013989 : V(30) = 125132.775852
*** Shear web in CRACKED state (er >= ecr) ***
*** Shear r/f in PLASTIC state (fst >= fsty) ***
*** Smeared long r/f in ELASTIC state (fsl < fsly_M_V) ***
Ie(30) = 229594945.483998 : dflex(30) = 3.402256 : dshear(30) = 4.476611 : dmax(30) = 7.878868
esl(30) = 0.001159 : Curv(30) = 0.000007
*** Flexural cracking has occurred (M >= Mcr) ***
CYCLE = 31 : No. of loops for er = 94
ed(31) = -0.000780 : er(31) = 0.019091 : el(31) = 0.002242 : et(31) = 0.016069
Xi(31) = 0.154277 : Sd(31) = -6.942457 : Sr(31) = 0.541304 : Sl(31) = 0.000000 : St(31) = 0.000000
Slc(31) = -5.804153 : Stc(31) = -0.597000
fst(31) = 597.000000 : fsl(31) = 448.489579
ALPHA(31) = 22.954754degs : vlt(31) = 2.687575 : glt(31) = 0.014272 : V(31) = 125294.750505
*** Shear web in CRACKED state (er >= ecr) ***
*** Shear r/f in PLASTIC state (fst >= fsty) ***
*** Smeared long r/f in ELASTIC state (fsl < fsly_M_V) ***
Ie(31) = 229587676.083391 : dflex(31) = 3.406768 : dshear(31) = 4.567106 : dmax(31) = 7.973875
esl(31) = 0.001160 : Curv(31) = 0.000007
*** Flexural cracking has occurred (M >= Mcr) ***
CYCLE = 32 : No. of loops for er = 95
ed(32) = -0.000805 : er(32) = 0.019531 : el(32) = 0.002260 : et(32) = 0.016466

Xi(32) = 0.155204 : Sd(32) = -6.984189 : Sr(32) = 0.536658 : Sl(32) =
 0.000000 : St(32) = 0.000000
 Slc(32) = -5.850531 : Stc(32) = -0.597000
 fst(32) = 597.000000 : fsl(32) = 452.073170
 ALPHA(32) = 22.845443degs : vlt(32) = 2.690890 : glt(32) = 0.014552 : V(32) =
 125449.294431
 *** Shear web in CRACKED state (er >= ecr) ***
 *** Shear r/f in PLASTIC state (fst >= fsty) ***
 *** Smeared long r/f in ELASTIC state (fsl < fsly_M_V) ***
 Ie(32) = 229580775.128711 : dflex(32) = 3.411073 : dshear(32) = 4.656677 :
 dmax(32) = 8.067750
 esl(32) = 0.001162 : Curv(32) = 0.000007
 *** Flexural cracking has occurred (M >= Mcr) ***
 CYCLE = 33 : No. of loops for er = 96
 ed(33) = -0.000830 : er(33) = 0.019968 : el(33) = 0.002278 : et(33) = 0.016860
 Xi(33) = 0.156104 : Sd(33) = -7.024659 : Sr(33) = 0.532173 : Sl(33) =
 0.000000 : St(33) = 0.000000
 Slc(33) = -5.895486 : Stc(33) = -0.597000
 fst(33) = 597.000000 : fsl(33) = 455.546923
 ALPHA(33) = 22.740256degs : vlt(33) = 2.694056 : glt(33) = 0.014829 : V(33) =
 125596.887875
 *** Shear web in CRACKED state (er >= ecr) ***
 *** Shear r/f in PLASTIC state (fst >= fsty) ***
 *** Smeared long r/f in ELASTIC state (fsl < fsly_M_V) ***
 Ie(33) = 229574216.209616 : dflex(33) = 3.415184 : dshear(33) = 4.745371 :
 dmax(33) = 8.160554
 esl(33) = 0.001163 : Curv(33) = 0.000007
 *** Flexural cracking has occurred (M >= Mcr) ***
 CYCLE = 34 : No. of loops for er = 96
 ed(34) = -0.000855 : er(34) = 0.020402 : el(34) = 0.002295 : et(34) = 0.017253
 Xi(34) = 0.156976 : Sd(34) = -7.063936 : Sr(34) = 0.527837 : Sl(34) =
 0.000000 : St(34) = 0.000000
 Slc(34) = -5.939099 : Stc(34) = -0.597000
 fst(34) = 597.000000 : fsl(34) = 458.916860
 ALPHA(34) = 22.638927degs : vlt(34) = 2.697082 : glt(34) = 0.015104 : V(34) =
 125737.967933
 *** Shear web in CRACKED state (er >= ecr) ***
 *** Shear r/f in PLASTIC state (fst >= fsty) ***
 *** Smeared long r/f in ELASTIC state (fsl < fsly_M_V) ***
 Ie(34) = 229567975.493984 : dflex(34) = 3.419113 : dshear(34) = 4.833232 :
 dmax(34) = 8.252344
 esl(34) = 0.001165 : Curv(34) = 0.000007
 *** Flexural cracking has occurred (M >= Mcr) ***
 CYCLE = 35 : No. of loops for er = 98
 ed(35) = -0.000880 : er(35) = 0.020834 : el(35) = 0.002311 : et(35) = 0.017643
 Xi(35) = 0.157824 : Sd(35) = -7.102082 : Sr(35) = 0.523643 : Sl(35) =
 0.000000 : St(35) = 0.000000
 Slc(35) = -5.981439 : Stc(35) = -0.597000
 fst(35) = 597.000000 : fsl(35) = 462.188515
 ALPHA(35) = 22.541215degs : vlt(35) = 2.699977 : glt(35) = 0.015376 : V(35) =
 125872.933529
 *** Shear web in CRACKED state (er >= ecr) ***
 *** Shear r/f in PLASTIC state (fst >= fsty) ***
 *** Smeared long r/f in ELASTIC state (fsl < fsly_M_V) ***
 Ie(35) = 229562031.410900 : dflex(35) = 3.422871 : dshear(35) = 4.920301 :
 dmax(35) = 8.343172
 esl(35) = 0.001166 : Curv(35) = 0.000007
 *** Flexural cracking has occurred (M >= Mcr) ***
 CYCLE = 36 : No. of loops for er = 99
 ed(36) = -0.000905 : er(36) = 0.021262 : el(36) = 0.002327 : et(36) = 0.018031

Xi(36) = 0.158648 : Sd(36) = -7.139155 : Sr(36) = 0.519582 : Sl(36) =
0.000000 : St(36) = 0.000000
Slc(36) = -6.022573 : Stc(36) = -0.597000
fst(36) = 597.000000 : fsl(36) = 465.366988
ALPHA(36) = 22.446900degs : vlt(36) = 2.702749 : glt(36) = 0.015646 : V(36) =
126002.149683
*** Shear web in CRACKED state (er >= ecr) ***
*** Shear r/f in PLASTIC state (fst >= fsty) ***
*** Smeared long r/f in ELASTIC state (fsl < fsly_M_V) ***
Ie(36) = 229556364.380273 : dflex(36) = 3.426470 : dshear(36) = 5.006616 :
dmax(36) = 8.433086
esl(36) = 0.001167 : Curv(36) = 0.000007
*** Flexural cracking has occurred (M >= Mcr) ***
CYCLE = 37 : No. of loops for er = 100
ed(37) = -0.000930 : er(37) = 0.021689 : el(37) = 0.002342 : et(37) = 0.018416
Xi(37) = 0.159449 : Sd(37) = -7.175208 : Sr(37) = 0.515645 : Sl(37) =
0.000000 : St(37) = 0.000000
Slc(37) = -6.062563 : Stc(37) = -0.597000
fst(37) = 597.000000 : fsl(37) = 468.456989
ALPHA(37) = 22.355781degs : vlt(37) = 2.705404 : glt(37) = 0.015913 : V(37) =
126125.951215
*** Shear web in CRACKED state (er >= ecr) ***
*** Shear r/f in PLASTIC state (fst >= fsty) ***
*** Smeared long r/f in ELASTIC state (fsl < fsly_M_V) ***
Ie(37) = 229550956.581155 : dflex(37) = 3.429917 : dshear(37) = 5.092212 :
dmax(37) = 8.522130
esl(37) = 0.001168 : Curv(37) = 0.000007
*** Flexural cracking has occurred (M >= Mcr) ***
CYCLE = 38 : No. of loops for er = 100
ed(38) = -0.000955 : er(38) = 0.022113 : el(38) = 0.002357 : et(38) = 0.018800
Xi(38) = 0.160229 : Sd(38) = -7.210291 : Sr(38) = 0.511827 : Sl(38) =
0.000000 : St(38) = 0.000000
Slc(38) = -6.101464 : Stc(38) = -0.597000
fst(38) = 597.000000 : fsl(38) = 471.462877
ALPHA(38) = 22.267674degs : vlt(38) = 2.707950 : glt(38) = 0.016179 : V(38) =
126244.645945
*** Shear web in CRACKED state (er >= ecr) ***
*** Shear r/f in PLASTIC state (fst >= fsty) ***
*** Smeared long r/f in ELASTIC state (fsl < fsly_M_V) ***
Ie(38) = 229545791.752361 : dflex(38) = 3.433222 : dshear(38) = 5.177122 :
dmax(38) = 8.610345
esl(38) = 0.001169 : Curv(38) = 0.000007
*** Flexural cracking has occurred (M >= Mcr) ***
CYCLE = 39 : No. of loops for er = 101
ed(39) = -0.000980 : er(39) = 0.022534 : el(39) = 0.002372 : et(39) = 0.019182
Xi(39) = 0.160988 : Sd(39) = -7.244448 : Sr(39) = 0.508120 : Sl(39) =
0.000000 : St(39) = 0.000000
Slc(39) = -6.139328 : Stc(39) = -0.597000
fst(39) = 597.000000 : fsl(39) = 474.388692
ALPHA(39) = 22.182409degs : vlt(39) = 2.710393 : glt(39) = 0.016442 : V(39) =
126358.517492
*** Shear web in CRACKED state (er >= ecr) ***
*** Shear r/f in PLASTIC state (fst >= fsty) ***
*** Smeared long r/f in ELASTIC state (fsl < fsly_M_V) ***
Ie(39) = 229540855.020164 : dflex(39) = 3.436393 : dshear(39) = 5.261377 :
dmax(39) = 8.697769
esl(39) = 0.001170 : Curv(39) = 0.000007
*** Flexural cracking has occurred (M >= Mcr) ***
CYCLE = 40 : No. of loops for er = 102
ed(40) = -0.001005 : er(40) = 0.022954 : el(40) = 0.002386 : et(40) = 0.019563

```

Xi(40) = 0.161727 : Sd(40) = -7.277724 : Sr(40) = 0.504519 : Sl(40) =
0.000000 : St(40) = 0.000000
Slc(40) = -6.176205 : Stc(40) = -0.597000
fst(40) = 597.000000 : fsl(40) = 477.238191
ALPHA(40) = 22.099829degs : vlt(40) = 2.712738 : glt(40) = 0.016703 : V(40) =
126467.827715
*** Shear web in CRACKED state (er >= ecr) ***
*** Shear r/f in PLASTIC state (fst >= fsty) ***
*** Smeared long r/f in ELASTIC state (fsl < fsly_M_V) ***
Ie(40) = 229536132.748831 : dflex(40) = 3.439436 : dshear(40) = 5.345003 :
dmax(40) = 8.784440
esl(40) = 0.001171 : Curv(40) = 0.000007
*** Flexural cracking has occurred (M >= Mcr) ***
CYCLE = 41 : No. of loops for er = 102
ed(41) = -0.001030 : er(41) = 0.023371 : el(41) = 0.002400 : et(41) = 0.019941
Xi(41) = 0.162448 : Sd(41) = -7.310158 : Sr(41) = 0.501018 : Sl(41) =
0.000000 : St(41) = 0.000000
Slc(41) = -6.212140 : Stc(41) = -0.597000
fst(41) = 597.000000 : fsl(41) = 480.014871
ALPHA(41) = 22.019792degs : vlt(41) = 2.714990 : glt(41) = 0.016963 : V(41) =
126572.818856
*** Shear web in CRACKED state (er >= ecr) ***
*** Shear r/f in PLASTIC state (fst >= fsty) ***
*** Smeared long r/f in ELASTIC state (fsl < fsly_M_V) ***
Ie(41) = 229531612.410472 : dflex(41) = 3.442360 : dshear(41) = 5.428029 :
dmax(41) = 8.870389
esl(41) = 0.001172 : Curv(41) = 0.000007
*** Flexural cracking has occurred (M >= Mcr) ***
CYCLE = 42 : No. of loops for er = 104
ed(42) = -0.001055 : er(42) = 0.023787 : el(42) = 0.002414 : et(42) = 0.020318
Xi(42) = 0.163151 : Sd(42) = -7.341786 : Sr(42) = 0.497612 : Sl(42) =
0.000000 : St(42) = 0.000000
Slc(42) = -6.247174 : Stc(42) = -0.597000
fst(42) = 597.000000 : fsl(42) = 482.721991
ALPHA(42) = 21.942163degs : vlt(42) = 2.717154 : glt(42) = 0.017220 : V(42) =
126673.715428
*** Shear web in CRACKED state (er >= ecr) ***
*** Shear r/f in PLASTIC state (fst >= fsty) ***
*** Smeared long r/f in ELASTIC state (fsl < fsly_M_V) ***
Ie(42) = 229527282.471312 : dflex(42) = 3.445169 : dshear(42) = 5.510480 :
dmax(42) = 8.955648
esl(42) = 0.001173 : Curv(42) = 0.000007
*** Flexural cracking has occurred (M >= Mcr) ***
CYCLE = 43 : No. of loops for er = 104
ed(43) = -0.001080 : er(43) = 0.024200 : el(43) = 0.002427 : et(43) = 0.020693
Xi(43) = 0.163837 : Sd(43) = -7.372644 : Sr(43) = 0.494297 : Sl(43) =
0.000000 : St(43) = 0.000000
Slc(43) = -6.281348 : Stc(43) = -0.597000
fst(43) = 597.000000 : fsl(43) = 485.362596
ALPHA(43) = 21.866820degs : vlt(43) = 2.719235 : glt(43) = 0.017476 : V(43) =
126770.725882
*** Shear web in CRACKED state (er >= ecr) ***
*** Shear r/f in PLASTIC state (fst >= fsty) ***
*** Smeared long r/f in ELASTIC state (fsl < fsly_M_V) ***
Ie(43) = 229523132.291995 : dflex(43) = 3.447869 : dshear(43) = 5.592377 :
dmax(43) = 9.040247
esl(43) = 0.001174 : Curv(43) = 0.000007
*** Flexural cracking has occurred (M >= Mcr) ***
CYCLE = 44 : No. of loops for er = 104
ed(44) = -0.001105 : er(44) = 0.024611 : el(44) = 0.002440 : et(44) = 0.021067

```

```

Xi(44) = 0.164506 : Sd(44) = -7.402764 : Sr(44) = 0.491067 : Sl(44) =
0.000000 : St(44) = 0.000000
Slc(44) = -6.314697 : Stc(44) = -0.597000
fst(44) = 597.000000 : fsl(44) = 487.939537
ALPHA(44) = 21.793649degs : vlt(44) = 2.721236 : glt(44) = 0.017730 : V(44) =
126864.044081
*** Shear web in CRACKED state (er >= ecr) ***
*** Shear r/f in PLASTIC state (fst >= fsty) ***
*** Smeared long r/f in ELASTIC state (fsl < fsly_M_V) ***
Ie(44) = 229519152.039893 : dflex(44) = 3.450467 : dshear(44) = 5.673745 :
dmax(44) = 9.124212
esl(44) = 0.001175 : Curv(44) = 0.000007
*** Flexural cracking has occurred (M >= Mcr) ***
CYCLE = 45 : No. of loops for er = 105
ed(45) = -0.001130 : er(45) = 0.025021 : el(45) = 0.002452 : et(45) = 0.021439
Xi(45) = 0.165159 : Sd(45) = -7.432177 : Sr(45) = 0.487919 : Sl(45) =
0.000000 : St(45) = 0.000000
Slc(45) = -6.347258 : Stc(45) = -0.597000
fst(45) = 597.000000 : fsl(45) = 490.455483
ALPHA(45) = 21.722542degs : vlt(45) = 2.723163 : glt(45) = 0.017983 : V(45) =
126953.850612
*** Shear web in CRACKED state (er >= ecr) ***
*** Shear r/f in PLASTIC state (fst >= fsty) ***
*** Smeared long r/f in ELASTIC state (fsl < fsly_M_V) ***
Ie(45) = 229515332.611757 : dflex(45) = 3.452967 : dshear(45) = 5.754603 :
dmax(45) = 9.207570
esl(45) = 0.001176 : Curv(45) = 0.000007
*** Flexural cracking has occurred (M >= Mcr) ***
CYCLE = 46 : No. of loops for er = 105
ed(46) = -0.001155 : er(46) = 0.025429 : el(46) = 0.002465 : et(46) = 0.021810
Xi(46) = 0.165798 : Sd(46) = -7.460911 : Sr(46) = 0.484850 : Sl(46) =
0.000000 : St(46) = 0.000000
Slc(46) = -6.379061 : Stc(46) = -0.597000
fst(46) = 597.000000 : fsl(46) = 492.912939
ALPHA(46) = 21.653402degs : vlt(46) = 2.725017 : glt(46) = 0.018234 : V(46) =
127040.313951
*** Shear web in CRACKED state (er >= ecr) ***
*** Shear r/f in PLASTIC state (fst >= fsty) ***
*** Smeared long r/f in ELASTIC state (fsl < fsly_M_V) ***
Ie(46) = 229511665.565285 : dflex(46) = 3.455374 : dshear(46) = 5.834970 :
dmax(46) = 9.290344
esl(46) = 0.001177 : Curv(46) = 0.000007
*** Flexural cracking has occurred (M >= Mcr) ***
CYCLE = 47 : No. of loops for er = 108
ed(47) = -0.001180 : er(47) = 0.025836 : el(47) = 0.002477 : et(47) = 0.022179
Xi(47) = 0.166422 : Sd(47) = -7.488992 : Sr(47) = 0.481855 : Sl(47) =
0.000000 : St(47) = 0.000000
Slc(47) = -6.410138 : Stc(47) = -0.597000
fst(47) = 597.000000 : fsl(47) = 495.314259
ALPHA(47) = 21.586135degs : vlt(47) = 2.726804 : glt(47) = 0.018484 : V(47) =
127123.591513
*** Shear web in CRACKED state (er >= ecr) ***
*** Shear r/f in PLASTIC state (fst >= fsty) ***
*** Smeared long r/f in ELASTIC state (fsl < fsly_M_V) ***
Ie(47) = 229508143.058412 : dflex(47) = 3.457692 : dshear(47) = 5.914866 :
dmax(47) = 9.372558
esl(47) = 0.001178 : Curv(47) = 0.000007
*** Flexural cracking has occurred (M >= Mcr) ***
CYCLE = 48 : No. of loops for er = 107
ed(48) = -0.001205 : er(48) = 0.026240 : el(48) = 0.002488 : et(48) = 0.022547

```

Xi(48) = 0.167032 : Sd(48) = -7.516448 : Sr(48) = 0.478931 : Sl(48) =
0.000000 : St(48) = 0.000000
Slc(48) = -6.440517 : Stc(48) = -0.597000
fst(48) = 597.000000 : fsl(48) = 497.661657
ALPHA(48) = 21.520656degs : vlt(48) = 2.728525 : glt(48) = 0.018732 : V(48) =
127203.830576
*** Shear web in CRACKED state (er >= ecr) ***
*** Shear r/f in PLASTIC state (fst >= fsty) ***
*** Smeared long r/f in ELASTIC state (fsl < fsly_M_V) ***
Ie(48) = 229504757.795315 : dflex(48) = 3.459926 : dshear(48) = 5.994308 :
dmax(48) = 9.454234
esl(48) = 0.001178 : Curv(48) = 0.000007
*** Flexural cracking has occurred (M >= Mcr) ***
CYCLE = 49 : No. of loops for er = 109
ed(49) = -0.001230 : er(49) = 0.026644 : el(49) = 0.002500 : et(49) = 0.022914
Xi(49) = 0.167629 : Sd(49) = -7.543300 : Sr(49) = 0.476075 : Sl(49) =
0.000000 : St(49) = 0.000000
Slc(49) = -6.470225 : Stc(49) = -0.597000
fst(49) = 597.000000 : fsl(49) = 499.957221
ALPHA(49) = 21.456883degs : vlt(49) = 2.730184 : glt(49) = 0.018979 : V(49) =
127281.169123
*** Shear web in CRACKED state (er >= ecr) ***
*** Shear r/f in PLASTIC state (fst >= fsty) ***
*** Smeared long r/f in ELASTIC state (fsl < fsly_M_V) ***
Ie(49) = 229501502.978260 : dflex(49) = 3.462078 : dshear(49) = 6.073312 :
dmax(49) = 9.535390
esl(49) = 0.001179 : Curv(49) = 0.000007
*** Flexural cracking has occurred (M >= Mcr) ***
CYCLE = 50 : No. of loops for er = 109
ed(50) = -0.001255 : er(50) = 0.027045 : el(50) = 0.002511 : et(50) = 0.023279
Xi(50) = 0.168213 : Sd(50) = -7.569573 : Sr(50) = 0.473285 : Sl(50) =
0.000000 : St(50) = 0.000000
Slc(50) = -6.499288 : Stc(50) = -0.597000
fst(50) = 597.000000 : fsl(50) = 502.202918
ALPHA(50) = 21.394742degs : vlt(50) = 2.731783 : glt(50) = 0.019225 : V(50) =
127355.736596
*** Shear web in CRACKED state (er >= ecr) ***
*** Shear r/f in PLASTIC state (fst >= fsty) ***
*** Smeared long r/f in ELASTIC state (fsl < fsly_M_V) ***
Ie(50) = 229498372.264572 : dflex(50) = 3.464154 : dshear(50) = 6.151893 :
dmax(50) = 9.616047
esl(50) = 0.001180 : Curv(50) = 0.000007
*** Flexural cracking has occurred (M >= Mcr) ***
CYCLE = 51 : No. of loops for er = 111
ed(51) = -0.001280 : er(51) = 0.027446 : el(51) = 0.002522 : et(51) = 0.023644
Xi(51) = 0.168784 : Sd(51) = -7.595286 : Sr(51) = 0.470557 : Sl(51) =
0.000000 : St(51) = 0.000000
Slc(51) = -6.527729 : Stc(51) = -0.597000
fst(51) = 597.000000 : fsl(51) = 504.400607
ALPHA(51) = 21.334162degs : vlt(51) = 2.733326 : glt(51) = 0.019469 : V(51) =
127427.654573
*** Shear web in CRACKED state (er >= ecr) ***
*** Shear r/f in PLASTIC state (fst >= fsty) ***
*** Smeared long r/f in ELASTIC state (fsl < fsly_M_V) ***
Ie(51) = 229495359.728066 : dflex(51) = 3.466156 : dshear(51) = 6.230067 :
dmax(51) = 9.696223
esl(51) = 0.001181 : Curv(51) = 0.000007
*** Flexural cracking has occurred (M >= Mcr) ***
CYCLE = 52 : No. of loops for er = 110
ed(52) = -0.001305 : er(52) = 0.027845 : el(52) = 0.002533 : et(52) = 0.024007

```

Xi(52) = 0.169344 : Sd(52) = -7.620461 : Sr(52) = 0.467889 : Sl(52) =
0.000000 : St(52) = 0.000000
Slc(52) = -6.555572 : Stc(52) = -0.597000
fst(52) = 597.000000 : fsl(52) = 506.552044
ALPHA(52) = 21.275077degs : vlt(52) = 2.734814 : glt(52) = 0.019712 : V(52) =
127497.037382
*** Shear web in CRACKED state (er >= ecr) ***
*** Shear r/f in PLASTIC state (fst >= fsty) ***
*** Smeared long r/f in ELASTIC state (fsl < fsly_M_V) ***
Ie(52) = 229492459.824437 : dflex(52) = 3.468087 : dshear(52) = 6.307847 :
dmax(52) = 9.775934
esl(52) = 0.001181 : Curv(52) = 0.000007
*** Flexural cracking has occurred (M >= Mcr) ***
CYCLE = 53 : No. of loops for er = 111
ed(53) = -0.001330 : er(53) = 0.028242 : el(53) = 0.002543 : et(53) = 0.024369
Xi(53) = 0.169891 : Sd(53) = -7.645117 : Sr(53) = 0.465279 : Sl(53) =
0.000000 : St(53) = 0.000000
Slc(53) = -6.582838 : Stc(53) = -0.597000
fst(53) = 597.000000 : fsl(53) = 508.658893
ALPHA(53) = 21.217423degs : vlt(53) = 2.736250 : glt(53) = 0.019954 : V(53) =
127563.992654
*** Shear web in CRACKED state (er >= ecr) ***
*** Shear r/f in PLASTIC state (fst >= fsty) ***
*** Smeared long r/f in ELASTIC state (fsl < fsly_M_V) ***
Ie(53) = 229489667.360098 : dflex(53) = 3.469950 : dshear(53) = 6.385248 :
dmax(53) = 9.855198
esl(53) = 0.001182 : Curv(53) = 0.000007
*** Flexural cracking has occurred (M >= Mcr) ***
CYCLE = 54 : No. of loops for er = 110
ed(54) = -0.001355 : er(54) = 0.028638 : el(54) = 0.002554 : et(54) = 0.024730
Xi(54) = 0.170428 : Sd(54) = -7.669271 : Sr(54) = 0.462724 : Sl(54) =
0.000000 : St(54) = 0.000000
Slc(54) = -6.609547 : Stc(54) = -0.597000
fst(54) = 597.000000 : fsl(54) = 510.722729
ALPHA(54) = 21.161142degs : vlt(54) = 2.737637 : glt(54) = 0.020195 : V(54) =
127628.621828
*** Shear web in CRACKED state (er >= ecr) ***
*** Shear r/f in PLASTIC state (fst >= fsty) ***
*** Smeared long r/f in ELASTIC state (fsl < fsly_M_V) ***
Ie(54) = 229486977.464099 : dflex(54) = 3.471749 : dshear(54) = 6.462281 :
dmax(54) = 9.934030
esl(54) = 0.001182 : Curv(54) = 0.000007
*** Flexural cracking has occurred (M >= Mcr) ***
CYCLE = 55 : No. of loops for er = 112
ed(55) = -0.001380 : er(55) = 0.029034 : el(55) = 0.002564 : et(55) = 0.025090
Xi(55) = 0.170954 : Sd(55) = -7.692941 : Sr(55) = 0.460222 : Sl(55) =
0.000000 : St(55) = 0.000000
Slc(55) = -6.635719 : Stc(55) = -0.597000
fst(55) = 597.000000 : fsl(55) = 512.745045
ALPHA(55) = 21.106180degs : vlt(55) = 2.738975 : glt(55) = 0.020434 : V(55) =
127691.020608
*** Shear web in CRACKED state (er >= ecr) ***
*** Shear r/f in PLASTIC state (fst >= fsty) ***
*** Smeared long r/f in ELASTIC state (fsl < fsly_M_V) ***
Ie(55) = 229484385.562747 : dflex(55) = 3.473486 : dshear(55) = 6.538958 :
dmax(55) = 10.012443
esl(55) = 0.001183 : Curv(55) = 0.000007
*** Flexural cracking has occurred (M >= Mcr) ***
CYCLE = 56 : No. of loops for er = 113
ed(56) = -0.001405 : er(56) = 0.029427 : el(56) = 0.002574 : et(56) = 0.025449

```



```

Xi(56) = 0.171470 : Sd(56) = -7.716143 : Sr(56) = 0.457771 : Sl(56) =
0.000000 : St(56) = 0.000000
Slc(56) = -6.661372 : Stc(56) = -0.597000
fst(56) = 597.000000 : fsl(56) = 514.727260
ALPHA(56) = 21.052483degs : vlt(56) = 2.740268 : glt(56) = 0.020673 : V(56) =
127751.279377
*** Shear web in CRACKED state (er >= ecr) ***
*** Shear r/f in PLASTIC state (fst >= fsty) ***
*** Smeared long r/f in ELASTIC state (fsl < fsly_M_V) ***
Ie(56) = 229481887.356637 : dflex(56) = 3.475163 : dshear(56) = 6.615291 :
dmax(56) = 10.090454
esl(56) = 0.001184 : Curv(56) = 0.000007
*** Flexural cracking has occurred (M >= Mcr) ***
CYCLE = 57 : No. of loops for er = 115
ed(57) = -0.001430 : er(57) = 0.029820 : el(57) = 0.002583 : et(57) = 0.025807
Xi(57) = 0.171975 : Sd(57) = -7.738893 : Sr(57) = 0.455370 : Sl(57) =
0.000000 : St(57) = 0.000000
Slc(57) = -6.686524 : Stc(57) = -0.597000
fst(57) = 597.000000 : fsl(57) = 516.670720
ALPHA(57) = 21.000002degs : vlt(57) = 2.741516 : glt(57) = 0.020910 : V(57) =
127809.483578
*** Shear web in CRACKED state (er >= ecr) ***
*** Shear r/f in PLASTIC state (fst >= fsty) ***
*** Smeared long r/f in ELASTIC state (fsl < fsly_M_V) ***
Ie(57) = 229479478.799828 : dflex(57) = 3.476782 : dshear(57) = 6.691291 :
dmax(57) = 10.168074
esl(57) = 0.001184 : Curv(57) = 0.000007
*** Flexural cracking has occurred (M >= Mcr) ***
CYCLE = 58 : No. of loops for er = 114
ed(58) = -0.001455 : er(58) = 0.030211 : el(58) = 0.002593 : et(58) = 0.026164
Xi(58) = 0.172471 : Sd(58) = -7.761205 : Sr(58) = 0.453015 : Sl(58) =
0.000000 : St(58) = 0.000000
Slc(58) = -6.711190 : Stc(58) = -0.597000
fst(58) = 597.000000 : fsl(58) = 518.576707
ALPHA(58) = 20.948691degs : vlt(58) = 2.742722 : glt(58) = 0.021147 : V(58) =
127865.714058
*** Shear web in CRACKED state (er >= ecr) ***
*** Shear r/f in PLASTIC state (fst >= fsty) ***
*** Smeared long r/f in ELASTIC state (fsl < fsly_M_V) ***
Ie(58) = 229477156.080923 : dflex(58) = 3.478347 : dshear(58) = 6.766969 :
dmax(58) = 10.245316
esl(58) = 0.001185 : Curv(58) = 0.000007
*** Flexural cracking has occurred (M >= Mcr) ***
CYCLE = 59 : No. of loops for er = 115
ed(59) = -0.001480 : er(59) = 0.030602 : el(59) = 0.002602 : et(59) = 0.026520
Xi(59) = 0.172958 : Sd(59) = -7.783094 : Sr(59) = 0.450707 : Sl(59) =
0.000000 : St(59) = 0.000000
Slc(59) = -6.735387 : Stc(59) = -0.597000
fst(59) = 597.000000 : fsl(59) = 520.446440
ALPHA(59) = 20.898506degs : vlt(59) = 2.743888 : glt(59) = 0.021382 : V(59) =
127920.047387
*** Shear web in CRACKED state (er >= ecr) ***
*** Shear r/f in PLASTIC state (fst >= fsty) ***
*** Smeared long r/f in ELASTIC state (fsl < fsly_M_V) ***
Ie(59) = 229474915.605851 : dflex(59) = 3.479859 : dshear(59) = 6.842333 :
dmax(59) = 10.322193
esl(59) = 0.001185 : Curv(59) = 0.000007
*** Flexural cracking has occurred (M >= Mcr) ***
CYCLE = 60 : No. of loops for er = 114
ed(60) = -0.001505 : er(60) = 0.030991 : el(60) = 0.002611 : et(60) = 0.026875

```

Xi(60) = 0.173435 : Sd(60) = -7.804573 : Sr(60) = 0.448442 : Sl(60) =
 0.000000 : St(60) = 0.000000
 Slc(60) = -6.759130 : Stc(60) = -0.597000
 fst(60) = 597.000000 : fsl(60) = 522.281080
 ALPHA(60) = 20.849405degs : vlt(60) = 2.745014 : glt(60) = 0.021617 : V(60) =
 127972.556148
 *** Shear web in CRACKED state (er >= ecr) ***
 *** Shear r/f in PLASTIC state (fst >= fsty) ***
 *** Smeared long r/f in ELASTIC state (fsl < fsly_M_V) ***
 Ie(60) = 229472753.982182 : dflex(60) = 3.481320 : dshear(60) = 6.917395 :
 dmax(60) = 10.398715
 esl(60) = 0.001186 : Curv(60) = 0.000007
 *** Flexural cracking has occurred (M >= Mcr) ***
 CYCLE = 61 : No. of loops for er = 115
 ed(61) = -0.001530 : er(61) = 0.031379 : el(61) = 0.002620 : et(61) = 0.027229
 Xi(61) = 0.173903 : Sd(61) = -7.825654 : Sr(61) = 0.446221 : Sl(61) =
 0.000000 : St(61) = 0.000000
 Slc(61) = -6.782434 : Stc(61) = -0.597000
 fst(61) = 597.000000 : fsl(61) = 524.081735
 ALPHA(61) = 20.801348degs : vlt(61) = 2.746103 : glt(61) = 0.021851 : V(61) =
 128023.309198
 *** Shear web in CRACKED state (er >= ecr) ***
 *** Shear r/f in PLASTIC state (fst >= fsty) ***
 *** Smeared long r/f in ELASTIC state (fsl < fsly_M_V) ***
 Ie(61) = 229470668.004802 : dflex(61) = 3.482733 : dshear(61) = 6.992162 :
 dmax(61) = 10.474895
 esl(61) = 0.001186 : Curv(61) = 0.000007
 *** Flexural cracking has occurred (M >= Mcr) ***
 CYCLE = 62 : No. of loops for er = 116
 ed(62) = -0.001555 : er(62) = 0.031767 : el(62) = 0.002629 : et(62) = 0.027582
 Xi(62) = 0.174363 : Sd(62) = -7.846350 : Sr(62) = 0.444040 : Sl(62) =
 0.000000 : St(62) = 0.000000
 Slc(62) = -6.805311 : Stc(62) = -0.597000
 fst(62) = 597.000000 : fsl(62) = 525.849460
 ALPHA(62) = 20.754299degs : vlt(62) = 2.747155 : glt(62) = 0.022083 : V(62) =
 128072.371919
 *** Shear web in CRACKED state (er >= ecr) ***
 *** Shear r/f in PLASTIC state (fst >= fsty) ***
 *** Smeared long r/f in ELASTIC state (fsl < fsly_M_V) ***
 Ie(62) = 229468654.642823 : dflex(62) = 3.484098 : dshear(62) = 7.066644 :
 dmax(62) = 10.550742
 esl(62) = 0.001187 : Curv(62) = 0.000007
 *** Flexural cracking has occurred (M >= Mcr) ***
 CYCLE = 63 : No. of loops for er = 116
 ed(63) = -0.001580 : er(63) = 0.032153 : el(63) = 0.002638 : et(63) = 0.027935
 Xi(63) = 0.174815 : Sd(63) = -7.866673 : Sr(63) = 0.441899 : Sl(63) =
 0.000000 : St(63) = 0.000000
 Slc(63) = -6.827775 : Stc(63) = -0.597000
 fst(63) = 597.000000 : fsl(63) = 527.585264
 ALPHA(63) = 20.708220degs : vlt(63) = 2.748173 : glt(63) = 0.022315 : V(63) =
 128119.806440
 *** Shear web in CRACKED state (er >= ecr) ***
 *** Shear r/f in PLASTIC state (fst >= fsty) ***
 *** Smeared long r/f in ELASTIC state (fsl < fsly_M_V) ***
 Ie(63) = 229466711.027588 : dflex(63) = 3.485418 : dshear(63) = 7.140849 :
 dmax(63) = 10.626267
 esl(63) = 0.001187 : Curv(63) = 0.000007
 *** Flexural cracking has occurred (M >= Mcr) ***
 CYCLE = 64 : No. of loops for er = 117
 ed(64) = -0.001605 : er(64) = 0.032538 : el(64) = 0.002646 : et(64) = 0.028287

Xi(64) = 0.175259 : Sd(64) = -7.886634 : Sr(64) = 0.439796 : Sl(64) =
0.000000 : St(64) = 0.000000
Slc(64) = -6.849838 : Stc(64) = -0.597000
fst(64) = 597.000000 : fsl(64) = 529.290111
ALPHA(64) = 20.663080degs : vlt(64) = 2.749156 : glt(64) = 0.022546 : V(64) =
128165.671842
*** Shear web in CRACKED state (er >= ecr) ***
*** Shear r/f in PLASTIC state (fst >= fsty) ***
*** Smeared long r/f in ELASTIC state (fsl < fsly_M_V) ***
Ie(64) = 229464834.441686 : dflex(64) = 3.486694 : dshear(64) = 7.214785 :
dmax(64) = 10.701479
esl(64) = 0.001188 : Curv(64) = 0.000007
*** Flexural cracking has occurred (M >= Mcr) ***
CYCLE = 65 : No. of loops for er = 117
ed(65) = -0.001630 : er(65) = 0.032922 : el(65) = 0.002655 : et(65) = 0.028638
Xi(65) = 0.175694 : Sd(65) = -7.906243 : Sr(65) = 0.437730 : Sl(65) =
0.000000 : St(65) = 0.000000
Slc(65) = -6.871513 : Stc(65) = -0.597000
fst(65) = 597.000000 : fsl(65) = 530.964922
ALPHA(65) = 20.618845degs : vlt(65) = 2.750108 : glt(65) = 0.022776 : V(65) =
128210.024352
*** Shear web in CRACKED state (er >= ecr) ***
*** Shear r/f in PLASTIC state (fst >= fsty) ***
*** Smeared long r/f in ELASTIC state (fsl < fsly_M_V) ***
Ie(65) = 229463022.308857 : dflex(65) = 3.487928 : dshear(65) = 7.288459 :
dmax(65) = 10.776387
esl(65) = 0.001188 : Curv(65) = 0.000007
*** Flexural cracking has occurred (M >= Mcr) ***
CYCLE = 66 : No. of loops for er = 118
ed(66) = -0.001655 : er(66) = 0.033306 : el(66) = 0.002663 : et(66) = 0.028988
Xi(66) = 0.176122 : Sd(66) = -7.925510 : Sr(66) = 0.435700 : Sl(66) =
0.000000 : St(66) = 0.000000
Slc(66) = -6.892810 : Stc(66) = -0.597000
fst(66) = 597.000000 : fsl(66) = 532.610577
ALPHA(66) = 20.575485degs : vlt(66) = 2.751028 : glt(66) = 0.023006 : V(66) =
128252.917517
*** Shear web in CRACKED state (er >= ecr) ***
*** Shear r/f in PLASTIC state (fst >= fsty) ***
*** Smeared long r/f in ELASTIC state (fsl < fsly_M_V) ***
Ie(66) = 229461272.184713 : dflex(66) = 3.489122 : dshear(66) = 7.361879 :
dmax(66) = 10.851000
esl(66) = 0.001188 : Curv(66) = 0.000007
*** Flexural cracking has occurred (M >= Mcr) ***
CYCLE = 67 : No. of loops for er = 118
ed(67) = -0.001680 : er(67) = 0.033689 : el(67) = 0.002671 : et(67) = 0.029337
Xi(67) = 0.176543 : Sd(67) = -7.944446 : Sr(67) = 0.433705 : Sl(67) =
0.000000 : St(67) = 0.000000
Slc(67) = -6.913741 : Stc(67) = -0.597000
fst(67) = 597.000000 : fsl(67) = 534.227922
ALPHA(67) = 20.532970degs : vlt(67) = 2.751918 : glt(67) = 0.023235 : V(67) =
128294.402371
*** Shear web in CRACKED state (er >= ecr) ***
*** Shear r/f in PLASTIC state (fst >= fsty) ***
*** Smeared long r/f in ELASTIC state (fsl < fsly_M_V) ***
Ie(67) = 229459581.748197 : dflex(67) = 3.490276 : dshear(67) = 7.435051 :
dmax(67) = 10.925327
esl(67) = 0.001189 : Curv(67) = 0.000007
*** Flexural cracking has occurred (M >= Mcr) ***
CYCLE = 68 : No. of loops for er = 119
ed(68) = -0.001705 : er(68) = 0.034070 : el(68) = 0.002679 : et(68) = 0.029686

```

Xi(68) = 0.176957 : Sd(68) = -7.963060 : Sr(68) = 0.431744 : Sl(68) =
0.000000 : St(68) = 0.000000
Slc(68) = -6.934316 : Stc(68) = -0.597000
fst(68) = 597.000000 : fsl(68) = 535.817763
ALPHA(68) = 20.491274degs : vlt(68) = 2.752778 : glt(68) = 0.023462 : V(68) =
128334.527580
*** Shear web in CRACKED state (er >= ecr) ***
*** Shear r/f in PLASTIC state (fst >= fsty) ***
*** Smeared long r/f in ELASTIC state (fsl < fsly_M_V) ***
Ie(68) = 229457948.793708 : dflex(68) = 3.491393 : dshear(68) = 7.507984 :
dmax(68) = 10.999376
esl(68) = 0.001189 : Curv(68) = 0.000007
*** Flexural cracking has occurred (M >= Mcr) ***
CYCLE = 69 : No. of loops for er = 120
ed(69) = -0.001730 : er(69) = 0.034451 : el(69) = 0.002687 : et(69) = 0.030034
Xi(69) = 0.177364 : Sd(69) = -7.981360 : Sr(69) = 0.429815 : Sl(69) =
0.000000 : St(69) = 0.000000
Slc(69) = -6.954545 : Stc(69) = -0.597000
fst(69) = 597.000000 : fsl(69) = 537.380877
ALPHA(69) = 20.450369degs : vlt(69) = 2.753611 : glt(69) = 0.023690 : V(69) =
128373.339586
*** Shear web in CRACKED state (er >= ecr) ***
*** Shear r/f in PLASTIC state (fst >= fsty) ***
*** Smeared long r/f in ELASTIC state (fsl < fsly_M_V) ***
Ie(69) = 229456371.223839 : dflex(69) = 3.492473 : dshear(69) = 7.580682 :
dmax(69) = 11.073155
esl(69) = 0.001190 : Curv(69) = 0.000007
*** Flexural cracking has occurred (M >= Mcr) ***
CYCLE = 70 : No. of loops for er = 121
ed(70) = -0.001755 : er(70) = 0.034831 : el(70) = 0.002695 : et(70) = 0.030382
Xi(70) = 0.177763 : Sd(70) = -7.999356 : Sr(70) = 0.427918 : Sl(70) =
0.000000 : St(70) = 0.000000
Slc(70) = -6.974438 : Stc(70) = -0.597000
fst(70) = 597.000000 : fsl(70) = 538.918006
ALPHA(70) = 20.410230degs : vlt(70) = 2.754416 : glt(70) = 0.023916 : V(70) =
128410.882736
*** Shear web in CRACKED state (er >= ecr) ***
*** Shear r/f in PLASTIC state (fst >= fsty) ***
*** Smeared long r/f in ELASTIC state (fsl < fsly_M_V) ***
Ie(70) = 229454847.042661 : dflex(70) = 3.493517 : dshear(70) = 7.653153 :
dmax(70) = 11.146670
esl(70) = 0.001190 : Curv(70) = 0.000007
*** Flexural cracking has occurred (M >= Mcr) ***
CYCLE = 71 : No. of loops for er = 121
ed(71) = -0.001780 : er(71) = 0.035211 : el(71) = 0.002702 : et(71) = 0.030728
Xi(71) = 0.178157 : Sd(71) = -8.017056 : Sr(71) = 0.426052 : Sl(71) =
0.000000 : St(71) = 0.000000
Slc(71) = -6.994004 : Stc(71) = -0.597000
fst(71) = 597.000000 : fsl(71) = 540.429863
ALPHA(71) = 20.370834degs : vlt(71) = 2.755195 : glt(71) = 0.024142 : V(71) =
128447.199403
*** Shear web in CRACKED state (er >= ecr) ***
*** Shear r/f in PLASTIC state (fst >= fsty) ***
*** Smeared long r/f in ELASTIC state (fsl < fsly_M_V) ***
Ie(71) = 229453374.349514 : dflex(71) = 3.494528 : dshear(71) = 7.725402 :
dmax(71) = 11.219929
esl(71) = 0.001190 : Curv(71) = 0.000007
*** Flexural cracking has occurred (M >= Mcr) ***
CYCLE = 72 : No. of loops for er = 123
ed(72) = -0.001805 : er(72) = 0.035589 : el(72) = 0.002710 : et(72) = 0.031075

```

```

Xi(72) = 0.178544 : Sd(72) = -8.034467 : Sr(72) = 0.424215 : Sl(72) =
0.000000 : St(72) = 0.000000
Slc(72) = -7.013251 : Stc(72) = -0.597000
fst(72) = 597.000000 : fsl(72) = 541.917134
ALPHA(72) = 20.332156degs : vlt(72) = 2.755949 : glt(72) = 0.024367 : V(72) =
128482.330097
*** Shear web in CRACKED state (er >= ecr) ***
*** Shear r/f in PLASTIC state (fst >= fsty) ***
*** Smeared long r/f in ELASTIC state (fsl < fsly_M_V) ***
Ie(72) = 229451951.333258 : dflex(72) = 3.495505 : dshear(72) = 7.797435 :
dmax(72) = 11.292940
esl(72) = 0.001191 : Curv(72) = 0.000007
*** Flexural cracking has occurred (M >= Mcr) ***
CYCLE = 73 : No. of loops for er = 123
ed(73) = -0.001830 : er(73) = 0.035967 : el(73) = 0.002717 : et(73) = 0.031420
Xi(73) = 0.178924 : Sd(73) = -8.051597 : Sr(73) = 0.422407 : Sl(73) =
0.000000 : St(73) = 0.000000
Slc(73) = -7.032189 : Stc(73) = -0.597000
fst(73) = 597.000000 : fsl(73) = 543.380475
ALPHA(73) = 20.294176degs : vlt(73) = 2.756678 : glt(73) = 0.024591 : V(73) =
128516.313569
*** Shear web in CRACKED state (er >= ecr) ***
*** Shear r/f in PLASTIC state (fst >= fsty) ***
*** Smeared long r/f in ELASTIC state (fsl < fsly_M_V) ***
Ie(73) = 229450576.266941 : dflex(73) = 3.496451 : dshear(73) = 7.869258 :
dmax(73) = 11.365708
esl(73) = 0.001191 : Curv(73) = 0.000007
*** Flexural cracking has occurred (M >= Mcr) ***
CYCLE = 74 : No. of loops for er = 123
ed(74) = -0.001855 : er(74) = 0.036344 : el(74) = 0.002724 : et(74) = 0.031765
Xi(74) = 0.179299 : Sd(74) = -8.068454 : Sr(74) = 0.420628 : Sl(74) =
0.000000 : St(74) = 0.000000
Slc(74) = -7.050826 : Stc(74) = -0.597000
fst(74) = 597.000000 : fsl(74) = 544.820521
ALPHA(74) = 20.256871degs : vlt(74) = 2.757383 : glt(74) = 0.024815 : V(74) =
128549.186910
*** Shear web in CRACKED state (er >= ecr) ***
*** Shear r/f in PLASTIC state (fst >= fsty) ***
*** Smeared long r/f in ELASTIC state (fsl < fsly_M_V) ***
Ie(74) = 229449247.502851 : dflex(74) = 3.497365 : dshear(74) = 7.940876 :
dmax(74) = 11.438241
esl(74) = 0.001191 : Curv(74) = 0.000007
*** Flexural cracking has occurred (M >= Mcr) ***
CYCLE = 75 : No. of loops for er = 122
ed(75) = -0.001880 : er(75) = 0.036720 : el(75) = 0.002731 : et(75) = 0.032109
Xi(75) = 0.179668 : Sd(75) = -8.085044 : Sr(75) = 0.418876 : Sl(75) =
0.000000 : St(75) = 0.000000
Slc(75) = -7.069169 : Stc(75) = -0.597000
fst(75) = 597.000000 : fsl(75) = 546.237879
ALPHA(75) = 20.220222degs : vlt(75) = 2.758065 : glt(75) = 0.025038 : V(75) =
128580.985641
*** Shear web in CRACKED state (er >= ecr) ***
*** Shear r/f in PLASTIC state (fst >= fsty) ***
*** Smeared long r/f in ELASTIC state (fsl < fsly_M_V) ***
Ie(75) = 229447963.467925 : dflex(75) = 3.498250 : dshear(75) = 8.012294 :
dmax(75) = 11.510543
esl(75) = 0.001191 : Curv(75) = 0.000007
*** Flexural cracking has occurred (M >= Mcr) ***
CYCLE = 76 : No. of loops for er = 124
ed(76) = -0.001905 : er(76) = 0.037096 : el(76) = 0.002738 : et(76) = 0.032453

```

Xi(76) = 0.180031 : Sd(76) = -8.101375 : Sr(76) = 0.417150 : Sl(76) =
 0.000000 : St(76) = 0.000000
 Slc(76) = -7.087225 : Stc(76) = -0.597000
 fst(76) = 597.000000 : fsl(76) = 547.633135
 ALPHA(76) = 20.184210degs : vlt(76) = 2.758725 : glt(76) = 0.025261 : V(76) =
 128611.743796
 *** Shear web in CRACKED state (er >= ecr) ***
 *** Shear r/f in PLASTIC state (fst >= fsty) ***
 *** Smeared long r/f in ELASTIC state (fsl < fsly_M_V) ***
 Ie(76) = 229446722.659470 : dflex(76) = 3.499106 : dshear(76) = 8.083517 :
 dmax(76) = 11.582622
 esl(76) = 0.001192 : Curv(76) = 0.000007
 *** Flexural cracking has occurred (M >= Mcr) ***
 CYCLE = 77 : No. of loops for er = 122
 ed(77) = -0.001930 : er(77) = 0.037471 : el(77) = 0.002745 : et(77) = 0.032796
 Xi(77) = 0.180388 : Sd(77) = -8.117453 : Sr(77) = 0.415450 : Sl(77) =
 0.000000 : St(77) = 0.000000
 Slc(77) = -7.105003 : Stc(77) = -0.597000
 fst(77) = 597.000000 : fsl(77) = 549.006852
 ALPHA(77) = 20.148815degs : vlt(77) = 2.759363 : glt(77) = 0.025483 : V(77) =
 128641.494003
 *** Shear web in CRACKED state (er >= ecr) ***
 *** Shear r/f in PLASTIC state (fst >= fsty) ***
 *** Smeared long r/f in ELASTIC state (fsl < fsly_M_V) ***
 Ie(77) = 229445523.641190 : dflex(77) = 3.499933 : dshear(77) = 8.154550 :
 dmax(77) = 11.654483
 esl(77) = 0.001192 : Curv(77) = 0.000007
 *** Flexural cracking has occurred (M >= Mcr) ***
 CYCLE = 78 : No. of loops for er = 126
 ed(78) = -0.001955 : er(78) = 0.037845 : el(78) = 0.002752 : et(78) = 0.033139
 Xi(78) = 0.180740 : Sd(78) = -8.133285 : Sr(78) = 0.413775 : Sl(78) =
 0.000000 : St(78) = 0.000000
 Slc(78) = -7.122510 : Stc(78) = -0.597000
 fst(78) = 597.000000 : fsl(78) = 550.359574
 ALPHA(78) = 20.114021degs : vlt(78) = 2.759980 : glt(78) = 0.025704 : V(78) =
 128670.267557
 *** Shear web in CRACKED state (er >= ecr) ***
 *** Shear r/f in PLASTIC state (fst >= fsty) ***
 *** Smeared long r/f in ELASTIC state (fsl < fsly_M_V) ***
 Ie(78) = 229444365.039479 : dflex(78) = 3.500734 : dshear(78) = 8.225398 :
 dmax(78) = 11.726131
 esl(78) = 0.001192 : Curv(78) = 0.000007
 *** Flexural cracking has occurred (M >= Mcr) ***
 CYCLE = 79 : No. of loops for er = 124
 ed(79) = -0.001980 : er(79) = 0.038219 : el(79) = 0.002758 : et(79) = 0.033481
 Xi(79) = 0.181086 : Sd(79) = -8.148876 : Sr(79) = 0.412125 : Sl(79) =
 0.000000 : St(79) = 0.000000
 Slc(79) = -7.139751 : Stc(79) = -0.597000
 fst(79) = 597.000000 : fsl(79) = 551.691823
 ALPHA(79) = 20.079809degs : vlt(79) = 2.760577 : glt(79) = 0.025925 : V(79) =
 128698.094489
 *** Shear web in CRACKED state (er >= ecr) ***
 *** Shear r/f in PLASTIC state (fst >= fsty) ***
 *** Smeared long r/f in ELASTIC state (fsl < fsly_M_V) ***
 Ie(79) = 229443245.539964 : dflex(79) = 3.501508 : dshear(79) = 8.296064 :
 dmax(79) = 11.797572
 esl(79) = 0.001193 : Curv(79) = 0.000007
 *** Flexural cracking has occurred (M >= Mcr) ***
 CYCLE = 80 : No. of loops for er = 125
 ed(80) = -0.002005 : er(80) = 0.038592 : el(80) = 0.002765 : et(80) = 0.033822

Xi(80) = 0.181427 : Sd(80) = -8.164232 : Sr(80) = 0.410498 : Sl(80) =
0.000000 : St(80) = 0.000000
Slc(80) = -7.156734 : Stc(80) = -0.597000
fst(80) = 597.000000 : fsl(80) = 553.004104
ALPHA(80) = 20.046165degs : vlt(80) = 2.761154 : glt(80) = 0.026145 : V(80) =
128725.003633
*** Shear web in CRACKED state (er >= ecr) ***
*** Shear r/f in PLASTIC state (fst >= fsty) ***
*** Smeared long r/f in ELASTIC state (fsl < fsly_M_V) ***
Ie(80) = 229442163.884282 : dflex(80) = 3.502257 : dshear(80) = 8.366554 :
dmax(80) = 11.868811
esl(80) = 0.001193 : Curv(80) = 0.000007
*** Flexural cracking has occurred (M >= Mcr) ***
CYCLE = 81 : No. of loops for er = 126
ed(81) = -0.002030 : er(81) = 0.038965 : el(81) = 0.002771 : et(81) = 0.034163
Xi(81) = 0.181764 : Sd(81) = -8.179359 : Sr(81) = 0.408895 : Sl(81) =
0.000000 : St(81) = 0.000000
Slc(81) = -7.173465 : Stc(81) = -0.597000
fst(81) = 597.000000 : fsl(81) = 554.296903
ALPHA(81) = 20.013071degs : vlt(81) = 2.761712 : glt(81) = 0.026365 : V(81) =
128751.022682
*** Shear web in CRACKED state (er >= ecr) ***
*** Shear r/f in PLASTIC state (fst >= fsty) ***
*** Smeared long r/f in ELASTIC state (fsl < fsly_M_V) ***
Ie(81) = 229441118.867067 : dflex(81) = 3.502980 : dshear(81) = 8.436872 :
dmax(81) = 11.939852
esl(81) = 0.001193 : Curv(81) = 0.000007
*** Flexural cracking has occurred (M >= Mcr) ***
CYCLE = 82 : No. of loops for er = 126
ed(82) = -0.002055 : er(82) = 0.039337 : el(82) = 0.002778 : et(82) = 0.034504
Xi(82) = 0.182095 : Sd(82) = -8.194263 : Sr(82) = 0.407314 : Sl(82) =
0.000000 : St(82) = 0.000000
Slc(82) = -7.189950 : Stc(82) = -0.597000
fst(82) = 597.000000 : fsl(82) = 555.570690
ALPHA(82) = 19.980513degs : vlt(82) = 2.762252 : glt(82) = 0.026584 : V(82) =
128776.178251
*** Shear web in CRACKED state (er >= ecr) ***
*** Shear r/f in PLASTIC state (fst >= fsty) ***
*** Smeared long r/f in ELASTIC state (fsl < fsly_M_V) ***
Ie(82) = 229440109.333131 : dflex(82) = 3.503680 : dshear(82) = 8.507021 :
dmax(82) = 12.010701
esl(82) = 0.001193 : Curv(82) = 0.000007
*** Flexural cracking has occurred (M >= Mcr) ***
CYCLE = 83 : No. of loops for er = 125
ed(83) = -0.002080 : er(83) = 0.039708 : el(83) = 0.002784 : et(83) = 0.034844
Xi(83) = 0.182421 : Sd(83) = -8.208949 : Sr(83) = 0.405755 : Sl(83) =
0.000000 : St(83) = 0.000000
Slc(83) = -7.206194 : Stc(83) = -0.597000
fst(83) = 597.000000 : fsl(83) = 556.825918
ALPHA(83) = 19.948476degs : vlt(83) = 2.762773 : glt(83) = 0.026803 : V(83) =
128800.495926
*** Shear web in CRACKED state (er >= ecr) ***
*** Shear r/f in PLASTIC state (fst >= fsty) ***
*** Smeared long r/f in ELASTIC state (fsl < fsly_M_V) ***
Ie(83) = 229439134.174832 : dflex(83) = 3.504357 : dshear(83) = 8.577006 :
dmax(83) = 12.081363
esl(83) = 0.001194 : Curv(83) = 0.000007
*** Flexural cracking has occurred (M >= Mcr) ***
CYCLE = 84 : No. of loops for er = 120
ed(84) = -0.002085 : er(84) = 0.039782 : el(84) = 0.002785 : et(84) = 0.034912

Xi(84) = 0.182486 : Sd(84) = -8.211860 : Sr(84) = 0.405445 : Sl(84) =
0.000000 : St(84) = 0.000000
Slc(84) = -7.209415 : Stc(84) = -0.597000
fst(84) = 597.000000 : fsl(84) = 557.074775
ALPHA(84) = 19.942130degs : vlt(84) = 2.762876 : glt(84) = 0.026847 : V(84) =
128805.261095
*** Shear web in CRACKED state (er >= ecr) ***
*** Shear r/f in PLASTIC state (fst >= fsty) ***
*** Smeared long r/f in ELASTIC state (fsl < fsly_M_V) ***
Ie(84) = 229438943.173976 : dflex(84) = 3.504489 : dshear(84) = 8.590983 :
dmax(84) = 12.095473
esl(84) = 0.001194 : Curv(84) = 0.000007
*** Flexural cracking has occurred (M >= Mcr) ***
CYCLE = 85 : No. of loops for er = 119
ed(85) = -0.002090 : er(85) = 0.039856 : el(85) = 0.002787 : et(85) = 0.034980
Xi(85) = 0.182550 : Sd(85) = -8.214763 : Sr(85) = 0.405137 : Sl(85) =
0.000000 : St(85) = 0.000000
Slc(85) = -7.212626 : Stc(85) = -0.597000
fst(85) = 597.000000 : fsl(85) = 557.322911
ALPHA(85) = 19.935804degs : vlt(85) = 2.762977 : glt(85) = 0.026890 : V(85) =
128809.993929
*** Shear web in CRACKED state (er >= ecr) ***
*** Shear r/f in PLASTIC state (fst >= fsty) ***
*** Smeared long r/f in ELASTIC state (fsl < fsly_M_V) ***
Ie(85) = 229438753.497215 : dflex(85) = 3.504621 : dshear(85) = 8.604955 :
dmax(85) = 12.109576
esl(85) = 0.001194 : Curv(85) = 0.000007
*** Flexural cracking has occurred (M >= Mcr) ***
CYCLE = 86 : No. of loops for er = 119
ed(86) = -0.002095 : er(86) = 0.039930 : el(86) = 0.002788 : et(86) = 0.035048
Xi(86) = 0.182615 : Sd(86) = -8.217658 : Sr(86) = 0.404830 : Sl(86) =
0.000000 : St(86) = 0.000000
Slc(86) = -7.215828 : Stc(86) = -0.597000
fst(86) = 597.000000 : fsl(86) = 557.570329
ALPHA(86) = 19.929498degs : vlt(86) = 2.763078 : glt(86) = 0.026934 : V(86) =
128814.694617
*** Shear web in CRACKED state (er >= ecr) ***
*** Shear r/f in PLASTIC state (fst >= fsty) ***
*** Smeared long r/f in ELASTIC state (fsl < fsly_M_V) ***
Ie(86) = 229438565.136326 : dflex(86) = 3.504752 : dshear(86) = 8.618919 :
dmax(86) = 12.123671
esl(86) = 0.001194 : Curv(86) = 0.000007
*** Flexural cracking has occurred (M >= Mcr) ***
CYCLE = 87 : No. of loops for er = 121
ed(87) = -0.002100 : er(87) = 0.040005 : el(87) = 0.002789 : et(87) = 0.035115
Xi(87) = 0.182679 : Sd(87) = -8.220544 : Sr(87) = 0.404523 : Sl(87) =
0.000000 : St(87) = 0.000000
Slc(87) = -7.219021 : Stc(87) = -0.597000
fst(87) = 597.000000 : fsl(87) = 557.817032
ALPHA(87) = 19.923213degs : vlt(87) = 2.763178 : glt(87) = 0.026978 : V(87) =
128819.363350
*** Shear web in CRACKED state (er >= ecr) ***
*** Shear r/f in PLASTIC state (fst >= fsty) ***
*** Smeared long r/f in ELASTIC state (fsl < fsly_M_V) ***
Ie(87) = 229438378.083151 : dflex(87) = 3.504882 : dshear(87) = 8.632878 :
dmax(87) = 12.137759
esl(87) = 0.001194 : Curv(87) = 0.000007
*** Flexural cracking has occurred (M >= Mcr) ***
CYCLE = 88 : No. of loops for er = 120
ed(88) = -0.002105 : er(88) = 0.040079 : el(88) = 0.002790 : et(88) = 0.035183

Xi(88) = 0.182743 : Sd(88) = -8.223421 : Sr(88) = 0.404217 : Sl(88) =
 0.000000 : St(88) = 0.000000
 Slc(88) = -7.222204 : Stc(88) = -0.597000
 fst(88) = 597.000000 : fsl(88) = 558.063024
 ALPHA(88) = 19.916947degs : vlt(88) = 2.763278 : glt(88) = 0.027021 : V(88) =
 128824.000314
 *** Shear web in CRACKED state (er >= ecr) ***
 *** Shear r/f in PLASTIC state (fst >= fsty) ***
 *** Smeared long r/f in ELASTIC state (fsl < fsly_M_V) ***
 Ie(88) = 229438192.329602 : dflex(88) = 3.505011 : dshear(88) = 8.646830 :
 dmax(88) = 12.151841
 esl(88) = 0.001194 : Curv(88) = 0.000007
 *** Flexural cracking has occurred (M >= Mcr) ***
 CYCLE = 89 : No. of loops for er = 119
 ed(89) = -0.002110 : er(89) = 0.040153 : el(89) = 0.002792 : et(89) = 0.035251
 Xi(89) = 0.182806 : Sd(89) = -8.226291 : Sr(89) = 0.403912 : Sl(89) =
 0.000000 : St(89) = 0.000000
 Slc(89) = -7.225379 : Stc(89) = -0.597000
 fst(89) = 597.000000 : fsl(89) = 558.308309
 ALPHA(89) = 19.910700degs : vlt(89) = 2.763376 : glt(89) = 0.027065 : V(89) =
 128828.605697
 *** Shear web in CRACKED state (er >= ecr) ***
 *** Shear r/f in PLASTIC state (fst >= fsty) ***
 *** Smeared long r/f in ELASTIC state (fsl < fsly_M_V) ***
 Ie(89) = 229438007.867654 : dflex(89) = 3.505139 : dshear(89) = 8.660776 :
 dmax(89) = 12.165915
 esl(89) = 0.001194 : Curv(89) = 0.000007
 *** Flexural cracking has occurred (M >= Mcr) ***
 CYCLE = 90 : No. of loops for er = 125
 ed(90) = -0.002111 : er(90) = 0.040160 : el(90) = 0.002792 : et(90) = 0.035258
 Xi(90) = 0.182813 : Sd(90) = -8.226577 : Sr(90) = 0.403882 : Sl(90) =
 0.000000 : St(90) = 0.000000
 Slc(90) = -7.225696 : Stc(90) = -0.597000
 fst(90) = 597.000000 : fsl(90) = 558.332798
 ALPHA(90) = 19.910077degs : vlt(90) = 2.763386 : glt(90) = 0.027069 : V(90) =
 128829.064506
 *** Shear web in CRACKED state (er >= ecr) ***
 *** Shear r/f in PLASTIC state (fst >= fsty) ***
 *** Smeared long r/f in ELASTIC state (fsl < fsly_M_V) ***
 Ie(90) = 229437989.492190 : dflex(90) = 3.505152 : dshear(90) = 8.662170 :
 dmax(90) = 12.167322
 esl(90) = 0.001194 : Curv(90) = 0.000007
 *** Flexural cracking has occurred (M >= Mcr) ***
 CYCLE = 91 : No. of loops for er = 109
 ed(91) = -0.002111 : er(91) = 0.040168 : el(91) = 0.002792 : et(91) = 0.035265
 Xi(91) = 0.182819 : Sd(91) = -8.226864 : Sr(91) = 0.403851 : Sl(91) =
 0.000000 : St(91) = 0.000000
 Slc(91) = -7.226013 : Stc(91) = -0.597000
 fst(91) = 597.000000 : fsl(91) = 558.357281
 ALPHA(91) = 19.909454degs : vlt(91) = 2.763396 : glt(91) = 0.027074 : V(91) =
 128829.523000
 *** Shear web in CRACKED state (er >= ecr) ***
 *** Shear r/f in PLASTIC state (fst >= fsty) ***
 *** Smeared long r/f in ELASTIC state (fsl < fsly_M_V) ***
 Ie(91) = 229437971.129555 : dflex(91) = 3.505164 : dshear(91) = 8.663564 :
 dmax(91) = 12.168728
 esl(91) = 0.001194 : Curv(91) = 0.000007
 *** Flexural cracking has occurred (M >= Mcr) ***
 CYCLE = 92 : No. of loops for er = 111
 ed(92) = -0.002112 : er(92) = 0.040175 : el(92) = 0.002792 : et(92) = 0.035272

Xi(92) = 0.182826 : Sd(92) = -8.227150 : Sr(92) = 0.403821 : Sl(92) =
0.000000 : St(92) = 0.000000
Slc(92) = -7.226329 : Stc(92) = -0.597000
fst(92) = 597.000000 : fsl(92) = 558.381756
ALPHA(92) = 19.908830degs : vlt(92) = 2.763406 : glt(92) = 0.027078 : V(92) =
128829.981181
*** Shear web in CRACKED state (er >= ecr) ***
*** Shear r/f in PLASTIC state (fst >= fsty) ***
*** Smeared long r/f in ELASTIC state (fsl < fsly_M_V) ***
Ie(92) = 229437952.779740 : dflex(92) = 3.505177 : dshear(92) = 8.664958 :
dmax(92) = 12.170135
esl(92) = 0.001194 : Curv(92) = 0.000007
*** Flexural cracking has occurred (M >= Mcr) ***
CYCLE = 93 : No. of loops for er = 109
ed(93) = -0.002112 : er(93) = 0.040182 : el(93) = 0.002792 : et(93) = 0.035278
Xi(93) = 0.182832 : Sd(93) = -8.227436 : Sr(93) = 0.403790 : Sl(93) =
0.000000 : St(93) = 0.000000
Slc(93) = -7.226646 : Stc(93) = -0.597000
fst(93) = 597.000000 : fsl(93) = 558.406225
ALPHA(93) = 19.908208degs : vlt(93) = 2.763416 : glt(93) = 0.027082 : V(93) =
128830.439049
*** Shear web in CRACKED state (er >= ecr) ***
*** Shear r/f in PLASTIC state (fst >= fsty) ***
*** Smeared long r/f in ELASTIC state (fsl < fsly_M_V) ***
Ie(93) = 229437934.442738 : dflex(93) = 3.505190 : dshear(93) = 8.666352 :
dmax(93) = 12.171542
esl(93) = 0.001194 : Curv(93) = 0.000007
*** Flexural cracking has occurred (M >= Mcr) ***
CYCLE = 94 : No. of loops for er = 111
ed(94) = -0.002113 : er(94) = 0.040190 : el(94) = 0.002792 : et(94) = 0.035285
Xi(94) = 0.182838 : Sd(94) = -8.227722 : Sr(94) = 0.403760 : Sl(94) =
0.000000 : St(94) = 0.000000
Slc(94) = -7.226962 : Stc(94) = -0.597000
fst(94) = 597.000000 : fsl(94) = 558.430686
ALPHA(94) = 19.907585degs : vlt(94) = 2.763425 : glt(94) = 0.027087 : V(94) =
128830.896604
*** Shear web in CRACKED state (er >= ecr) ***
*** Shear r/f in PLASTIC state (fst >= fsty) ***
*** Smeared long r/f in ELASTIC state (fsl < fsly_M_V) ***
Ie(94) = 229437916.118540 : dflex(94) = 3.505203 : dshear(94) = 8.667746 :
dmax(94) = 12.172949
esl(94) = 0.001194 : Curv(94) = 0.000007
*** Flexural cracking has occurred (M >= Mcr) ***
CYCLE = 95 : No. of loops for er = 110
ed(95) = -0.002113 : er(95) = 0.040197 : el(95) = 0.002792 : et(95) = 0.035292
Xi(95) = 0.182845 : Sd(95) = -8.228008 : Sr(95) = 0.403729 : Sl(95) =
0.000000 : St(95) = 0.000000
Slc(95) = -7.227279 : Stc(95) = -0.597000
fst(95) = 597.000000 : fsl(95) = 558.455141
ALPHA(95) = 19.906962degs : vlt(95) = 2.763435 : glt(95) = 0.027091 : V(95) =
128831.353845
*** Shear web in CRACKED state (er >= ecr) ***
*** Shear r/f in PLASTIC state (fst >= fsty) ***
*** Smeared long r/f in ELASTIC state (fsl < fsly_M_V) ***
Ie(95) = 229437897.807139 : dflex(95) = 3.505215 : dshear(95) = 8.669140 :
dmax(95) = 12.174355
esl(95) = 0.001194 : Curv(95) = 0.000007
*** Flexural cracking has occurred (M >= Mcr) ***
CYCLE = 96 : No. of loops for er = 110
ed(96) = -0.002114 : er(96) = 0.040205 : el(96) = 0.002792 : et(96) = 0.035299

```

Xi(96) = 0.182851 : Sd(96) = -8.228294 : Sr(96) = 0.403699 : Sl(96) =
0.000000 : St(96) = 0.000000
Slc(96) = -7.227595 : Stc(96) = -0.597000
fst(96) = 597.000000 : fsl(96) = 558.479588
ALPHA(96) = 19.906340degs : vlt(96) = 2.763445 : glt(96) = 0.027095 : V(96) =
128831.810774
*** Shear web in CRACKED state (er >= ecr) ***
*** Shear r/f in PLASTIC state (fst >= fsty) ***
*** Smeared long r/f in ELASTIC state (fsl < fsly_M_V) ***
Ie(96) = 229437879.508528 : dflex(96) = 3.505228 : dshear(96) = 8.670534 :
dmax(96) = 12.175762
esl(96) = 0.001194 : Curv(96) = 0.000007
*** Flexural cracking has occurred (M >= Mcr) ***
CYCLE = 97 : No. of loops for er = 110
ed(97) = -0.002114 : er(97) = 0.040212 : el(97) = 0.002793 : et(97) = 0.035305
Xi(97) = 0.182857 : Sd(97) = -8.228580 : Sr(97) = 0.403669 : Sl(97) =
0.000000 : St(97) = 0.000000
Slc(97) = -7.227912 : Stc(97) = -0.597000
fst(97) = 597.000000 : fsl(97) = 558.504028
ALPHA(97) = 19.905718degs : vlt(97) = 2.763455 : glt(97) = 0.027100 : V(97) =
128832.267389
*** Shear web in CRACKED state (er >= ecr) ***
*** Shear r/f in PLASTIC state (fst >= fsty) ***
*** Smeared long r/f in ELASTIC state (fsl < fsly_M_V) ***
Ie(97) = 229437861.222697 : dflex(97) = 3.505241 : dshear(97) = 8.671928 :
dmax(97) = 12.177169
esl(97) = 0.001194 : Curv(97) = 0.000007
*** Flexural cracking has occurred (M >= Mcr) ***
CYCLE = 98 : No. of loops for er = 111
ed(98) = -0.002115 : er(98) = 0.040219 : el(98) = 0.002793 : et(98) = 0.035312
Xi(98) = 0.182864 : Sd(98) = -8.228866 : Sr(98) = 0.403638 : Sl(98) =
0.000000 : St(98) = 0.000000
Slc(98) = -7.228228 : Stc(98) = -0.597000
fst(98) = 597.000000 : fsl(98) = 558.528462
ALPHA(98) = 19.905096degs : vlt(98) = 2.763465 : glt(98) = 0.027104 : V(98) =
128832.723693
*** Shear web in CRACKED state (er >= ecr) ***
*** Shear r/f in PLASTIC state (fst >= fsty) ***
*** Smeared long r/f in ELASTIC state (fsl < fsly_M_V) ***
Ie(98) = 229437842.949639 : dflex(98) = 3.505253 : dshear(98) = 8.673322 :
dmax(98) = 12.178575
esl(98) = 0.001194 : Curv(98) = 0.000007
*** Flexural cracking has occurred (M >= Mcr) ***
CYCLE = 99 : No. of loops for er = 110
ed(99) = -0.002115 : er(99) = 0.040227 : el(99) = 0.002793 : et(99) = 0.035319
Xi(99) = 0.182870 : Sd(99) = -8.229152 : Sr(99) = 0.403608 : Sl(99) =
0.000000 : St(99) = 0.000000
Slc(99) = -7.228544 : Stc(99) = -0.597000
fst(99) = 597.000000 : fsl(99) = 558.552888
ALPHA(99) = 19.904474degs : vlt(99) = 2.763474 : glt(99) = 0.027108 : V(99) =
128833.179684
*** Shear web in CRACKED state (er >= ecr) ***
*** Shear r/f in PLASTIC state (fst >= fsty) ***
*** Smeared long r/f in ELASTIC state (fsl < fsly_M_V) ***
Ie(99) = 229437824.689347 : dflex(99) = 3.505266 : dshear(99) = 8.674715 :
dmax(99) = 12.179981
esl(99) = 0.001194 : Curv(99) = 0.000007
*** Flexural cracking has occurred (M >= Mcr) ***
CYCLE = 100 : No. of loops for er = 110
ed(100) = -0.002116 : er(100) = 0.040234 : el(100) = 0.002793 : et(100) =
0.035326

```

```

Xi(100) = 0.182876 : Sd(100) = -8.229437 : Sr(100) = 0.403577 : Sl(100) =
0.000000 : St(100) = 0.000000
Slc(100) = -7.228860 : Stc(100) = -0.597000
fst(100) = 597.000000 : fsl(100) = 558.577308
ALPHA(100) = 19.903852degs : vlt(100) = 2.763484 : glt(100) = 0.027113 : V(100)
= 128833.635363
*** Shear web in CRACKED state (er >= ecr) ***
*** Shear r/f in PLASTIC state (fst >= fsty) ***
*** Smeared long r/f in ELASTIC state (fsl < fsly_M_V) ***
Ie(100) = 229437806.441812 : dflex(100) = 3.505279 : dshear(100) = 8.676109 :
dmax(100) = 12.181388
esl(100) = 0.001194 : Curv(100) = 0.000007
*** Flexural cracking has occurred (M >= Mcr) ***
CYCLE = 101 : No. of loops for er = 110
ed(101) = -0.002116 : er(101) = 0.040242 : el(101) = 0.002793 : et(101) =
0.035333
Xi(101) = 0.182883 : Sd(101) = -8.229723 : Sr(101) = 0.403547 : Sl(101) =
0.000000 : St(101) = 0.000000
Slc(101) = -7.229176 : Stc(101) = -0.597000
fst(101) = 597.000000 : fsl(101) = 558.601720
ALPHA(101) = 19.903231degs : vlt(101) = 2.763494 : glt(101) = 0.027117 : V(101)
= 128834.090730
*** Shear web in CRACKED state (er >= ecr) ***
*** Shear r/f in PLASTIC state (fst >= fsty) ***
*** Smeared long r/f in ELASTIC state (fsl < fsly_M_V) ***
Ie(101) = 229437788.207026 : dflex(101) = 3.505291 : dshear(101) = 8.677502 :
dmax(101) = 12.182794
esl(101) = 0.001194 : Curv(101) = 0.000007
*** Flexural cracking has occurred (M >= Mcr) ***
CYCLE = 102 : No. of loops for er = 110
ed(102) = -0.002117 : er(102) = 0.040249 : el(102) = 0.002793 : et(102) =
0.035339
Xi(102) = 0.182889 : Sd(102) = -8.230009 : Sr(102) = 0.403517 : Sl(102) =
0.000000 : St(102) = 0.000000
Slc(102) = -7.229492 : Stc(102) = -0.597000
fst(102) = 597.000000 : fsl(102) = 558.626125
ALPHA(102) = 19.902610degs : vlt(102) = 2.763504 : glt(102) = 0.027122 : V(102)
= 128834.545785
*** Shear web in CRACKED state (er >= ecr) ***
*** Shear r/f in PLASTIC state (fst >= fsty) ***
*** Smeared long r/f in ELASTIC state (fsl < fsly_M_V) ***
Ie(102) = 229437769.984983 : dflex(102) = 3.505304 : dshear(102) = 8.678896 :
dmax(102) = 12.184200
esl(102) = 0.001194 : Curv(102) = 0.000007
*** Flexural cracking has occurred (M >= Mcr) ***
CYCLE = 103 : No. of loops for er = 109
ed(103) = -0.002117 : er(103) = 0.040256 : el(103) = 0.002793 : et(103) =
0.035346
Xi(103) = 0.182895 : Sd(103) = -8.230294 : Sr(103) = 0.403486 : Sl(103) =
0.000000 : St(103) = 0.000000
Slc(103) = -7.229808 : Stc(103) = -0.597000
fst(103) = 597.000000 : fsl(103) = 558.650523
ALPHA(103) = 19.901989degs : vlt(103) = 2.763514 : glt(103) = 0.027126 : V(103)
= 128835.000529
*** Shear web in CRACKED state (er >= ecr) ***
*** Shear r/f in PLASTIC state (fst >= fsty) ***
*** Smeared long r/f in ELASTIC state (fsl < fsly_M_V) ***
Ie(103) = 229437751.775673 : dflex(103) = 3.505317 : dshear(103) = 8.680289 :
dmax(103) = 12.185606
esl(103) = 0.001194 : Curv(103) = 0.000007
*** Flexural cracking has occurred (M >= Mcr) ***

```

CYCLE = 104 : No. of loops for er = 111
 ed(104) = -0.002118 : er(104) = 0.040264 : el(104) = 0.002793 : et(104) = 0.035353
 Xi(104) = 0.182902 : Sd(104) = -8.230579 : Sr(104) = 0.403456 : Sl(104) = 0.000000 : St(104) = 0.000000
 Slc(104) = -7.230123 : Stc(104) = -0.597000
 fst(104) = 597.000000 : fsl(104) = 558.674915
 ALPHA(104) = 19.901368degs : vlt(104) = 2.763523 : glt(104) = 0.027130 : V(104) = 128835.454961
 *** Shear web in CRACKED state (er >= ecr) ***
 *** Shear r/f in PLASTIC state (fst >= fsty) ***
 *** Smeared long r/f in ELASTIC state (fsl < fsly_M_V) ***
 Ie(104) = 229437733.579089 : dflex(104) = 3.505329 : dshear(104) = 8.681683 : dmax(104) = 12.187012
 esl(104) = 0.001194 : Curv(104) = 0.000007
 *** Flexural cracking has occurred (M >= Mcr) ***
 CYCLE = 105 : No. of loops for er = 111
 ed(105) = -0.002118 : er(105) = 0.040271 : el(105) = 0.002793 : et(105) = 0.035360
 Xi(105) = 0.182908 : Sd(105) = -8.230865 : Sr(105) = 0.403426 : Sl(105) = 0.000000 : St(105) = 0.000000
 Slc(105) = -7.230439 : Stc(105) = -0.597000
 fst(105) = 597.000000 : fsl(105) = 558.699299
 ALPHA(105) = 19.900747degs : vlt(105) = 2.763533 : glt(105) = 0.027135 : V(105) = 128835.909082
 *** Shear web in CRACKED state (er >= ecr) ***
 *** Shear r/f in PLASTIC state (fst >= fsty) ***
 *** Smeared long r/f in ELASTIC state (fsl < fsly_M_V) ***
 Ie(105) = 229437715.395223 : dflex(105) = 3.505342 : dshear(105) = 8.683076 : dmax(105) = 12.188418
 esl(105) = 0.001194 : Curv(105) = 0.000007
 *** Flexural cracking has occurred (M >= Mcr) ***
 CYCLE = 106 : No. of loops for er = 110
 ed(106) = -0.002119 : er(106) = 0.040279 : el(106) = 0.002794 : et(106) = 0.035367
 Xi(106) = 0.182914 : Sd(106) = -8.231150 : Sr(106) = 0.403395 : Sl(106) = 0.000000 : St(106) = 0.000000
 Slc(106) = -7.230754 : Stc(106) = -0.597000
 fst(106) = 597.000000 : fsl(106) = 558.723676
 ALPHA(106) = 19.900127degs : vlt(106) = 2.763543 : glt(106) = 0.027139 : V(106) = 128836.362892
 *** Shear web in CRACKED state (er >= ecr) ***
 *** Shear r/f in PLASTIC state (fst >= fsty) ***
 *** Smeared long r/f in ELASTIC state (fsl < fsly_M_V) ***
 Ie(106) = 229437697.224068 : dflex(106) = 3.505355 : dshear(106) = 8.684469 : dmax(106) = 12.189824
 esl(106) = 0.001194 : Curv(106) = 0.000007
 *** Flexural cracking has occurred (M >= Mcr) ***
 CYCLE = 107 : No. of loops for er = 112
 ed(107) = -0.002119 : er(107) = 0.040286 : el(107) = 0.002794 : et(107) = 0.035373
 Xi(107) = 0.182921 : Sd(107) = -8.231435 : Sr(107) = 0.403365 : Sl(107) = 0.000000 : St(107) = 0.000000
 Slc(107) = -7.231070 : Stc(107) = -0.597000
 fst(107) = 597.000000 : fsl(107) = 558.748047
 ALPHA(107) = 19.899507degs : vlt(107) = 2.763552 : glt(107) = 0.027143 : V(107) = 128836.816391
 *** Shear web in CRACKED state (er >= ecr) ***
 *** Shear r/f in PLASTIC state (fst >= fsty) ***
 *** Smeared long r/f in ELASTIC state (fsl < fsly_M_V) ***

Ie(107) = 229437679.065615 : dflex(107) = 3.505367 : dshear(107) = 8.685862 :
 dmax(107) = 12.191230
 esl(107) = 0.001194 : Curv(107) = 0.000007
 *** Flexural cracking has occurred (M >= Mcr) ***
 CYCLE = 108 : No. of loops for er = 110
 ed(108) = -0.002120 : er(108) = 0.040293 : el(108) = 0.002794 : et(108) =
 0.035380
 Xi(108) = 0.182927 : Sd(108) = -8.231720 : Sr(108) = 0.403335 : Sl(108) =
 0.000000 : St(108) = 0.000000
 Slc(108) = -7.231385 : Stc(108) = -0.597000
 fst(108) = 597.000000 : fsl(108) = 558.772410
 ALPHA(108) = 19.898887degs : vlt(108) = 2.763562 : glt(108) = 0.027148 : V(108)
 = 128837.269580
 *** Shear web in CRACKED state (er >= ecr) ***
 *** Shear r/f in PLASTIC state (fst >= fsty) ***
 *** Smeared long r/f in ELASTIC state (fsl < fsly_M_V) ***
 Ie(108) = 229437660.919857 : dflex(108) = 3.505380 : dshear(108) = 8.687256 :
 dmax(108) = 12.192635
 esl(108) = 0.001194 : Curv(108) = 0.000007
 *** Flexural cracking has occurred (M >= Mcr) ***
 CYCLE = 109 : No. of loops for er = 110
 ed(109) = -0.002120 : er(109) = 0.040301 : el(109) = 0.002794 : et(109) =
 0.035387
 Xi(109) = 0.182933 : Sd(109) = -8.232005 : Sr(109) = 0.403305 : Sl(109) =
 0.000000 : St(109) = 0.000000
 Slc(109) = -7.231700 : Stc(109) = -0.597000
 fst(109) = 597.000000 : fsl(109) = 558.796767
 ALPHA(109) = 19.898267degs : vlt(109) = 2.763572 : glt(109) = 0.027152 : V(109)
 = 128837.722458
 *** Shear web in CRACKED state (er >= ecr) ***
 *** Shear r/f in PLASTIC state (fst >= fsty) ***
 *** Smeared long r/f in ELASTIC state (fsl < fsly_M_V) ***
 Ie(109) = 229437642.786785 : dflex(109) = 3.505392 : dshear(109) = 8.688649 :
 dmax(109) = 12.194041
 esl(109) = 0.001194 : Curv(109) = 0.000007
 *** Flexural cracking has occurred (M >= Mcr) ***
 CYCLE = 110 : No. of loops for er = 113
 ed(110) = -0.002121 : er(110) = 0.040308 : el(110) = 0.002794 : et(110) =
 0.035394
 Xi(110) = 0.182940 : Sd(110) = -8.232289 : Sr(110) = 0.403274 : Sl(110) =
 0.000000 : St(110) = 0.000000
 Slc(110) = -7.232015 : Stc(110) = -0.597000
 fst(110) = 597.000000 : fsl(110) = 558.821116
 ALPHA(110) = 19.897647degs : vlt(110) = 2.763582 : glt(110) = 0.027156 : V(110)
 = 128838.175026
 *** Shear web in CRACKED state (er >= ecr) ***
 *** Shear r/f in PLASTIC state (fst >= fsty) ***
 *** Smeared long r/f in ELASTIC state (fsl < fsly_M_V) ***
 Ie(110) = 229437624.666393 : dflex(110) = 3.505405 : dshear(110) = 8.690042 :
 dmax(110) = 12.195447
 esl(110) = 0.001194 : Curv(110) = 0.000007
 *** Flexural cracking has occurred (M >= Mcr) ***
 CYCLE = 111 : No. of loops for er = 112
 ed(111) = -0.002121 : er(111) = 0.040316 : el(111) = 0.002794 : et(111) =
 0.035400
 Xi(111) = 0.182946 : Sd(111) = -8.232574 : Sr(111) = 0.403244 : Sl(111) =
 0.000000 : St(111) = 0.000000
 Slc(111) = -7.232330 : Stc(111) = -0.597000
 fst(111) = 597.000000 : fsl(111) = 558.845458
 ALPHA(111) = 19.897028degs : vlt(111) = 2.763591 : glt(111) = 0.027161 : V(111)
 = 128838.627283

```

*** Shear web in CRACKED state (er >= ecr) ***
*** Shear r/f in PLASTIC state (fst >= fsty) ***
*** Smeared long r/f in ELASTIC state (fsl < fsly_M_V) ***
Ie(111) = 229437606.558672 : dflex(111) = 3.505418 : dshear(111) = 8.691435 :
dmax(111) = 12.196852
esl(111) = 0.001194 : Curv(111) = 0.000007
*** Flexural cracking has occurred (M >= Mcr) ***
CYCLE = 112 : No. of loops for er = 109
ed(112) = -0.002122 : er(112) = 0.040323 : el(112) = 0.002794 : et(112) =
0.035407
Xi(112) = 0.182952 : Sd(112) = -8.232859 : Sr(112) = 0.403214 : Sl(112) =
0.000000 : St(112) = 0.000000
Slc(112) = -7.232645 : Stc(112) = -0.597000
fst(112) = 597.000000 : fsl(112) = 558.869794
ALPHA(112) = 19.896409degs : vlt(112) = 2.763601 : glt(112) = 0.027165 : V(112)
= 128839.079231
*** Shear web in CRACKED state (er >= ecr) ***
*** Shear r/f in PLASTIC state (fst >= fsty) ***
*** Smeared long r/f in ELASTIC state (fsl < fsly_M_V) ***
Ie(112) = 229437588.463615 : dflex(112) = 3.505430 : dshear(112) = 8.692827 :
dmax(112) = 12.198258
esl(112) = 0.001194 : Curv(112) = 0.000007
*** Flexural cracking has occurred (M >= Mcr) ***
CYCLE = 113 : No. of loops for er = 111
ed(113) = -0.002122 : er(113) = 0.040330 : el(113) = 0.002794 : et(113) =
0.035414
Xi(113) = 0.182959 : Sd(113) = -8.233143 : Sr(113) = 0.403183 : Sl(113) =
0.000000 : St(113) = 0.000000
Slc(113) = -7.232960 : Stc(113) = -0.597000
fst(113) = 597.000000 : fsl(113) = 558.894122
ALPHA(113) = 19.895790degs : vlt(113) = 2.763611 : glt(113) = 0.027169 : V(113)
= 128839.530869
*** Shear web in CRACKED state (er >= ecr) ***
*** Shear r/f in PLASTIC state (fst >= fsty) ***
*** Smeared long r/f in ELASTIC state (fsl < fsly_M_V) ***
Ie(113) = 229437570.381213 : dflex(113) = 3.505443 : dshear(113) = 8.694220 :
dmax(113) = 12.199663
esl(113) = 0.001194 : Curv(113) = 0.000007
*** Flexural cracking has occurred (M >= Mcr) ***
CYCLE = 114 : No. of loops for er = 111
ed(114) = -0.002123 : er(114) = 0.040338 : el(114) = 0.002795 : et(114) =
0.035421
Xi(114) = 0.182965 : Sd(114) = -8.233428 : Sr(114) = 0.403153 : Sl(114) =
0.000000 : St(114) = 0.000000
Slc(114) = -7.233275 : Stc(114) = -0.597000
fst(114) = 597.000000 : fsl(114) = 558.918444
ALPHA(114) = 19.895171degs : vlt(114) = 2.763620 : glt(114) = 0.027174 : V(114)
= 128839.982197
*** Shear web in CRACKED state (er >= ecr) ***
*** Shear r/f in PLASTIC state (fst >= fsty) ***
*** Smeared long r/f in ELASTIC state (fsl < fsly_M_V) ***
Ie(114) = 229437552.311459 : dflex(114) = 3.505455 : dshear(114) = 8.695613 :
dmax(114) = 12.201068
esl(114) = 0.001194 : Curv(114) = 0.000007
*** Flexural cracking has occurred (M >= Mcr) ***
CYCLE = 115 : No. of loops for er = 109
ed(115) = -0.002123 : er(115) = 0.040345 : el(115) = 0.002795 : et(115) =
0.035428
Xi(115) = 0.182971 : Sd(115) = -8.233712 : Sr(115) = 0.403123 : Sl(115) =
0.000000 : St(115) = 0.000000
Slc(115) = -7.233590 : Stc(115) = -0.597000

```

```

fst(115) = 597.000000 : fsl(115) = 558.942758
ALPHA(115) = 19.894552degs : vlt(115) = 2.763630 : glt(115) = 0.027178 : V(115)
= 128840.433216
*** Shear web in CRACKED state (er >= ecr) ***
*** Shear r/f in PLASTIC state (fst >= fsty) ***
*** Smeared long r/f in ELASTIC state (fsl < fsly_M_V) ***
Ie(115) = 229437534.254346 : dflex(115) = 3.505468 : dshear(115) = 8.697006 :
dmax(115) = 12.202474
esl(115) = 0.001194 : Curv(115) = 0.000007
*** Flexural cracking has occurred (M >= Mcr) ***
CYCLE = 116 : No. of loops for er = 109
ed(116) = -0.002124 : er(116) = 0.040353 : el(116) = 0.002795 : et(116) =
0.035434
Xi(116) = 0.182978 : Sd(116) = -8.233997 : Sr(116) = 0.403093 : Sl(116) =
0.000000 : St(116) = 0.000000
Slc(116) = -7.233904 : Stc(116) = -0.597000
fst(116) = 597.000000 : fsl(116) = 558.967066
ALPHA(116) = 19.893934degs : vlt(116) = 2.763640 : glt(116) = 0.027182 : V(116)
= 128840.883926
*** Shear web in CRACKED state (er >= ecr) ***
*** Shear r/f in PLASTIC state (fst >= fsty) ***
*** Smeared long r/f in ELASTIC state (fsl < fsly_M_V) ***
Ie(116) = 229437516.209865 : dflex(116) = 3.505480 : dshear(116) = 8.698398 :
dmax(116) = 12.203879
esl(116) = 0.001194 : Curv(116) = 0.000007
*** Flexural cracking has occurred (M >= Mcr) ***

#####Max Shear Cycle #####
CYCLE = 117 : No. of loops for er = 107
ed(117) = -0.002124 : er(117) = 0.040360 : el(117) = 0.002795 : et(117) =
0.035441
Xi(117) = 0.182984 : Sd(117) = -8.234281 : Sr(117) = 0.403062 : Sl(117) =
0.000000 : St(117) = 0.000000
Slc(117) = -7.234219 : Stc(117) = -0.597000
fst(117) = 597.000000 : fsl(117) = 558.991366
ALPHA(117) = 19.893315degs : vlt(117) = 2.763649 : glt(117) = 0.027187 : V(117)
= 128841.334327
*** Shear web in CRACKED state (er >= ecr) ***
*** Shear r/f in PLASTIC state (fst >= fsty) ***
*** Smeared long r/f in ELASTIC state (fsl < fsly_M_V) ***
Ie(117) = 229437498.178008 : dflex(117) = 3.505493 : dshear(117) = 8.699791 :
dmax(117) = 12.205284
esl(117) = 0.001194 : Curv(117) = 0.000007
*** Flexural cracking has occurred (M >= Mcr) ***

#####Max Shear Cycle #####
CYCLE = 118 : No. of loops for er = 27
ed(118) = -0.002125 : er(118) = 0.040369 : el(118) = 0.002795 : et(118) =
0.035449
Xi(118) = 0.182986 : Sd(118) = -8.234356 : Sr(118) = 0.403026 : Sl(118) =
0.000000 : St(118) = 0.000000
Slc(118) = -7.234330 : Stc(118) = -0.597000
fst(118) = 597.000000 : fsl(118) = 559.000000
ALPHA(118) = 19.892890degs : vlt(118) = 2.763613 : glt(118) = 0.027192 : V(118)
= 128839.615603
*** Shear web in CRACKED state (er >= ecr) ***
*** Shear r/f in PLASTIC state (fst >= fsty) ***
*** Smeared long r/f in PLASTIC state (fsl >= fsly_M_V) ***

```


Ie(118) = 229437566.988712 : dflex(118) = 3.505445 : dshear(118) = 8.701570 :
 dmax(118) = 12.207015
 esl(118) = 0.001194 : Curv(118) = 0.000007
 *** Flexural cracking has occurred (M >= Mcr) ***
 CYCLE = 119 : No. of loops for er = 133
 ed(119) = -0.002375 : er(119) = 0.042012 : el(119) = 0.002773 : et(119) =
 0.036865
 Xi(119) = 0.191811 : Sd(119) = -8.170579 : Sr(119) = 0.396491 : Sl(119) =
 0.000000 : St(119) = 0.000000
 Slc(119) = -7.177089 : Stc(119) = -0.597000
 fst(119) = 597.000000 : fsl(119) = 554.576908
 ALPHA(119) = 19.909662degs : vlt(119) = 2.743042 : glt(119) = 0.028424 : V(119)
 = 127880.614275
 *** Shear web in CRACKED state (er >= ecr) ***
 *** Shear r/f in PLASTIC state (fst >= fsty) ***
 *** Smeared long r/f in ELASTIC state (fsl < fsly_M_V) ***
 Ie(119) = 229476541.280470 : dflex(119) = 3.478762 : dshear(119) = 9.095683 :
 dmax(119) = 12.574445
 esl(119) = 0.001185 : Curv(119) = 0.000007
 *** Flexural cracking has occurred (M >= Mcr) ***
 CYCLE = 120 : No. of loops for er = 130
 ed(120) = -0.002625 : er(120) = 0.041257 : el(120) = 0.002658 : et(120) =
 0.035974
 Xi(120) = 0.207170 : Sd(120) = -7.877330 : Sr(120) = 0.399452 : Sl(120) =
 0.000000 : St(120) = 0.000000
 Slc(120) = -6.880878 : Stc(120) = -0.597000
 fst(120) = 597.000000 : fsl(120) = 531.688605
 ALPHA(120) = 20.302368degs : vlt(120) = 2.693418 : glt(120) = 0.028560 : V(120)
 = 125567.151470
 *** Shear web in CRACKED state (er >= ecr) ***
 *** Shear r/f in PLASTIC state (fst >= fsty) ***
 *** Smeared long r/f in ELASTIC state (fsl < fsly_M_V) ***
 Ie(120) = 229575535.188471 : dflex(120) = 3.414355 : dshear(120) = 9.139096 :
 dmax(120) = 12.553451
 esl(120) = 0.001163 : Curv(120) = 0.000007
 *** Flexural cracking has occurred (M >= Mcr) ***
 CYCLE = 121 : No. of loops for er = 130
 ed(121) = -0.002875 : er(121) = 0.038910 : el(121) = 0.002484 : et(121) =
 0.033551
 Xi(121) = 0.227923 : Sd(121) = -7.436087 : Sr(121) = 0.409130 : Sl(121) =
 0.000000 : St(121) = 0.000000
 Slc(121) = -6.429957 : Stc(121) = -0.597000
 fst(121) = 597.000000 : fsl(121) = 496.845724
 ALPHA(121) = 20.984580degs : vlt(121) = 2.623168 : glt(121) = 0.027942 : V(121)
 = 122292.091672
 *** Shear web in CRACKED state (er >= ecr) ***
 *** Shear r/f in PLASTIC state (fst >= fsty) ***
 *** Smeared long r/f in ELASTIC state (fsl < fsly_M_V) ***
 Ie(121) = 229728795.858685 : dflex(121) = 3.323083 : dshear(121) = 8.941570 :
 dmax(121) = 12.264653
 esl(121) = 0.001132 : Curv(121) = 0.000007
 *** Flexural cracking has occurred (M >= Mcr) ***
 CYCLE = 122 : No. of loops for er = 123
 ed(122) = -0.003125 : er(122) = 0.035640 : el(122) = 0.002274 : et(122) =
 0.030241
 Xi(122) = 0.253512 : Sd(122) = -6.907041 : Sr(122) = 0.423972 : Sl(122) =
 0.000000 : St(122) = 0.000000
 Slc(122) = -5.886070 : Stc(122) = -0.597000
 fst(122) = 597.000000 : fsl(122) = 454.819306
 ALPHA(122) = 21.912213degs : vlt(122) = 2.538183 : glt(122) = 0.026842 : V(122)
 = 118330.087999

```

*** Shear web in CRACKED state (er >= ecr) ***
*** Shear r/f in PLASTIC state (fst >= fsty) ***
*** Smeared long r/f in ELASTIC state (fsl < fsly_M_V) ***
Ie(122) = 229937602.338331 : dflex(122) = 3.212502 : dshear(122) = 8.589545 :
dmax(122) = 11.802047
esl(122) = 0.001094 : Curv(122) = 0.000007
*** Flexural cracking has occurred (M >= Mcr) ***
CYCLE = 123 : No. of loops for er = 116
ed(123) = -0.003375 : er(123) = 0.032012 : el(123) = 0.002048 : et(123) =
0.026590
Xi(123) = 0.283242 : Sd(123) = -6.341642 : Sr(123) = 0.442673 : Sl(123) =
0.000000 : St(123) = 0.000000
Slc(123) = -5.301970 : Stc(123) = -0.597000
fst(123) = 597.000000 : fsl(123) = 409.685630
ALPHA(123) = 23.045818degs : vlt(123) = 2.443879 : glt(123) = 0.025495 : V(123)
= 113933.659801
*** Shear web in CRACKED state (er >= ecr) ***
*** Shear r/f in PLASTIC state (fst >= fsty) ***
*** Smeared long r/f in ELASTIC state (fsl < fsly_M_V) ***
Ie(123) = 230204578.338342 : dflex(123) = 3.089558 : dshear(123) = 8.158251 :
dmax(123) = 11.247809
esl(123) = 0.001052 : Curv(123) = 0.000006
*** Flexural cracking has occurred (M >= Mcr) ***
CYCLE = 124 : No. of loops for er = 106
ed(124) = -0.003625 : er(124) = 0.028405 : el(124) = 0.001822 : et(124) =
0.022959
Xi(124) = 0.316375 : Sd(124) = -5.776749 : Sr(124) = 0.464223 : Sl(124) =
0.000000 : St(124) = 0.000000
Slc(124) = -4.715526 : Stc(124) = -0.597000
fst(124) = 597.000000 : fsl(124) = 364.370816
ALPHA(124) = 24.353216degs : vlt(124) = 2.344540 : glt(124) = 0.024065 : V(124)
= 109302.477512
*** Shear web in CRACKED state (er >= ecr) ***
*** Shear r/f in PLASTIC state (fst >= fsty) ***
*** Smeared long r/f in ELASTIC state (fsl < fsly_M_V) ***
Ie(124) = 230534215.549805 : dflex(124) = 2.959735 : dshear(124) = 7.700817 :
dmax(124) = 10.660553
esl(124) = 0.001008 : Curv(124) = 0.000006
*** Flexural cracking has occurred (M >= Mcr) ***

Vu = 128841.334327
    = 128.8 kN

```

#####Analysis Completed#####

APPENDIX E
INPUT DATA FOR ANALYSIS USING VECTOR2

Beam S1-1

* * * * *
* V E C T O R *
* J O B D A T A *
* * * * *

Job Title (30 char. max.) : S1-1
Job File Name (8 char. max.) : S1-1
Date (30 char. max.) : 13 Jan 2007

STRUCTURE DATA

Structure Type : 2
File Name (8 char. max.) : S1-1

LOADING DATA

No. of Load Stages : 161
Starting Load Stage No. : 1
Load Series ID (5 char. max.) : S1-1

Load Case	File Name (8 char. max.)	Initial	Final	Factors LS-Inc	Type	Reps	C-Inc
1	S1-1	0.000000	40.000000	0.250000	1	1	0.000
2	NULL	0.000000	0.000000	0.000000	1	1	0.000
3	NULL	0.000000	0.000000	0.000000	1	1	0.000
4	NULL	0.000000	0.000000	0.000000	1	1	0.000
5	NULL	0.000000	0.000000	0.000000	1	1	0.000

ANALYSIS PARAMETERS

Analysis Mode (1-2) : 1
Seed File Name (8 char. max.) : NULL
Convergence Limit (>1.0) : 1.000010
Averaging Factor (<1.0) : 0.500
Maximum No. of Iterations : 60
Convergence Criteria (1-5) : 2
Results Files (1-4) : 2
Output Format (1-3) : 1

MATERIAL BEHAVIOUR MODELS

Concrete Compression Base Curve (0-3) : 1
Concrete Compression Post-Peak (0-3) : 1
Concrete Compression Softening (0-8) : 1
Concrete Tension Stiffening (0-6) : 1
Concrete Tension Softening (0-3) : 1
Concrete Tension Splitting (0-1) : 1
Concrete Confined Strength (0-2) : 1
Concrete Dilation (0-1) : 1
Concrete Cracking Criterion (0-4) : 1
Concrete Crack Slip Check (0-2) : 1
Concrete Crack Width Check (0-2) : 0
Concrete Bond or Adhesion (0-3) : 1
Concrete Creep and Relaxation (0-1) : 1
Concrete Hysteresis (0-2) : 1
Reinforcement Hysteresis (0-2) : 1

```

Reinforcement Dowel Action          (0-1) : 1
Reinforcement Buckling              (0-1) : 1
Element Strain Histories            (0-1) : 1
Element Slip Distortions           (0-4) : 1
Strain Rate Effects                 (0-1) : 1
Structural Damping                  (0-1) : 1
Geometric Nonlinearity             (0-1) : 1
Crack Allocation Process            (0-1) : 1

```

<<< JOB FILE NOTES>>>

```

* * * * *
*                               *
*           V e c T o r 2       *
*                               *
*   S T R U C T U R E   D A T A   *
* * * * *

```

STRUCTURAL PARAMETERS

```

Structure Title          : Enter Structure Title
Structure File Name     : S1-1
Working Units           : METRIC

No. of RC Material Types : 8
No. of Steel Material Types : 2
No. of Bond Material Types : 0
No. of Rectangular Elements : 562
No. of Quadrilateral Elements : 0
No. of Triangular Elements : 0
No. of Truss Elements : 80
No. of Linkage Elements : 0
No. of Contact Elements : 0
No. of Joints : 618
No. of Restraints : 17

```

MATERIAL SPECIFICATIONS

REINFORCED CONCRETE

=====

CONCRETE

MAT TYP	REINF CMP	f'c (MPa)	f't (MPa)	e0 (me)	Ec (MPa)	MU	Cc (u/C)	T (mm)
1	0	45.00	3.80	3.91	23000.	0.15	10.00	200.0
2	1	45.00	3.80	3.91	23000.	0.15	10.00	200.0
3	1	45.00	3.80	3.91	23000.	0.15	10.00	200.0
4	2	45.00	3.80	3.91	23000.	0.15	10.00	200.0

5	1	45.00	3.80	3.91	23000.	0.15	10.00	200.0
6	1	45.00	3.80	3.91	23000.	0.15	10.00	200.0
7	1	45.00	3.80	3.91	23000.	0.15	10.00	200.0
8	1	45.00	3.80	3.91	23000.	0.15	10.00	200.0

MAT TYP	Agg (mm)	Scrx (mm)	Scry (mm)
1	10.0	0.0	0.0
2	10.0	0.0	0.0
3	10.0	0.0	0.0
4	10.0	0.0	0.0
5	10.0	0.0	0.0
6	10.0	0.0	0.0
7	10.0	0.0	0.0
8	10.0	0.0	0.0

REINFORCEMENT COMPONENTS

MAT TYP	SRF TYP	DIR (deg)	AMNT (%)	DIA (mm)	Fy (MPa)	Fu (MPa)	Es (MPa)
2	1	90.0	0.100	4.00	597.0	658.0	200000.
3	1	90.0	0.200	4.00	597.0	658.0	200000.
4	1	90.0	0.100	4.00	597.0	658.0	200000.
	1	361.0	2.500	4.00	400.0	600.0	200000.
5	1	361.0	2.500	4.00	400.0	600.0	200000.
6	1	361.0	5.000	4.00	400.0	600.0	200000.
7	1	361.0	10.000	4.00	400.0	600.0	200000.
8	1	90.0	1.000	24.00	559.0	651.0	200000.

MAT TYP	DIR (deg)	esh (me)	Esh (MPa)	Cs (u/C)	Dep (me)
2	90.0	10.00	500.0	0.00	0.000
3	90.0	10.00	500.0	0.00	0.000
4	90.0	10.00	500.0	0.00	0.000
	361.0	10.00	500.0	0.00	0.000
5	361.0	10.00	500.0	0.00	0.000
6	361.0	10.00	500.0	0.00	0.000
7	361.0	10.00	500.0	0.00	0.000
8	90.0	10.00	500.0	0.00	0.000

STEEL
=====

MAT TYP	SRF TYP	AREA (mm2)	DIA (mm)	Fy (MPa)	Fu (MPa)	Es (MPa)
1	1	900.0	24.00	559.0	651.00	200000.
2	1	220.0	12.00	570.0	699.00	200000.

MAT TYP	esh (me)	Esh (MPa)	Cs (u/C)	Dep (me)
1	8.00	5000.0	0.00	0.000
2	8.00	5000.0	0.00	0.000

* * * * *
* V e c T o r 2 *
* L O A D D A T A *
* * * * *

LOAD CASE PARAMETERS

Structure Title (30 char. max.) : Enter Structure Title
Load Case Title (30 char. max.) : Enter load case title
Load Case File Name (8 char. max.) : S1-1
No. of Loaded Joints : 0
No. of Prescribed Support Displacements : 1
No. of Elements with Gravity Loads : 0
No. of Elements with Temperature Loads : 0
No. of Elements with Concrete Prestrain : 0
No. of Elements with Ingress Pressure : 0
No. of Element Surfaces w/ Thermal Load : 0
No. of Nodes with Lumped Masses : 0
No. of Nodes with Impulse Forces : 0
Ground Acceleration Record (0-1) : 0

JOINT LOADS

<NOTE:> UNITS: KIPS OR KN
<<<<< FORMAT >>>>>
NODE Fx Fy [#NODE d(NODE) d(Fx) d(Fy)] /
/

SUPPORT DISPLACEMENTS

<NOTE:> UNITS: MM OR IN
<<<<< FORMAT >>>>>
JNT DOF DISPL [#JNT d(JNT)] /
 617 2 -1.000 1 1/
/

GRAVITY LOADS

<NOTE:> UNITS: KG/M3

```

<<<<< FORMAT >>>>>
ELMT DENS GX GY [#ELMT d(ELMT)] [#ELMT d(ELMT)] /
/
                                TEMPERATURE LOADS
                                *****

<NOTE:> UNITS: F OR C
<<<<< FORMAT >>>>>
ELMT TEMP [#ELMT d(ELMT) d(TEMP)] [#ELMT d(ELMT) d(TEMP)] /
/
                                CONCRETE PRESTRAINS
                                *****

<NOTE:> UNITS: me
<<<<< FORMAT >>>>>
ELMT STRAIN [#ELMT d(ELMT) d(STRAIN)] [#ELMT d(ELMT) d(STRAIN)] /
/
                                INGRESS PRESSURES
                                *****

<NOTE:> UNITS: MPa
<<<<< FORMAT >>>>>
ELMT PRESSURE [#ELMT d(ELMT) d(PRS)] [#ELMT d(ELMT) d(PRS)] /
/
                                SURFACE THERMAL LOADS
                                *****

<NOTE:> UNITS: Sec, Degrees C
<<<<< FORMAT >>>>>
NODE1 NODE2 Tm1 Tp1 Tm2 Tp2 Tm3 Tp3 [#SURF d(NODE)] [#SURF d(NODE)] /
/
                                LUMPED MASSES
                                *****

<NOTE:> UNITS: kg, m/s
<<<<< FORMAT >>>>>
NODE DOF-X DOF-Y MASS GF-X GF-Y Vo-X Vo-Y [#NODE d(NODE)] /
/
                                IMPULSE FORCES
                                *****

<NOTE:> UNITS: Sec, kN
<<<<< FORMAT >>>>>
NODE DOF T1 F1 T2 F2 T3 F3 T4 F4 [#NODE d(NODE)] /
/
                                GROUND ACCELERATION
                                *****

<NOTE:> UNITS: Sec, G
<<<<< FORMAT >>>>>
TIME ACC-X ACC-Y
/

<<< LOAD FILE NOTES >>>

```


Beam S1-2

```

* * * * *
*       V E C T O R       *
*       J O B   D A T A   *
* * * * *

```

```

Job Title      (30 char. max.)      : S1-2
Job File Name  ( 8 char. max.)      : S1-2
Date           (30 char. max.)      : 13 Jan 2007

```

STRUCTURE DATA

```

-----
Structure Type                : 2
File Name      ( 8 char. max.) : S1-2

```

LOADING DATA

```

-----
No. of Load Stages           : 161
Starting Load Stage No.      : 1
Load Series ID  ( 5 char. max.) : S1-2

```

Load Case	File Name (8 char. max.)	Initial	Final	Factors LS-Inc	Type	Reps	C-Inc
1	S1-2	0.000000	40.000000	0.250000	1	1	0.000000
2	NULL	0.000000	0.000000	0.000000	1	1	0.000000
3	NULL	0.000000	0.000000	0.000000	1	1	0.000000
4	NULL	0.000000	0.000000	0.000000	1	1	0.000000
5	NULL	0.000000	0.000000	0.000000	1	1	0.000000

ANALYSIS PARAMETERS

```

-----
Analysis Mode                (1-2) : 1
Seed File Name      (8 char. max.) : NULL
Convergence Limit          (>1.0) : 1.000010
Averaging Factor          (<1.0) : 0.500
Maximum No. of Iterations                : 60
Convergence Criteria        (1-5) : 2
Results Files                (1-4) : 2
Output Format                (1-3) : 1

```

MATERIAL BEHAVIOUR MODELS

```

-----
Concrete Compression Base Curve        (0-3) : 1
Concrete Compression Post-Peak         (0-3) : 1
Concrete Compression Softening         (0-8) : 1
Concrete Tension Stiffening            (0-6) : 1
Concrete Tension Softening             (0-3) : 1
Concrete Tension Splitting             (0-1) : 1
Concrete Confined Strength              (0-2) : 1
Concrete Dilation                      (0-1) : 1
Concrete Cracking Criterion            (0-4) : 1
Concrete Crack Slip Check              (0-2) : 1
Concrete Crack Width Check             (0-2) : 0
Concrete Bond or Adhesion              (0-3) : 1
Concrete Creep and Relaxation          (0-1) : 1

```

```

Concrete Hysteresis           (0-2) : 1
Reinforcement Hysteresis     (0-2) : 1
Reinforcement Dowel Action   (0-1) : 1
Reinforcement Buckling       (0-1) : 1
Element Strain Histories     (0-1) : 1
Element Slip Distortions     (0-4) : 1
Strain Rate Effects          (0-1) : 1
Structural Damping           (0-1) : 1
Geometric Nonlinearity       (0-1) : 1
Crack Allocation Process     (0-1) : 1

```

<<< JOB FILE NOTES>>>

```

* * * * *
*
*           V e c T o r 2
*
*   S T R U C T U R E   D A T A
* * * * *

```

STRUCTURAL PARAMETERS

```

Structure Title           : Enter Structure Title
Structure File Name       : S1-2
Working Units             : METRIC

No. of RC Material Types : 8
No. of Steel Material Types : 2
No. of Bond Material Types : 0
No. of Rectangular Elements : 562
No. of Quadrilateral Elements : 0
No. of Triangular Elements : 0
No. of Truss Elements : 80
No. of Linkage Elements : 0
No. of Contact Elements : 0
No. of Joints : 618
No. of Restraints : 17

```

MATERIAL SPECIFICATIONS

REINFORCED CONCRETE
=====

CONCRETE

MAT TYP	REINF CMP	f'c (MPa)	f't (MPa)	e0 (me)	Ec (MPa)	MU	Cc (u/C)	T (mm)
1	0	45.00	3.80	3.91	23000.	0.15	10.00	200.0
2	1	45.00	3.80	3.91	23000.	0.15	10.00	200.0

3	1	45.00	3.80	3.91	23000.	0.15	10.00	200.0
4	2	45.00	3.80	3.91	23000.	0.15	10.00	200.0
5	1	45.00	3.80	3.91	23000.	0.15	10.00	200.0
6	1	45.00	3.80	3.91	23000.	0.15	10.00	200.0
7	1	45.00	3.80	3.91	23000.	0.15	10.00	200.0
8	1	45.00	3.80	3.91	23000.	0.15	10.00	200.0

MAT TYP	Agg (mm)	Scrx (mm)	Scry (mm)
1	10.0	0.0	0.0
2	10.0	0.0	0.0
3	10.0	0.0	0.0
4	10.0	0.0	0.0
5	10.0	0.0	0.0
6	10.0	0.0	0.0
7	10.0	0.0	0.0
8	10.0	0.0	0.0

REINFORCEMENT COMPONENTS

MAT TYP	SRF TYP	DIR (deg)	AMNT (%)	DIA (mm)	Fy (MPa)	Fu (MPa)	Es (MPa)
2	1	90.0	0.130	4.00	597.0	658.0	200000.
3	1	90.0	0.260	4.00	597.0	658.0	200000.
4	1	90.0	0.130	4.00	597.0	658.0	200000.
	1	361.0	2.500	4.00	400.0	600.0	200000.
5	1	361.0	2.500	4.00	400.0	600.0	200000.
6	1	361.0	5.000	4.00	400.0	600.0	200000.
7	1	361.0	10.000	4.00	400.0	600.0	200000.
8	1	90.0	1.000	24.00	559.0	651.0	200000.

MAT TYP	DIR (deg)	esh (me)	Esh (MPa)	Cs (u/C)	Dep (me)
2	90.0	10.00	500.0	0.00	0.000
3	90.0	10.00	500.0	0.00	0.000
4	90.0	10.00	500.0	0.00	0.000
	361.0	10.00	500.0	0.00	0.000
5	361.0	10.00	500.0	0.00	0.000
6	361.0	10.00	500.0	0.00	0.000
7	361.0	10.00	500.0	0.00	0.000
8	90.0	10.00	500.0	0.00	0.000

STEEL
=====

MAT TYP	SRF TYP	AREA (mm2)	DIA (mm)	Fy (MPa)	Fu (MPa)	Es (MPa)
1	1	900.0	24.00	559.0	651.00	200000.
2	1	220.0	12.00	570.0	699.00	200000.

MAT TYP	esh (me)	Esh (MPa)	Cs (u/C)	Dep (me)
1	8.00	5000.0	0.00	0.000
2	8.00	5000.0	0.00	0.000

* * * * *
* V e c T o r 2 *
* L O A D D A T A *
* * * * *

LOAD CASE PARAMETERS

Structure Title (30 char. max.) : Enter Structure Title
 Load Case Title (30 char. max.) : Enter load case title
 Load Case File Name (8 char. max.) : S1-2
 No. of Loaded Joints : 0
 No. of Prescribed Support Displacements : 1
 No. of Elements with Gravity Loads : 0
 No. of Elements with Temperature Loads : 0
 No. of Elements with Concrete Prestrain : 0
 No. of Elements with Ingress Pressure : 0
 No. of Element Surfaces w/ Thermal Load : 0
 No. of Nodes with Lumped Masses : 0
 No. of Nodes with Impulse Forces : 0
 Ground Acceleration Record (0-1) : 0

JOINT LOADS

<NOTE:> UNITS: KIPS OR KN
 <<<<< FORMAT >>>>>
 NODE Fx Fy [#NODE d(NODE) d(Fx) d(Fy)] /
 /

SUPPORT DISPLACEMENTS

<NOTE:> UNITS: MM OR IN
 <<<<< FORMAT >>>>>
 JNT DOF DISPL [#JNT d(JNT)] /
 617 2 -1.000 1 1/
 /

GRAVITY LOADS

<NOTE:> UNITS: KG/M3
 <<<<< FORMAT >>>>>
 ELMT DENS GX GY [#ELMT d(ELMT)] [#ELMT d(ELMT)] /
 /

TEMPERATURE LOADS

<NOTE:> UNITS: F OR C
<<<<< FORMAT >>>>>
ELMT TEMP [#ELMT d(ELMT) d(TEMP)] [#ELMT d(ELMT) d(TEMP)] /
/

CONCRETE PRESTRAINS

<NOTE:> UNITS: me
<<<<< FORMAT >>>>>
ELMT STRAIN [#ELMT d(ELMT) d(STRAIN)] [#ELMT d(ELMT) d(STRAIN)] /
/

INGRESS PRESSURES

<NOTE:> UNITS: MPa
<<<<< FORMAT >>>>>
ELMT PRESSURE [#ELMT d(ELMT) d(PRS)] [#ELMT d(ELMT) d(PRS)] /
/

SURFACE THERMAL LOADS

<NOTE:> UNITS: Sec, Degrees C
<<<<< FORMAT >>>>>
NODE1 NODE2 Tm1 Tp1 Tm2 Tp2 Tm3 Tp3 [#SURF d(NODE)] [#SURF d(NODE)] /
/

LUMPED MASSES

<NOTE:> UNITS: kg, m/s
<<<<< FORMAT >>>>>
NODE DOF-X DOF-Y MASS GF-X GF-Y Vo-X Vo-Y [#NODE d(NODE)] /
/

IMPULSE FORCES

<NOTE:> UNITS: Sec, kN
<<<<< FORMAT >>>>>
NODE DOF T1 F1 T2 F2 T3 F3 T4 F4 [#NODE d(NODE)] /
/

GROUND ACCELERATION

<NOTE:> UNITS: Sec, G
<<<<< FORMAT >>>>>
TIME ACC-X ACC-Y
/

<<< LOAD FILE NOTES >>>

Beam S1-3

```
* * * * *
*   V E C T O R   *
*   J O B   D A T A   *
* * * * *
```

Job Title (30 char. max.) : S1-3
Job File Name (8 char. max.) : S1-3
Date (30 char. max.) : 13 Jan 2007

STRUCTURE DATA

Structure Type : 2
File Name (8 char. max.) : S1-3

LOADING DATA

No. of Load Stages : 161
Starting Load Stage No. : 1
Load Series ID (5 char. max.) : S1-3

Load Case	File Name (8 char. max.)	Initial	Final	Factors LS-Inc	Type	Reps	C-Inc
1	S1-3	0.000000	40.000000	0.250000	1	1	0.000000
2	NULL	0.000000	0.000000	0.000000	1	1	0.000000
3	NULL	0.000000	0.000000	0.000000	1	1	0.000000
4	NULL	0.000000	0.000000	0.000000	1	1	0.000000
5	NULL	0.000000	0.000000	0.000000	1	1	0.000000

ANALYSIS PARAMETERS

Analysis Mode (1-2) : 1
Seed File Name (8 char. max.) : NULL
Convergence Limit (>1.0) : 1.000010
Averaging Factor (<1.0) : 0.500
Maximum No. of Iterations : 60
Convergence Criteria (1-5) : 2
Results Files (1-4) : 2
Output Format (1-3) : 1

MATERIAL BEHAVIOUR MODELS

Concrete Compression Base Curve (0-3) : 1
Concrete Compression Post-Peak (0-3) : 1
Concrete Compression Softening (0-8) : 1
Concrete Tension Stiffening (0-6) : 1
Concrete Tension Softening (0-3) : 1
Concrete Tension Splitting (0-1) : 1
Concrete Confined Strength (0-2) : 1
Concrete Dilation (0-1) : 1
Concrete Cracking Criterion (0-4) : 1
Concrete Crack Slip Check (0-2) : 1
Concrete Crack Width Check (0-2) : 0
Concrete Bond or Adhesion (0-3) : 1
Concrete Creep and Relaxation (0-1) : 1
Concrete Hysteresis (0-2) : 1
Reinforcement Hysteresis (0-2) : 1
Reinforcement Dowel Action (0-1) : 1
Reinforcement Buckling (0-1) : 1

Element Strain Histories (0-1) : 1
 Element Slip Distortions (0-4) : 1
 Strain Rate Effects (0-1) : 1
 Structural Damping (0-1) : 1
 Geometric Nonlinearity (0-1) : 1
 Crack Allocation Process (0-1) : 1

* * * * *
 *
 * V e c T o r 2 *
 *
 * S T R U C T U R E D A T A *
 * * * * *

STRUCTURAL PARAMETERS

Structure Title : Enter Structure Title
 Structure File Name : S1-3
 Working Units : METRIC

No. of RC Material Types : 8
 No. of Steel Material Types : 2
 No. of Bond Material Types : 0
 No. of Rectangular Elements : 562
 No. of Quadrilateral Elements : 0
 No. of Triangular Elements : 0
 No. of Truss Elements : 80
 No. of Linkage Elements : 0
 No. of Contact Elements : 0
 No. of Joints : 618
 No. of Restraints : 17

MATERIAL SPECIFICATIONS

REINFORCED CONCRETE
 =====

CONCRETE

MAT TYP	REINF CMP	f'c (MPa)	f't (MPa)	e0 (me)	Ec (MPa)	MU	Cc (u/C)	T (mm)
1	0	44.00	3.80	3.91	23000.	0.15	10.00	200.0
2	1	44.00	3.80	3.91	23000.	0.15	10.00	200.0
3	1	44.00	3.80	3.91	23000.	0.15	10.00	200.0
4	2	44.00	3.80	3.91	23000.	0.15	10.00	200.0
5	1	44.00	3.80	3.91	23000.	0.15	10.00	200.0
6	1	44.00	3.80	3.91	23000.	0.15	10.00	200.0
7	1	44.00	3.80	3.91	23000.	0.15	10.00	200.0
8	1	44.00	3.80	3.91	23000.	0.15	10.00	200.0

MAT TYP	Agg (mm)	Scrx (mm)	Scry (mm)
1	10.0	0.0	0.0
2	10.0	0.0	0.0
3	10.0	0.0	0.0
4	10.0	0.0	0.0
5	10.0	0.0	0.0
6	10.0	0.0	0.0
7	10.0	0.0	0.0
8	10.0	0.0	0.0

REINFORCEMENT COMPONENTS

MAT TYP	SRF TYP	DIR (deg)	AMNT (%)	DIA (mm)	Fy (MPa)	Fu (MPa)	Es (MPa)
2	1	90.0	0.170	4.00	597.0	658.0	200000.
3	1	90.0	0.340	4.00	597.0	658.0	200000.
4	1	90.0	0.170	4.00	597.0	658.0	200000.
	1	361.0	2.500	4.00	400.0	600.0	200000.
5	1	361.0	2.500	4.00	400.0	600.0	200000.
6	1	361.0	5.000	4.00	400.0	600.0	200000.
7	1	361.0	10.000	4.00	400.0	600.0	200000.
8	1	90.0	1.000	24.00	559.0	651.0	200000.

MAT TYP	DIR (deg)	esh (me)	Esh (MPa)	Cs (u/C)	Dep (me)
2	90.0	10.00	500.0	0.00	0.000
3	90.0	10.00	500.0	0.00	0.000
4	90.0	10.00	500.0	0.00	0.000
	361.0	10.00	500.0	0.00	0.000
5	361.0	10.00	500.0	0.00	0.000
6	361.0	10.00	500.0	0.00	0.000
7	361.0	10.00	500.0	0.00	0.000
8	90.0	10.00	500.0	0.00	0.000

STEEL
=====

MAT TYP	SRF TYP	AREA (mm2)	DIA (mm)	Fy (MPa)	Fu (MPa)	Es (MPa)
------------	------------	---------------	-------------	-------------	-------------	-------------

1	1	900.0	24.00	559.0	651.00	200000.
2	1	220.0	12.00	570.0	699.00	200000.

MAT TYP	esh (me)	Esh (MPa)	Cs (u/C)	Dep (me)
1	8.00	5000.0	0.00	0.000
2	8.00	5000.0	0.00	0.000

<<< JOB FILE NOTES>>>

```

* * * * *
*       V e c T o r 2       *
*     L O A D   D A T A     *
* * * * *

```

LOAD CASE PARAMETERS

```

Structure Title      (30 char. max.)      : Enter Structure Title
Load Case Title      (30 char. max.)      : Enter load case title
Load Case File Name  (8 char. max.)       : S1-3
No. of Loaded Joints : 0
No. of Prescribed Support Displacements  : 1
No. of Elements with Gravity Loads       : 0
No. of Elements with Temperature Loads   : 0
No. of Elements with Concrete Prestrain  : 0
No. of Elements with Ingress Pressure    : 0
No. of Element Surfaces w/ Thermal Load  : 0
No. of Nodes with Lumped Masses          : 0
No. of Nodes with Impulse Forces         : 0
Ground Acceleration Record (0-1)         : 0

```

JOINT LOADS

```

<NOTE:> UNITS: KIPS OR KN
<<<<< FORMAT >>>>>
NODE   Fx   Fy   [ #NODE d(NODE) d(Fx) d(Fy) ] /
/

```

SUPPORT DISPLACEMENTS

```

<NOTE:> UNITS: MM OR IN
<<<<< FORMAT >>>>>
JNT   DOF   DISPL   [ #JNT d(JNT) ] /
    617   2   -1.000   1   1/
/

```

GRAVITY LOADS

```

<NOTE:> UNITS: KG/M3
<<<<< FORMAT >>>>>
ELMT  DENS  GX  GY  [#ELMT d(ELMT)] [ #ELMT d(ELMT)] /
/

```

TEMPERATURE LOADS

```

<NOTE:> UNITS: F OR C

```

```

<<<<< FORMAT >>>>>
ELMT  TEMP  [ #ELMT d(ELMT) d(TEMP) ] [ #ELMT d(ELMT) d(TEMP) ] /
/

CONCRETE PRESTRAINS
*****

<NOTE:> UNITS:  me
<<<<< FORMAT >>>>>
ELMT  STRAIN  [ #ELMT d(ELMT) d(STRAIN) ] [ #ELMT d(ELMT) d(STRAIN) ] /
/

INGRESS PRESSURES
*****

<NOTE:> UNITS:  MPa
<<<<< FORMAT >>>>>
ELMT  PRESSURE  [ #ELMT d(ELMT) d(PRS) ] [ #ELMT d(ELMT) d(PRS) ] /
/

SURFACE THERMAL LOADS
*****

<NOTE:> UNITS:  Sec, Degrees C
<<<<< FORMAT >>>>>
NODE1 NODE2  Tm1 Tp1  Tm2 Tp2  Tm3 Tp3  [#SURF d(NODE)] [#SURF d(NODE)] /
/

LUMPED MASSES
*****

<NOTE:> UNITS:  kg, m/s
<<<<< FORMAT >>>>>
NODE  DOF-X  DOF-Y  MASS  GF-X  GF-Y  Vo-X  Vo-Y  [ #NODE d(NODE) ] /
/

IMPULSE FORCES
*****

<NOTE:> UNITS:  Sec, kN
<<<<< FORMAT >>>>>
NODE  DOF  T1  F1  T2  F2  T3  F3  T4  F4  [ #NODE d(NODE) ] /
/

GROUND ACCELERATION
*****

<NOTE:> UNITS:  Sec, G
<<<<< FORMAT >>>>>
TIME  ACC-X  ACC-Y
/

<<< LOAD FILE NOTES >>>

```

Beam S2-1

```
* * * * *
*   V E C T O R   *
*   J O B   D A T A   *
* * * * *
```

Job Title (30 char. max.) : S2-1
Job File Name (8 char. max.) : S2-1
Date (30 char. max.) : 12 Jan 2007

STRUCTURE DATA

Structure Type : 2
File Name (8 char. max.) : S2-1

LOADING DATA

No. of Load Stages : 161
Starting Load Stage No. : 1
Load Series ID (5 char. max.) : S2-1

Load Case	File Name (8 char. max.)	Initial	Final	Factors LS-Inc	Type	Reps	C-Inc
1	S2-1	0.000000	40.000000	0.250000	1	1	0.000000
2	NULL	0.000000	0.000000	0.000000	1	1	0.000000
3	NULL	0.000000	0.000000	0.000000	1	1	0.000000
4	NULL	0.000000	0.000000	0.000000	1	1	0.000000
5	NULL	0.000000	0.000000	0.000000	1	1	0.000000

ANALYSIS PARAMETERS

Analysis Mode (1-2) : 1
Seed File Name (8 char. max.) : NULL
Convergence Limit (>1.0) : 1.000010
Averaging Factor (<1.0) : 0.500
Maximum No. of Iterations : 60
Convergence Criteria (1-5) : 2
Results Files (1-4) : 2
Output Format (1-3) : 1

MATERIAL BEHAVIOUR MODELS

Concrete Compression Base Curve (0-3) : 1
Concrete Compression Post-Peak (0-3) : 1
Concrete Compression Softening (0-8) : 1
Concrete Tension Stiffening (0-6) : 1
Concrete Tension Softening (0-3) : 1
Concrete Tension Splitting (0-1) : 1
Concrete Confined Strength (0-2) : 1
Concrete Dilation (0-1) : 1
Concrete Cracking Criterion (0-4) : 1
Concrete Crack Slip Check (0-2) : 1
Concrete Crack Width Check (0-2) : 0
Concrete Bond or Adhesion (0-3) : 1
Concrete Creep and Relaxation (0-1) : 1
Concrete Hysteresis (0-2) : 1
Reinforcement Hysteresis (0-2) : 1
Reinforcement Dowel Action (0-1) : 1

```

Reinforcement Buckling           (0-1) : 1
Element Strain Histories         (0-1) : 1
Element Slip Distortions        (0-4) : 1
Strain Rate Effects              (0-1) : 1
Structural Damping               (0-1) : 1
Geometric Nonlinearity          (0-1) : 1
Crack Allocation Process         (0-1) : 1

```

<<< JOB FILE NOTES>>>

```

* * * * *
*
*           V e c T o r 2
*
*   S T R U C T U R E   D A T A
* * * * *

```

STRUCTURAL PARAMETERS

```

Structure Title           : Enter Structure Title
Structure File Name       : S2-1
Working Units             : METRIC

No. of RC Material Types : 8
No. of Steel Material Types : 2
No. of Bond Material Types : 0
No. of Rectangular Elements : 562
No. of Quadrilateral Elements : 0
No. of Triangular Elements : 0
No. of Truss Elements : 80
No. of Linkage Elements : 0
No. of Contact Elements : 0
No. of Joints : 618
No. of Restraints : 17

```

MATERIAL SPECIFICATIONS

REINFORCED CONCRETE
=====

CONCRETE

MAT TYP	REINF CMP	f'c (MPa)	f't (MPa)	e0 (me)	Ec (MPa)	MU	Cc (u/C)	T (mm)
1	0	56.00	4.40	4.29	26100.	0.15	10.00	200.0
2	1	56.00	4.40	4.29	26100.	0.15	10.00	200.0
3	1	56.00	4.40	4.29	26100.	0.15	10.00	200.0
4	2	56.00	4.40	4.29	26100.	0.15	10.00	200.0

5	1	56.00	4.40	4.29	26100.	0.15	10.00	200.0
6	1	56.00	4.40	4.29	26100.	0.15	10.00	200.0
7	1	56.00	4.40	4.29	26100.	0.15	10.00	200.0
8	1	56.00	4.40	4.29	26100.	0.15	10.00	200.0

MAT TYP	Agg (mm)	Scrx (mm)	Scry (mm)
1	10.0	0.0	0.0
2	10.0	0.0	0.0
3	10.0	0.0	0.0
4	10.0	0.0	0.0
5	10.0	0.0	0.0
6	10.0	0.0	0.0
7	10.0	0.0	0.0
8	10.0	0.0	0.0

REINFORCEMENT COMPONENTS

MAT TYP	SRF TYP	DIR (deg)	AMNT (%)	DIA (mm)	Fy (MPa)	Fu (MPa)	Es (MPa)
2	1	90.0	0.100	4.00	597.0	658.0	200000.
3	1	90.0	0.200	4.00	597.0	658.0	200000.
4	1	90.0	0.100	4.00	597.0	658.0	200000.
	1	361.0	2.500	4.00	400.0	600.0	200000.
5	1	361.0	2.500	4.00	400.0	600.0	200000.
6	1	361.0	5.000	4.00	400.0	600.0	200000.
7	1	361.0	10.000	4.00	400.0	600.0	200000.
8	1	90.0	1.000	28.00	560.0	662.0	200000.

MAT TYP	DIR (deg)	esh (me)	Esh (MPa)	Cs (u/C)	Dep (me)
2	90.0	10.00	500.0	0.00	0.000
3	90.0	10.00	500.0	0.00	0.000
4	90.0	10.00	500.0	0.00	0.000
	361.0	10.00	500.0	0.00	0.000
5	361.0	10.00	500.0	0.00	0.000
6	361.0	10.00	500.0	0.00	0.000
7	361.0	10.00	500.0	0.00	0.000
8	90.0	10.00	500.0	0.00	0.000

STEEL
=====

MAT TYP	SRF TYP	AREA (mm2)	DIA (mm)	Fy (MPa)	Fu (MPa)	Es (MPa)
1	1	1240.0	28.00	560.0	662.00	200000.
2	1	220.0	12.00	570.0	699.00	200000.

MAT TYP	esh (me)	Esh (MPa)	Cs (u/C)	Dep (me)
1	8.00	5000.0	0.00	0.000
2	8.00	5000.0	0.00	0.000

* * * * *
* V e c T o r 2 *
* L O A D D A T A *
* * * * *

LOAD CASE PARAMETERS

Structure Title (30 char. max.) : Enter Structure Title
Load Case Title (30 char. max.) : Enter load case title
Load Case File Name (8 char. max.) : S2-1
No. of Loaded Joints : 0
No. of Prescribed Support Displacements : 1
No. of Elements with Gravity Loads : 0
No. of Elements with Temperature Loads : 0
No. of Elements with Concrete Prestrain : 0
No. of Elements with Ingress Pressure : 0
No. of Element Surfaces w/ Thermal Load : 0
No. of Nodes with Lumped Masses : 0
No. of Nodes with Impulse Forces : 0
Ground Acceleration Record (0-1) : 0

JOINT LOADS

<NOTE:> UNITS: KIPS OR KN
<<<<< FORMAT >>>>>
NODE Fx Fy [#NODE d(NODE) d(Fx) d(Fy)] /
/

SUPPORT DISPLACEMENTS

<NOTE:> UNITS: MM OR IN
<<<<< FORMAT >>>>>
JNT DOF DISPL [#JNT d(JNT)] /
 617 2 -1.000 1 1/
/

GRAVITY LOADS

<NOTE:> UNITS: KG/M3
<<<<< FORMAT >>>>>
ELMT DENS GX GY [#ELMT d(ELMT)] [#ELMT d(ELMT)] /
/

TEMPERATURE LOADS

<NOTE:> UNITS: F OR C
<<<<< FORMAT >>>>>

```

ELMT  TEMP  [ #ELMT d(ELMT) d(TEMP) ] [ #ELMT d(ELMT) d(TEMP) ] /
/

CONCRETE PRESTRAINS
*****

<NOTE:> UNITS:  me
<<<<< FORMAT >>>>>
ELMT  STRAIN  [ #ELMT d(ELMT) d(STRAIN) ] [ #ELMT d(ELMT) d(STRAIN) ] /
/

INGRESS PRESSURES
*****

<NOTE:> UNITS:  MPa
<<<<< FORMAT >>>>>
ELMT  PRESSURE  [ #ELMT d(ELMT) d(PRS) ] [ #ELMT d(ELMT) d(PRS) ] /
/

SURFACE THERMAL LOADS
*****

<NOTE:> UNITS:  Sec, Degrees C
<<<<< FORMAT >>>>>
NODE1 NODE2  Tm1 Tp1  Tm2 Tp2  Tm3 Tp3  [#SURF d(NODE)] [#SURF d(NODE)] /
/

LUMPED MASSES
*****

<NOTE:> UNITS:  kg, m/s
<<<<< FORMAT >>>>>
NODE  DOF-X  DOF-Y  MASS  GF-X  GF-Y  Vo-X  Vo-Y  [ #NODE d(NODE) ] /
/

IMPULSE FORCES
*****

<NOTE:> UNITS:  Sec, kN
<<<<< FORMAT >>>>>
NODE  DOF  T1  F1  T2  F2  T3  F3  T4  F4  [ #NODE d(NODE) ] /
/

GROUND ACCELERATION
*****

<NOTE:> UNITS:  Sec, G
<<<<< FORMAT >>>>>
TIME  ACC-X  ACC-Y
/

<<< LOAD FILE NOTES >>>

```

Beam S2-2

```

* * * * *
*       V E C T O R       *
*     J O B   D A T A     *
* * * * *

```

```

Job Title      (30 char. max.)      : S2-2
Job File Name  ( 8 char. max.)      : S2-2
Date          (30 char. max.)      : 12 Jan 2007

```

STRUCTURE DATA

```

-----
Structure Type                : 2
File Name      ( 8 char. max.) : S2-2

```

LOADING DATA

```

-----
No. of Load Stages           : 161
Starting Load Stage No.      : 1
Load Series ID  ( 5 char. max.) : S2-2

```

Load Case	File Name (8 char. max.)	Initial	Final	Factors LS-Inc	Type	Reps	C-Inc
1	S2-2	0.000000	40.000000	0.250000	1	1	0.000000
2	NULL	0.000000	0.000000	0.000000	1	1	0.000000
3	NULL	0.000000	0.000000	0.000000	1	1	0.000000
4	NULL	0.000000	0.000000	0.000000	1	1	0.000000
5	NULL	0.000000	0.000000	0.000000	1	1	0.000000

ANALYSIS PARAMETERS

```

-----
Analysis Mode                (1-2) : 1
Seed File Name      (8 char. max.) : NULL
Convergence Limit          (>1.0) : 1.000010
Averaging Factor          (<1.0) : 0.500
Maximum No. of Iterations                : 60
Convergence Criteria        (1-5) : 2
Results Files              (1-4) : 2
Output Format              (1-3) : 1

```

MATERIAL BEHAVIOUR MODELS

```

-----
Concrete Compression Base Curve        (0-3) : 1
Concrete Compression Post-Peak         (0-3) : 1
Concrete Compression Softening         (0-8) : 1
Concrete Tension Stiffening            (0-6) : 1
Concrete Tension Softening             (0-3) : 1
Concrete Tension Splitting            (0-1) : 1
Concrete Confined Strength             (0-2) : 1
Concrete Dilation                     (0-1) : 1
Concrete Cracking Criterion            (0-4) : 1
Concrete Crack Slip Check              (0-2) : 1
Concrete Crack Width Check             (0-2) : 0
Concrete Bond or Adhesion              (0-3) : 1
Concrete Creep and Relaxation          (0-1) : 1

```



```

Concrete Hysteresis           (0-2) : 1
Reinforcement Hysteresis     (0-2) : 1
Reinforcement Dowel Action   (0-1) : 1
Reinforcement Buckling      (0-1) : 1
Element Strain Histories     (0-1) : 1
Element Slip Distortions     (0-4) : 1
Strain Rate Effects          (0-1) : 1
Structural Damping           (0-1) : 1
Geometric Nonlinearity      (0-1) : 1
Crack Allocation Process     (0-1) : 1

```

<<< JOB FILE NOTES>>>

```

* * * * *
*                               *
*           V e c T o r 2       *
*                               *
*   S T R U C T U R E   D A T A   *
* * * * *

```

STRUCTURAL PARAMETERS

```

Structure Title           : Enter Structure Title
Structure File Name       : S2-2
Working Units             : METRIC

No. of RC Material Types  :      8
No. of Steel Material Types :      2
No. of Bond Material Types :      0
No. of Rectangular Elements :    562
No. of Quadrilateral Elements :      0
No. of Triangular Elements :      0
No. of Truss Elements     :     80
No. of Linkage Elements   :      0
No. of Contact Elements   :      0
No. of Joints             :    618
No. of Restraints         :     17

```

MATERIAL SPECIFICATIONS

REINFORCED CONCRETE
=====

CONCRETE

MAT	REINF	f'c	f't	e0	Ec	MU	Cc	T
TYP	CMP	(MPa)	(MPa)	(me)	(MPa)		(u/C)	(mm)

1	0	50.00	4.08	4.00	25000.	0.15	10.00	200.0
2	1	50.00	4.08	4.00	25000.	0.15	10.00	200.0
3	1	50.00	4.08	4.00	25000.	0.15	10.00	200.0
4	2	50.00	4.08	4.00	25000.	0.15	10.00	200.0
5	1	50.00	4.08	4.00	25000.	0.15	10.00	200.0
6	1	50.00	4.08	4.00	25000.	0.15	10.00	200.0
7	1	50.00	4.08	4.00	25000.	0.15	10.00	200.0
8	1	50.00	4.08	4.00	25000.	0.15	10.00	200.0

MAT TYP	Agg (mm)	Scrx (mm)	Scry (mm)
1	10.0	0.0	0.0
2	10.0	0.0	0.0
3	10.0	0.0	0.0
4	10.0	0.0	0.0
5	10.0	0.0	0.0
6	10.0	0.0	0.0
7	10.0	0.0	0.0
8	10.0	0.0	0.0

REINFORCEMENT COMPONENTS

MAT TYP	SRF TYP	DIR (deg)	AMNT (%)	DIA (mm)	Fy (MPa)	Fu (MPa)	Es (MPa)
2	1	90.0	0.130	4.00	597.0	658.0	200000.
3	1	90.0	0.260	4.00	597.0	658.0	200000.
4	1	90.0	0.130	4.00	597.0	658.0	200000.
	1	361.0	2.500	4.00	400.0	600.0	200000.
5	1	361.0	2.500	4.00	400.0	600.0	200000.
6	1	361.0	5.000	4.00	400.0	600.0	200000.
7	1	361.0	10.000	4.00	400.0	600.0	200000.
8	1	90.0	1.000	28.00	560.0	662.0	200000.

MAT TYP	DIR (deg)	esh (me)	Esh (MPa)	Cs (u/C)	Dep (me)
2	90.0	10.00	500.0	0.00	0.000
3	90.0	10.00	500.0	0.00	0.000
4	90.0	10.00	500.0	0.00	0.000
	361.0	10.00	500.0	0.00	0.000
5	361.0	10.00	500.0	0.00	0.000
6	361.0	10.00	500.0	0.00	0.000
7	361.0	10.00	500.0	0.00	0.000

8 90.0 10.00 500.0 0.00 0.000

STEEL
=====

MAT TYP	SRF TYP	AREA (mm2)	DIA (mm)	Fy (MPa)	Fu (MPa)	Es (MPa)
1	1	1240.0	28.00	560.0	662.00	200000.
2	1	220.0	12.00	570.0	699.00	200000.

MAT TYP	esh (me)	Esh (MPa)	Cs (u/C)	Dep (me)
1	8.00	5000.0	0.00	0.000
2	8.00	5000.0	0.00	0.000

* * * * *
 * V e c T o r 2 *
 * L O A D D A T A *
 * * * * *

LOAD CASE PARAMETERS

Structure Title (30 char. max.) : Enter Structure Title
 Load Case Title (30 char. max.) : Enter load case title
 Load Case File Name (8 char. max.) : S2-2
 No. of Loaded Joints : 0
 No. of Prescribed Support Displacements : 1
 No. of Elements with Gravity Loads : 0
 No. of Elements with Temperature Loads : 0
 No. of Elements with Concrete Prestrain : 0
 No. of Elements with Ingress Pressure : 0
 No. of Element Surfaces w/ Thermal Load : 0
 No. of Nodes with Lumped Masses : 0
 No. of Nodes with Impulse Forces : 0
 Ground Acceleration Record (0-1) : 0

JOINT LOADS

<NOTE:> UNITS: KIPS OR KN
 <<<<< FORMAT >>>>>
 NODE Fx Fy [#NODE d(NODE) d(Fx) d(Fy)] /
 /

SUPPORT DISPLACEMENTS

<NOTE:> UNITS: MM OR IN
 <<<<< FORMAT >>>>>
 JNT DOF DISPL [#JNT d(JNT)] /
 617 2 -1.000 1 1/
 /

GRAVITY LOADS

<NOTE:> UNITS: KG/M3
 <<<<< FORMAT >>>>>

```

ELMT DENS GX GY [#ELMT d(ELMT)] [#ELMT d(ELMT)] /
/
TEMPERATURE LOADS
*****

<NOTE:> UNITS: F OR C
<<<<< FORMAT >>>>>
ELMT TEMP [#ELMT d(ELMT) d(TEMP)] [#ELMT d(ELMT) d(TEMP)] /
/
CONCRETE PRESTRAINS
*****

<NOTE:> UNITS: me
<<<<< FORMAT >>>>>
ELMT STRAIN [#ELMT d(ELMT) d(STRAIN)] [#ELMT d(ELMT) d(STRAIN)] /
/
INGRESS PRESSURES
*****

<NOTE:> UNITS: MPa
<<<<< FORMAT >>>>>
ELMT PRESSURE [#ELMT d(ELMT) d(PRS)] [#ELMT d(ELMT) d(PRS)] /
/
SURFACE THERMAL LOADS
*****

<NOTE:> UNITS: Sec, Degrees C
<<<<< FORMAT >>>>>
NODE1 NODE2 Tm1 Tp1 Tm2 Tp2 Tm3 Tp3 [#SURF d(NODE)] [#SURF d(NODE)] /
/
LUMPED MASSES
*****

<NOTE:> UNITS: kg, m/s
<<<<< FORMAT >>>>>
NODE DOF-X DOF-Y MASS GF-X GF-Y Vo-X Vo-Y [#NODE d(NODE)] /
/
IMPULSE FORCES
*****

<NOTE:> UNITS: Sec, kN
<<<<< FORMAT >>>>>
NODE DOF T1 F1 T2 F2 T3 F3 T4 F4 [#NODE d(NODE)] /
/
GROUND ACCELERATION
*****

<NOTE:> UNITS: Sec, G
<<<<< FORMAT >>>>>
TIME ACC-X ACC-Y
/

<<< LOAD FILE NOTES >>>

```

Beam S2-3

```

* * * * *
*       V E C T O R       *
*     J O B   D A T A     *
* * * * *

```

```

Job Title      (30 char. max.)      : S2-3
Job File Name  ( 8 char. max.)      : S2-3
Date          (30 char. max.)      : 13 Jan 2007

```

STRUCTURE DATA

```

Structure Type      : 2
File Name          ( 8 char. max.) : S2-3

```

LOADING DATA

```

No. of Load Stages      : 161
Starting Load Stage No. : 1
Load Series ID   ( 5 char. max.) : S2-3

```

Load Case	File Name (8 char. max.)	Initial	Final	Factors LS-Inc	Type	Reps	C-Inc
1	S2-3	0.000000	40.000000	0.250000	1	1	0.000000
2	NULL	0.000000	0.000000	0.000000	1	1	0.000000
3	NULL	0.000000	0.000000	0.000000	1	1	0.000000
4	NULL	0.000000	0.000000	0.000000	1	1	0.000000
5	NULL	0.000000	0.000000	0.000000	1	1	0.000000

ANALYSIS PARAMETERS

```

Analysis Mode      (1-2) : 1
Seed File Name    (8 char. max.) : NULL
Convergence Limit (>1.0) : 1.000010
Averaging Factor  (<1.0) : 0.500
Maximum No. of Iterations : 60
Convergence Criteria (1-5) : 2
Results Files     (1-4) : 2
Output Format      (1-3) : 1

```

MATERIAL BEHAVIOUR MODELS

```

Concrete Compression Base Curve (0-3) : 1
Concrete Compression Post-Peak  (0-3) : 1
Concrete Compression Softening  (0-8) : 1
Concrete Tension Stiffening     (0-6) : 1
Concrete Tension Softening      (0-3) : 1
Concrete Tension Splitting      (0-1) : 1
Concrete Confined Strength      (0-2) : 1
Concrete Dilation                (0-1) : 1
Concrete Cracking Criterion      (0-4) : 1
Concrete Crack Slip Check       (0-2) : 1
Concrete Crack Width Check      (0-2) : 0
Concrete Bond or Adhesion       (0-3) : 1
Concrete Creep and Relaxation    (0-1) : 1

```

Concrete Hysteresis	(0-2) : 1
Reinforcement Hysteresis	(0-2) : 1
Reinforcement Dowel Action	(0-1) : 1
Reinforcement Buckling	(0-1) : 1
Element Strain Histories	(0-1) : 1
Element Slip Distortions	(0-4) : 1
Strain Rate Effects	(0-1) : 1
Structural Damping	(0-1) : 1
Geometric Nonlinearity	(0-1) : 1
Crack Allocation Process	(0-1) : 1

<<< JOB FILE NOTES>>>

```

* * * * *
*                               *
*           V e c T o r 2       *
*                               *
*   S T R U C T U R E   D A T A   *
* * * * *

```

STRUCTURAL PARAMETERS

Structure Title	:	Enter Structure Title
Structure File Name	:	S2-3
Working Units	:	METRIC
No. of RC Material Types	:	8
No. of Steel Material Types	:	2
No. of Bond Material Types	:	0
No. of Rectangular Elements	:	562
No. of Quadrilateral Elements	:	0
No. of Triangular Elements	:	0
No. of Truss Elements	:	80
No. of Linkage Elements	:	0
No. of Contact Elements	:	0
No. of Joints	:	618
No. of Restraints	:	17

MATERIAL SPECIFICATIONS

REINFORCED CONCRETE
=====

CONCRETE

MAT	REINF	f'c	f't	e0	Ec	MU	Cc	T
TYP	CMP	(MPa)	(MPa)	(me)	(MPa)		(u/C)	(mm)

1	0	50.00	4.08	4.00	25000.	0.15	10.00	200.0
2	1	50.00	4.08	4.00	25000.	0.15	10.00	200.0
3	1	50.00	4.08	4.00	25000.	0.15	10.00	200.0
4	2	50.00	4.08	4.00	25000.	0.15	10.00	200.0
5	1	50.00	4.08	4.00	25000.	0.15	10.00	200.0
6	1	50.00	4.08	4.00	25000.	0.15	10.00	200.0
7	1	50.00	4.08	4.00	25000.	0.15	10.00	200.0
8	1	50.00	4.08	4.00	25000.	0.15	10.00	200.0

MAT TYP	Agg (mm)	Scrx (mm)	Scry (mm)
1	10.0	0.0	0.0
2	10.0	0.0	0.0
3	10.0	0.0	0.0
4	10.0	0.0	0.0
5	10.0	0.0	0.0
6	10.0	0.0	0.0
7	10.0	0.0	0.0
8	10.0	0.0	0.0

REINFORCEMENT COMPONENTS

MAT TYP	SRF TYP	DIR (deg)	AMNT (%)	DIA (mm)	Fy (MPa)	Fu (MPa)	Es (MPa)
2	1	90.0	0.170	4.00	597.0	658.0	200000.
3	1	90.0	0.340	4.00	597.0	658.0	200000.
4	1	90.0	0.170	4.00	597.0	658.0	200000.
	1	361.0	2.500	4.00	400.0	600.0	200000.
5	1	361.0	2.500	4.00	400.0	600.0	200000.
6	1	361.0	5.000	4.00	400.0	600.0	200000.
7	1	361.0	10.000	4.00	400.0	600.0	200000.
8	1	90.0	1.000	28.00	560.0	662.0	200000.

MAT TYP	DIR (deg)	esh (me)	Esh (MPa)	Cs (u/C)	Dep (me)
2	90.0	10.00	500.0	0.00	0.000
3	90.0	10.00	500.0	0.00	0.000
4	90.0	10.00	500.0	0.00	0.000
	361.0	10.00	500.0	0.00	0.000
5	361.0	10.00	500.0	0.00	0.000
6	361.0	10.00	500.0	0.00	0.000
7	361.0	10.00	500.0	0.00	0.000

8 90.0 10.00 500.0 0.00 0.000

STEEL
=====

MAT TYP	SRF TYP	AREA (mm2)	DIA (mm)	Fy (MPa)	Fu (MPa)	Es (MPa)
1	1	1240.0	28.00	560.0	662.00	200000.
2	1	220.0	12.00	570.0	699.00	200000.

MAT TYP	esh (me)	Esh (MPa)	Cs (u/C)	Dep (me)
1	8.00	5000.0	0.00	0.000
2	8.00	5000.0	0.00	0.000

* * * * *
* V e c T o r 2 *
* L O A D D A T A *
* * * * *

LOAD CASE PARAMETERS

Structure Title (30 char. max.) : Enter Structure Title
 Load Case Title (30 char. max.) : Enter load case title
 Load Case File Name (8 char. max.) : S2-3
 No. of Loaded Joints : 0
 No. of Prescribed Support Displacements : 1
 No. of Elements with Gravity Loads : 0
 No. of Elements with Temperature Loads : 0
 No. of Elements with Concrete Prestrain : 0
 No. of Elements with Ingress Pressure : 0
 No. of Element Surfaces w/ Thermal Load : 0
 No. of Nodes with Lumped Masses : 0
 No. of Nodes with Impulse Forces : 0
 Ground Acceleration Record (0-1) : 0

JOINT LOADS

<NOTE:> UNITS: KIPS OR KN
 <<<<< FORMAT >>>>>
 NODE Fx Fy [#NODE d(NODE) d(Fx) d(Fy)] /
 /

SUPPORT DISPLACEMENTS

<NOTE:> UNITS: MM OR IN
 <<<<< FORMAT >>>>>
 JNT DOF DISPL [#JNT d(JNT)] /
 617 2 -1.000 1 1/
 /

GRAVITY LOADS

<NOTE:> UNITS: KG/M3
 <<<<< FORMAT >>>>>
 ELMT DENS GX GY [#ELMT d(ELMT)] [#ELMT d(ELMT)] /


```

/
                                TEMPERATURE LOADS
                                *****

<NOTE:> UNITS: F OR C
<<<<< FORMAT >>>>>
ELMT  TEMP  [ #ELMT d(ELMT) d(TEMP) ] [ #ELMT d(ELMT) d(TEMP) ] /
/

                                CONCRETE PRESTRAINS
                                *****

<NOTE:> UNITS: me
<<<<< FORMAT >>>>>
ELMT  STRAIN  [ #ELMT d(ELMT) d(STRAIN) ] [ #ELMT d(ELMT) d(STRAIN) ] /
/

                                INGRESS PRESSURES
                                *****

<NOTE:> UNITS: MPa
<<<<< FORMAT >>>>>
ELMT  PRESSURE  [ #ELMT d(ELMT) d(PRS) ] [ #ELMT d(ELMT) d(PRS) ] /
/

                                SURFACE THERMAL LOADS
                                *****

<NOTE:> UNITS: Sec, Degrees C
<<<<< FORMAT >>>>>
NODE1 NODE2  Tm1 Tp1  Tm2 Tp2  Tm3 Tp3  [#SURF d(NODE)] [#SURF d(NODE)] /
/

                                LUMPED MASSES
                                *****

<NOTE:> UNITS: kg, m/s
<<<<< FORMAT >>>>>
NODE  DOF-X  DOF-Y  MASS  GF-X  GF-Y  Vo-X  Vo-Y  [ #NODE d(NODE) ] /
/

                                IMPULSE FORCES
                                *****

<NOTE:> UNITS: Sec, kN
<<<<< FORMAT >>>>>
NODE  DOF  T1  F1  T2  F2  T3  F3  T4  F4  [ #NODE d(NODE) ] /
/

                                GROUND ACCELERATION
                                *****

<NOTE:> UNITS: Sec, G
<<<<< FORMAT >>>>>
TIME  ACC-X  ACC-Y
/

<<< LOAD FILE NOTES >>>

```

Beam S3-1

```
* * * * *
*       V E C T O R       *
*     J O B   D A T A     *
* * * * *
```

```
Job Title      (30 char. max.)      : S3-1
Job File Name  ( 8 char. max.)      : S3-1
Date           (30 char. max.)      : 12 Jan 2007
```

STRUCTURE DATA

```
-----
Structure Type                : 2
File Name      ( 8 char. max.) : S3-1
```

LOADING DATA

```
-----
No. of Load Stages           : 161
Starting Load Stage No.      : 1
Load Series ID ( 5 char. max.) : S3-1
```

Load Case	File Name (8 char. max.)	Initial	Final	Factors LS-Inc	Type	Reps	C-Inc
1	S3-1	0.000000	40.000000	0.250000	1	1	0.000000
2	NULL	0.000000	0.000000	0.000000	1	1	0.000000
3	NULL	0.000000	0.000000	0.000000	1	1	0.000000
4	NULL	0.000000	0.000000	0.000000	1	1	0.000000
5	NULL	0.000000	0.000000	0.000000	1	1	0.000000

ANALYSIS PARAMETERS

```
-----
Analysis Mode                (1-2) : 1
Seed File Name (8 char. max.) : NULL
Convergence Limit            (>1.0) : 1.000010
Averaging Factor             (<1.0) : 0.500
Maximum No. of Iterations    : 60
Convergence Criteria         (1-5) : 2
Results Files                 (1-4) : 2
Output Format                  (1-3) : 1
```

MATERIAL BEHAVIOUR MODELS

```
-----
Concrete Compression Base Curve (0-3) : 1
Concrete Compression Post-Peak (0-3) : 1
Concrete Compression Softening (0-8) : 1
Concrete Tension Stiffening     (0-6) : 1
Concrete Tension Softening      (0-3) : 1
Concrete Tension Splitting      (0-1) : 1
Concrete Confined Strength      (0-2) : 1
Concrete Dilation                (0-1) : 1
Concrete Cracking Criterion      (0-4) : 1
Concrete Crack Slip Check        (0-2) : 1
Concrete Crack Width Check       (0-2) : 0
Concrete Bond or Adhesion        (0-3) : 1
Concrete Creep and Relaxation    (0-1) : 1
Concrete Hysteresis              (0-2) : 1
```

Reinforcement Hysteresis (0-2) : 1
 Reinforcement Dowel Action (0-1) : 1
 Reinforcement Buckling (0-1) : 1
 Element Strain Histories (0-1) : 1
 Element Slip Distortions (0-4) : 1
 Strain Rate Effects (0-1) : 1
 Structural Damping (0-1) : 1
 Geometric Nonlinearity (0-1) : 1
 Crack Allocation Process (0-1) : 1

<<< JOB FILE NOTES>>>

```

* * * * *
*                               *
*           V e c T o r 2       *
*                               *
*   S T R U C T U R E   D A T A   *
* * * * *
  
```

STRUCTURAL PARAMETERS

Structure Title : Enter Structure Title
 Structure File Name : S3-1
 Working Units : METRIC

No. of RC Material Types : 8
 No. of Steel Material Types : 2
 No. of Bond Material Types : 0
 No. of Rectangular Elements : 562
 No. of Quadrilateral Elements : 0
 No. of Triangular Elements : 0
 No. of Truss Elements : 80
 No. of Linkage Elements : 0
 No. of Contact Elements : 0
 No. of Joints : 618
 No. of Restraints : 17

MATERIAL SPECIFICATIONS

REINFORCED CONCRETE
 =====

CONCRETE

MAT TYP	REINF CMP	f 'c (MPa)	f 't (MPa)	e0 (me)	Ec (MPa)	MU	Cc (u/C)	T (mm)
1	0	49.00	4.02	3.92	25000.	0.15	10.00	200.0
2	1	49.00	4.02	3.92	25000.	0.15	10.00	200.0
3	1	49.00	4.02	3.92	25000.	0.15	10.00	200.0

4	1	49.00	4.02	3.92	25000.	0.15	10.00	200.0
5	0	49.00	4.02	3.92	25000.	0.15	10.00	200.0
6	0	49.00	4.02	3.92	25000.	0.15	10.00	200.0
7	1	49.00	4.02	3.92	25000.	0.15	10.00	200.0
8	1	49.00	4.02	3.92	25000.	0.15	10.00	200.0

MAT TYP	Agg (mm)	Scrx (mm)	Scry (mm)
1	10.0	0.0	0.0
2	10.0	0.0	0.0
3	10.0	0.0	0.0
4	10.0	0.0	0.0
5	10.0	0.0	0.0
6	10.0	0.0	0.0
7	10.0	0.0	0.0
8	10.0	0.0	0.0

REINFORCEMENT COMPONENTS

MAT TYP	SRF TYP	DIR (deg)	AMNT (%)	DIA (mm)	Fy (MPa)	Fu (MPa)	Es (MPa)
2	1	90.0	0.100	4.00	597.0	658.0	200000.
3	1	90.0	0.200	4.00	597.0	658.0	200000.
4	1	90.0	0.100	4.00	597.0	658.0	200000.
7	1	361.0	10.000	4.00	400.0	600.0	200000.
8	1	90.0	1.000	32.00	571.0	664.0	200000.

MAT TYP	DIR (deg)	esh (me)	Esh (MPa)	Cs (u/C)	Dep (me)
2	90.0	10.00	500.0	0.00	0.000
3	90.0	10.00	500.0	0.00	0.000
4	90.0	10.00	500.0	0.00	0.000
7	361.0	10.00	500.0	0.00	0.000
8	90.0	10.00	500.0	0.00	0.000

STEEL

=====

MAT TYP	SRF TYP	AREA (mm2)	DIA (mm)	Fy (MPa)	Fu (MPa)	Es (MPa)
1	1	1600.0	32.00	571.0	664.00	200000.
2	1	400.0	16.00	563.0	669.00	200000.

MAT TYP	esh (me)	Esh (MPa)	Cs (u/C)	Dep (me)
1	8.00	5000.0	0.00	0.000
2	8.00	5000.0	0.00	0.000

* * * * *

* V e c T o r 2 *
 * L O A D D A T A *
 * * * * * * * * * * * * *

LOAD CASE PARAMETERS

Structure Title (30 char. max.) : Enter Structure Title
 Load Case Title (30 char. max.) : Enter load case title
 Load Case File Name (8 char. max.) : S3-1
 No. of Loaded Joints : 0
 No. of Prescribed Support Displacements : 1
 No. of Elements with Gravity Loads : 0
 No. of Elements with Temperature Loads : 0
 No. of Elements with Concrete Prestrain : 0
 No. of Elements with Ingress Pressure : 0
 No. of Element Surfaces w/ Thermal Load : 0
 No. of Nodes with Lumped Masses : 0
 No. of Nodes with Impulse Forces : 0
 Ground Acceleration Record (0-1) : 0

JOINT LOADS

<NOTE:> UNITS: KIPS OR KN
 <<<<< FORMAT >>>>>
 NODE Fx Fy [#NODE d(NODE) d(Fx) d(Fy)] /
 /

SUPPORT DISPLACEMENTS

<NOTE:> UNITS: MM OR IN
 <<<<< FORMAT >>>>>
 JNT DOF DISPL [#JNT d(JNT)] /
 617 2 -1.000 1 1/
 /

GRAVITY LOADS

<NOTE:> UNITS: KG/M3
 <<<<< FORMAT >>>>>
 ELMT DENS GX GY [#ELMT d(ELMT)] [#ELMT d(ELMT)] /
 /

TEMPERATURE LOADS

<NOTE:> UNITS: F OR C
 <<<<< FORMAT >>>>>
 ELMT TEMP [#ELMT d(ELMT) d(TEMP)] [#ELMT d(ELMT) d(TEMP)] /
 /

CONCRETE PRESTRAINS

<NOTE:> UNITS: me
 <<<<< FORMAT >>>>>
 ELMT STRAIN [#ELMT d(ELMT) d(STRAIN)] [#ELMT d(ELMT) d(STRAIN)] /
 /

INGRESS PRESSURES

<NOTE:> UNITS: MPa
 <<<<< FORMAT >>>>>
 ELMT PRESSURE [#ELMT d(ELMT) d(PRS)] [#ELMT d(ELMT) d(PRS)] /
 /

SURFACE THERMAL LOADS

<NOTE:> UNITS: Sec, Degrees C

```

<<<<< FORMAT >>>>>
NODE1 NODE2 Tm1 Tp1 Tm2 Tp2 Tm3 Tp3 [#SURF d(NODE)] [#SURF d(NODE)] /
/
                                LUMPED MASSES
                                *****

<NOTE:> UNITS: kg, m/s
<<<<< FORMAT >>>>>
NODE DOF-X DOF-Y MASS GF-X GF-Y Vo-X Vo-Y [ #NODE d(NODE) ] /
/
                                IMPULSE FORCES
                                *****

<NOTE:> UNITS: Sec, kN
<<<<< FORMAT >>>>>
NODE DOF T1 F1 T2 F2 T3 F3 T4 F4 [ #NODE d(NODE) ] /
/
                                GROUND ACCELERATION
                                *****

<NOTE:> UNITS: Sec, G
<<<<< FORMAT >>>>>
TIME ACC-X ACC-Y
/

<<< LOAD FILE NOTES >>>

```

Beam S3-2

```

* * * * *
*   V E C T O R   *
*   J O B   D A T A   *
* * * * *

```

```

Job Title      (30 char. max.)      : S3-2
Job File Name  ( 8 char. max.)      : S3-2
Date           (30 char. max.)      : 12 Jan 2007

```

STRUCTURE DATA

```

-----
Structure Type                : 2
File Name      ( 8 char. max.) : S3-2

```

LOADING DATA

```

-----
No. of Load Stages           : 161
Starting Load Stage No.      : 1
Load Series ID ( 5 char. max.) : S3-2

```

Load Case	File Name (8 char. max.)	Initial	Final	Factors LS-Inc	Type	Reps	C-Inc
1	S3-2	0.000000	40.000000	0.250000	1	1	0.000000
2	Case2	0.000000	0.000000	0.000000	1	1	0.000000
3	NULL	0.000000	0.000000	0.000000	1	1	0.000000
4	NULL	0.000000	0.000000	0.000000	1	1	0.000000
5	NULL	0.000000	0.000000	0.000000	1	1	0.000000

ANALYSIS PARAMETERS

```

-----
Analysis Mode                (1-2) : 1
Seed File Name (8 char. max.) : NULL
Convergence Limit            (>1.0) : 1.000010
Averaging Factor             (<1.0) : 0.500
Maximum No. of Iterations    : 60
Convergence Criteria         (1-5) : 2
Results Files                 (1-4) : 2
Output Format                  (1-3) : 1

```

MATERIAL BEHAVIOUR MODELS

```

-----
Concrete Compression Base Curve (0-3) : 1
Concrete Compression Post-Peak (0-3) : 1
Concrete Compression Softening (0-8) : 1
Concrete Tension Stiffening     (0-6) : 1
Concrete Tension Softening      (0-3) : 1
Concrete Tension Splitting      (0-1) : 1
Concrete Confined Strength      (0-2) : 1
Concrete Dilation                (0-1) : 1
Concrete Cracking Criterion      (0-4) : 1
Concrete Crack Slip Check        (0-2) : 1
Concrete Crack Width Check       (0-2) : 0
Concrete Bond or Adhesion        (0-3) : 1
Concrete Creep and Relaxation    (0-1) : 1
Concrete Hysteresis              (0-2) : 1
Reinforcement Hysteresis         (0-2) : 1
Reinforcement Dowel Action       (0-1) : 1

```

Reinforcement Buckling (0-1) : 1
 Element Strain Histories (0-1) : 1
 Element Slip Distortions (0-4) : 1
 Strain Rate Effects (0-1) : 1
 Structural Damping (0-1) : 1
 Geometric Nonlinearity (0-1) : 1
 Crack Allocation Process (0-1) : 1

<<< JOB FILE NOTES>>>

```

* * * * *
*
*           V e c T o r 2
*
*   S T R U C T U R E   D A T A
* * * * *

```

STRUCTURAL PARAMETERS

Structure Title : Enter Structure Title
 Structure File Name : S3-2
 Working Units : METRIC

No. of RC Material Types : 8
 No. of Steel Material Types : 2
 No. of Bond Material Types : 0
 No. of Rectangular Elements : 562
 No. of Quadrilateral Elements : 0
 No. of Triangular Elements : 0
 No. of Truss Elements : 80
 No. of Linkage Elements : 0
 No. of Contact Elements : 0
 No. of Joints : 618
 No. of Restraints : 17

MATERIAL SPECIFICATIONS

REINFORCED CONCRETE
 =====

CONCRETE

MAT TYP	REINF CMP	f'c (MPa)	f't (MPa)	e0 (me)	Ec (MPa)	MU	Cc (u/C)	T (mm)
1	0	49.00	4.02	3.92	25000.	0.15	10.00	200.0
2	1	49.00	4.02	3.92	25000.	0.15	10.00	200.0
3	1	49.00	4.02	3.92	25000.	0.15	10.00	200.0
4	2	49.00	4.02	3.92	25000.	0.15	10.00	200.0

5	1	49.00	4.02	3.92	25000.	0.15	10.00	200.0
6	1	49.00	4.02	3.92	25000.	0.15	10.00	200.0
7	1	49.00	4.02	3.92	25000.	0.15	10.00	200.0
8	1	49.00	4.02	3.92	25000.	0.15	10.00	200.0

MAT TYP	Agg (mm)	Scrx (mm)	Scry (mm)
1	10.0	0.0	0.0
2	10.0	0.0	0.0
3	10.0	0.0	0.0
4	10.0	0.0	0.0
5	10.0	0.0	0.0
6	10.0	0.0	0.0
7	10.0	0.0	0.0
8	10.0	0.0	0.0

REINFORCEMENT COMPONENTS

MAT TYP	SRF TYP	DIR (deg)	AMNT (%)	DIA (mm)	Fy (MPa)	Fu (MPa)	Es (MPa)
2	1	90.0	0.130	4.00	597.0	658.0	200000.
3	1	90.0	0.260	4.00	597.0	658.0	200000.
4	1	90.0	0.130	4.00	597.0	658.0	200000.
	1	361.0	2.500	4.00	400.0	600.0	200000.
5	1	361.0	2.500	4.00	400.0	600.0	200000.
6	1	361.0	5.000	4.00	400.0	600.0	200000.
7	1	361.0	10.000	4.00	400.0	600.0	200000.
8	1	90.0	1.000	32.00	571.0	664.0	200000.

MAT TYP	DIR (deg)	esh (me)	Esh (MPa)	Cs (u/C)	Dep (me)
2	90.0	10.00	500.0	0.00	0.000
3	90.0	10.00	500.0	0.00	0.000
4	90.0	10.00	500.0	0.00	0.000
	361.0	10.00	500.0	0.00	0.000
5	361.0	10.00	500.0	0.00	0.000
6	361.0	10.00	500.0	0.00	0.000
7	361.0	10.00	500.0	0.00	0.000
8	90.0	10.00	500.0	0.00	0.000

STEEL
=====

MAT TYP	SRF TYP	AREA (mm2)	DIA (mm)	Fy (MPa)	Fu (MPa)	Es (MPa)
1	1	1600.0	32.00	571.0	664.00	200000.
2	1	400.0	16.00	563.0	669.00	200000.

MAT TYP	esh (me)	Esh (MPa)	Cs (u/C)	Dep (me)
1	8.00	5000.0	0.00	0.000
2	8.00	5000.0	0.00	0.000

* * * * *
* V e c T o r 2 *
* L O A D D A T A *
* * * * *

LOAD CASE PARAMETERS

Structure Title (30 char. max.) : Enter Structure Title
Load Case Title (30 char. max.) : Enter load case title
Load Case File Name (8 char. max.) : S3-2
No. of Loaded Joints : 0
No. of Prescribed Support Displacements : 1
No. of Elements with Gravity Loads : 0
No. of Elements with Temperature Loads : 0
No. of Elements with Concrete Prestrain : 0
No. of Elements with Ingress Pressure : 0
No. of Element Surfaces w/ Thermal Load : 0
No. of Nodes with Lumped Masses : 0
No. of Nodes with Impulse Forces : 0
Ground Acceleration Record (0-1) : 0

JOINT LOADS

<NOTE:> UNITS: KIPS OR KN
<<<<< FORMAT >>>>>
NODE Fx Fy [#NODE d(NODE) d(Fx) d(Fy)] /
/

SUPPORT DISPLACEMENTS

<NOTE:> UNITS: MM OR IN
<<<<< FORMAT >>>>>
JNT DOF DISPL [#JNT d(JNT)] /
 617 2 -1.000 1 1/
/

GRAVITY LOADS

<NOTE:> UNITS: KG/M3
<<<<< FORMAT >>>>>
ELMT DENS GX GY [#ELMT d(ELMT)] [#ELMT d(ELMT)] /
/

TEMPERATURE LOADS

<NOTE:> UNITS: F OR C

```

<<<<< FORMAT >>>>>
ELMT  TEMP  [ #ELMT d(ELMT) d(TEMP) ] [ #ELMT d(ELMT) d(TEMP) ] /
/

CONCRETE PRESTRAINS
*****

<NOTE:> UNITS:  me
<<<<< FORMAT >>>>>
ELMT  STRAIN  [ #ELMT d(ELMT) d(STRAIN) ] [ #ELMT d(ELMT) d(STRAIN) ] /
/

INGRESS PRESSURES
*****

<NOTE:> UNITS:  MPa
<<<<< FORMAT >>>>>
ELMT  PRESSURE  [ #ELMT d(ELMT) d(PRS) ] [ #ELMT d(ELMT) d(PRS) ] /
/

SURFACE THERMAL LOADS
*****

<NOTE:> UNITS:  Sec, Degrees C
<<<<< FORMAT >>>>>
NODE1 NODE2  Tm1 Tp1  Tm2 Tp2  Tm3 Tp3  [#SURF d(NODE)] [#SURF d(NODE)] /
/

LUMPED MASSES
*****

<NOTE:> UNITS:  kg, m/s
<<<<< FORMAT >>>>>
NODE  DOF-X  DOF-Y  MASS  GF-X  GF-Y  Vo-X  Vo-Y  [ #NODE d(NODE) ] /
/

IMPULSE FORCES
*****

<NOTE:> UNITS:  Sec, kN
<<<<< FORMAT >>>>>
NODE  DOF  T1  F1  T2  F2  T3  F3  T4  F4  [ #NODE d(NODE) ] /
/

GROUND ACCELERATION
*****

<NOTE:> UNITS:  Sec, G
<<<<< FORMAT >>>>>
TIME  ACC-X  ACC-Y
/

<<< LOAD FILE NOTES >>>

```

Beam S3-3

* * * * *
* V E C T O R *
* J O B D A T A *
* * * * *

Job Title (30 char. max.) : S3-3
Job File Name (8 char. max.) : S3-3
Date (30 char. max.) : 12 Jan 2007

STRUCTURE DATA

Structure Type : 2
File Name (8 char. max.) : S3-3

LOADING DATA

No. of Load Stages : 161
Starting Load Stage No. : 1
Load Series ID (5 char. max.) : S3-3

Load Case	File Name (8 char. max.)	Initial	Final	Factors LS-Inc	Type	Reps	C-Inc
1	S3-3	0.000000	40.000000	0.250000	1	1	0.000000
2	NULL	0.000000	0.000000	0.000000	1	1	0.000000
3	NULL	0.000000	0.000000	0.000000	1	1	0.000000
4	NULL	0.000000	0.000000	0.000000	1	1	0.000000
5	NULL	0.000000	0.000000	0.000000	1	1	0.000000

ANALYSIS PARAMETERS

Analysis Mode (1-2) : 1
Seed File Name (8 char. max.) : NULL
Convergence Limit (>1.0) : 1.000010
Averaging Factor (<1.0) : 0.500
Maximum No. of Iterations : 60
Convergence Criteria (1-5) : 2
Results Files (1-4) : 2
Output Format (1-3) : 1

MATERIAL BEHAVIOUR MODELS

Concrete Compression Base Curve (0-3) : 1
Concrete Compression Post-Peak (0-3) : 1
Concrete Compression Softening (0-8) : 1
Concrete Tension Stiffening (0-6) : 1
Concrete Tension Softening (0-3) : 1
Concrete Tension Splitting (0-1) : 1
Concrete Confined Strength (0-2) : 1
Concrete Dilation (0-1) : 1
Concrete Cracking Criterion (0-4) : 1
Concrete Crack Slip Check (0-2) : 1
Concrete Crack Width Check (0-2) : 0
Concrete Bond or Adhesion (0-3) : 1
Concrete Creep and Relaxation (0-1) : 1
Concrete Hysteresis (0-2) : 1
Reinforcement Hysteresis (0-2) : 1

```

Reinforcement Dowel Action          (0-1) : 1
Reinforcement Buckling              (0-1) : 1
Element Strain Histories             (0-1) : 1
Element Slip Distortions            (0-4) : 1
Strain Rate Effects                  (0-1) : 1
Structural Damping                   (0-1) : 1
Geometric Nonlinearity              (0-1) : 1
Crack Allocation Process             (0-1) : 1

```

<<< JOB FILE NOTES>>>

```

* * * * *
*                               *
*           V e c T o r 2       *
*                               *
*   S T R U C T U R E   D A T A   *
* * * * *

```

STRUCTURAL PARAMETERS

```

Structure Title          : Enter Structure Title
Structure File Name     : S3-3
Working Units           : METRIC

No. of RC Material Types : 8
No. of Steel Material Types : 2
No. of Bond Material Types : 0
No. of Rectangular Elements : 562
No. of Quadrilateral Elements : 0
No. of Triangular Elements : 0
No. of Truss Elements : 80
No. of Linkage Elements : 0
No. of Contact Elements : 0
No. of Joints : 618
No. of Restraints : 17

```

MATERIAL SPECIFICATIONS

REINFORCED CONCRETE

=====

CONCRETE

MAT TYP	REINF CMP	f'c (MPa)	f't (MPa)	e0 (me)	Ec (MPa)	MU	Cc (u/C)	T (mm)
1	0	56.00	4.40	4.29	26100.	0.15	10.00	200.0
2	1	56.00	4.40	4.29	26100.	0.15	10.00	200.0
3	1	56.00	4.40	4.29	26100.	0.15	10.00	200.0
4	2	56.00	4.40	4.29	26100.	0.15	10.00	200.0

5	1	56.00	4.40	4.29	26100.	0.15	10.00	200.0
6	1	56.00	4.40	4.29	26100.	0.15	10.00	200.0
7	1	56.00	4.40	4.29	26100.	0.15	10.00	200.0
8	1	56.00	4.40	4.29	26100.	0.15	10.00	200.0

MAT TYP	Agg (mm)	Scrx (mm)	Scry (mm)
1	10.0	0.0	0.0
2	10.0	0.0	0.0
3	10.0	0.0	0.0
4	10.0	0.0	0.0
5	10.0	0.0	0.0
6	10.0	0.0	0.0
7	10.0	0.0	0.0
8	10.0	0.0	0.0

REINFORCEMENT COMPONENTS

MAT TYP	SRF TYP	DIR (deg)	AMNT (%)	DIA (mm)	Fy (MPa)	Fu (MPa)	Es (MPa)
2	1	90.0	0.170	4.00	597.0	658.0	200000.
3	1	90.0	0.340	4.00	597.0	658.0	200000.
4	1	90.0	0.170	4.00	597.0	658.0	200000.
	1	361.0	2.500	4.00	400.0	600.0	200000.
5	1	361.0	2.500	4.00	400.0	600.0	200000.
6	1	361.0	5.000	4.00	400.0	600.0	200000.
7	1	361.0	10.000	4.00	400.0	600.0	200000.
8	1	90.0	1.000	32.00	571.0	664.0	200000.

MAT TYP	DIR (deg)	esh (me)	Esh (MPa)	Cs (u/C)	Dep (me)
2	90.0	10.00	500.0	0.00	0.000
3	90.0	10.00	500.0	0.00	0.000
4	90.0	10.00	500.0	0.00	0.000
	361.0	10.00	500.0	0.00	0.000
5	361.0	10.00	500.0	0.00	0.000
6	361.0	10.00	500.0	0.00	0.000
7	361.0	10.00	500.0	0.00	0.000
8	90.0	10.00	500.0	0.00	0.000

STEEL
=====

MAT TYP	SRF TYP	AREA (mm2)	DIA (mm)	Fy (MPa)	Fu (MPa)	Es (MPa)
1	1	1600.0	32.00	571.0	664.00	200000.
2	1	400.0	16.00	563.0	669.00	200000.

MAT TYP	esh (me)	Esh (MPa)	Cs (u/C)	Dep (me)
1	8.00	5000.0	0.00	0.000
2	8.00	5000.0	0.00	0.000

* * * * *
* V e c T o r 2 *
* L O A D D A T A *
* * * * *

LOAD CASE PARAMETERS

Structure Title (30 char. max.) : Enter Structure Title
Load Case Title (30 char. max.) : Enter load case title
Load Case File Name (8 char. max.) : S3-3
No. of Loaded Joints : 0
No. of Prescribed Support Displacements : 1
No. of Elements with Gravity Loads : 0
No. of Elements with Temperature Loads : 0
No. of Elements with Concrete Prestrain : 0
No. of Elements with Ingress Pressure : 0
No. of Element Surfaces w/ Thermal Load : 0
No. of Nodes with Lumped Masses : 0
No. of Nodes with Impulse Forces : 0
Ground Acceleration Record (0-1) : 0

JOINT LOADS

<NOTE:> UNITS: KIPS OR KN
<<<<< FORMAT >>>>>
NODE Fx Fy [#NODE d(NODE) d(Fx) d(Fy)] /
/

SUPPORT DISPLACEMENTS

<NOTE:> UNITS: MM OR IN
<<<<< FORMAT >>>>>
JNT DOF DISPL [#JNT d(JNT)] /
 617 2 -1.000 1 1/
/

GRAVITY LOADS

<NOTE:> UNITS: KG/M3
<<<<< FORMAT >>>>>
ELMT DENS GX GY [#ELMT d(ELMT)] [#ELMT d(ELMT)] /
/

TEMPERATURE LOADS

```

<NOTE:> UNITS: F OR C
<<<<< FORMAT >>>>>
ELMT TEMP [ #ELMT d(ELMT) d(TEMP) ] [ #ELMT d(ELMT) d(TEMP) ] /
/
CONCRETE PRESTRAINS
*****

<NOTE:> UNITS: me
<<<<< FORMAT >>>>>
ELMT STRAIN [ #ELMT d(ELMT) d(STRAIN) ] [ #ELMT d(ELMT) d(STRAIN) ] /
/
INGRESS PRESSURES
*****

<NOTE:> UNITS: MPa
<<<<< FORMAT >>>>>
ELMT PRESSURE [ #ELMT d(ELMT) d(PRS) ] [ #ELMT d(ELMT) d(PRS) ] /
/
SURFACE THERMAL LOADS
*****

<NOTE:> UNITS: Sec, Degrees C
<<<<< FORMAT >>>>>
NODE1 NODE2 Tm1 Tp1 Tm2 Tp2 Tm3 Tp3 [#SURF d(NODE)] [#SURF d(NODE)] /
/
LUMPED MASSES
*****

<NOTE:> UNITS: kg, m/s
<<<<< FORMAT >>>>>
NODE DOF-X DOF-Y MASS GF-X GF-Y Vo-X Vo-Y [ #NODE d(NODE) ] /
/
IMPULSE FORCES
*****

<NOTE:> UNITS: Sec, kN
<<<<< FORMAT >>>>>
NODE DOF T1 F1 T2 F2 T3 F3 T4 F4 [ #NODE d(NODE) ] /
/
GROUND ACCELERATION
*****

<NOTE:> UNITS: Sec, G
<<<<< FORMAT >>>>>
TIME ACC-X ACC-Y
/

<<< LOAD FILE NOTES >>>

```


APPENDIX F
CRACK PATTERN OF EACH PAIR OF GEOPOLYMER CONCRETE BEAMS FOR D-
SERIES AND L-SERIES (SIDE VIEW AND BOTTOM VIEW)

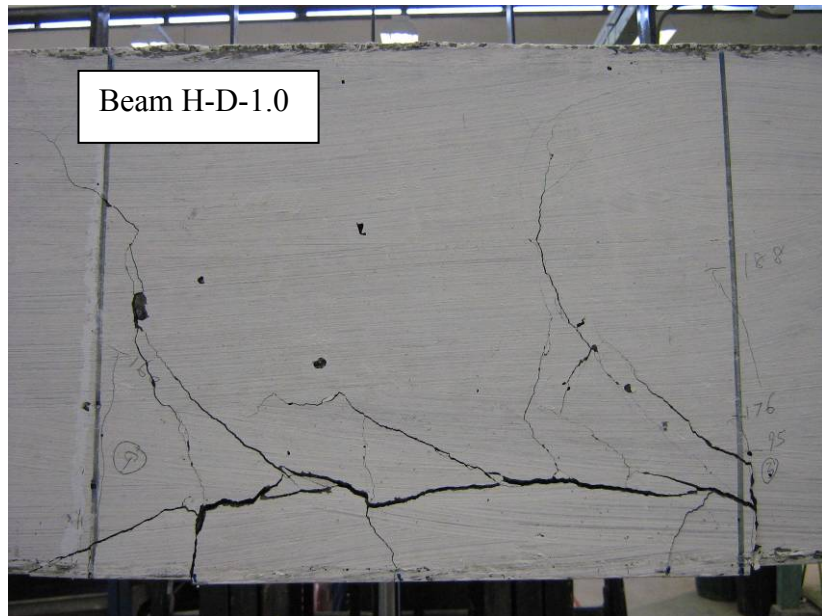
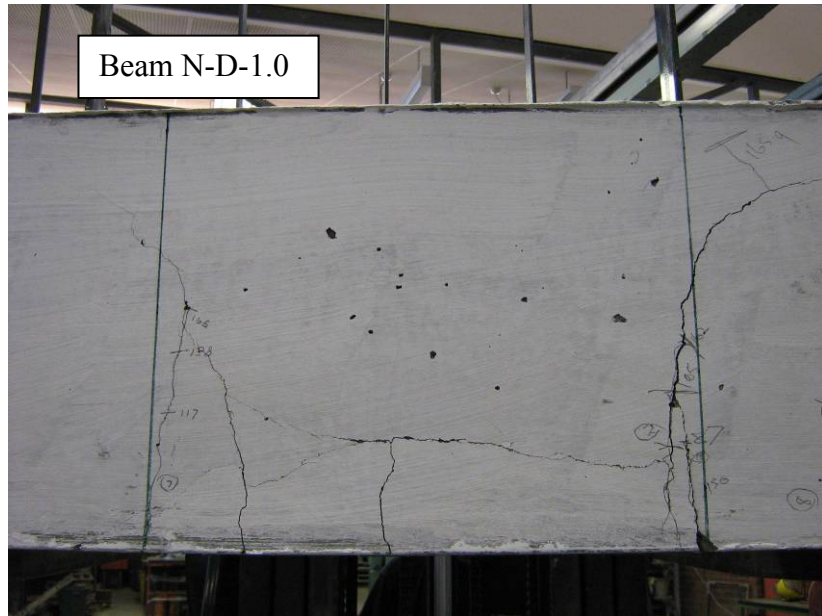


Figure F.1: Crack Pattern for Beam N-D-1.0 and H-D-1.0 (Side View)

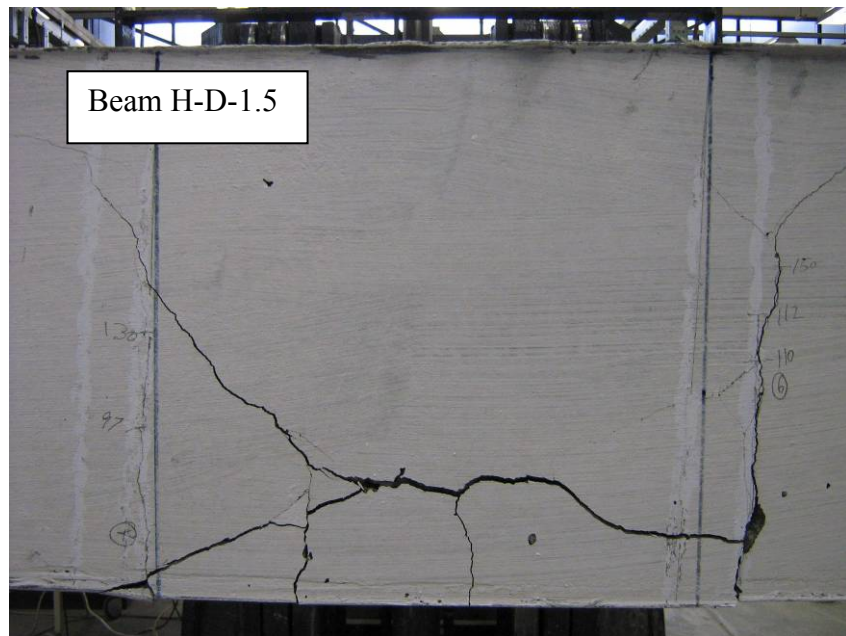
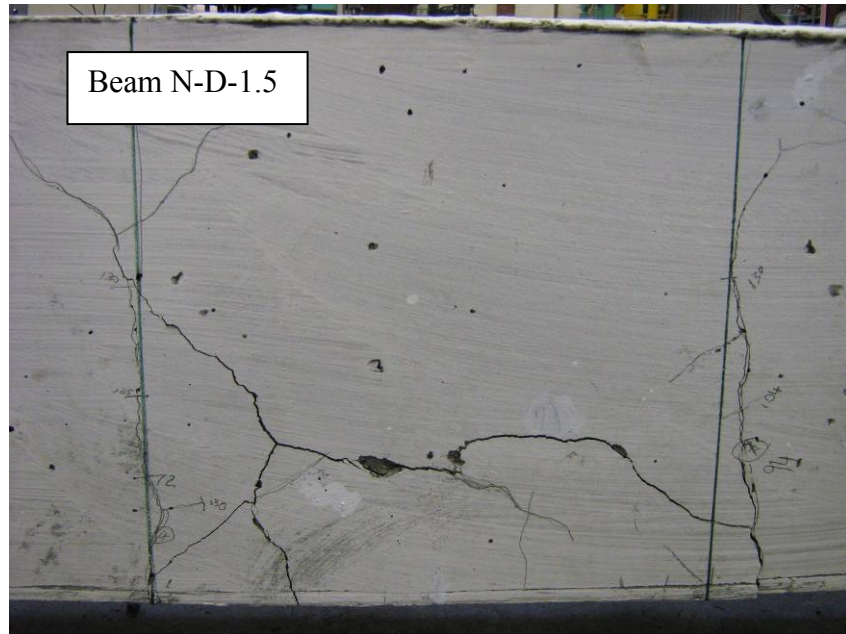


Figure F.2: Crack Pattern for Beam N-D-1.5 and H-D-1.5 (Side View)

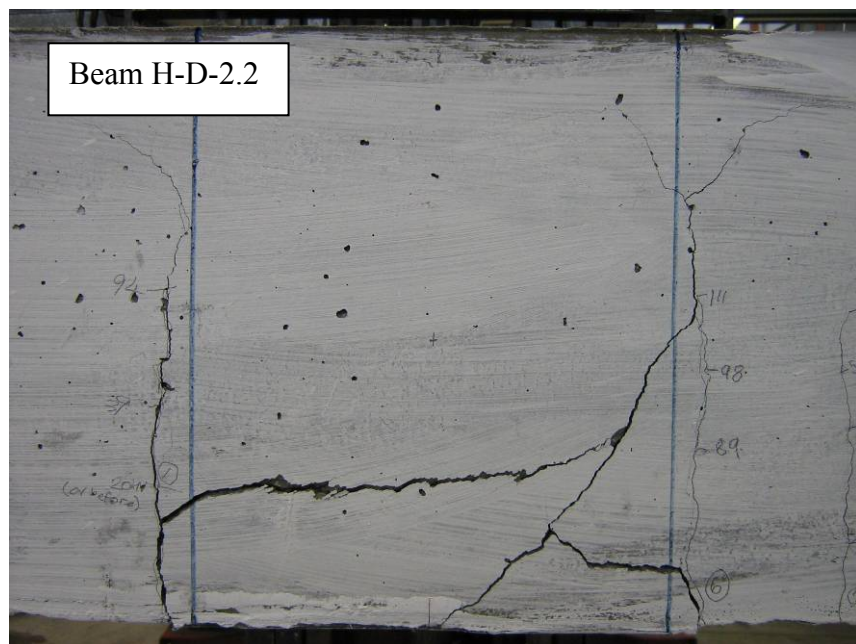
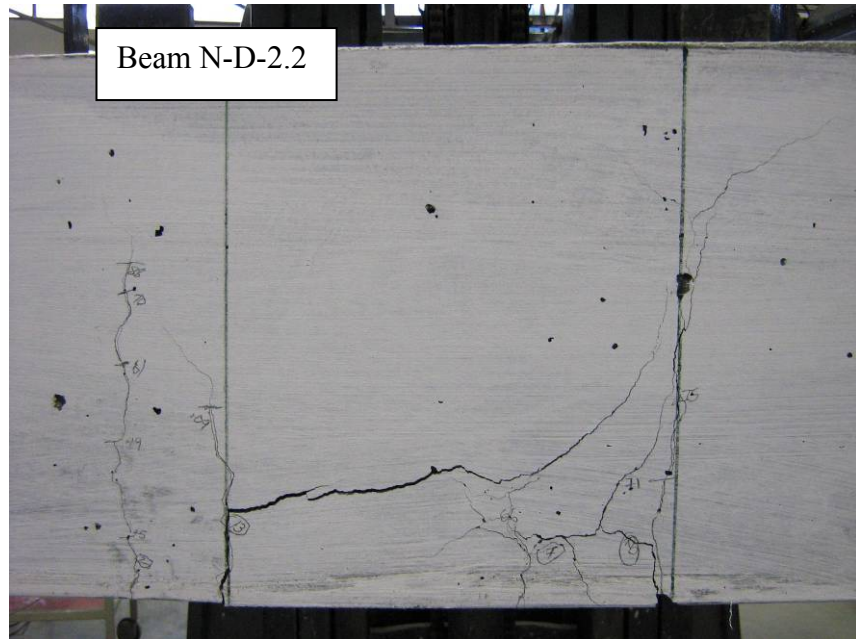


Figure F.3: Crack Pattern for Beam N-D-2.2 and H-D-2.2 (Side View)

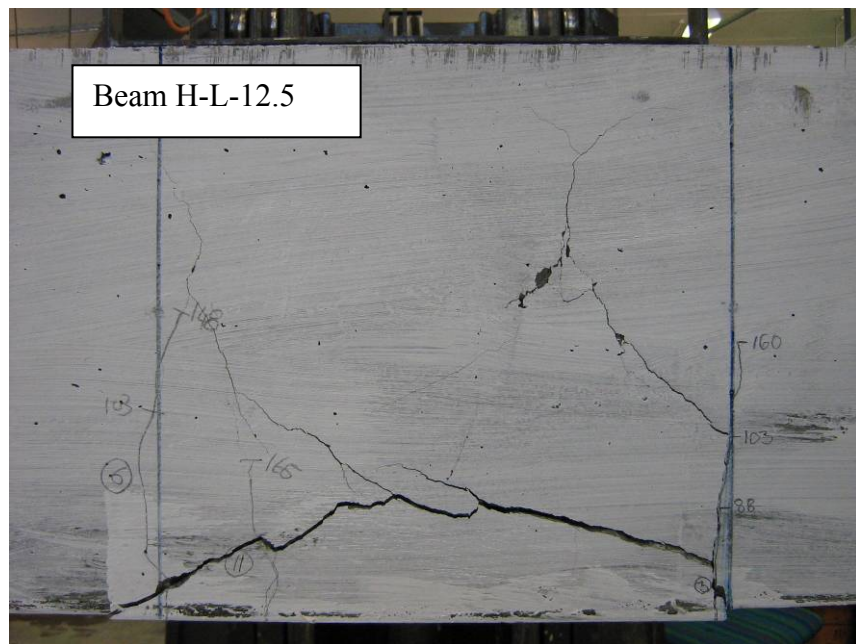
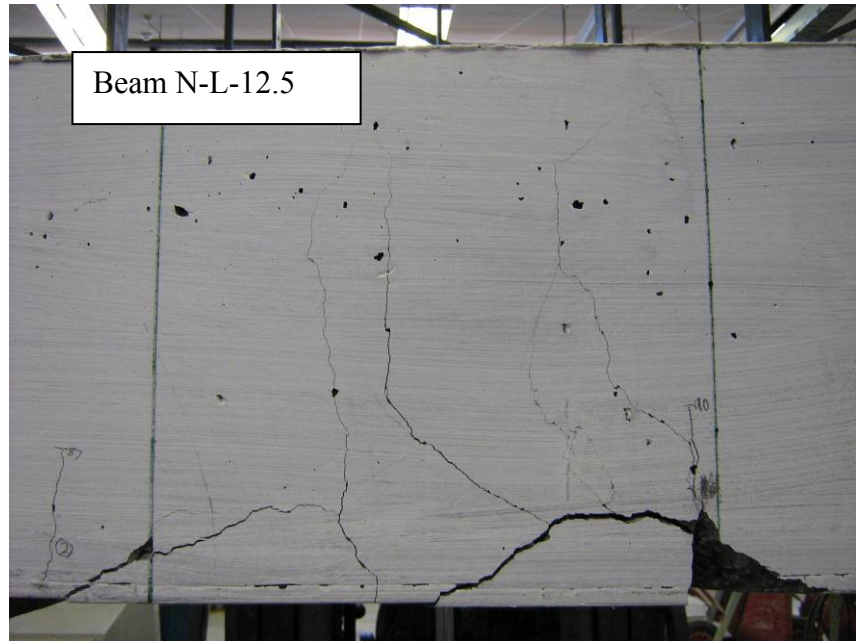


Figure F.4: Crack Pattern for Beam N-L-12.5 and H-L-12.5 (Side View)

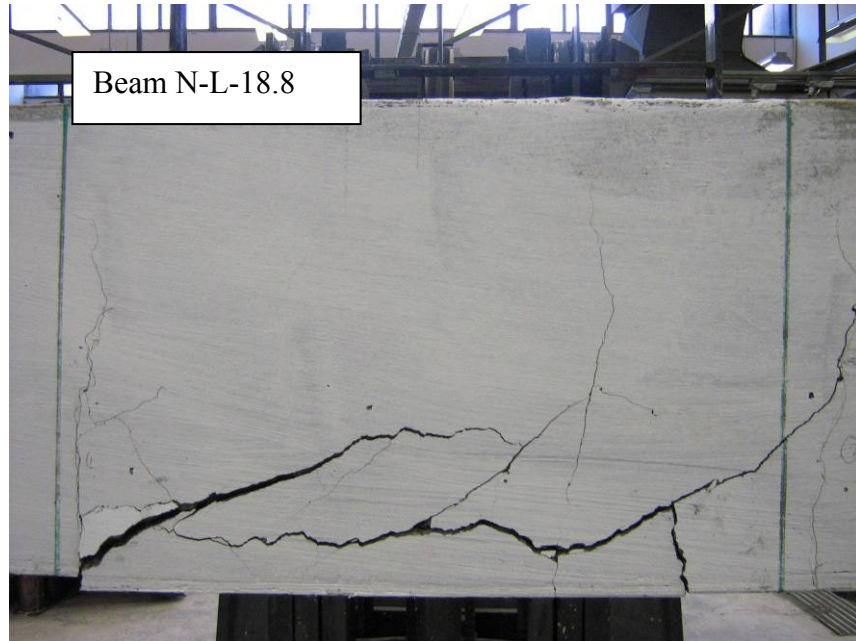


Figure F.5: Crack Pattern for Beam N-L-18.8 and H-L-18.8 (Side View)

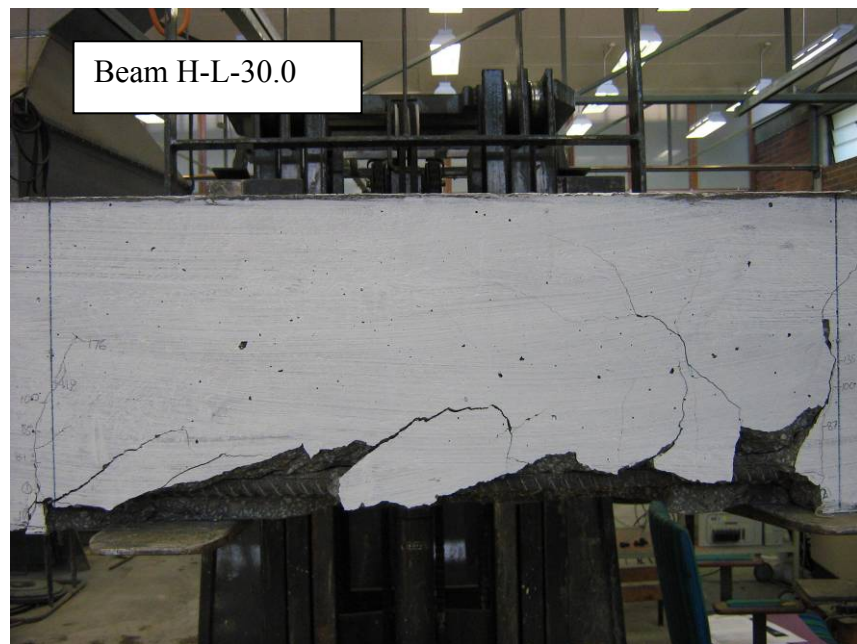


Figure F.6: Crack Pattern for Beam N-L-30.0 and H-L-30.0 (Side View)

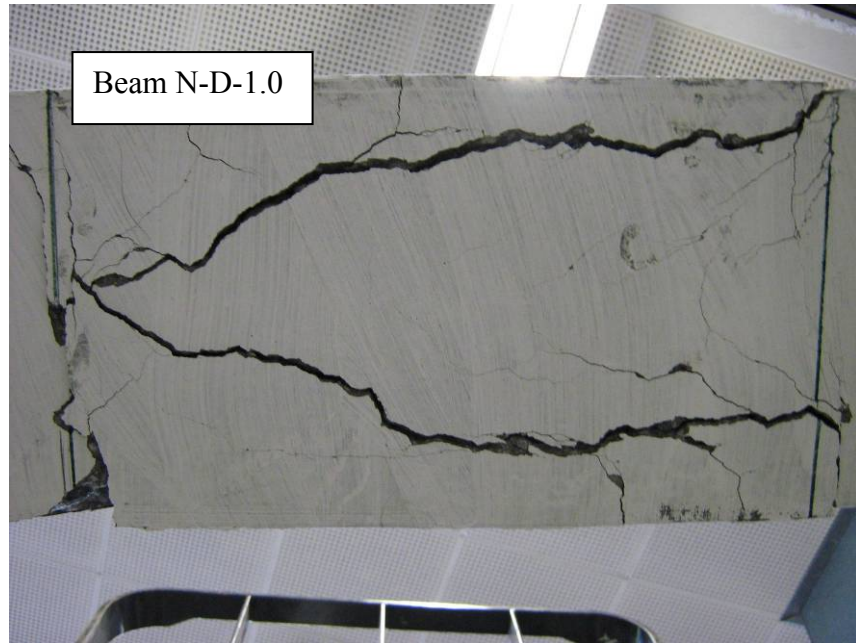


Figure F.7: Crack Pattern for Beam N-D-1.0 and H-D-1.0 (Bottom View)

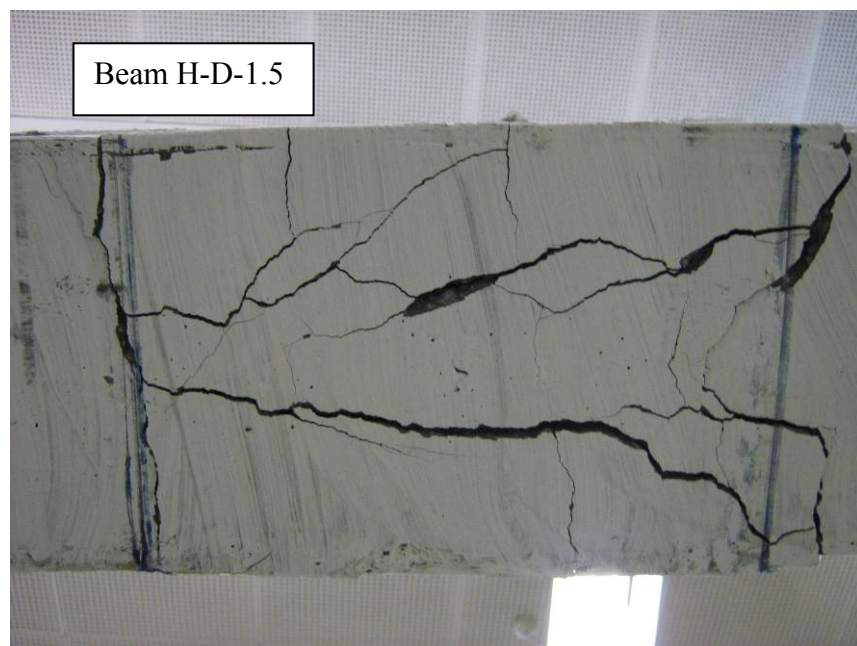
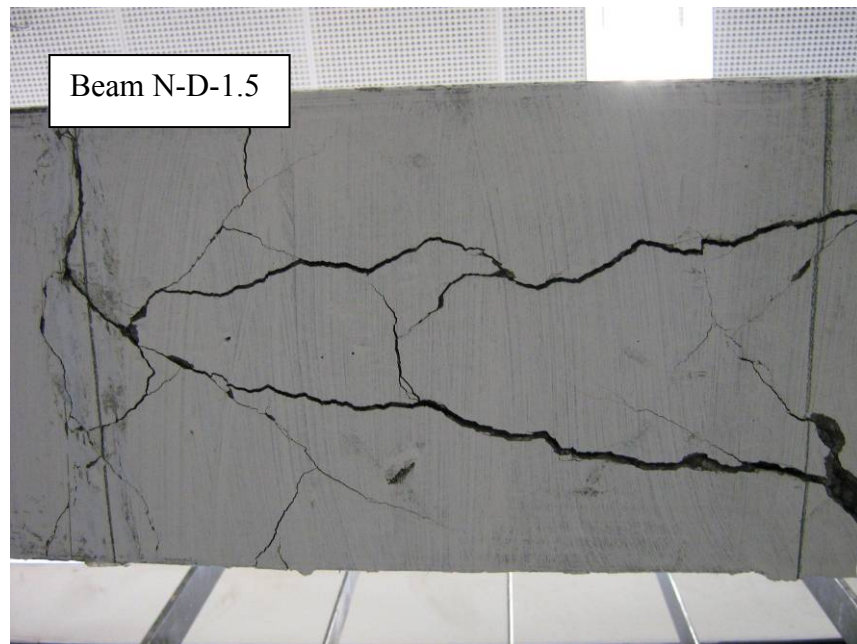


Figure F.8: Crack Pattern for Beam N-D-1.5 and H-D-1.5 (Bottom View)

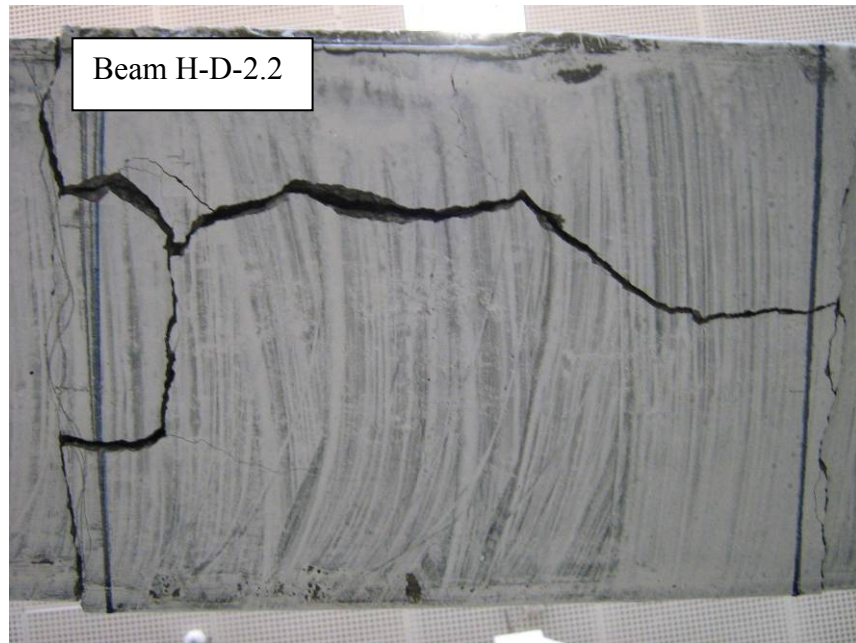
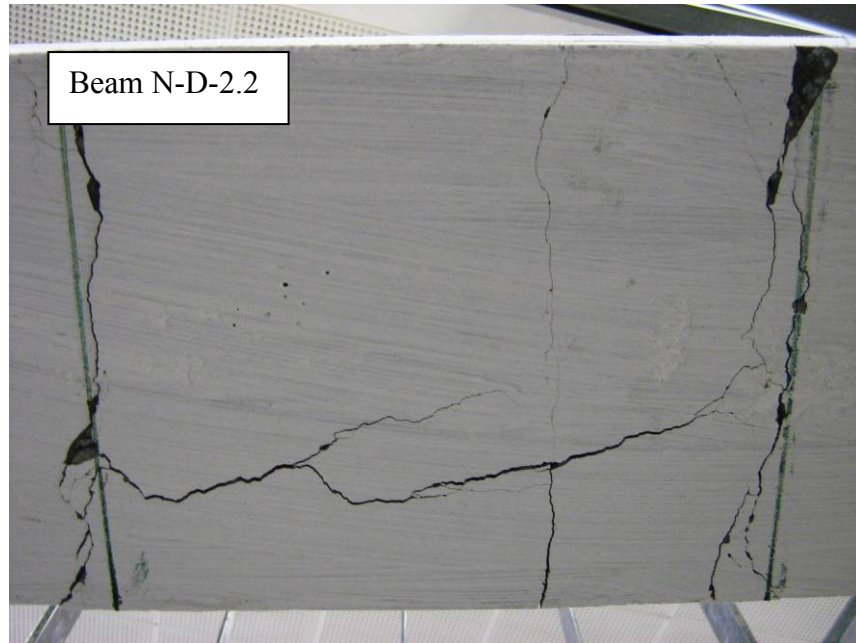


Figure F.9: Crack Pattern for Beam N-D-2.2 and H-D-2.2 (Bottom View)

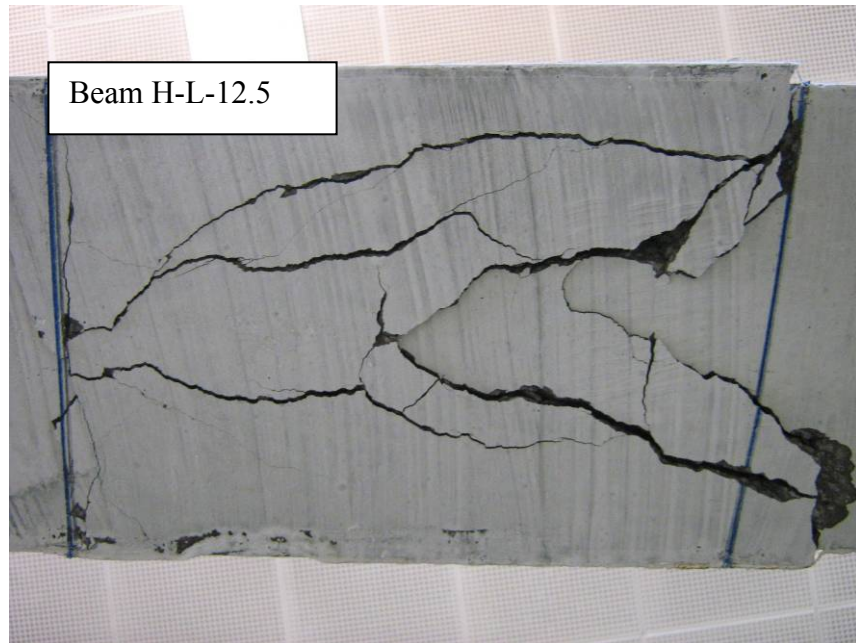
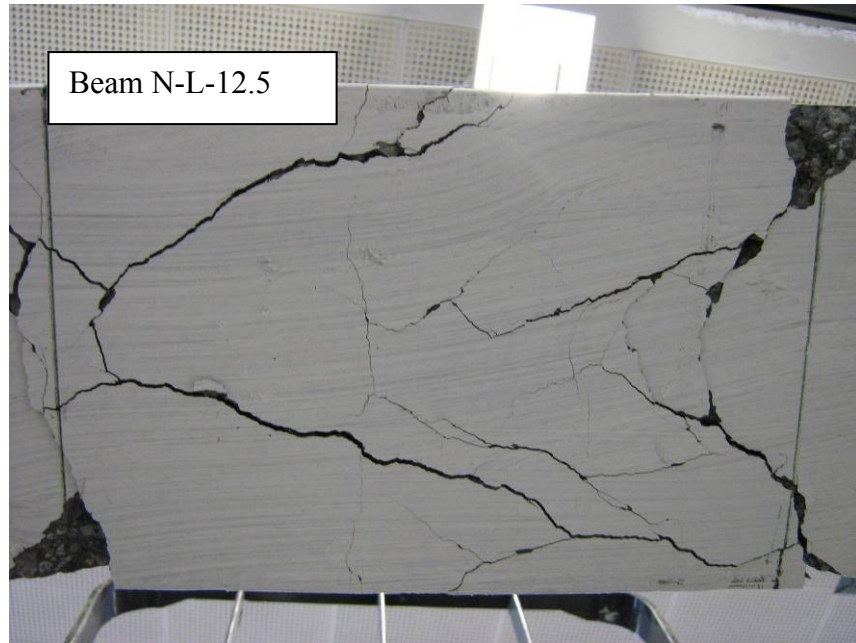


Figure F.10: Crack Pattern for Beam N-L-12.5 and H-L-12.5 (Bottom View)

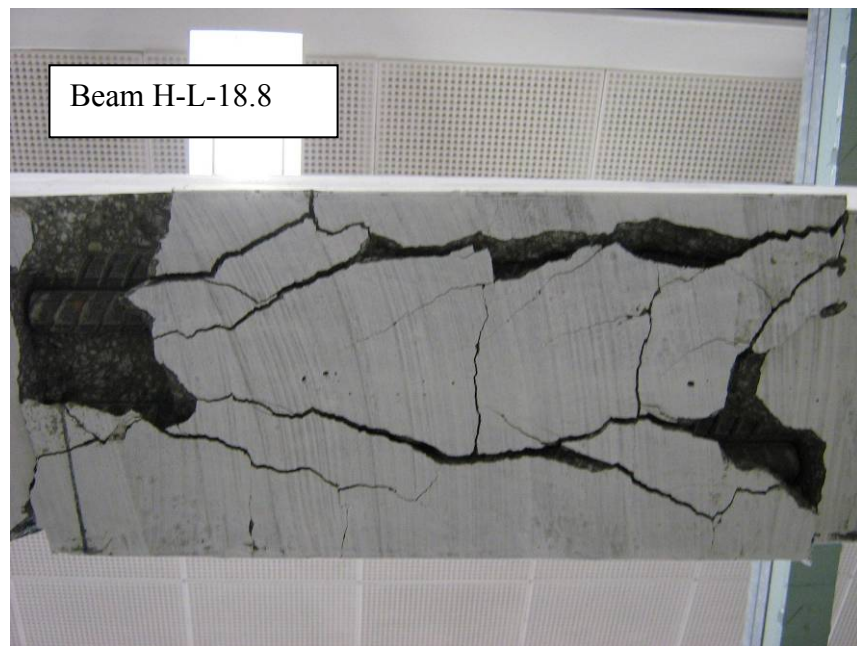
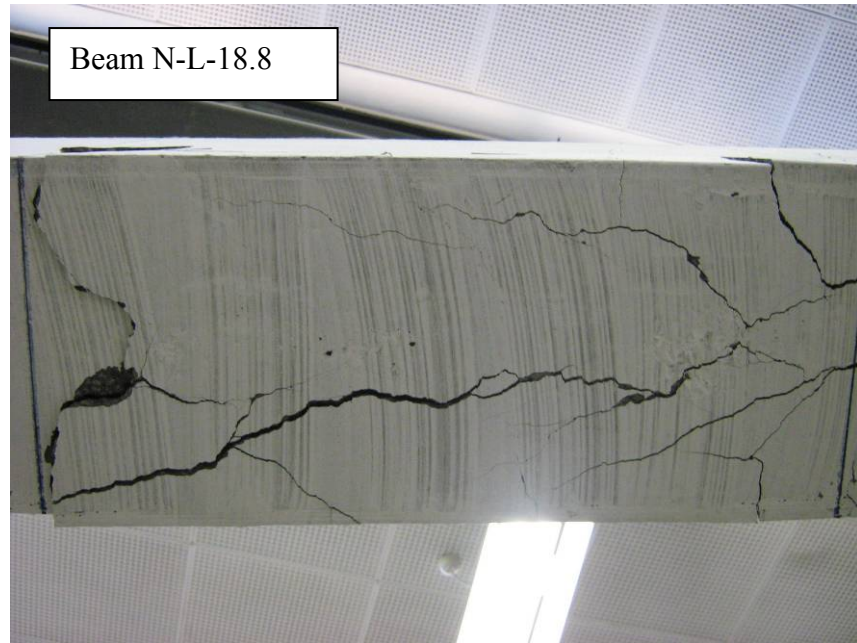


Figure F.11: Crack Pattern for Beam N-L-18.8 and H-L-18.8 (Bottom View)

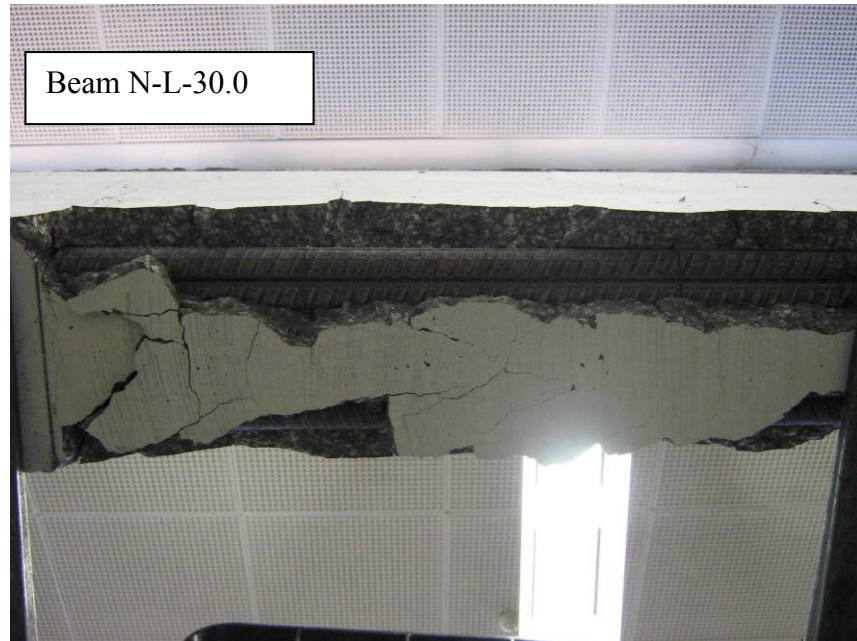


Figure F.12: Crack Pattern for Beam N-L-30.0 and H-L-30.0 (Bottom View)

APPENDIX G
STEEL- GEOPOLYMER CONCRETE INTERFACE AT SPLICE REGION
AFTER FAILURE

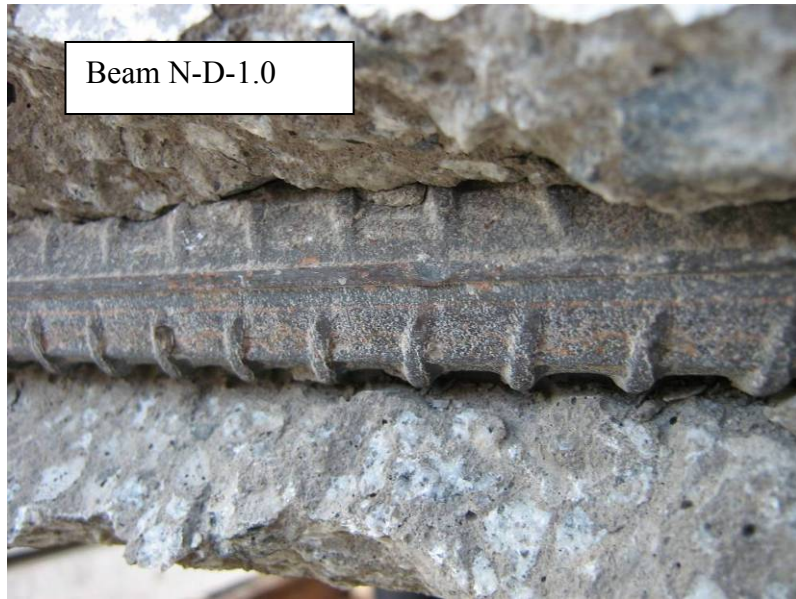


Figure G.1: Steel-Geopolymer Concrete Interface for Beam N-D-1.0 and H-D-1.0



Figure G.2: Steel-Geopolymer Concrete Interface for Beam N-D-1.5 and H-D-1.5



Figure G.3: Steel-Geopolymer Concrete Interface for Beam N-D-2.2 and H-D-2.2



Figure G.4: Steel-Geopolymer Concrete Interface for Beam N-L-12.5 and H-L-12.5



Figure G.5: Steel-Geopolymer Concrete Interface for Beam N-L-18.8 and H-L-18.8



Figure G.6: Steel-Geopolymer Concrete Interface for Beam N-L-30.0 and H-L-30.0

APPENDIX H
TEST DATA FOR BEAMS (BOND STUDY)

Table H.1: Test Data for Beam N-D-1.0

Load (kN)	Mid-span Deflection (mm)
0	0
9.87	0.44
19.73	0.67
29.6	0.83
39.5	1.01
49.33	1.21
59.19	1.58
71.52	1.93
81.39	2.3
91.25	2.63
101.12	2.96
110.98	3.3
120.85	3.64
130.71	3.98
140.58	4.42
150.44	4.89
157.84	5.16
160.31	5.35
162.78	5.49
165.24	5.62
162.78	5.69
157.84	5.73
152.91	5.84

Table H.2: Test Data for Beam N-D-1.5

Load (kN)	Mid-span Deflection (mm)
0	0
9.87	0.53
19.73	0.71
29.6	0.91
39.46	1.08
51.79	1.33
61.66	1.79
71.52	2.21
81.38	2.72
91.25	3.11
98.65	3.44
101.11	3.64
110.98	4.13
120.85	4.62
130.71	5.15
138.11	5.52
143.05	5.79
145.51	5.89
143.05	5.99
140.58	6.02
138.11	6.06

Table H.3: Test Data for Beam N-D-2.2

Load (kN)	Mid-span Deflection (mm)
0	0
9.87	0.24
19.73	0.47
29.6	0.64
39.46	0.83
44.39	1.15
49.32	1.42
54.26	1.87
61.66	2.26
64.12	2.42
69.06	2.69
73.99	3.21
78.92	3.37
81.39	3.59
83.85	3.72
88.79	4.01
91.25	4.37
96.19	4.64
101.12	5.11
106.05	5.66
108.52	5.77
110.98	6.03
108.52	6.03
106.05	6.05
103.59	6.16

Table H.4: Test Data for Beam H-D-1.0

Load (kN)	Mid-span Deflection (mm)
0	0
9.98	0.33
19.73	0.55
29.6	0.7
39.46	0.81
49.33	0.97
59.19	1.12
69.06	1.35
81.39	1.65
91.26	1.93
101.12	2.32
110.98	2.69
120.85	3.00
130.71	3.39
140.58	3.67
150.44	4.01
160.314	4.34
170.18	4.68
180.04	5.06
189.91	5.46
194.84	5.74
192.37	5.79
189.9	5.83

Table H.5: Test Data for Beam H-D-1.5

Load (kN)	Mid-span Deflection (mm)
0	0
9.87	0.29
19.73	0.51
29.6	0.67
39.46	0.84
49.33	0.99
59.19	1.17
69.06	1.56
81.39	2
91.25	2.43
101.12	2.99
110.98	3.44
120.85	3.84
130.71	4.34
140.58	4.77
150.45	5.22
160.31	5.73
170.18	6.11
172.64	6.42
170.18	6.49
167.71	6.53
162.78	6.56

Table H.6: Test Data for Beam H-D-2.2

Load (kN)	Mid-span Deflection (mm)
0	0
9.87	0.34
19.73	0.59
29.6	0.85
39.46	1.16
49.33	1.48
59.19	1.79
69.06	2.17
81.39	2.88
91.25	3.68
101.11	4.76
110.98	5.43
120.85	6.15
130.71	7.37
133.18	7.66
135.65	7.86
133.18	8.02
130.7	8.07

Table H.7: Test Data for Beam N-L-12.5

Load (kN)	Mid-span Deflection (mm)
0	0
9.87	0.73
22.19	0.94
29.6	1.09
39.46	1.27
49.33	1.46
61.66	1.79
71.52	2.09
81.39	2.46
91.25	2.8
101.12	3.2
110.98	3.58
120.85	3.91
130.71	4.32
133.18	4.51
135.65	4.65
133.18	4.67
130.71	4.85
123.31	4.95

Table H.8: Test Data for Beam N-L-18.8

Load (kN)	Mid-span Deflection (mm)
0	0
9.86	0.043
19.73	0.242
27.13	0.32
32.06	0.48
36.99	0.55
41.92	0.64
49.33	0.75
51.79	0.82
54.26	0.88
59.19	0.95
61.65	1.04
66.59	1.18
69.06	1.25
73.99	1.39
76.46	1.48
81.39	1.59
86.32	1.79
93.72	2.1
98.65	2.23
103.59	2.34
108.52	2.63
115.92	2.79
120.85	2.9
125.78	3.1
135.64	3.39
140.59	3.61
150.44	3.99
155.38	4.11
162.78	4.39
167.71	4.54
172.64	4.74
177.57	4.96
184.97	5.22
187.44	5.45
192.37	5.54
194.84	5.56
189.91	5.6
187.44	5.62
180.04	5.62
177.57	5.62
172.64	5.64
170.18	5.69
167.7	5.71

Table H.9: Test Data for Beam N-L-30.0

Load (kN)	Mid-span Deflection (mm)
0	0
9.865	0.2987
19.7	0.52
29.59	0.73
39.46	0.91
49.33	1.14
59.19	1.41
69.06	1.74
81.39	2.15
91.25	2.45
101.12	2.76
110.98	3.11
120.85	3.54
130.71	3.85
140.57	4.25
150.44	4.64
160.31	5.02
170.18	5.48
180.04	5.85
189.9	6.33
199.78	6.43
212.1	7.34
221.97	7.75
231.83	8.11
241.1	8.68
244.16	8.87
246.63	8.87
249.1	9.03
249.1	9.27
244.1	9.33
241.7	9.57

Table H.10: Test Data for Beam H-L-12.5

Load (kN)	Mid-span Deflection (mm)
0	0
9.86	0.27
19.73	0.49
29.6	0.66
39.46	0.83
49.33	0.99
59.19	1.17
69.06	1.4
81.39	1.81
91.25	2.1
101.12	2.51
110.98	2.89
120.85	3.23
130.71	3.57
140.58	3.92
150.44	4.27
160.31	4.69
165.24	4.98
167.71	5.18
165.24	5.24
162.78	5.28
160.31	5.32

Table H.11: Test Data for Beam H-L-18.8

Load (kN)	Mid-span Deflection (mm)
0	0
9.87	0.41
19.73	0.64
29.6	0.8
39.46	0.96
51.79	1.14
61.66	1.31
71.52	1.51
81.39	1.76
91.25	2.03
101.12	2.33
110.98	2.68
120.85	2.99
130.71	3.27
140.58	3.51
150.44	3.84
160.31	4.12
170.17	4.4
180.04	4.66
189.91	4.98
199.77	5.31
209.64	5.59
219.5	5.9
231.83	6.28
241.7	6.7
251.56	7.16
249.1	7.23
246.63	7.28
241.7	7.32

Table H.12: Test Data for Beam H-L-30.0

Load (kN)	Mid-span Deflection (mm)
0	0
9.87	0.32
19.73	0.59
29.6	0.76
39.46	0.92
49.33	1.1
59.19	1.31
69.06	1.54
81.39	1.82
91.25	2.09
101.12	2.36
110.98	2.6
120.85	2.89
130.71	3.17
140.58	3.43
150.44	3.78
160.31	4.08
170.18	4.32
180.04	4.67
189.9	4.95
199.77	5.25
209.64	5.56
221.97	5.94
231.83	6.24
241.7	6.6
251.56	6.97
261.43	7.3
271.29	7.69
281.16	8.03
291.03	8.48
300.89	8.89
310.76	9.27
320.62	9.75
323.09	9.97
320.62	10